SIMULATING CHLORAMINE DISSIPATION IN STORMWATER NETWORKS: A DECISION SUPPORT FRAMEWORK FOR POLLUTANT HAZARD ASSESSMENT

by

Mohamed Gaafar

A thesis submitted in partial fulfillment of the requirements for the degree of

Doctor of Philosophy

in

Water Resources Engineering

Department of Civil and Environmental Engineering
University of Alberta

ABSTRACT

Chloramine, a widely-used water disinfectant with long-lasting residuals, can pose serious environmental risks when reaches the aquatic environment through its introduction to storm sewers after different outdoor tap water uses, and consequently harm receiving water bodies and their aquatic biota. Although the allowable chloramine concentration in stormwater effluents is 0.02 mg/L, recent sampling results in Edmonton found concentrations as high as 0.39 mg/L. To date, there is no analytical framework capable of simulating chloramine decay and then predicting its related concentrations throughout a drainage system. And with recent studies about chloramine decay coefficients variability spatially and temporally, no available stormwater quality tool can adequately simulate this complex decay. Therefore, this knowledge gap provides an opportunity to structure a hazard assessment framework for stormwater quality to assess chloramine loads in stormwater effluents. This framework comprises 1) a stormwater model for runoff and pipe flow quantitative routing, 2) a new stormwater quality model to simulate chloramine decay in the sewer, 3) a hazard assessment framework for system operators that can quickly and accurately assess chloramine release incidents.

A stormwater model was built in MIKE URBAN that used rainfall data for hydrological input and pipe flow data of monitoring stations for model validation. High correlation between model predictions and observed pipe flows was found. Next, a new Variable Decay Coefficient Simulator model (VDCS) was developed to predict chloramine concentrations in the sewer system considering the spatial and temporal variability of its decay coefficients. The model inputs include the hydrodynamic simulations results of the stormwater model, the sewer system attributes, and the pollutant loads and decay characteristics. Then, the model outputs pollutographs at all system

manholes and outlets. Results of the VDCS simulations were validated showing very high agreements at all system points.

Running stormwater simulation models can be very time-consuming, and by the time results are available, mitigation actions may no longer be necessary. Stormwater system managers need reliable and fast tools to assess stormwater quality hazards at system outlets as a result of releases from any point in the stormwater basin. The solution comes in the form of new standalone maps that can be used as tools to quickly assess the severity of release incidents. Under different weather conditions, two types of maps were devised; 1) concentration maps show pollutant concentrations at the system outlet resulting from point-source pollutant releases anywhere in the stormwater basin, 2) hazard maps work similarly but show the spatial variation of pollution hazards instead of concentrations.

The hazard assessment framework was applied to study chloramine pollution in a stormwater basin in Edmonton, Alberta, in which results of stormwater MIKE URBAN and VDCS were used to develop concentrations and hazard maps. Concentration maps showed that under dry weather conditions chloramine over the entire basin was higher than the regulatory limit. For design storms of 2 and 5-year, it was found that 60% and 80% of the study area generated concentrations within the safe range. Storms with higher return periods, more than 5-year, posed no significant environmental concerns. Chloramine hazard maps were developed using two approaches. In the first, chloramine hazard scores were calculated based on event mean concentrations (EMC) which include total pollutant mass, concentrations and total stormwater volumes. This EMC-based hazard scores showed that approximately 25% of the basin at moderate to high risk of chloramine-related water pollution. In the second, fuzzy logic was utilized to include more chloramine-affecting

factors to better represent contaminant hazard in the study area. These factors included EMC values, land-use types, the spatial variation of chloramine decay, annual rainfall, ground slopes, property assessment values and proximity to the drainage network. The fuzzy-based hazard maps generated a different hazard pattern as a result of incorporating more pollutant-inducing factors, predicting that approximately 54% of the basin at moderate to high risk of chloramine-related water pollution.

This study shows that the development of a reliable concentration and hazard maps is achievable even for a complex pollutant like chloramine, and hence can be adopted to other stormwater pollutants. Applying the hazard assessment framework presented here, stormwater pollution and unregulated release incidents can be effectively controlled, focusing resources on areas with higher hazard susceptibility without the need for long simulations that preclude taking required measures in time.

PREFACE

This thesis is my original work. The thesis is organized in two formats. Chapter 2 and 3 are presented in a thesis chapter format. Chapter 2 provides a literature review on the topic of modeling stormwater networks and chloramine dissipation. Chapter 3 presents information about the process of stormwater modeling including model structure, computations and validation of results. Each of Chapter 4 and 5 is organized in a journal article format, as a standalone article for journal submission. Finally, Chapter 1 provides an overall introduction to the thesis, and Chapter 6 summarizes and concludes this research, and presents recommendations for future studies. Due to the mixed format of this thesis, duplication of some ideas, data presentation and figures could not be totally avoided; however, it was kept to the minimum. The task of preparing this thesis has been to produce from those activities a single piece of work. Hence, all chapters are integrated into a cohesive unit with a logical progression from one chapter to the next. Each chapter has its own introduction, hypothesis, and conclusions.

To date, this work has led to the submission of two manuscript for publication in peer-reviewed academic journals. For Chapter 5, Mr. Shereif Mahmoud provided advice on conducting geospatial analyses in ArcGIS and recommendations on the formulation of Section 5.2.3. My supervisor, Dr. Evan Davies contributed to all manuscripts composition and editing for all chapters and provided recommendations on the models' development.

Some of the research conducted for this thesis forms a part of a research project led by Drs. Evan Davies, Yang Liu, and James Bolton. The project received ethics approval from the University of Alberta Research Ethics Board, and support of NSERC and the City of Edmonton Drainage Services department through a Collaborative Research and Development grant to Dr. Evan Davies (principal investigator), called "A study of chlorine transport and dissipation in stormwater systems", No. CRDPJ 468429-14, September 2014.

A research is never finished.

Even when it seems so.

It is a work in progress.

And ever will be.

To everyone who helped me along the way,

and my parents, my wife, and my daughter.

ACKNOWLEDGEMENTS

Above all, I thank my mother and my father. There are not enough words to express my gratitude and appreciation. I would not be anything in life without their hard work, patience, sacrifices and encouragement. I am forever indebted to them. I want to thank my wife for her support and apologize for all the time I was not around.

I am greatly thankful to my supervisor for giving me the opportunity, support and guidance over the course of my research. I would like to thank him for all his devoted time and effort which improved the outcome of this work considerably.

I would also extend my gratitude to the members of my supervisory committee along with the examination committees on my defence and candidacy exams. I thank them for their contributed time, efforts and suggestions.

I am grateful for the financial support of NSERC and the City of Edmonton. I also received funding through E. Davies' Discovery Grant, the University of Alberta Doctoral Recruitment Scholarship, the University of Alberta Bursaries program, the Sustainability Scholars program and the Graduate Student Internship Program.

I would like also to thank of the help of all the City of Edmonton/EPCOR personnel during the sampling collection, field measurements and site visits.

Thank you to all my fellow graduate students and friends for their endless help and encouragement.

I thank every person who helped me, taught me anything, offered me an advice, gifted me a new idea, alleviated my stress, lent me some time or effort, or encouraged me; in any way; in my work, study or personal life.

TABLE OF CONTENTS

LIST OF FIGURES

LIST OF TABLES

LIST OF ABBREVIATIONS

AD	**:**	Advection-Dispersion
AOB	**:**	Ammonia oxidizing bacteria
ASCE	**:**	American society of civil engineers
BKM	**:**	Bayesian Kriging Model
BMP	**:**	Best management practices
BOD	**:**	Biochemical oxygen demand
CCME	**:**	Canadian Council of Ministers of the Environment
Cl	**:**	Chlorine
CN	**:**	Curve number
CoE	**:**	The City of Edmonton
COD	**:**	Chemical oxygen demand
COM	**:**	Commercial land-use/Location
DBPs	**:**	Disinfection by-products
DEM	**:**	Digital elevation model
DNA	**:**	Deoxyribonucleic acid
DO	**:**	Dissolved oxygen
DOC	**:**	total organic carbon
DWF	**:**	Dry weather flow
EMC	**:**	Event mean concentration
GIS	**:**	Geographic information systems
IA	**:**	Index of agreement
IDF	**:**	Intensity duration frequency curves
IDW	**:**	Inverse Distance Weighted
IND	**:**	Industrial land-use/Location
ln(NSE)	**:**	Logarithmic NSE
MAE	**:**	Mean absolute error
MOUSE	**:**	The model for urban sewers
NCl_3	**:**	Trichloramine

NH_2Cl	**:**	Monochloramine
$NHCl_2$	**:**	Dichloramine
NOB	**:**	Nitrite oxidizing bacteria
NOM	**:**	Natural organic matter
NRC	**:**	United States National Research Counsil
NSE	**:**	Nash-Sutcliffe efficiency
NSERC	**:**	Natural Sciences and Engineering Research Council of Canada
Pb	**:**	Lead
PBIAS	**:**	Percent bias
PRK	**:**	Park land-use/Location
RES	**:**	Residential land-use/Location
RMSE	**:**	Root mean square error
SWMM	**:**	StormWater Management Model
TAC	**:**	Total active chlorine
TKN	**:**	Total Kjeldahl nitrogen
TOC	**:**	Total organic carbon
TSS	**:**	Total suspended solids
UH	**:**	Unit hydrograph
US EPA	**:**	United States Environmental Protection Agency
VDCS	**:**	The variable decay coefficient simulator
WDS	**:**	Water distribution systems

CHAPTER 1

INTRODUCTION

1.1 Background

Although chlorine was discovered in the mid-18th century in Sweden, it took about one-and-a-half centuries to recognize chlorine and chlorine-containing products as effective disinfectants (Connell, 1996; Zhang et al., 2017); instead, early chlorine applications aimed to control the foul odors in water, which were believed to be responsible for waterborne diseases (AWWA, 2006). By the 1940s, chlorine disinfection became a standard, widely-used approach for water treatment that is still used today by many municipalities (Crittenden et al., 2012). In spite of its wide acceptance, chlorine has some known disadvantages, including the volatility of chlorine which causes it to dissipate rapidly in distribution systems, and the reactivity of chlorine with naturally found organic matters in water systems, which results in the production of disinfection by-products (DBPs) that pose considerable risks to public health (AWWA, 2006; Hrudey, 2009). Since the first report of DBPs in 1974, research has focused on understanding the producing reactions, method of prevention and acceptable concentrations of DBPs, along with looking for alternative disinfection methods (AWWA, 2006).

An alternative to chlorine, called chloramine, was first used by a water treatment plant in Ottawa in 1916 to reduce treatment costs (Connell, 1996). During chloramination, ammonia is added to convert the residual chlorine to chloramines including monochloramine (NH_2Cl), dichloramine ($NHCl_2$) and trichloramine (NCl_3) (Vikesland et al., 2001). NH_2Cl is the dominant chloramine species, and so the term "chloramine" is used in this work to describe all chloramine species – monochloramine, dichloramine and trichloramine – for simplicity. Initially, chlorine and chloramine were used widely for disinfection purposes; however, the U.S. Public Health Service observed chlorine's rapid effect on several bacteria in 1943, which reduced the use of chloramine significantly (Crittenden et al., 2012). Thus, it was not until the discovery of chlorine DBPs in the 1970s that chloramine started to be used widely as a disinfectant (AWWA, 2006; Zhang et al., 2018a), because (1) although chloramines do form DBPs, they do so to a much lesser degree than chlorine (Duirk et al., 2005; Moradi et al., 2017); and (2) monochloramine has a desirable longer-lasting residual that prolongs its disinfection efficiency (WHO, 2004). By 2004, approximately

30% of U.S water suppliers were using chloramination for disinfection (Maestre et al., 2016), and today it is widely used worldwide (Wahman and Speitel, 2012), including by the City of Edmonton (CoE) (Zhang et al., 2018c).

Given its long-lasting residual, a concern is that the DBPs and chloramines in treated drinking water may reach the aquatic environment through their introduction to stormwater drainage systems after outdoor or industrial tap water use (Zhang et al., 2018c, 2017). Sources include distribution system leaks and breaks, lawn and garden watering, car and driveway washing, pool emptying, street cleaning, firefighting, construction activities, hydro-testing of industrial pressure-vessels and boilers, and industrial or commercial wash-down activities (Balling et al., 2008; Manning et al., 1996; Mayer and DeOreo, 1998; Zhang et al., 2018c, 2017). In Edmonton, stormwater eventually enters the North Saskatchewan River or tributary creeks from over 200 storm sewer outfalls, in which some of the stormwater system discharges flow directly from the point of discharge into receiving waters (CoE, 2013).

In growing recognition of the detrimental environmental effects of stormwater runoff, the past several decades have witnessed a broader shift toward management of stormwater quality (Goulden et al., 2018; Tsihrintzis and Hamid, 1997a; Zoppou, 1999). In terms of chlorine, it was found that the long-lasting NH_2Cl disinfectant poses considerable environmental risk for receiving water bodies and their aquatic biota (Zhang et al., 2018a). Typically, water treatment produces a total active chlorine (TAC) concentration of 2.0 mg/L (Milne et al., 1993). Many studies demonstrated the chlorine-induced harmful, and potentially fatal, influences on fish habitat and possible changes in species composition (Bellanca et al., 1977; Grothe and Eaton, 1975; Manning et al., 1996; NRC, 2008; Svecevicius et al., 2005; US EPA, 1988, 1984; Zillich, 1972; Zvinavashe et al., 2008). However, the chlorine effects of exposure depend on the concentration, duration, fish species, and other environmental factors. Field studies and biological surveys found a TAC exceeding only 0.02 mg/L to harm aquatic life. Consequently, the Canadian Council of Ministers of the Environment issued new Canada-wide guidelines for the protection of aquatic life that reduced the maximum TAC concentration in municipal effluents discharged to surface waters to 0.02 mg/L (CCME, 2009). In this light, the CoE has recently adjusted its Sewers Use Bylaw (Bylaw 16200, 2016) to reduce the permissible total chlorine discharge concentration to 0.02 mg/L (CoE, 2018); however, monitoring of the TAC concentrations at selected locations of Edmonton

storm sewers showed TAC concentrations up to 0.39 mg/L, which is substantially greater than the reported detrimental level. Further, a new study has found TAC concentrations as high as 0.77 mg/L in stormwater samples (Zhang et al., 2018c). Therefore, there is a need to understand and anticipate chloramine dissipation behaviour in stormwater systems.

1.2 On urbanization

Chloramine contamination results from many problems driven by urban development and growth in today's world. With more than 50% of human beings inhabiting cities and over 500 cities with over 1 million residents (Fletcher et al., 2013), urbanization has several serious impacts on receiving waters in terms of water quality and flood intensity (Wang et al., 2019). As it alters the natural ground surface, urban growth increases impervious land area, which leads to less infiltration, and more and peakier runoff (Butler and Davies, 2011). In addition to more intensive floods as a result of suburban development, urbanization contributes to more severe pollutant loadings (Lee and Heaney, 2003). Related factors coinciding with urbanization such as land-use changes, human activities and population growth aggravate the impact of urban sprawl on the quality of stormwater effluents that eventually reach surface waters (Zhang et al., 2018c). There are many sources of urban water pollution such as precipitation, soil erosion, and the accumulation and wash-off of street dirt, fertilizers, pesticides and harmful chemical constituents, as well as direct pollutant inflows to the drainage system (Brezonik and Stadelmann, 2002). In many cities, stormwater is a significant contributor to water bodies, thus exacerbating pollution that is often routed directly to receiving streams and rivers, impairing local water supplies and causing unnecessary risks to human and aquatic health (Bernhardt and Palmer, 2007; Davis et al., 2001; Eriksson et al., 2007; Gnecco et al., 2005; Howell et al., 2012; Makepeace et al., 1995; Roy et al., 2008).

Over decades, urbanization-inducing effects on stormwater quality have been discussed and proven (Haris et al., 2016). Several studies have reported the impact of polluted stormwater on freshwater ecosystems and human health (Konrad, 2005; Paul and Meyer, 2001; Roy et al., 2008; Walsh, 2000). The large amounts of pollutants released to receiving watercourses lead to water-quality degradation, and in return may cause potential health risk of waterborne diseases in many urban streams (Jiang et al., 2015). For instance, it was found that 91% of the UK river basins

considered at risk were located downstream of heavily altered urban waters (Ellis et al., 2012); while in the US, urban stormwater is regarded as the primary source of water quality impairments of 13%, 18% and 32% of all rivers, lakes and estuaries respectively (NRC, 2008). Many studies have found similar patterns regarding urban water pollution, see Meyer et al. (2005).

In conclusion, because of the detrimental impacts on receiving waters, the uncertainty about decay processes, the value for planning purposes and the expense of obtaining pollution data, interest has grown in developing predictive models for urban stormwater pollutant loads (Dotto et al., 2012; Zhang et al., 2015). Such models can help both stormwater management practitioners and scientists make estimates for pollution loading over the watershed (Brezonik and Stadelmann, 2002).

1.3 Problem statement

Although research over the past two decades has increasingly focused on modeling stormwater quality, as discussed later in Section 2.2 and 2.3, studies on modeling chloramine dissipation in stormwater networks are lacking. There is not, to-date, a comprehensive analytical framework capable of simulating chloramine dissipation and then predicting its related concentrations throughout a drainage system. The complex nature of chloramine decay pathways makes a full representation of the interacting chemical and biological mechanisms of formation, transport, decomposition and decay of chloramines challenging, and a tool capable of modeling them extremely helpful. Such a tool would help managers and engineers, in both public and private sectors, to predict chloramine concentrations in stormwater networks according to defined inputs and to support decision makers in maintaining released concentrations below the assimilation capacity of receiving streams in the future.

The research presented here was part of a research project to study the decay of chloramine in Edmonton's storm sewers in a collaboration between the University of Alberta and City of Edmonton. The other part of the project – conducted by Dr. Yang Liu's research group – studied the chemistry of chloramine decay. Recent findings based on field sampling results, laboratory experiments and an analytical chemistry model (Zhang et al., 2018a, 2018c, 2018b) showed that chloramine decay characteristics can vary temporally and spatially because of the complex

interactions with biofilms and natural organic matter (NOM), which no available stormwater simulation tool is capable of modeling, as further discussed in Section 2.3.

This knowledge gap provides opportunities to (1) expand our knowledge and capability of simulating chloramine dissipation in storm sewers, (2) investigate the necessary input parameters, equations and variables for proper simulations, (3) examine the effects of including chloramine decay coefficient variability in chloramine simulations, and (4) study the effect of different pipe flow characteristics, weather conditions, and rainfall properties on chloramine dissipation rates, using the simulation tool.

1.4 Research objectives

The ultimate aim of this research is to provide a hazard assessment framework for water quality in stormwater systems that can project chloramine concentrations and consequently anticipate related water quality hazards in the storm sewer system before chloramine pollution reaches surface water bodies. Such a tool can be generalizable to other Canadian cities and internationally, and can be made flexible enough to apply in the future to study the dissipation of other constituents in sewer systems. Implementing this hazard assessment framework for a complex stormwater pollutant with many decay mechanisms and pathways like chloramine means that the framework is applicable to many other stormwater pollutants.

Toward this overall aim, specific objectives are,

1. To build, calibrate and validate a stormwater simulation model including the surface runoff hydrological routing and hydrodynamic pipe flow computation. This entails improvement of GIS-based catchment property estimations, such as imperviousness and ground slope estimations for different surfaces and ground slopes. Quantitative simulations of this model will be tested against rainfall and pipe flow data records provided by CoE's Drainage Services. Validity will be assessed using a group of statistical measures to evaluate model predictions.
2. To build a new water quality simulation model that can simulate chloramine decay in the stormwater system considering the variability of its decay coefficients both temporally and spatially.

3. To study the effect of including the variability of chloramine decay rates on the predictions of the water quality models under different weather conditions and pollution source types.
4. To develop a GIS model for mapping chloramine concentration in a GIS application like ArcGIS, in which suitable mapping techniques are tested and validated using available chloramine concentration records and results of field sampling and laboratory experiments.
5. To structure an analytical hazard assessment framework for chloramine dissipation in stormwater systems that incorporates the stormwater simulation model, the stormwater quality model and the GIS-mapping model to generate GIS-based decision support tool.
6. To estimate chloramine hazard probabilities across the study area considering, i) different weather conditions, ii) various chloramine-pollution release factors, and iii) both pollutant mass and concentration at the system outlet.
7. To produce standalone, easy-to-use chloramine hazard maps that can help system operators to quickly assess stormwater-induced pollution in the study area.

1.5 Novelty and contribution

For simulating degradable chemical constituents, all commercial stormwater modeling tools are basic and do not include necessary modeling options. The water quality model to be developed in this work will support modeling of different decay orders such as zero, first and second orders, considering variable decay coefficients over the study period and area. It will readily accept hydrodynamic simulation results from any stormwater software to produce a complete system for stormwater modeling.

The chloramine hazard assessment framework introduced in this work can be applied to any stormwater model to predict stormwater quality risk associated with point-source release incidents. That hazard assessment framework can be generalized to different chemical substances that can harm receiving waters environment. This framework is built to function as one whole model structure, which is new. The developed hazard map in this work adopts a new concept of assessing chloramine concentration at the most critical points in the sewer system such as outfalls. The hazard maps are new to stormwater quality assessment and would help save municipal resources.

With the growing public awareness of the necessity of protecting water resources and aquatic life, a need to predict the concentrations of chloraminated water discharged in stormwater systems is

required. Many local governments are required to develop sustainable water usage management plans, which demand stormwater quality management options and contaminated discharge controls. Ideally, the proposed research will support many municipalities and water industries, which aim to minimize urban pollution and environmental footprint, by developing cost-effective techniques to simulate and subsequently predict chloramine dissipation in drainage systems, and thus pollutant concentrations that may enter surface waters. Furthermore, the intended research here will expand our capabilities of simulating chloramine dissipation in stormwater networks. It is hoped that the analytical modeling framework developed here will be applicable to a larger range of pollutant discharges from stormwater systems. On a broader scale, the outcomes of this project will contribute to the efforts of reducing negative environmental impacts of polluted urban water discharges to surface waters.

1.6 Thesis layout

This thesis is organized into six chapters. Both Chapter 4 and Chapter 5 are formatted as two main contributions and paper submissions to peer-reviewed journals.

Chapter 1 gives a background, defines the problem statement, and provides the motivation, objectives, and the novel contribution of the research.

Chapter 2 summaries the available material in the literature about stormwater models, stormwater quality simulations and the dissipation of chlorine and chloramine in both water distribution and stormwater networks.

Chapter 3 describes the analytical framework of stormwater modeling including the runoff, pipe flow and water quality computations. In addition, the chapter addresses details of stormwater modeling efforts including the selection of study areas, data collection, selection of efficiency measures, model sensitivity analysis, calibration and validation of the stormwater models.

Chapter 4 introduces the Variable Decay Coefficient Simulator (VDCS) that integrates results of the model described from Chapter 3 in order to simulate the dissipation of chloramine considering the variability of its decay coefficients spatially and temporally. This chapter was submitted to the Journal of Hydrology, April 2019.

Chapter 5 presents the "4-stage-3-model" hazard assessment framework for stormwater quality and applies the framework to the study of chloramine pollution in a stormwater basin in Edmonton, Alberta. This chapter was submitted to the Journal of Cleaner Production, April 2019.

Chapter 6 provides a concluding overall summary of the thesis. It includes the research summary and principal conclusions of the study. It also sets recommendations for future studies on similar topics.

Bibliography and Appendices from all chapters are combined and presented after Chapter 6. Six appendices are included in the thesis. Appendix A comprises a description for all the data collected for this research, along with their source, format type and application. Appendix B sheds more light upon the definition of the stormwater model in MIKE URBAN. Appendix C provides a detailed model description, user guide, and code required to reproduce the VDCS model. Appendices D and E are the supporting material for Chapter 4 and Chapter 5, respectively. Finally, Appendix F lists a group of associated literature on chloramine dissipation in stormwater networks.

CHAPTER 2

LITERATURE REVIEW

This chapter aims to summarise the material found in the literature related to simulation of chloramine in stormwater systems. First, the available simulation models of stormwater systems are reviewed, and their capabilities are analysed. Second, related published studies on water quality in the storm and combined sewers are presented. Finally, due to lack of enough research on chloramine dissipation in stormwater systems, a focused review on studies of chlorine or chloramine decay in water distribution and stormwater networks is conducted. An extended discussion of available decay models then follows, compiling alterations and modifications of chloramine models over the years.

2.1 Available stormwater models

With advances in computer technologies, complex stormwater quality and quantity models capable of simulating stormwater processes started to be developed in the early 1970s (Butler and Davies, 2011). The following decades have witnessed the development of a large number of such models and more are being developed continuously. Today, there are literally hundreds of models available for urban stormwater modeling with varying capabilities and applications (Zoppou, 2001).

Many factors differentiate these models from one another. First, there are two main uses for such models: design of new systems and simulation of existing systems (Elliott and Trowsdale, 2007). Design models determine the physical details of different components of a proposed drainage system, while simulation models test system responses to particular conditions, including surface flooding and water quality (Butler and Davies, 2011). In addition, depending on the type of model inputs, models can be either deterministic or stochastic, and both may be further subdivided into conceptual or empirical (Devi et al., 2015). Stormwater models can be further distinguished according to temporal resolution. Event-based models are used for simulation during and after individual storm events, especially ones that may cause flooding and transport large amounts of sediment, while continuous models are usually used for studying the effects of hydrological

changes and management practices over longer terms like months or seasons (Borah et al., 2006). In terms of spatial variability, a model is described as distributed when it acknowledges spatial variability, or lumped when it does not (Zoppou, 1999). For quantity computations, models apply different methods for representation of runoff generation, routing to and within the drainage network, and estimating infiltration and groundwater movement (Obropta and Kardos, 2007). Further, in water quality simulations, the types of contaminants included in each model and methods used in generation and transport of contamination also vary considerably (Elliott and Trowsdale, 2007). There are many published reviews for these models with helpful comparisons for application and capability such as Borah et al. (2019, 2009), Borah and Bera (2004a), Elliott and Trowsdale (2007), Gironas et al. (2009), Haris et al. (2016), Jayasooriya and Ng (2014), Mitchell et al. (2007), Obropta and Kardos (2007), Rubinato et al. (2013) and Zoppou (2001). Table 2.1 compares some popular stormwater models.

Table 2.1 Characteristics of some available stormwater packages

Model, developer, first release year	Access		Function			Time scale		Spatial scale		Routing level			Pollution transport			
	Public Domain	Commercial	Planning	Operational	Design	Continuous	Event	Lumped	Distributed	Simple Storage	Hydrological	Hydraulic	Advective	Completely mixed	First order decay	Plug flow
DRAINS, Watercom Pty Ltd, 1998		■	■	■	■	■	■			■	■	■				
HEC-HMS, Hydrologic Engineering Center, 1992		■		■		■	■		■			■	■			
HSPF, US EPA, 1980	■		■		■	■	■		■	■	■			■		■
Infoworks ICM SE, Innovyze, 1990s		■		■	■	■	■	■	■	■	■	■	■	■	■	
MIKE-SWMM, DHI, 1990s		■	■	■	■	■	■		■	■	■	■	■	■	■	■
MIKE URBAN (MOUSE), DHI, 2008		■	■	■	■	■	■		■	■	■	■	■	■	■	
MOUSE, DHI, 1985	■			■	■	■	■		■	■	■	■	■		■	
MUSIC, Monash University, 2000		■		■	■	■	■		■	■	■			■	■	
QQS, (Geiger and Dorsch, 1980)	■		■		■	■	■		■	■	■	■			■	■
RUNQUAL, Cornell University, 1999	■		■	■			■	■		■					■	
SLAMM, USGS, 1970s		■	■	■			■	■		■					■	
STORM, US Army Corps of Engineers, 1977	■		■				■		■	■				■		
SWAT, USDA, 1986	■		■	■		■			■	■	■					
SWMM, USEPA, 1971	■		■	■	■	■	■		■	■[1]	■	■[2]		■	■	■
UVQ, Monash University, 2000	■			■		■			■	■					■	
WBM, Greater Vancouver Regional District, 2004		■[5]	■	■	■		■	■		■					■	
Wallingford 3, Hydraulic Research Institute, 1978		■	■	■	■	■	■		■	■	■	■	■[4]		■	

[1] Flow balance only, [2] with EXTRAN module, [3] Including WASSP, MOSQITO, and WALLRUS, [4] Advection only, [5] Free basic package.

2.2 Water quality simulations in stormwater systems

Many models have been used over the last two decades to study stormwater quality in urban water systems, including the transport mechanisms of a variety of pollutants such as total suspended solids, nitrogenous and phosphorus compounds, biochemical oxygen demand (BOD) or chemical oxygen demand (COD), total organic carbon (DOC), dissolved oxygen (DO), and heavy metals. However, modeling studies on chloramine dissipation within storm sewer networks are lacking.

Available stormwater models range from (1) loading models, like GWLF and PLOAD, that estimate sediment or chemicals loads from a watershed outlet into a receiving water body; (2) receiving water models, like WASP, AQUATOX, CE-QUAL-W2 and QUAL2K, that simulate water quality in a receiving water body based on contributing watershed loadings; and (3) watershed models, like HSPF, SWAT, STORM, Wallingford, SWMM, and DHI's MOUSE model, which combine the capacities of loading models with features of receiving water models (Borah et al., 2006; Zoppou, 2001). A variety of model reviews provide comparisons of their applications and capabilities; see for example Borah and Bera (2004b, 2003), Brabec et al. (2002), Duncan (1995), Elliott and Trowsdale (2007), Marsalek (1991), Obropta and Kardos (2007), Tsihrintzis and Hamid (1997a), Vaze and Chiew (2003), and Zoppou (2001). Table 2.2 lists a number of recent simulation studies for water quality parameters in stormwater systems.

Table 2.2 Review of some recent stormwater quality models

Author, year	Model	Water quality parameters								Sewer system	
		Suspended solids	Nitrogen	Phosphorus	COD/ BOD	DO (on site)	Organic matter	Turbidity	Heavy metals	Stormwater	Combined
Artina et al. (2007)	Mouse/Wallingford	■								■	
Becouze-Lareure et al. (2019)			■				■		■	■	■
Dembélé et al. (2011)		■								■	■
Fraga et al. (2016)	MEDUSA	■							■	■	
Gamerith et al. (2009)	SMUSI 5.0				■					■	■
Goonetilleke et al. (2005)		■	■	■		■	■			■	
Heineman et al. (2013)	SWMM	■	■	■	■				■	■	
Hussein et al. (2015)	SWMM	■			■					■	
Lee et al. (2009)	SWMM	■	■	■	■						■
Lee et al. (2010)	SWMM/HSPF	■	■	■	■					■	
Mannina and Viviani (2010)		■			■					■	
Maruéjouls et al. (2014)		■			■					■	■
May and Sivakumar (2009)		■	■	■	■				Pb	■	
Metadier and Bertrand-Krajewski (2012)		■			■			■		■	■
Miguntanna et al. (2010)		■	■	■			■				
Rossi et al. (2013)	REBEKA II	■									■
Shon et al. (2012)	SWMM	■	■	■	■	■				■	
Shorshani et al. (2014)	SWMM	■							■	■	■
Shrestha and He (2017)	SWMM	■								■	
Temprano et al. (2006)	SWMM	■	■	■	■						■
Tsihrintzis and Hamid (1997b)		■	■		■				Pb	■	
Tsihrintzis and Hamid (1998)	SWMM	■	■	■	■				Pb	■	
Zhang et al. (2012)		■	■	■	■					■	

Several factors affect the generation and transport of pollutants in urban stormwater systems. Regarding the generation of pollutants, urban sprawl and land-use type are major factors contributing to changes in generated pollutants (Bian et al., 2011), increasing concentrations of chemical contaminants produced by human activities which differ significantly from the naturally-produced chemicals in any catchment (House et al., 1993). Other group of factors control the transport of pollutants to receiving waters. One are the characteristics of the surface identified by the surface type, material composition, surface slope, local losses, exposure and spatial location, and imperviousness degree (Gobel et al., 2007). Second are the rainfall characteristics, because pollutants detach from surfaces as a result of rainfall impact and then may be transported by excess surface runoff (Bian et al., 2011). Rainfall intensity, duration and volume considerably influence pollutant concentrations and loads (Brezonik and Stadelmann, 2002). Finally, third are the characteristics of the sewer system identified by the following interrelated components: physical properties of the system's static elements, hydrodynamic properties, environmental conditions, and biological, chemical and physical processes in sewer system (Kowalska et al., 2013).

In conclusion, practical use of physically-based water quality models is limited due to the complexity of processes, the change in governing mechanisms among different pollutants and the source of the pollutant (He et al., 2011; Obropta and Kardos, 2007). The generation and transport of pollutants in urban drainage systems depends on a group of combined factors that do not lend themselves to a simple mathematical model, and oversimplification of modeling assumptions and approaches can lead to gross errors in model predictions (Goonetilleke et al., 2005). Hence, a special investigation of chloramine dissipation characteristics is needed to build an accurate simulation tool, as discussed in the next section.

2.3 Chlorine/Chloramine dissipation models for water networks

Comprehensive studies on chloramine dissipation in storm sewer networks are lacking in the literature (Zhang et al., 2018c). At the time our research team started the current research, the decay of chloramine/chlorine in stormwater systems had not well-studied previously. To date, our research team's work is the only work published on the topic; in Gaafar et al. (under review) and Zhang et al. (2018b, 2018c, 2018a). Since there no enough research on the dissipation of chlorine

and/or chloramine in stormwater networks, this review includes some important published work on the dissipation of such compounds in water distribution systems (WDS), as well.

In WDS, chlorine (Cl) has been used to reduce numbers of microorganisms in drinking water (WHO, 2004), despite being relatively chemically-unstable and highly-reactive with a variety of inorganic and organic substances, which cause its gradual dissipation within the supply system (Ahn et al., 2012). Maintaining an effective residual Cl concentration from the system entry to its farthest end is important to prevent waterborne diseases (Fisher et al., 2012). Still, excessive concentrations may leave unpleasant tastes and odours, and increase the potential of producing by-products, some of which are suspected carcinogens (Al-omari et al., 2004). In large WDS, booster-dosing stations are used to keep uniform Cl residuals throughout the system by allowing lower entry concentrations while maintaining adequate downstream-end residual (VanBriesen et al., 2011). Therefore, there is a real need for powerful modeling tools that can simulate Cl decay which, in spite of much effort, is still complex as it depends on improvements both in hydraulic and Cl decay kinetic models (Monteiro et al., 2014).

Cl decay starts immediately after the dose application, rapidly at first and then relatively slower after 4 to 5 hours. The oxidation of inorganic compounds is a rapid process while the substitution reactions with natural organic matter (NOM) are relatively slow; however, the overall decay rates in WDS depend on characteristics of the source water and the distribution system as well (Boccelli et al., 2003). Models that include both stages are known as two-reactant models (2R), and represent an approach first proposed by Kastl et al. (1999). The fast stage is typically modeled by zeroth-order or second-order decay models. As rapid decay is considered complete by the time water leaves the treatment plant (Boccelli et al., 2003), the main focus here is the slower decay in the water network which is generally modeled according to first-order kinetics (Ahn et al., 2012; Rossman et al., 1994; Savic et al., 2009), as:

$$\frac{dC}{dt} = -KC \tag{2.1}$$

where C is the chlorine concentration, K is the first-order decay constant and t is the time. This phase of *Cl* decay involves two distinct processes. As *Cl* travels in pipes, it reacts with chlorine-

consuming substances in the bulk fluid, and with the pipe's internal wall material and biofilms; these coefficients are known as the bulk decay (K_b) and wall decay (K_w) coefficients, respectively (Rossman et al., 1994), so that,

$$K = K_b + K_w \tag{2.2}$$

A number of studies have attempted to determine K_b and K_w and their associated processes, using laboratory experiments or field measurements with regression analysis; see for instance Ahn et al. (2012), Al-omari et al. (2004), Boccelli et al. (2003), Castro and Neves (2003), Clark et al. (1995), Fisher et al. (2011b), Hallam et al. (2002), Powell et al. (2000), and Vasconcelos et al. (1997). The K_b is usually described in terms of temperature, total organic carbon (TOC), transport time and initial *Cl* concentration and contaminant, while K_w is affected by pipe age, diameter, material, roughness, corrosion and biofilm. In some WDS models, the decay coefficient is simply calibrated to minimize the model error against field measurements (Ahn et al., 2012; Mostafa et al., 2013; VanBriesen et al., 2011).

However, the first-order model of Eq. 2.1 is not the only description available in this regard. Some other modified versions of the first-order decay model were examined, e.g. parallel and limited first-order models, as listed in Table 2.3. Some of these models provided a better fit to available data sets, although not significantly or consistently better in most cases – see, for instance, Ahn et al. (2012), Helbling and VanBriesen (2009), and Vasconcelos et al. (1997). Other groups focused on a second-order decay kinetic model – see, for example, Clark (1998), Fisher et al. (2011b), and Islam et al. (1997). Typically, only small differences existed between first- and second-order models in terms of Cl decay. For instance, Boccelli et al. (2003) found second-order models generally equaled or bettered the performance of first-order models, while Kim et al. (2015) compared the performance of nine different chlorine decay models for a pilot scale water network and found that the first-order model outperformed all others under all studied conditions.

On one hand, as a water disinfectant, chloramine poses additional challenges for modeling compared with chlorine (Mutoti et al., 2007). During chloramination, ammonia is added to convert residual chlorine to chloramines (Connell, 1996). Chloramination produces different residuals in the WDS, including NH_2Cl, $NHCl_2$, and NCl_3, as well as organic chloramines (Milne et al., 1993). On the other hand, in stormwater systems, chloramine behaves differently compared to other

stormwater pollutants. Unlike many stormwater pollutants generated from deposition on different urban surfaces and accumulated over antecedent dry periods between rainfalls (Wei et al., 2019), chloramine does not exhibit build-up and wash-off characteristics. In either WDS or storm sewers, the reactivity between chloramines and the following physical factors and substances naturally found in water environments adds more challenges to studying chloramine dissipation (Crittenden et al., 2012; Zhang et al., 2018a).

The predominant chloramine residual, NH_2Cl, dissipates through auto-decomposition, bio-degradation and direct chemical reactivity with waterborne constituents (Sung et al., 2005; Zhang et al., 2018c). The auto-decomposition process allows formation of free ammonia added to excess ammonia from chloramine formation (Vikesland et al., 2001), and causes an increased availability of assimilable organic carbon that promotes growth of nitrifying bacteria in bulk water (Moradi et al., 2017; Sathasivan et al., 2009). Nitrification is a two-step microbiological process where ammonia is oxidized to nitrite by ammonia oxidizing bacteria (AOB), and then nitrite is oxidized to nitrate by nitrite oxidizing bacteria (NOB), which in turn consumes chloramine and accelerates its decay (Sathasivan et al., 2008). Moreover, sediments and biofilms have interchangeable effects (Adhikari et al., 2012). Sediments provide habitat to microbial growth, which enhances microbial activity and biofilm development (Herath et al., 2015; Sathasivan et al., 2009): the more sediments and biofilms in a water system, the faster chloramine decays (Adhikari et al., 2012). In contrast, higher pH (pH>8.5) reduces the activity of nitrifiers and, in turn, decelerates chloramine decay (Sarker and Sathasivan, 2012). Various other factors have been linked to NH_2Cl decay including bromide (Vikesland et al., 2001), temperature (Adhikari et al., 2012; Regan et al., 2002), cometabolism (Maestre et al., 2016), alkalinity (Zhang et al., 2017), corrosion (Clark et al., 2006), flow velocity (Westbrook and Digiano, 2009) and pipe materials (Mutoti et al., 2007). The presence of natural organic matter (NOM) significantly accelerates the NH_2Cl loss rate (Hrudey, 2009; Zhang et al., 2017). A study on chloramine dissipation in stormwater systems (Zhang et al., 2018c) has shown the NOM concentration to be the dominant factor in monochloramine dissipation in stormwater. They also found that, like in WDS, ammonium can decrease the decay rate because it promotes regeneration of NH_2Cl during its auto-decomposition, while reactivity with nitrite, organic components, and biofilm accelerates the decay process.

Table 2.3 Recent models of chlorine/chloramine decay in WDSs

Author, year	Kinetic modeling*								Chlorine	Chloramine	Focus	Model
	1st order decay	2nd order decay	Overall decay	Bulk decay	Wall decay	Mass transfer	2 Reactant model	Multiple-species				
Ahn et al. (2012)	■ AB C			■	■	■			■		Cl decay & Predicting DBPs	EPANET
Al-omari and Chaudhry (2001)	■		■						■		Inverse Cl modeling	Inv. Math. Model
Al-omari et al. (2004)	■			■	■	■					Modeling Cl residuals	WaterCAD
Blokker et al. (2014)	■		■					■	■		Residual Cl at WDS extremities	EPANET / EPANET-MSX
Castro and Neves (2003)	■			■		■			■		Modeling Cl decay	EPANET
Constans et al. (2003)	■		■						■		Simulating Cl decay	EPANET/Numerical model
Dukan et al. (1996)	■		■	■					■		Cl and bacterial growth in WDS	Piccolo
Fisher et al. (2011a)	■			■			■		■		Cl bulk decay models	2R-Model
Fisher et al. (2016)	■			■			■		■		Simulating Cl residuals in WDS	2RA / AQUASIM
Hamdy et al. (2014)	■		■						■		Free residual Cl	WaterCAD
Helbling and VanBriesen (2009)	■ AB CD	■	■					■	■		Microbial contamination effects	EPANET-MSX
Huang and Mcbean (2008)	■	■		■	■	■			■		Estimating Cl decay	EPANET
Islam et al. (1997)	■		■						■		Inverse Cl modeling	Inv. Math. Model
Kohpaei et al. (2011)	■	■ E	■					■	■		Second-order Cl Decay	EPANET-MSX
Monteiro et al. (2014)	■ C	■			■	■	■	■	■		Modeling Cl decay	EPANET / EPANET-MSX
Mostafa et al. (2013)	■			■	■	■			■		Simulating Cl decay	EPANET
Nagatani et al. (2006)	■			■	■ F				■		Simulating free residual Cl	MIKE URBAN/EPANET
Nejjari et al. (2014)	■	■					■		■		Modeling Cl decay	Piccolo / EPANET
Ozdemir and Ucak (2002)	■			■	■				■		2D simulation of Cl decay	EPANET / DYNAQ
Rossman et al. (1994)	■			■	■	■			■		Modeling Cl decay	EPANET
Tamminen et al. (2008)	■			■	■				■		Pipe material effects	EPANET
Vuţă and Pîrăianu (2008)	■			■	■				■		Simulating Cl residuals	Infoworks / EPANET

VanBriesen et al. (2011)	■			■	■				■		Cl residuals - Booster response	EPANET
Vasconcelos et al. (1997)	■ [AB C]		■	■	■	■			■		Cl decay kinetics	EPANET
Alexander and Boccelli (2010)	■		■				■			■	NH_2Cl decay in WDS	EPANET-MSX
Clark et al. (2006)	■			■	■	■			■	■	Decay in metallic pipes	EPANET /mass trans. model
Lee et al. (2003)	■		■							■	Combined chlorine variation	EPANET /mass trans. model
Maier et al. (2000)	■		■	■	■				■	■	Cl and NH_2Cl decay in WDS	EPANET
Shang et al. (2008)	■							■	■	■	Multiple species in WDS	EPANET-MSX
Zhang et al. (2017)	■					■				■	NH_2Cl decay	Kinetic model

*Some authors provided additional versions to model decay kinetics, as follows; [A] Limited first-order kinetics, [B] Parallel first-order kinetics, [C] n^{th} order decay kinetics, [D] Limited n^{th} order kinetics, [F] Parallel second-order, and [E] Zero-order.

There has been some effort on modeling chloramine decay in WDS. The EPANET-MSX (Multi-Species extension model (Shang et al., 2007) can simulate complex reactions in both bulk flow and at the pipe wall. Citing literatures, using EPANET-MSX, Shang et al. (2008) studied the auto-decomposition of NH_2Cl to ammonia in the presence of NOM and Alexander and Boccelli (2010) investigated the reactions take place in bulk fluid within chloraminated water system. Despite the complexity of its decay chemistry, chloramine decay is better represented as a first-order process than chlorine (Fisher et al., 2009). In general, NH_2Cl is considered to act like free chlorine but with slower dissipation (Lee et al., 2003). Maier et al. (2000) developed two different models to simulate chloramine decay using EPANET: a constant overall first-order decay coefficient and a bulk-wall coefficient. Their results were similar for cases with higher flow conditions, while the second model performed better in lower flows. Second-order equations have not yet been used in simulating chloramine decay. A review of previous studies on chlorine/chloramine dissipation in WDS is provided in Table 2.3.

Spatial and temporal variability within the stormwater system plays an important role in chloramine decay (Marsalek, 1991): spatially, with varying characteristics of stormwater effluents per land-use type and human activities (Zhang et al., 2018c), distribution of the decay-inducing parameters within the sewers (Potgieter et al., 2018) such as biofilms, and change in the properties of the sewer network itself (Savic et al., 2009), which produces varying velocities and

consequently travel times; and temporally, as a result of fluctuations in the pollutant mass fluxes over time (Clark, 1998), changes in the levels of the decay-affecting parameters such as temperature (VanBriesen et al., 2011), and the dynamic nature of pipe hydraulics (Westbrook and Digiano, 2009) and decay rates (Jonkergouw et al., 2009). In partcular, decay rates are known to decrease with time (Courtis et al., 2009), because chloraminated flows traveling in a pipe react with chloramine-consuming substances where present (Sathasivan et al., 2008), both in bulk water and in biofilms at the pipe wall (Hallam et al., 2002). These reactions slow over time as reactants are consumed (Kohpaei et al., 2011; Zhang et al., 2018b). To represent these temporal and spatial changes, chloramine decay in stormwater systems can be better modeled using varying decay coefficients than constant values (Kohpaei et al., 2011; Zhang et al., 2018b). Based on field sampling results, laboratory experiments (Zhang et al., 2018c, 2018a), and model development in COMSOL (Zhang et al., 2018b), the temporal variation of chloramine decay rates can be described with the following relationship,

$$K_{t,i} = \frac{1}{\alpha\, t + \beta} * (f_i) \tag{2.3}$$

where $K_{t,i}$ is the decay coefficient at time t for land-use i, f is a land-use dependent coefficient derived from the analytical chemistry COMSOL model using water quality characteristics, t is the discharge time in minutes, $\alpha = 1.73$, and $\beta = 1.0$.

In summary, Sections 2.2 and 2.3 showed that enough research on simulating chloramine dissipation in stormwater systems is lacking. The proposed research here is intended to address this gap and requires a powerful simulation tool to perform accurate water quality simulations for chloramine dissipation. Section 2.1 reviewed capabilities of the available stormwater models, and Table 2.1 showed that MIKE URBAN can simulate distributed rainfall-runoff and unsteady flow in pipe and channel networks, and contains one of the most comprehensive water quality modules. It promises a high ability to simulate pollution transport, dissipation and interaction between different water quality processes such as advection, dispersion, sediment transport and biological processes. MIKE URBAN was selected for the present study for its capabilities in serving the research objectives adequately, and because it is used by the CoE. A detailed discussion on the MIKE URBAN model in the next chapter.

CHAPTER 3

STORMWATER MODELING IN MIKE URAN

3.1 Analytical framework in MIKE URBAN

Drainage system simulations and computations are conducted in two distinct stages in many software packages (Butler and Davies, 2011), including MIKE URBAN. The first stage is the runoff computations, which simulate the hydrological surface processes and routing of surface flow in modeled catchment areas based on precipitation input and selected hydrological model parameters and processes (Borah et al., 2009). Where network simulations are included, catchment connections to the drainage network must be defined (DHI, 2017a). In the second stage, the network computations, the computed runoff from the previous stage is typically used as a hydraulic load to the collection system (Guan et al., 2015). MIKE URBAN can represent different sewer system components such as pipes, manholes, curb inlets, outfalls and structures including orifices, weirs and pumps. Finally, the model applies the selected routing model to simulate the hydrodynamics of the pipe flow (DHI, 2017a). These steps are shown in Fig. 3.1.

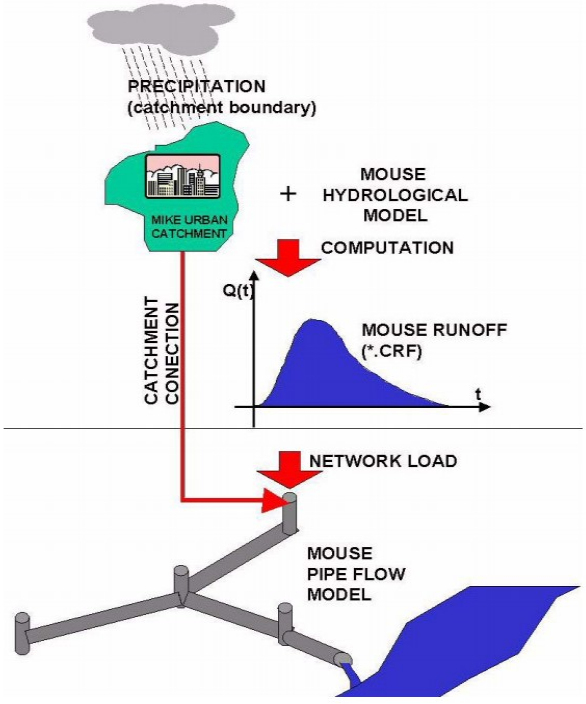

Fig. 3.1 Information flow of in hydrological modeling (DHI, 2017a)

3.2 Runoff computations

MIKE URBAN provides four different options for runoff computations. The selection of the appropriate runoff routing method is an essential step in modeling that may result in very different simulated runoffs (DHI, 2017b). Further, each method uses different sets of input data and model parameters, and applies different runoff computation concepts as well (Zoppou, 2001), making it critical to understand the assumptions and hence the limitations of the runoff model applied (Borah and Bera, 2004a). Some sets of the runoff model data are independent of the choice of the runoff model – for example, the basic catchment information such as size, geographical location and connection point to the drainage network (Overton and Meadows, 1976). In turn, each runoff method accounts for hydrological losses and ground surface properties differently, which requires different input parameters. Model-specific data requirements for each runoff method depend on the adopted runoff computations. For example, land-use types are accounted differently in each runoff technique, which necessitates specific input parameters (Butler and Davies, 2011). The available runoff methods in MIKE URBAN are the,

- Time-area method, which can be viewed as an extension and improvement of the rational method (Chow et al., 1988). The outlet discharge is the summation of flow contribution from subdivisions of the catchment defined by time contours, or isochrones, which are lines of equal travel times to the outlet where the discharge is required (Butler and Davies, 2011). A time–area diagram is constructed by summing the areas between the isochrones that define the hydrological response of a catchment (Karamouz et al., 2010), as illustrated in Fig. 3.2. When combined with rainfall in depth increments of I_N flow at any time, $Q(t)$ is:

$$Q(t) = \sum_{m=1}^{N} \frac{dA(j)}{dt} I_m \qquad (3.1)$$

where $dA(j)/dt$ is the slope of the time–area diagram at time j, and I_m is the rainfall depth in the mth of N blocks of duration dt. Water first flows from areas close to the outlet and thus the percentage of total contributing area increases progressively with time (Bedient and Huber, 2013). This simple method applies assumptions that (1) all catchment storage is neglected in all sub-

catchments by assuming that the outlet hydrograph results from pure translation of runoff through the watershed (Karamouz et al., 2010), (2) the runoff amount is only controlled by an assumed initial loss and size of the contributing area and by a continuous hydrological loss, and (3) the shape of the runoff hydrograph is only controlled by the time of concentration and by the time-area curve (DHI, 2017b). These two parameters represent a conceptual description of the catchment reaction speed and the catchment shape (Butler and Davies, 2011). These assumptions and the method representation in MIKE URBAN preclude proper modeling for different surfaces within the same catchment – for example, differences in the imperviousness ratio – and impose a simplified conceptual description of only homogenous basins with constant properties, which is not the case for most urban areas.

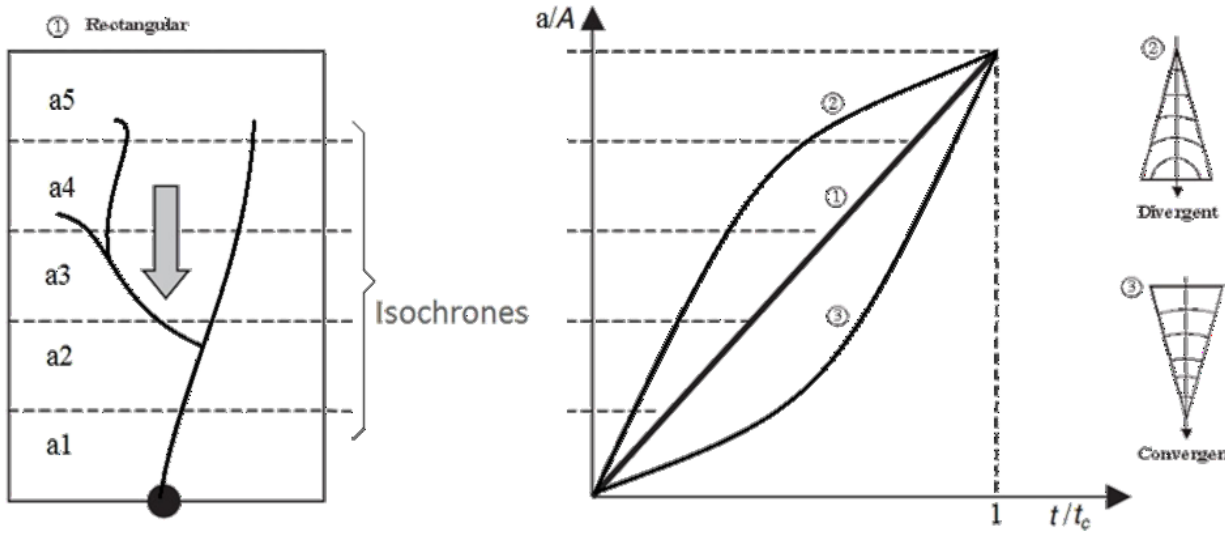

Fig. 3.2 Time-area method , modified from (Butler and Davies, 2011; DHI, 2017b)

MIKE URBAN provides three pre-defined types of time-area curves, namely, rectangular, divergent and convergent catchment, see Fig. 3.2, along with user-specified curve option for irregularly shaped catchments. In order to account for directly connected impervious areas, this model applies a hydrological reduction factor to reduce runoff from impervious surfaces of a catchment (DHI, 2017b).

- Unit hydrograph method (UH), which is defined as the direct runoff produced from a unit depth of rainfall excess falling uniformly over the basin (Butler and Davies, 2011). This approach

assumes that each basin has one UH that does not change in shape as long as the basin characteristics, e.g. drainage area, slope, etc., remain unchanged (Karamouz et al., 2010). Firstly, the UH should be derived in areas under consideration, then the concept of hydrograph convolution can be used to construct the catchment response to any rainfall event, as described by Butler and Davies (2011),

$$Q(t) = \sum_{i=1}^{N} U_j \, P_i \tag{3.2}$$

where $Q(t)$ is the runoff hydrograph ordinate at time t, U_j is the unit hydrograph ordinate at time j, P_i is the rainfall excess in the i^{th} of N blocks of a rainfall event, and $j = t - (i-1)$.

In MIKE URBAN, the UH module provides an alternative for areas where a unit hydrograph has already been established. As spatial variations of physical characteristics within the watershed are not represented – each catchment is considered as one unit and therefore the parameters represent average values for the catchment – it is classified as a lumped method (DHI, 2017b). Some inherent assumptions limit the applicability of the approach (Chow et al., 1988). Specifically, the UH (1) can only account for single storm events for any number of pre-defined catchments, (2) distributes excess rainfall uniformly spatially and temporally for all storms of equal duration, (3) produces hydrographs with equivalent time bases for rainfall excesses of equal duration, regardless of rain intensity, (4) holds the time distribution of direct runoff as independent of preceding precipitation, and (5) produces direct runoff values that are directly proportional to rainfall excess volumes for all hydrographs of a common base time (Bedient and Huber, 2013).

- The linear reservoir, which represents overland flow processes as one or more reservoirs connected in series (DHI, 2017b), where outputs from one reservoir are considered as inputs to the next one, is based on the two equations of storage and continuity:

$$Q(t) = C \, y(t) \tag{3.3}$$

$$\frac{\partial y}{\partial t} + \frac{1}{A} Q(t) = I_e \tag{3.4}$$

where $y(t)$ is the runoff depth at time t, I_e is the effective precipitation depth, A is the contributing catchment surface area, and C is a linear reservoir constant that can be determined from an

empirical equation as a function of the imperviousness ratio and the slope, length and area of the catchment; or alternatively can be used as a calibration parameter (Artina et al., 2007).

In this method, the reservoir is linear, by definition, as represented by the storage equation. This method enables surface runoff modeling with minimum data requirements (DHI, 2017a); however, the runoff routing is less detailed and depends only on one empirical constant that should be estimated via calibration (Butler and Davies, 2011). MIKE URBAN provides this method in two versions developed for two basins, one in France and one in the Netherlands. The representation of catchment-related properties purely as the routing of surface runoff with a single coefficient is unrealistic and may affect validation results.

- Kinematic wave method for overland flow, which is a more physically-based approach that solves a simplified version of the Saint-Venant Equations (Stephenson and Meadows, 1986), with surface runoff based on gravitational and friction forces (Borah et al., 2009). Further, the different hydrological losses and size of the contributing area determine the runoff volume, while the runoff hydrograph is shaped by catchment-related parameters including length, slope and surface roughness coefficients (Miller, 1984).

In MIKE URBAN, the kinematic wave runoff computations comprise two processes: runoff computations and runoff routing (DHI, 2017b). In the first step, the runoff computations, different hydrological losses are included in calculating the effective precipitation intensity, I_e, i.e., the net rainfall depth that contributes to surface runoff. In this process, the total precipitation intensity (I_P) is assumed to be uniformly distributed over each catchment. Then, portions of storm events are lost to wet the ground surface (I_{WL}), fill depressions (I_{SL}), and infiltrate soil (I_{IL}) – see Fig. 3.3. MIKE URBAN provides reference values to be used for assuming these losses on different surfaces, which is not the case in other software packages such as the Wallingford model that apply empirical equations to determine these losses (Mansell and Rollet, 2008). It is then through evaporation that depression storage is recovered and water in detention ponds is reduced (Gironas et al., 2009). In the water balances of urban areas, evaporation is typically neglected, since attention is usually paid to the runoff from short-duration or single rainfall events, which are insensitive to evaporation losses (Mansell and Rollet, 2008). Also, infiltration is assumed to start when the wetting loss of any surface is completed. The kinematic wave method applies the well-known

Horton infiltration model. In summary, hydrological simulation accounts for all those losses according to this equation:

$$I_e(t) = I_P(t) - I_{EL}(t) - I_{WL}(t) - I_{IL}(t) - I_{SL}(t) \quad (3.5)$$

where I_e is the effective precipitation intensity at time *t*, $I_P(t)$ is the total precipitation intensity, $I_{EL}(t)$ is the Evaporation loss, $I_{WL}(t)$ is the wetting loss, $I_{IL}(t)$ is the infiltration loss, $I_{SL}(t)$ is the surface storage loss (DHI, 2017b).

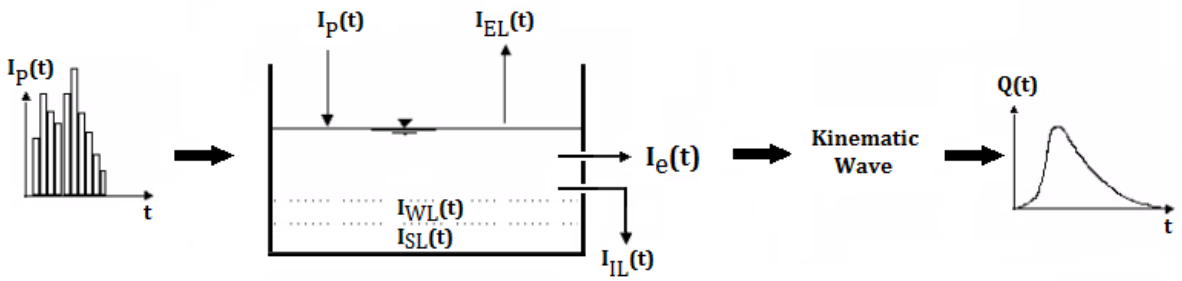

Fig. 3.3 The simulated processes in kinematic wave model, based on (DHI, 2017b)

The kinematic wave model can distinguish up to five different surface types so that the individual catchment area can be divided into up to five sub-catchments, with percentages of each area specified by the modeler. The input dialogue box of the kinematic wave runoff routing method is shown in Fig. 3.4. For each surface type, only the relevant loss types are applied. For example, infiltration losses are associated with pervious sub-catchments exclusively, while wetting losses are considered for all surfaces. At the end, the excess rainfall from a catchment is obtained as a sum of the fractional contribution of each sub-catchment.

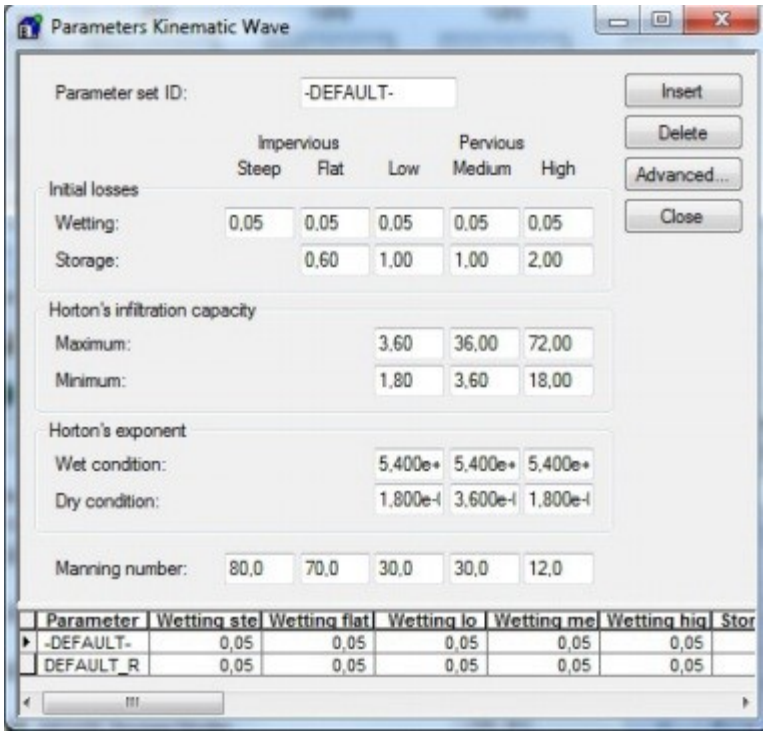

Fig. 3.4 The kinematic wave parameters editor in MIKE URBAN

In order to calculate surface runoff discharges, the one-dimensional Saint-Venant Equations are commonly used to model surface runoff and transient channel flow in many models, including HEC-RAS, SWMM5, MIKE 11, InfoWorks, MOUSE and MIKE SHE (Wong, 2009; Zoppou, 2001). It is a simplification of the shallow water equations that neglects the spatial and temporal variations in lateral and transverse directions, such that flow in a river or channel system can be represented as a unidimensional process along the longitudinal direction (Miller, 1984). Common applications of the 1-D Saint-Venant Equations include dam break analyses, storm pulses in an open channel, as well as storm runoff in overland flow (Kowalska et al., 2013). Based on the Navier-Stokes equations, a clear derivation of these equations is available in Henderson (1966). The full one-dimensional theoretical treatment leads to a pair of equations – the continuity and dynamic equations – that are usually referred to as the Saint-Venant Equations (Borah and Bera, 2003). The continuity equation is,

$$\frac{\partial Q}{\partial x} + \frac{\partial A}{\partial t} = 0 \tag{3.6}$$

and the dynamic equation is either in terms of velocity,

$$\frac{1}{g}\frac{\partial v}{\partial t} + \frac{\partial y}{\partial x} + \frac{v}{g}\frac{\partial v}{\partial x} + S_f = S_O \tag{3.7}$$

or in terms of discharge,

$$\frac{\partial Q}{\partial t} + \frac{\partial}{\partial x}\left(\alpha \frac{Q^2}{A}\right) + gA\frac{\partial y}{\partial x} - gA\left(S_O - S_f\right) = 0 \tag{3.8}$$

Where x is the longitudinal distance, Q is the flow rate, A is the area of the flow cross-section, t is time, y is the flow depth, v is the velocity, α is the velocity distribution coefficient, S_o is the average overland slope, and S_f is the friction slope. The Saint-Venant Equations are based on the following assumptions (Liggett, 1994; Overton and Meadows, 1976; Zoppou, 1999)**:** (1) water is incompressible and homogeneous, i.e. there is negligible variation in density, and the vertical pressure distribution is hydrostatic; (2) the sewer bed slope is small so that flow depth measured vertically is almost the same as that normal to the bed and so that the cosine of its angle may be replaced by unity; (3) wave lengths are large compared to water depth; (4) lateral flow is negligible, and for a channel cross-section, the velocity distribution is uniform and the water level is horizontal; (5) the boundary friction and turbulence losses estimated by steady flow equations are valid in unsteady flow; and (6) the flow is primarily sub-critical.

In addition, there are three different levels of flow description simplifications (dynamic, diffusion and kinematic), that are further discussed in Section 3.3 on pipe hydraulics. For surface runoff computations, the kinematic wave simplification is commonly applied. This is the greatest simplification, and assumes that the relation between Q and y can be described as steady uniform flow, which reduces Eq. 3.8 to,

$$S_O = S_f \tag{3.9}$$

Then, following an approach first proposed by Henderson and Wooding (1964) and Wooding (1965), hydraulic routing is applied to compute the overland flow based on the continuity equation and the kinematic wave formula with Manning's equation. The continuity and momentum equations for overland kinematic waves can be reduced to the following two equations (Zoppou, 2001). First, the continuity equation for a unit width is,

$$\frac{\partial q}{\partial x} + \frac{\partial y}{\partial t} = I_e \tag{3.10}$$

and with Eq. 3.9, a simplified form of Eq. 3.8 is,

$$q = a\, y^m \tag{3.11}$$

In these equations, y is the depth of overland flow, t is the time, x is the longitudinal distance, q is the overland flow per unit width, and a and m are the conveyance factor and a constant, respectively, both depending on the applied resistance equation. If Manning's equation is used, m = 5/3 and a = $S_o^{0.5}$/n , where n is the Manning roughness coefficient (Wong, 2009). Together, Eq. 3.10 and 3.11 form the kinematic wave equation for overland flow. Substituting for q in Eq. 3.10, q and y at any (x, t) can be obtained as,

$$\frac{\partial y}{\partial t} + a\, m\, y^{m-1} \frac{\partial y}{\partial x} = I_e \tag{3.12}$$

Eq. 3.12 has only one dependent variable in terms of x, t and I_e. Once solved, the discharge can be obtained from the momentum equation (Henderson, 1966). A schematic of the computations is shown in Fig. 3.3.

The Kinematic Wave module uses a relatively large number of parameters and allows for full spatial variation by applying local values of these parameters for individual catchments. However, for practical applications, MIKE URBAN applies a default set of parameters that enables running the entire model with a small amount of available data, as depicted in Fig. 3.4. It is then up to the modeler to define sufficient parameters, as needed, to represent the spatial variability adequately.

The kinematic wave module was chosen for the current study to ensure maximum accuracy. In order to assess the individual effect of each term in the dynamic equation, Eq. 3.7, sample values from previous studies are listed in Table 3.1 from which conclusions can be drawn about the relative weights of each term in the equation. Note that lower bed slope reduced the significance of the neglected terms by the kinematic wave, which favors its use in modeling drainage networks where most slopes are relatively low.

Table 3.1 Relative weight of the dynamic equation terms

Dynamic equation terms	S_O	$\partial y/\partial x$	$v/g \cdot \partial v/\partial x$	$1/g \cdot \partial v/\partial t$
Stephenson and Meadows (1986)	76.9%	7.7%	7.7%	7.7%
Henderson (1966), alluvial river flow	98.9%	0.2%	0.7%	0.2%
Miller (1984), gutter flow	90.3%	4.8%	2.4%	2.4%
Miller (1984), overland flow	91.5%	7.1%	0.7%	0.7%

3.3 Pipe flow computations

After calculating the surface runoff, the hydrodynamic calculations follow in order to route stormwater flows through the sewer system. The pipe flow computations in MIKE URBAN also apply the 1-D Saint-Venant Equations; however, additionally, all the three different levels of flow description approximations are available in the MIKE URBAN Pipe Flow Module, as follows:

- Kinematic wave, which assumes a balance between friction and gravity forces. The approach is valid when the changes in wave height over distance and velocity over distance and time are negligible; for instance, in shallow flows in steep pipes (Wong, 2009). In addition, the kinematic wave is independent of the downstream conditions, meaning that waves only propagate downstream and so the approach cannot simulate backwater effects (Novak et al., 2010).

- Diffusive wave, which includes the pressure, friction, and gravity terms in Eq. 3.8, but neglects the inertia terms, leading to the following simplified form:

$$\frac{\partial y}{\partial x} + S_f = S_o \tag{3.13}$$

The approach accounts for downstream boundary conditions and thus enables simulation of backwater profiles. With the assumption of negligible inertial acceleration, this approach is appropriate for slowly propagating waves where bed and wall resistance dominate (Borah and Bera, 2003).

- Dynamic wave, which is valid for all channel flow scenarios, as it uses the full one-dimensional Saint-Venant Equations including acceleration forces, which allows simulation of fast transients and backwater effects (Novak et al., 2010). The dynamic flow description should be used when

both inertial and pressure forces are important and backwater effects are not negligible (Miller, 1984). For instance, in cases with mild slope channels with downstream control. A Simple comparison of the three approximations is shown in Table 3.2.

Depending on the problem under consideration, the most appropriate and efficient description should be selected. In general, the dynamic wave is recommended in all cases except when either the diffusive or kinematic waves provides higher computational efficiency, in terms of computation time and/or when the ignored terms have an insignificant effect on model predictions (DHI, 2017b). In the current study, the dynamic wave description was adopted in all pipe flow simulations for two reasons: 1) the focus here was on single storm events, so that computational time was not a critical condition, and 2) some pipes have downstream control such as control structures or external water levels, which may cause backwater effects. In addition, the dynamic wave should be used when the change in inertia of the water body over time and space is important, which is the case with rapid changes in flows and water depths in the sewer system due to storm events with varying duration and intensity.

Table 3.2 Different simplifications of wave equations (Butler and Davies, 2011)

Accounts for	Kinematic wave	Diffusion wave	Dynamic wave
Wave translation	✓	✓	✓
Backwater	X	✓	✓
Wave attenuation	X	✓	✓
Flow acceleration	X	X	✓

3.4 Water quality computations

MIKE URBAN provides several modules for simulating water quality in stormwater systems for both catchment surfaces and pipe systems. These modules are called Surface Runoff Quality, Pipe Sediment Transport, Biological Processes, and Pipe Advection-Dispersion. Using these modules, many water quality problems can be simulated within MIKE-URBAN such as build-up and wash-off of sediment particles, transport of pollutants attached to sediment particles, transport of dissolved substances and suspended fine sediments in pipe flow, sediment erosion,

biofilms, water age, decay of BOD/COD in biofilm and water phases, re-aeration and bacterial fate (DHI, 2017a).

The main focus here is the Pipe Advection-Dispersion (AD) module that simulates the transport and dissipation of dissolved materials in the stormwater pipe-flow system (DHI, 2017c). This module can simulate conservative substances as well as non-conservative substances subject to a linear decay. A Pipe Advection-Dispersion simulation must be preceded by a hydrodynamic model simulation in order to provide the pipe flow discharges, water levels and cross-sectional flow areas that are used in the AD computations.

The transport of dissolved substances is typically described by the advection-dispersion equations (DHI, 2017c). The one-dimensional advection-dispersion equation used in MIKE-URBAN accounts for both advective and dispersive transport (DHI, 2017d), and is given as,

$$\frac{\partial(AC)}{\partial t} + \frac{\partial(QC)}{\partial x} - \frac{\partial}{\partial x}\left(AD\,\frac{\partial C}{\partial x}\right) = -A\,K\,C + C_S\,q \qquad (3.14)$$

where C is the concentration, A is the flow cross-sectional area, K is the linear decay coefficient, C_S the source/sink concentration, q is the lateral inflow, x is distance, t is time, and D is the dispersion coefficient, which is calculated as a function of the mean flow velocity as,

$$\mathrm{D} = \mathrm{a}\,\mathrm{u}^{\mathrm{b}} \qquad (3.15)$$

where u is the mean flow velocity, a is the dispersion factor, and b is a dimensionless exponent. Both a and b are user-specified constants.

The main assumptions of this module are (1) complete mixing over cross-sections, (2) transport of conservative substances or substances subject to first-order decay, and (3) proportionality of dispersive transport to concentration gradients of dissolved matter (Zoppou, 2001). Although dispersion includes several phenomena such as molecular diffusion, turbulent diffusion and the effect of a non-uniform velocity distribution over the cross-section, the first two processes are less significant than the third (DHI, 2017c).

The two main inputs to the AD module are a concentration time series at the system boundaries and data for defining the modeled substance, such as initial concentrations, dispersion coefficients and decay rates that allow non-conservative compounds to decay according to a first-order expression, as discussed earlier. The output of a water quality simulation is a set of longitudinal concentration profiles and pollutographs at points of interest, typically control structures or storm sewer outfalls.

3.5 The modeling process in MIKE URBAN

3.5.1 Selection of study locations

A field sampling program was designed to collect stormwater samples from four locations with different land-use types to understand chloramine dissipation better, and for model validation later. Thus, four Edmonton neighborhoods were selected to represent four major land-use types: (1) residential, as a reference for comparison with other land-uses; (2) parks and recreation, for their extensive green areas and correspondingly more-uniform irrigation and fertilizer use than residential areas; (3) commercial, with a focus on areas with a high density of automobile dealerships and rental businesses; and (4) industrial, with a focus on areas with pressure vessel fabricators. Each neighbourhood lies within one of two stormwater catchments, Kennedale in north Edmonton and 30th Avenue in south Edmonton, which were selected in consultation with City of Edmonton Drainage Services personnel because of their relatively long monitoring records and existing preliminary MIKE URBAN drainage models. The 30th Avenue stormwater basin is the main focus of this study to study chloramine decay; however, the Kennedale basin was used because a potential park could not be found in the 30th Avenue basin. The Kennedale and 30th Avenue catchment maps are shown in Fig. 3.5.

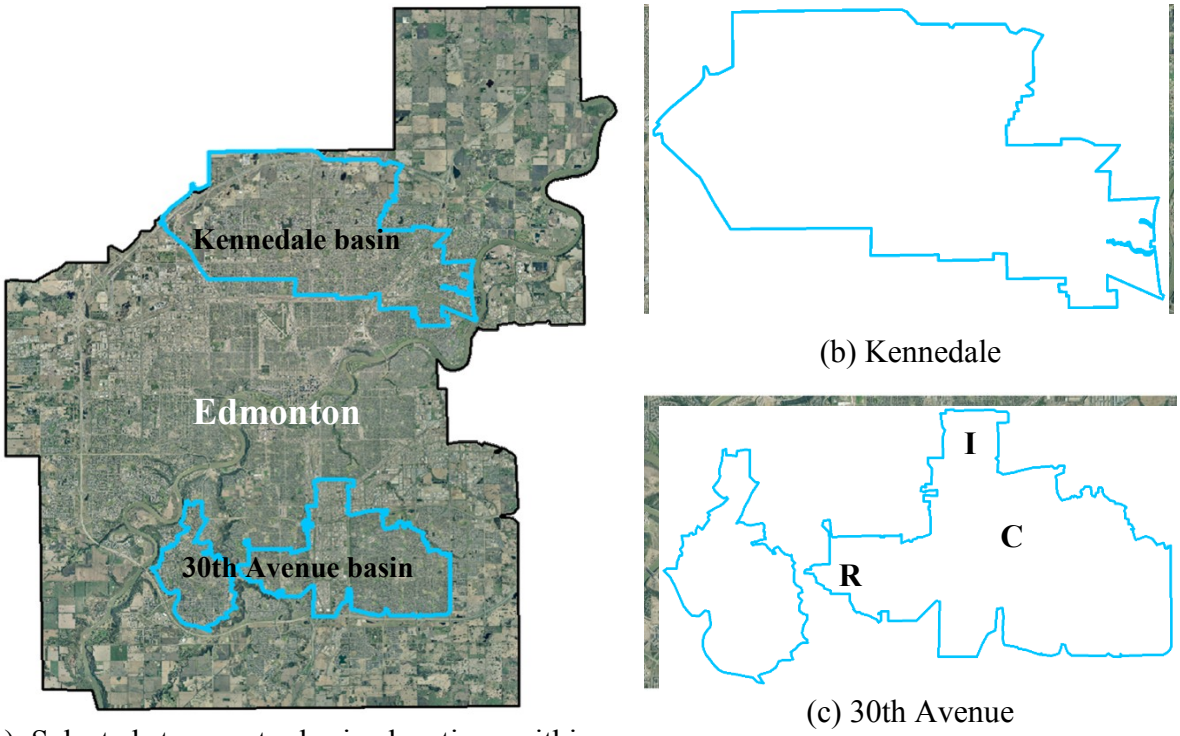

(a) Selected stormwater basins locations within the City of Edmonton boundaries

(b) Kennedale

(c) 30th Avenue

Fig. 3.5 Selected stormwater basins maps, labels for selected neighborhoods (R) residential, (P) parks, (I) industrial and (C) commercial

Within these two catchments, the four neighborhoods were then selected according to the following criteria and process of elimination. Stormwater drainage system characteristics of potential neighborhoods played a key role, particularly the location of the neighborhood within the pipe network, the presence of stormwater ponds upstream, availability of access points for water sampling, and existence of monitoring data for water quality and flow. Two of the criteria – the location of the neighborhood within the pipe network and availability of access points for sampling – produced conflicting requirements: 1) sampling near the sewer network's upstream-end would ensure that stormwater flows originated in the catchment under consideration, while sampling farther downstream would make it difficult to attribute pollutants to probable sources, but 2) sampling too near the upstream-end of the network might not provide sufficient sample volumes. In addition, for the observation of total active chlorine (TAC) dissipation, as described in Section

2.3, the presence of long, uninterrupted sections of pipe was important, since the absence of additional inflows at pipe junctions would permit attribution of changes in water quality to chemical and biological interactions within the pipe section, and give more time for such interactions to occur. Potential locations with mixed land- uses within or upstream of the neighborhood were excluded. Finally, several potential neighborhoods were eliminated because of logistical hurdles, such as traffic conditions, poor accessibility and sampling difficulty (e.g. manhole location and sewer depth).

Additional criteria were applied for specific land-use types, based on Marsalek (1991) and Zhang et al. (2018c). In selecting the residential location, low-density neighborhoods with relatively higher property values were favored because of their larger lawn and garden areas (cf. the Albuquerque, New Mexico, study conducted by Al-Kofahi et al., 2012), and were identified from CoE data and aerial photos, as shown in Fig. 3.6(a). Then, the property assessed-values were categorized into three sets based on the assessed value of each property: low <$300k), medium ($300k-$600k), and high (>$600k), as shown in Fig. 3.6(b). Application of the above criteria resulted in selection of the high property-value Blue Quill Estates neighborhood, shown in Fig. 3.7(a).

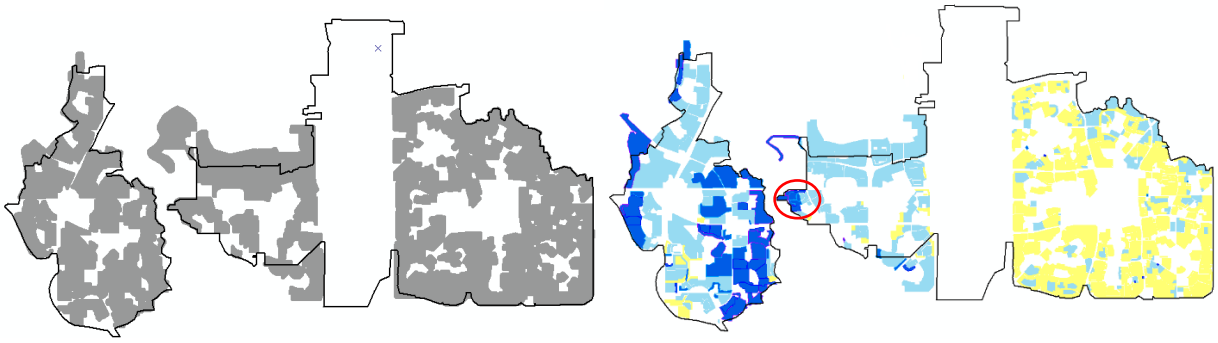

(a) Low-density residency (b) Property assessed value

Fig. 3.6 Selection of the residential study location

The M. E. Lazerte Park in the Kennedale catchment was selected among the irrigated parks of the two catchments, based on data availability for determining irrigation volumes, type of water used for irrigation (potable), and park location within the neighborhood and sewer pipe network, along with the aforementioned criteria. Its location is shown in Fig. 3.7(b). Note that this was the only

study location outside the 30th Avenue catchment, in the Kennedale stormwater catchment instead, since no suitable park within the 30th Avenue catchment was available.

For the commercial site, a cluster of approximately two dozen automobile-related service providers such as car rental agencies, car washers and dealerships was selected. The location selected – at 93rd Street near 34th Avenue – had the largest number of automotive services businesses and met the pipe network based criteria described above, see Fig. 3.7(c).

Last, for the industrial location, the pressure vessel industry is potentially a large point-source contributor of chloramine pollution. Pressure-vessel fabricators rely on large volumes of potable water for testing vessel integrity; this testing water is occasionally discharged to storm sewers rather than the sanitary system. Many pressure-vessel manufacturers were near the intersection of 97th Street and 45th Avenue in the 30th Avenue basin, as presented in Fig. 3.7(d). The selected locations along with their associated stormwater networks are shown in Fig. 3.7, and the average stormwater network properties are listed in Table 4.1.

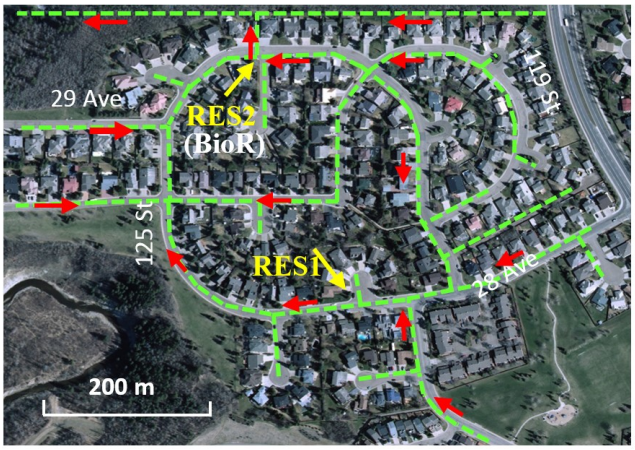

(a) Blue Quill Estates, residential

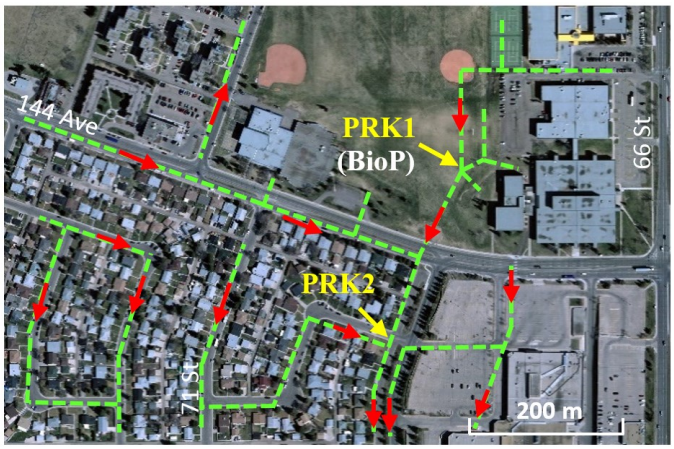

(b) M. E. Lazerte, park

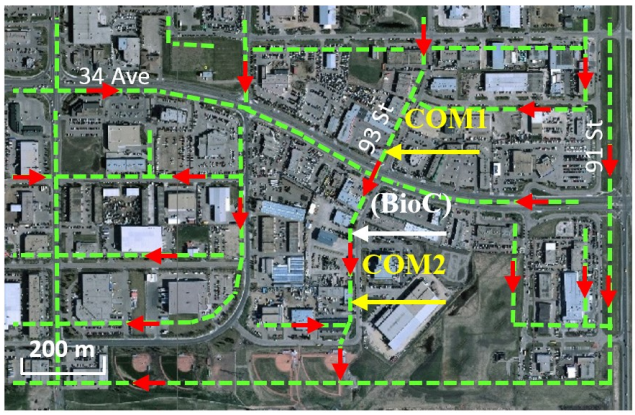

(c) Parsons Industrial, commercial

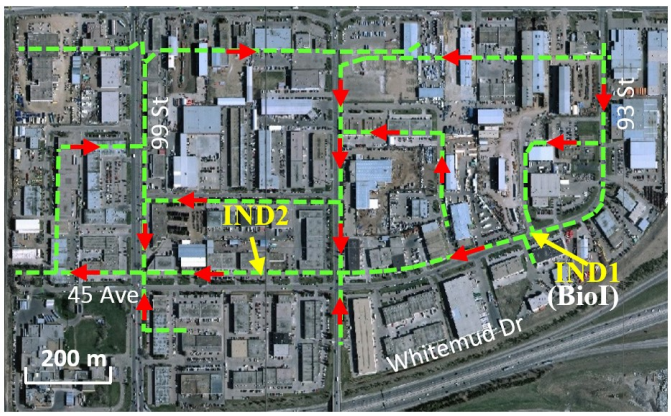

(d) Papaschase, industrial

Fig. 3.7 Aerial maps and storm sewer network for study sites
(red arrows represent flow directions)

Table 3.3 Average stormwater network properties of the study locations

Study site	Residential	Commercial	Industrial	Park
Material	Concrete	Concrete	Concrete	Concrete
Diameter (mm)	610	1050	750	375
Slope (%)	0.99	2.03	0.48	0.84
Length (m)	45	95	110	70
Drainage area, ha	34	104	148	27
Imperviousness	62%	90	65	51
BMP	No	No	No	No

3.5.2 Data collection

The City of Edmonton provided a variety of data sets that were used both to establish study site selection criteria and to select the sites themselves. The data included (1) GIS data, including aerial images, land-use maps, property assessment maps and digital elevation models (DEM) with spatial resolution of 1.5 m, and resolution of topography of 0.1 m; (2) attributes and layouts of the stormwater network components from the DRAINS database; (3) MIKE URBAN sewer system models built to the trunk level (which means that only the main drainage features – lines with diameters approximately larger than 800 mm – were included); and (4) data about the city's parklands, i.e. area, irrigation status and type of watering source. Online sources including Google

maps and telephone listings were used to find locations of pressure vessel manufacturers and commercial car dealerships in the two basins. Some of these data sets are shown in Fig. 3.8.

Field sampling was conducted every 2-3 weeks during the summers of 2015 and 2016 under both dry and wet weather conditions. Stormwater measurements included TAC concentrations, temperature, pH, conductivity, and dissolved oxygen (DO). The eight sampling locations are shown in Fig. 3.7. Also, microbial biofilm concentrations were measured for each land-use type at the following locations: BioR, BioP, BioC, and BioI in the sewer system, see Fig. 3.7. Then, laboratory analyses were conducted to estimate different physical, biological and chemical characteristics including DOC, COD, TSS, alkalinity, turbidity and biofilm genomic DNA. Most of these data sets were used to study chloramine decay mechanisms and determine decay coefficients of different land-use types. For more details on data acquired from stormwater samples and laboratory experiments, and their application, see Zhang et al. (2018c, 2018b).

In addition, the following data sets were collected for the case study locations: (1) temporary pipe flow monitoring values for the summer seasons of 2015 and 2016 at three locations, one for each of the commercial, industrial and parks land-uses, see Fig. 3.8 and 3.9; (2) long-term pipe flow records from other permanent metering stations; and finally (3) long-term rain gauge data for the two stormwater basins, as shown in Fig. 3.8.

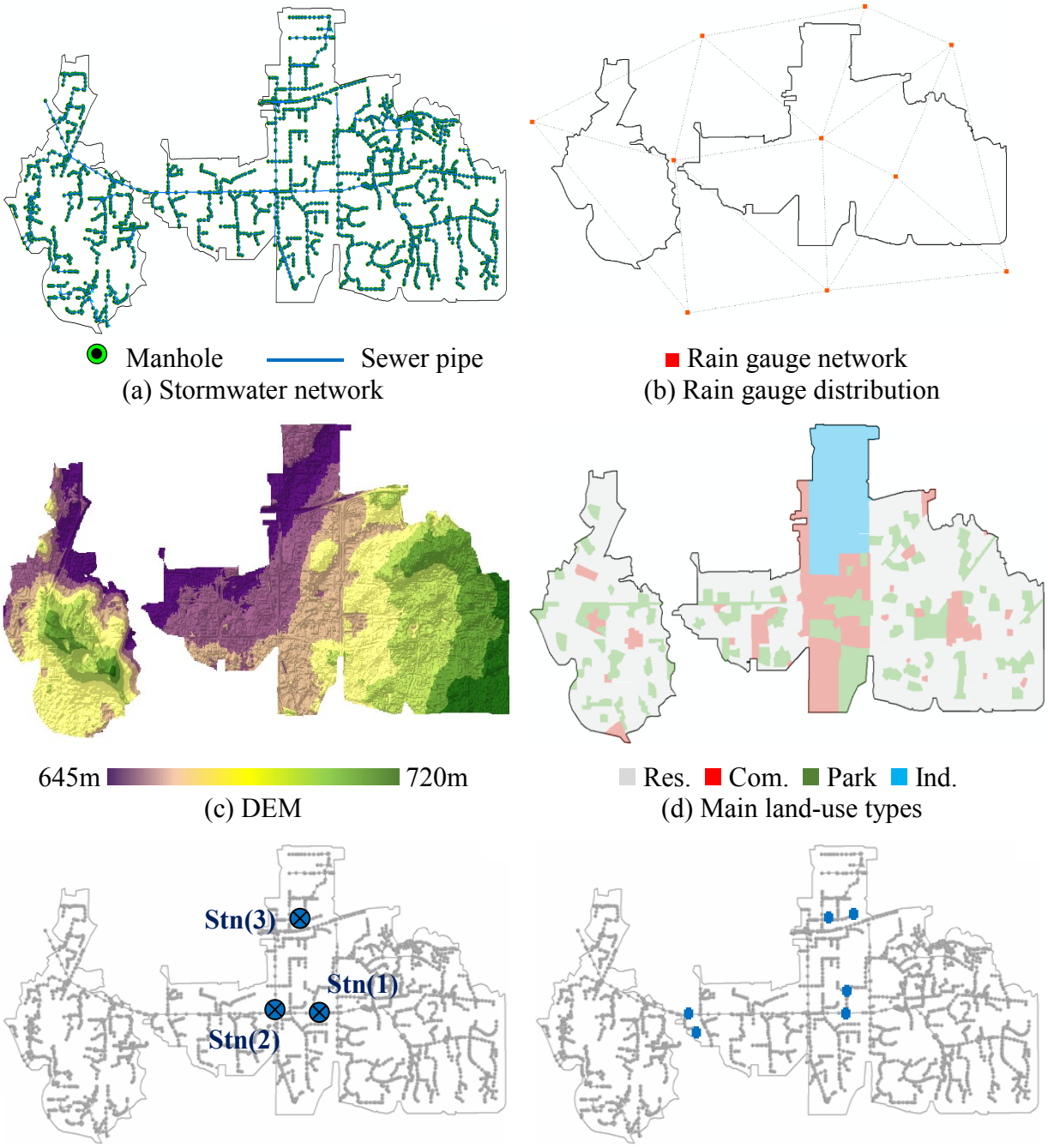

Fig. 3.8 Collected data for the 30th Avenue stormwater basin

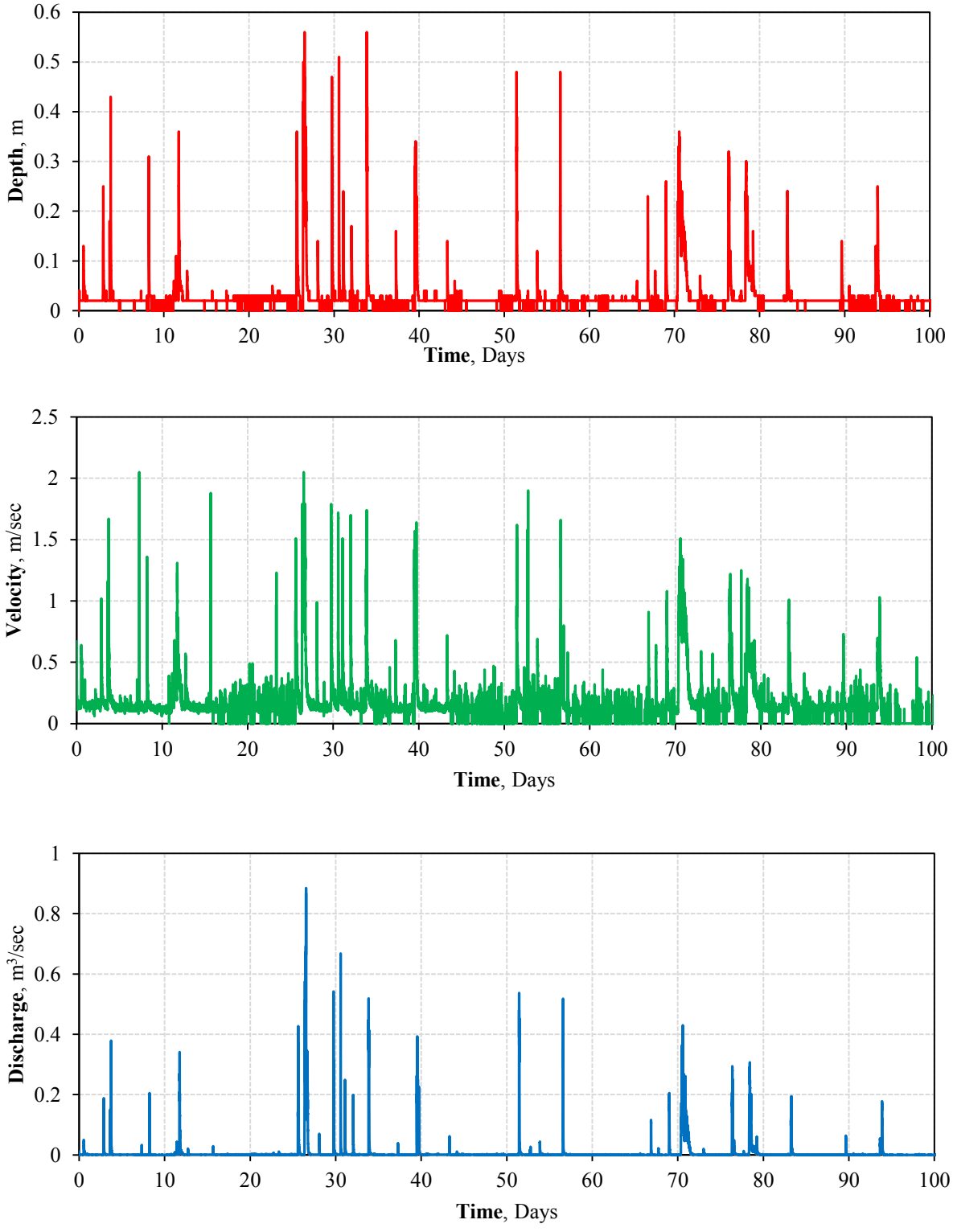

Fig. 3.9 Sample pipe flow data collected at a monotoring station, Stn(2)

3.5.3 Preliminary MIKE URBAN models

The City of Edmonton had built MIKE URBAN stormwater models for the 30th Avenue and Kennedale catchments to the trunk level. This level of detail was intended for the study of urban floods, but was not sufficient for water quality in sewers. Therefore, stormwater basin and sub-catchment delineations was conducted by standard geospatial analytical tools and GRASS GIS (GRASS, 2016), with data obtained from local administrators, using digital elevation model (DEM), land-use data records and stormwater network characteristics. Hence, the first goal was to improve the models by including all the real stormwater network components for the study locations.

Second, the catchment drainage models were uncalibrated, and so model inputs were based on assumptions that needed further investigation in some cases. Some parameters were set to a constant value for the entire model, such as catchment slopes. Thus, the model computed pipe flows that were significantly higher than the observed values, as shown in Fig. 3.10, with peak values about 2.5 times higher than the monitored values.

As model input, rainfall data collected by the City from a large group of rain gauges in and around the two stormwater basins were available, from approximately mid-June to mid-October, for most of the rain gauges. Fig. 3.8(b) shows the rain gauges for the 30th Avenue basin. Moreover, flow-metering records of flow depth, velocity and discharge were collected at three stations (COM2, IND2, and PRK2), see Fig. 3.7, for 2015 and 2016 from mid-May to the end of October.

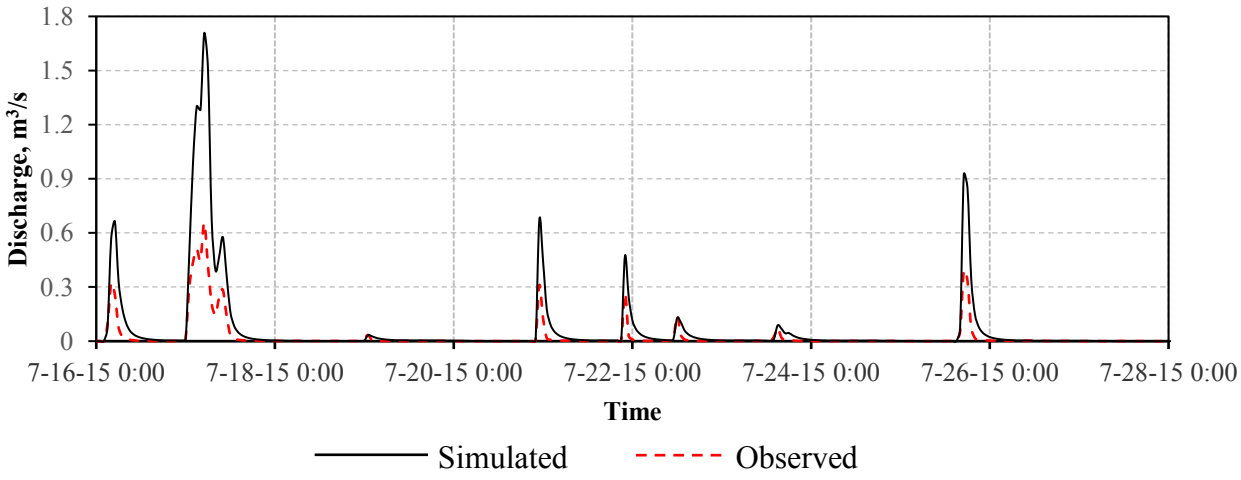

Fig. 3.10 Example of comparison between observed and simulated pipe flows

Improving the match between simulated and observed flows required, (1) selecting appropriate statistical measures to assess the model performance and improvements through model calibration, (2) analyzing the model sensitivity to specific parameter variations, (3) fine-tuning identified parameters, and (4) calibrating and validating the model results, as elaborated in the next sections.

3.6 Selecting the model efficiency assessment measures

Models are intended to reflect physical processes (McCuen et al., 2006). However, in order to trust model outputs, the model should be scientifically robust and defensible, and the criteria by which model performance is assessed should be discussed before starting model evaluation (US EPA, 2002). Models used for simulating hydrological processes typically require calibration prior to application, in which having reliable goodness-of-fit criteria, or efficiency assessment measures, is essential for the modeling process (Ritter and Munoz-Carpena, 2013). In theory, efficiency measures provide a mathematical evaluation of model's prediction accuracy compared to independently obtained observations (Ye et al., 1998). Although the coefficient of determination, R^2, is well defined and therefore its statistical significance is easily assessed (Legates and McCabe, 1999), it provides a biased view of the model performance (Kessler and Neas, 1994) and is oversensitive to extreme values (Willmott, 1981).

For a first assessment of the model performance, graphical techniques are essential (Moriasi et al., 2007). Indeed, it is recommended to evaluate models using graphical techniques along with other quantitative statistics (ASCE 1993; Legates & McCabe 1999; Moriasi et al. 2007). Firstly, visual inspection for hydrographs of predicted and observed flows throughout the modelled periods helps to identify model bias to over- or under-prediction (ASCE, 1993), as well as differences in timing, base and peak flows, rising and falling limbs, and runoff volumes (Krause and Boyle, 2005). This method can make it easier to identify potential outliers or to examine the homogeneity of model performance throughout the prediction period (Ritter and Munoz-Carpena, 2013). In addition, scatter plots are an important tool that may reveal definite conclusions about model performance (Jain and Sudheer, 2008). For example, in a scatter plot of observations against predictions, the degree to which the slope of the best-fit regression line is close to one and y-intercept is close to zero indicates how good the predictions are (Ritter and Munoz-Carpena, 2013).

Then, quantitative measures are applied to statistically evaluate model predictions. These can be divided into three main groups: (1) absolute criteria such as the widely used root mean square error (RMSE) and mean absolute error (MAE), (2) normalized criteria such as the index of agreement (IA) and percent bias (PBIAS), and (3) indicators modified for particular cases such as logarithmic and relative measures. Definitions and examples of these indices, including discussions on the limitations and suitability of each index, can be found in ASCE (1993), Legates and McCabe (1999), Krause and Boyle (2005), Moriasi et al. (2007), Reusser et al. (2009), Pushpalatha et al. (2012), Jain and Sudheer (2008), Ritter and Munoz-Carpena (2013), and Zambrano-Bigiarini (2015).

The choice of appropriate efficiency measures is critical as each measure allows different interpretations of the model predictions. These interpretations guide the calibration to emphasize different aspects of model output and thus dramatically affect the model predictions (Ye et al., 1998). Efficiency measure selection can be a challenge even for experienced hydrologists (Krause and Boyle, 2005), since each measure emphasizes different factors, including sample size, outliers and magnitude bias (McCuen et al., 2006). As emphasized by many authors, the hydrological community has struggled to identify the most appropriate statistical measures even in the relatively simple terms of the best measure of goodness-of-fit. The problem is magnified by a lack of agreement on the most suitable measure in each case for evaluating model accuracy (Gupta et al., 2009).

There is no best statistical efficiency criterion for hydrological models (Węglarczyk, 1998), and hence, studies have recommended and demonstrated the advantages of using multiple efficiency measures over a single one (Krause and Boyle, 2005; Pushpalatha et al., 2012; Yapo et al., 1998). The modeler should take into account the interdependency among measures (Węglarczyk, 1998), and suitability for the model's intended use (Janssen and Heuberger, 1995). Generally, at least one absolute measure and one normalized or relative measure should be selected to quantify the model's goodness-of-fit (Legates and McCabe, 1999; Pushpalatha et al., 2012). Therefore, in the current study, graphical techniques will be applied and the coefficient of determination (R^2) and bR^2 will be reported, but the calibration and validation will be driven by the following three efficiency measures**:**

- The Nash-Sutcliffe efficiency (NSE). Since it was first introduced by Nash and Sutcliffe (1970), the NSE has been widely used in hydrological modeling (Garrick et al., 1978; McCuen et al., 2006; Ritter and Munoz-Carpena, 2013; Wong and Koh, 2008) and received the most attention, modification and discussion (Gupta et al., 2009; Jain and Sudheer, 2008; Krause and Boyle, 2005; Legates and McCabe, 1999; McCuen et al., 2006; Moriasi et al., 2007; Oudin et al., 2006; Pushpalatha et al., 2012; Ye et al., 1998) of all efficiency measures. The NSE has three main advantages: (1) it was recommended by ASCE (1993); (2) its wide use provides an extensive record of reported values (Moriasi et al., 2007); and (3) it is flexible enough to be applied to a variety of model types (McCuen et al., 2006). The NSE is given by,

$$NSE = 1 - \frac{\sum_{i=1}^{N}(O_i - P_i)^2}{\sum_{i=1}^{N}(O_i - \bar{O})^2} \tag{3.16}$$

where O_i is the i^{th} observed value, P_i is the i^{th} predicted value, $\bar{O}$ is the mean of the observed values, and N is the total number of observations. The NSE ranges between $-\infty$ and 1.0, where 1.0 indicates a perfect fit, and values < 0.0 mean that $\bar{O}$ is a better predictor than the model and hence a poor agreement (Wilcox et al., 1990). Statistically speaking, R^2=0.8 and NSE=0.8 have different meanings, where the R^2 value shows that the model can predict 80% of the variance in the observed data, while the NSE indicates that the model mean squared error represents 20% of the observed variance (Ritter and Munoz-Carpena, 2013). There is currently no widely-accepted interpretation for NSE values between 0.0 and 1.0 (Ritter and Munoz-Carpena, 2013), since interpretation of different levels of performance depends on model type and purpose (Moriasi et al., 2007). A review of values from the literature can be found in Table 3.4.

- The root mean square error (RMSE). This well-established statistical index has been widely used in evaluating hydrological models, and is recommended to be reported for all models (Legates and McCabe, 1999). The RMSE is defined as,

$$RMSE = \sqrt{\frac{1}{N}\sum_{i=1}^{N}(O_i - P_i)^2} \tag{3.17}$$

It ranges between 0.0 and ∞, where 0.0 indicates a perfect fit. Also, due its absolute nature, it shows the actual size of model-produced errors in units of the constituent of interest (Willmott, 1981). Ritter and Munoz-Carpena (2013) provides criteria to which RMSE can be compared and on the basis of which it can be interpreted, see Table 3.4.

- Logarithmic NSE, ln(NSE). The NSE has been criticized over the years for emphasizing high flows and outliers over low flows (Pushpalatha et al., 2012). This occurs because the differences between the observed and predicted values are calculated as squared values (Legates and McCabe, 1999). Calibrations depending only on NSE tend to fit higher and peak flows at the expense of lower flows (Krause and Boyle, 2005). Therefore, many researchers have argued that NSE is unsuitable for low flows (Ye et al., 1998), and have instead suggested modified versions, including the modified NSE (Legates and McCabe, 1999), the logarithmic NSE (Krause and Boyle, 2005), the relative NSE, and the squared root transformation (Oudin et al., 2006). However, none of these measures have been sufficiently tested or used and reported values are lacking (Moriasi et al., 2007; Pushpalatha et al., 2012). In this work, owing to the need to obtain accurate low flows, the ln(NSE) is used as it is more affected by low flows, and it shows nearly no correlation with NSE (Krause and Boyle, 2005). It is defined as,

$$ln(NSE) = 1 - \frac{\sum_{i=1}^{N} | \ln O_i - \ln P_i|^2}{\sum_{i=1}^{N} \left| \ln O_i - \overline{\ln O} \right|^2} \tag{3.18}$$

with

$$\overline{\ln O} = \frac{1}{N} \sum_{i=1}^{N} \ln O_i \tag{3.19}$$

Table 3.4 Reported performance ratings and interpretations of NSE, RMSE and ln(NSE)

Reference	Criteria	Model	Value	Performance
Donigian et al. (1983)[A]	NSE	HSPF	> 0.80	Satisfactory
Ramanarayanan et al. (1997) [A]	NSE	APEX	> 0.40	Satisfactory
Gupta et al. (1999) [A]	NSE	SAC-SMA	< 0.70	Poor
Gupta et al. (1999) [A]	NSE	SAC-SMA	> 0.80	Efficient
Saleh et al. (2000) [A]	NSE	SWAT	> 0.65	Very good
Saleh et al. (2000) [A]	NSE	SWAT	0.54 to 0.65	Adequate
Santhi et al. (2001) [A]	NSE	SWAT	> 0.50	Satisfactory

Singh et al. (2004) [A]	NSE	SWAT and HSPF	> 0.65	Satisfactory
Porretta-Brandyk et al. (2011)	NSE	WetSpa	0.65 to 0.85	Very good
Porretta-Brandyk et al. (2011)	NSE	WetSpa	0.50 to 0.65	Good
Shamseldin (1997)	NSE	SLM and LPM	0.80 to 0.90	Satisfactory
Shamseldin (1997)	NSE	SLM and LPM	< 0.80	Unsatisfactory
Ritter and Munoz-Carpena (2013)	RMSE	Compared to the standard deviation (SD)	< 0.32 SD	Very good
Ritter and Munoz-Carpena (2013)	RMSE		0.32 SD to 0.46 SD	Good
Ritter and Munoz-Carpena (2013)	RMSE		0.46 SD to 0.59 SD	Acceptable
Ritter and Munoz-Carpena (2013)	RMSE		> 0.59 SD	Unsatisfactory
Porretta-Brandyk et al. (2011)	ln(NSE)	WetSpa	0.65 to 0.85	Very good
Porretta-Brandyk et al. (2011)	ln(NSE)	WetSpa	0.50 to 0.65	Good

[A] As provided by Moriasi et al. (2007)

3.7 Sensitivity analysis

Calibration efficiency improves when modelers concentrate on the parameters to which model outputs are most sensitive (US EPA, 2002). Therefore, calibration usually begins by evaluating the sensitivity of outputs to changes in model inputs or initial boundary conditions, and determining the accuracy needed in estimating model parameters, through an approach called sensitivity analysis (Zoppou, 2001). Sensitivity analysis is defined as the process applied to determine the relative change in model output corresponding to changes in model inputs or initial boundary conditions, and the accuracy needed in estimating model parameters (Moriasi et al., 2007).

In a simple, commonly applied technique, a sensitivity analysis proceeds by keeping all parameters constant, and perturbing parameter values one at a time so that the related variation in the fit between observations and model predictions can be examined (James, 2005). If large changes are found, the model is sensitive to that parameter, while parameters to which model results are not sensitive may not need to be accurately estimated, or could possibly be ignored during calibration (Overton and Meadows, 1976). Consequently, parameters can be ranked by sensitivity gradient of each parameter around its mean or expected value (Loucks and van Beek, 2017).

In this work, a sensitivity analysis identified critical parameters. The main categories investigated were imperviousness, catchment surface properties, infiltration indices, depression and initial

losses, and surface roughness, which are represented in MIKE URBAN by approximately 34 global parameters. In each case, the parameter under investigation was altered by a certain percentage (e.g., ±10%) and the corresponding changes in model outputs, represented by the selected efficiency measures discussed earlier in Section 3.6, were reported. The results showed that model performance was very sensitive to surface roughness, imperviousness and depression storage, while changes in catchment length and infiltration parameters were relatively ineffective, as shown in Fig. 3.11. These findings matched the results of previous studies, such as Brabec et al. (2002), Goonetilleke et al. (2005), Lee et al. (2009), and Tsihrintzis and Hamid (1998). Therefore, the next step was to adjust the identified parameters during model calibration and validation.

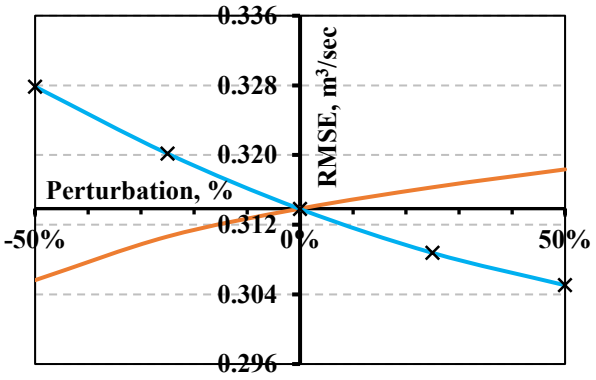

(a) Catchment properties

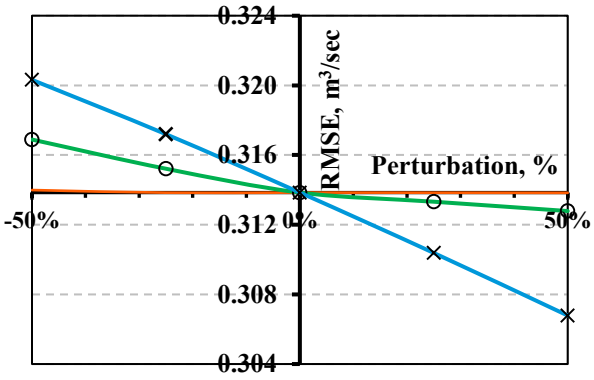

(b) Storage/Wetting losses

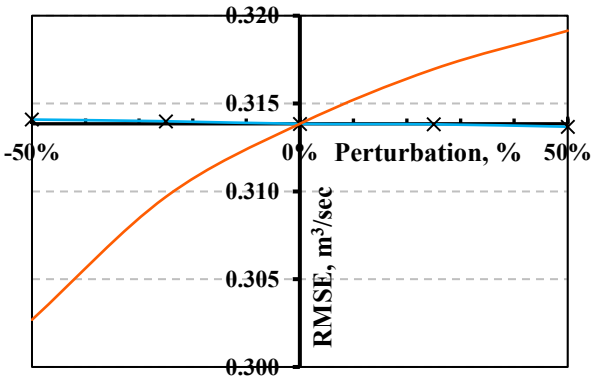

(c) Manning coefficient

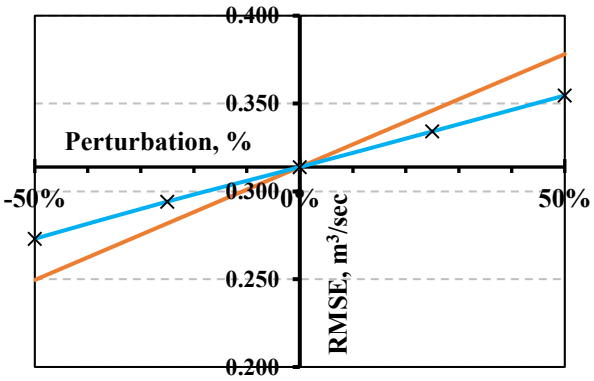

(d) Imperviousness ratio

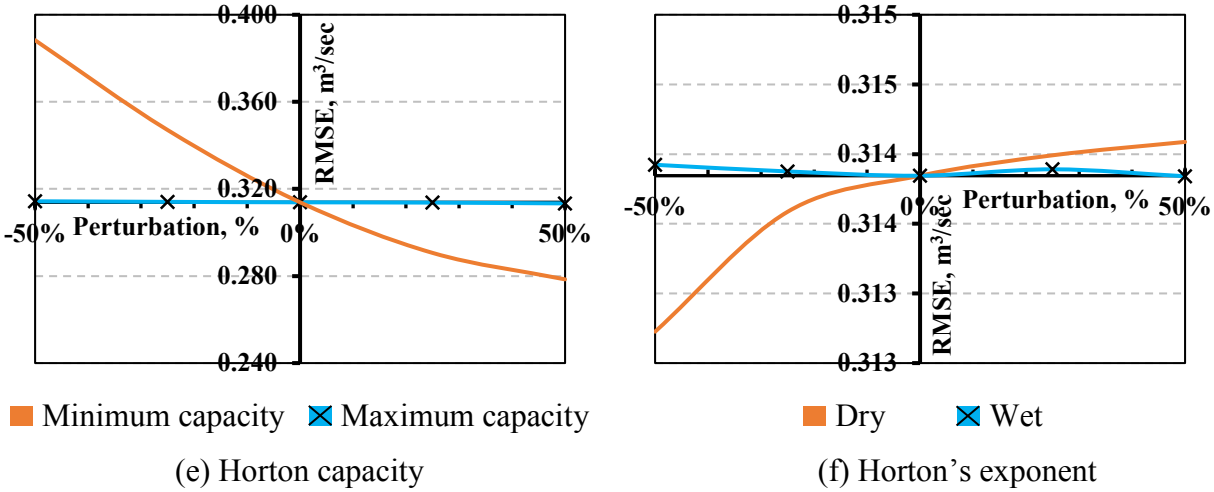

(e) Horton capacity (f) Horton's exponent

Fig. 3.11 Sensitivity analysis of the 30th Avenue stormwater model

Table 3.5 Results of Sensitivity analysis of the MIKE URBAN model

	Percentage change in average RMSE				
Perturbation %	**-50**	**-25**	**0**	**25**	**50**
Catchment slope	-2.62	-1.02	0	0.78	1.44
Catchment length	4.46	2.01	0	-1.62	-2.80
Wetting losses	0.05	0.00	0	0.00	0.00
Depression storage (Impervious)	0.97	0.44	0	-0.17	-0.34
Depression storage (Pervious)	2.06	1.07	0	-1.10	-2.25
Manning number (Impervious all)*	-3.56	-1.32	0	0.99	1.69
Manning number (Pervious)	-2.55	-1.04	0	0.76	1.33
Horton's max capacity	0.16	0.07	0	-0.04	-0.16
Horton's min capacity*	23.72	10.58	0	-7.40	-11.27
Imperviousness ratio (Impervious flat)*	-20.49	-10.23	0	10.25	20.48
Imperviousness ratio (Impervious steep)*	-13.01	-6.27	0	6.46	12.98

(*) Indicating relatively sensitive model variables

3.8 Model validation

The process of adjusting parameters in a model to cause its predictions to represent measured variables accurately is called calibration (James, 2005). Variables used for model calibration may be flow rates, depths or velocities. Since any model inherently incorporates simplifications to a

physical system, calibration is necessary for all hydrological models (Butler and Davies, 2011). Further, because simplifications entail errors in model predictions (Savic et al., 2009), adjustments of model parameters are necessary to reduce them and improve the goodness-of-fit between model predictions and physical observations (Gironas et al., 2009). With increasing improvements in software and hardware capabilities, the selection of appropriate values of the model parameters should be given more care so as to simulate rainfall-runoff models accurately (Loucks and van Beek, 2017).

3.8.1 Improving estimations of GIS-dependent parameters

GIS applications can improve the estimates of some model parameters. Here, the most sensitive parameters, as determined from the sensitivity analysis, include the percentage of impervious surfaces and catchment slopes.

Impervious surfaces include roadways, parking lots, driveways, sidewalks and roofs. The imperviousness ratio plays a key role in model performance in terms of runoff volumes and hydrograph shapes (Zoppou, 1999). Lee and Heaney (2003) found that when a directly connected impervious area represented 44% of the total catchment area, it contributed to 72% of the total surface runoff, since it transmits 100% of its runoff. Aerial images and land-use maps were used to prepare specific GIS-layers to identify the imperviousness ratio of each catchment. As an example, an aerial image of the commercial location is shown in Fig. 3.12 with superimposed layers representing different types of impervious surfaces. Roofs were also recognized as flat or inclined. These layers were then used to identify the imperviousness ratio of each catchment – see Fig. 3.13 – in which the upper chart shows the default surface percentages used in the CoE's model based on city zoning, while the lower charts display the GIS-based percentages of the seven sub-catchments contributing to runoff at this location. These values were used to improve the model's hydrological estimations.

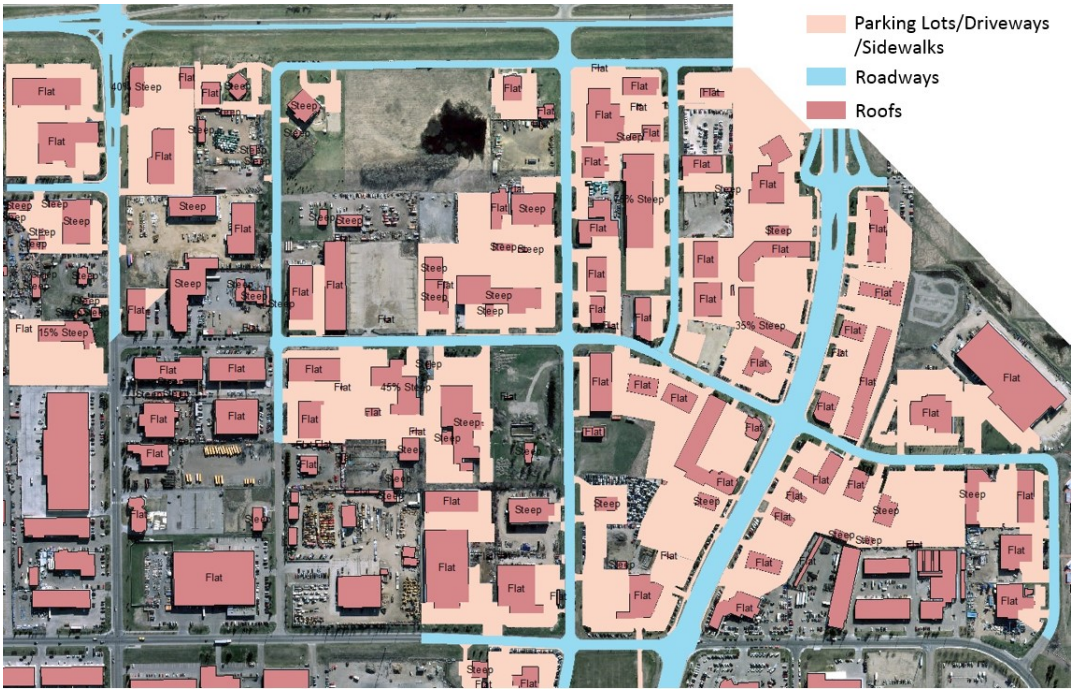

Fig. 3.12 Special GIS layers to improve imperviousness estimations

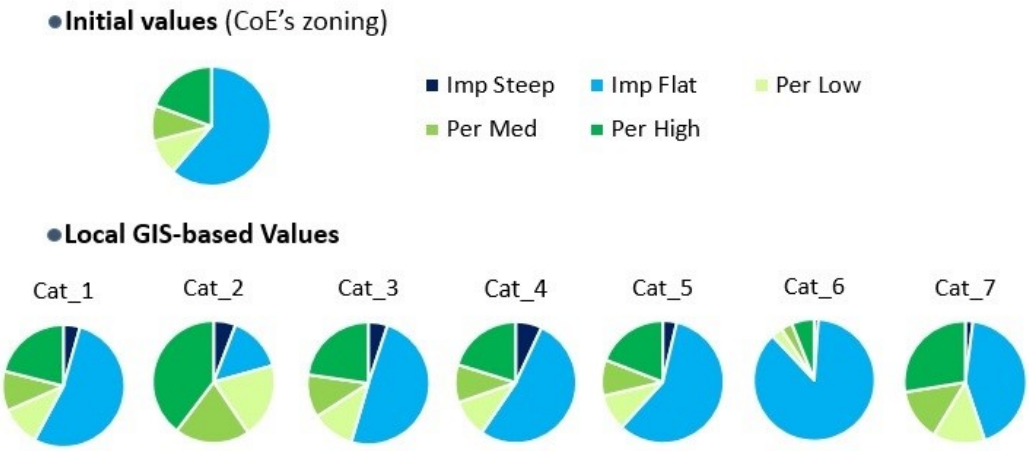

Fig. 3.13 Change in surface percentages among commercial sub-catchments

Further, the digital elevation map provided by the CoE in ArcGIS format permitted the calculation of actual slopes for each catchment. The outcome of this step, shown in Fig. 3.14, was used to improve the model's parameter values.

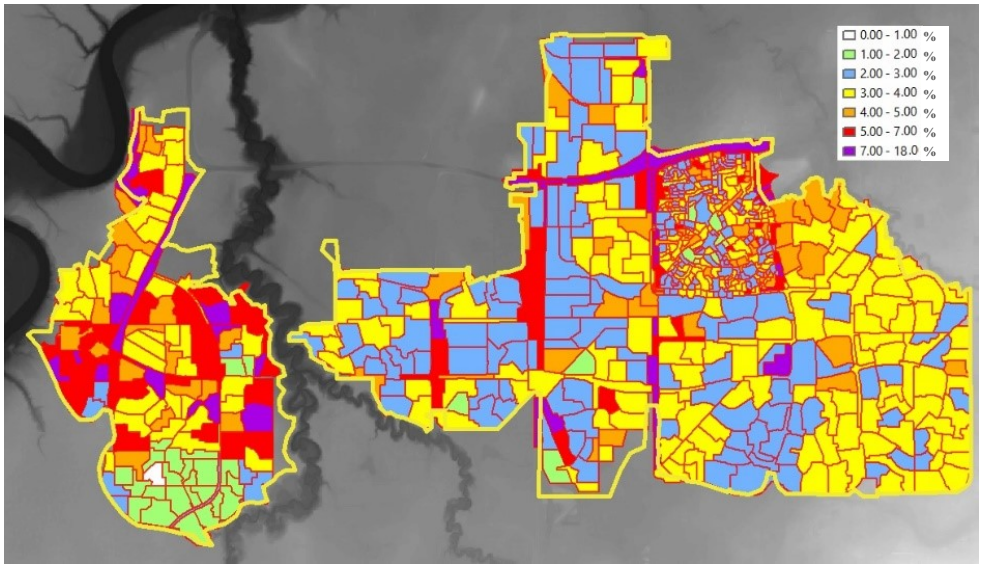

Fig. 3.14 Catchments slopes of the 30th Avenue stormwater basin

3.8.2 Calibration and validation results

The application of the kinematic wave runoff module requires a basic group of 34 parameters, neglecting spatial variability. The model was calibrated by adjusting the 34 parameters including the wetting losses, depression storage losses, maximum and minimum infiltration capacity, roughness coefficients and Horton's exponents for different type of ground surfaces. Appendix B shows the kinematic wave module global parameters after model calibration. In addition, model calibration also included introducing of GIS-estimated parameters to the MIKE URBAN stormwater model, such as catchment slope, length and percent imperviousness. Although these parameters are computed, it is common practice to adjust the computed values iteratively to enhance model performance (DHI, 2017b). For example, catchment length and slope are inherently approximations, even where they are measured. Moreover, GIS-based imperviousness values require reduction, because some fraction of these areas is not directly connected to the system, and thus their related runoff remains as surface or subsurface storage and does not contribute to hydrological loads (Lee and Heaney, 2003). Other calibration parameters that cannot be directly measured are usually adjusted to represent measured data. However, estimating these parameters individually for each catchment presents a challenge, and so global values are used as much as possible (DHI, 2017a). Finally, unmeasured parameters that are included in the model but do not

contribute significantly to calibration, as determined through the sensitivity analysis, were kept constant (wetting losses, for example).

Flows are the primary parameter used for calibration. The goal of calibration depends on the specific use of the model (Elliott and Trowsdale, 2007); in this case, this model must represent discharges, flow volumes and hydrograph shape accurately. In the present study, the calibration goals were adapted from a similar study , Carr et al. (2010), defined by a discharge correlation coefficient ($R^2 \geq 0.80$), a maximum volume difference ($\pm 15\%$), a total volume error ($\pm 10\%$), and a peak volume error ($\pm 10\%$). Additionally, the monitoring conducted by the CoE provided rainfall, flow, depth and velocity measurements at 5-min intervals.

The basis of the calibration was a data set from the CoE, which conducted monitoring of rainfall, flow, depth and velocity measurements at 5-min intervals over the summers of 2015 and 2016. Therefore, despite the fact that the model was run at smaller time steps (10 or 30 seconds), the model output was aggregated to 5-minute intervals to match the time step of the observed data. Shrestha and He (2017) used a total of 12 storm events to calibrate the runoff computations of their SWMM stormwater model, in which 8 events were used in calibration and the rest were used in model validation. Similarly, in the current work, for the summers of 2015 and 2016, a total of 21 independent storm events were identified along with their related observed pipe flows, with peak flows ranging from 0.12 to 0.63 m^3/sec, and flow durations of between 24 and 60 hours. Examples of some of the pre-calibration model sewer pipe hydrographs are shown in Fig. 3.15, and the related statistical measures are listed in Table 3.6(a).

These hydrographs were divided into two groups with similar hydrograph shapes, peaks and durations. Half of the data were used for model calibration and the other half were used for model validation. In the manual calibration, each efficiency assessment measure was tracked according to adjustments in model parameters in order to balance the model performance over the entire hydrograph while noting the produced errors compared to the observed data (Savic et al., 2009). In general, higher performance ratings should be pursued for the model calibration stage than for the validation stage (James, 2005), because parameter values are optimized during model calibration but are kept constant in validation, where ideally different conditions are encountered compared than for calibration (Moriasi et al., 2007).

Ultimately, the model performed well for the selected storms. The assessment measures and calibration goal statistics were within the acceptable criteria. In summary, the data correlation was good (R^2 = 0.95, NSE = 0.91, RMSE = 0.024 m^3/sec, maximum volume difference+11.3%, total volume error+8.8%, and peak volume error+9.8%). These results were considered very good compared to previous studies in the literature (Carr et al., 2010; Shrestha and He, 2017). For two storm events, storm C5 and V4, the model performance was relatively poor because of low peak flows for the C5 and V4 storms, and the predicted flows were highly affected by hydrological losses, which in turn affected all their statistical measures, see Fig. 3.16. These cases were retained to illustrate the limitations of the model. Table 3.6(b) summarizes the results of the post-calibration model and validation in addition to the calculated assessment measures for both.

A water quality model can provide reliable results only when flows are accurately represented (Savic et al., 2009); therefore, after calibration and validation, the model is now ready for the next step: water quality simulations.

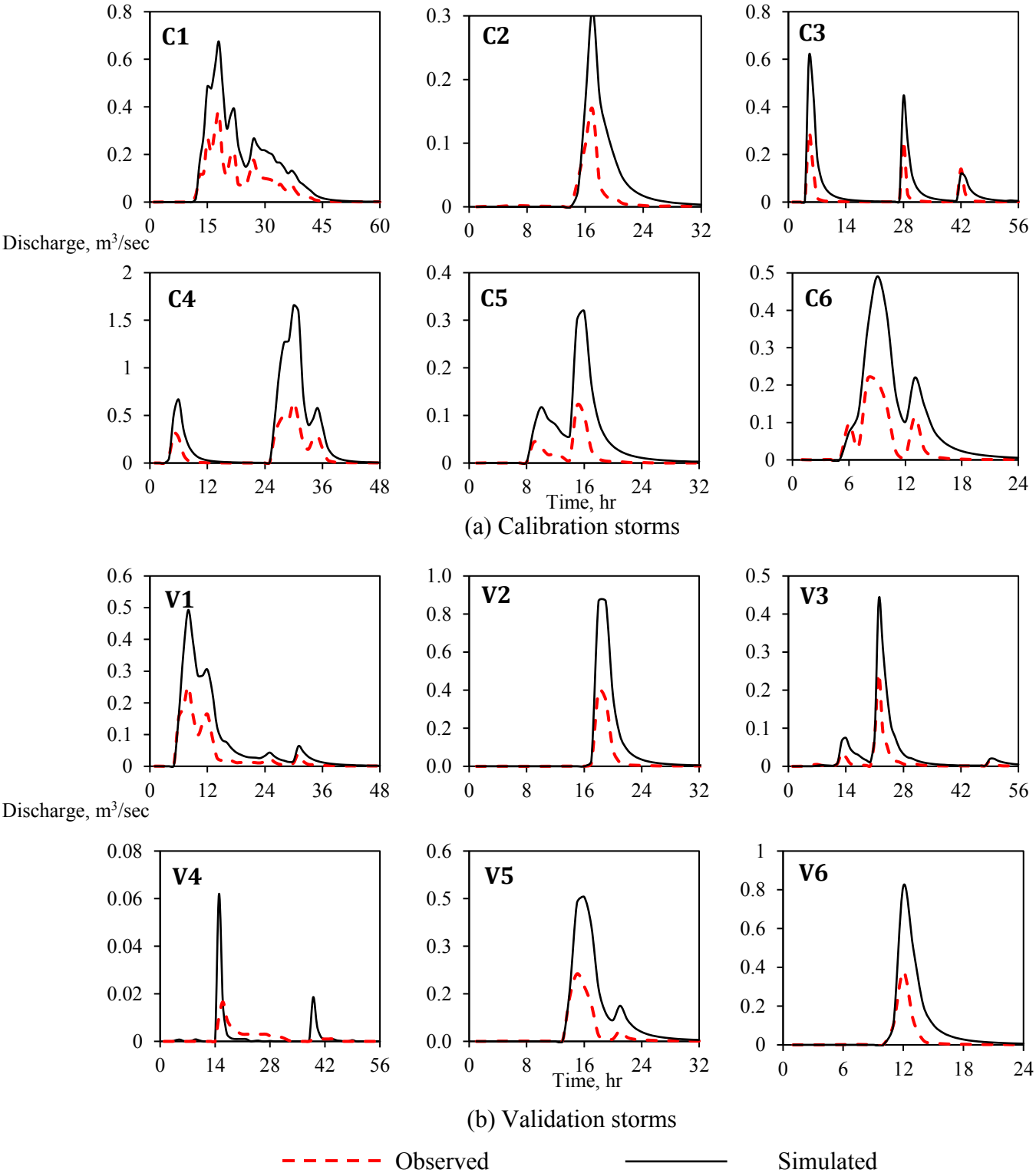

Fig. 3.15 A sample of pre-calibration model results for some storm events for Stn(1)

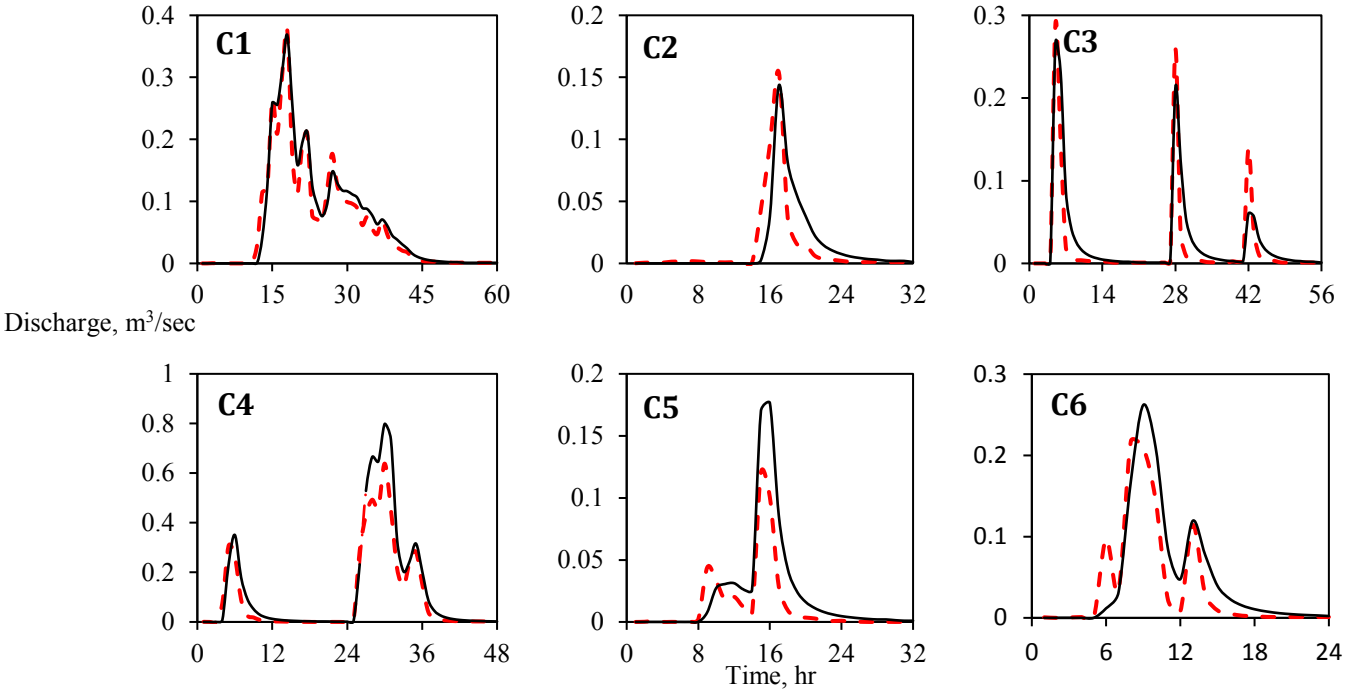

(a) Calibration storms

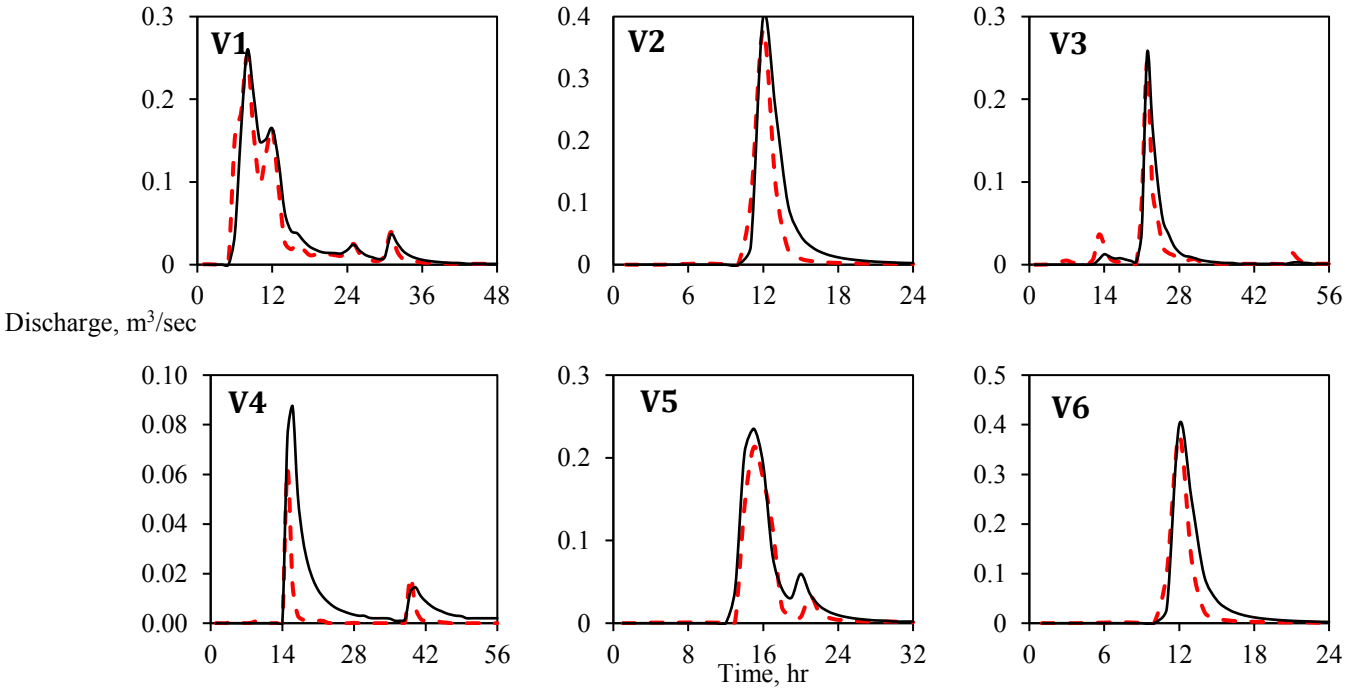

(b) Validation storms

Observed — Simulated

Fig. 3.16 A sample of post-calibration model results for some storm events for Stn(1)

Table 3.6 Efficency assessment measures for the sample group of storm events for Stn(1)

(a) Pre-calibration model stasistics

Storm	C1	C2	C3	C4	C5	C6	V1	V2	V3	V4	V5	V6	Average
Duration	60	32	56	48	32	24	48	24	56	56	32	48	
NSE	-0.621	-1.082	-1.070	-2.719	-4.485	-1.259	-0.620	-1.487	-0.786	-1.484	-1.551	-1.267	-1.536
RMSE	0.106	0.045	0.081	0.315	0.064	0.099	0.074	0.125	0.048	0.014	0.086	0.112	0.098
R^2	0.956	0.823	0.828	0.941	0.899	0.848	0.930	0.894	0.869	0.490	0.871	0.966	0.860
Slope (b)	0.500	0.426	0.429	0.371	0.331	0.447	0.480	0.404	0.447	0.364	0.408	0.409	0.418
Ln (NSE)	0.384	2.045	0.247	0.901	0.831	1.802	3.622	0.999	0.868	0.953	2.683	0.601	2.862
bR^2	0.478	0.351	0.355	0.349	0.297	0.379	0.446	0.361	0.388	0.178	0.356	0.395	0.361

(b) Post-calibration model stasistics

Storm	C1	C2	C3	C4	C5	C6	V1	V2	V3	V4	V5	V6	Average
Duration	60	32	56	48	32	24	48	24	56	56	32	48	
NSE	0.939	0.692	0.805	0.814	0.353	0.748	0.863	0.817	0.823	0.253	0.874	0.939	0.912
RMSE	0.021	0.017	0.025	0.071	0.022	0.033	0.022	0.034	0.015	0.008	0.019	0.021	0.022
R^2	0.949	0.704	0.826	0.953	0.865	0.803	0.876	0.878	0.883	0.299	0.925	0.949	0.961
Slope (b)	0.927	0.892	0.920	0.751	0.597	0.827	0.905	0.814	0.800	1.598	0.844	0.927	0.829
Ln (NSE)	0.374	2.029	0.140	0.805	0.763	1.738	3.517	0.980	2.645	0.638	2.385	0.374	0.592
bR^2	0.880	0.627	0.760	0.715	0.517	0.664	0.793	0.715	0.706	0.187	0.780	0.880	0.797

CONNECTING TEXT TO CHAPTER 4

The stormwater simulation model developed using MIKE URBAN package in Chapter 3 is integrated with a newly-developed model in Python programming language. The variable decay coefficient simulator (VDCS) was created in order to conduct stormwater quality simulations for monochloramine dissipation. The VDCS model computes pollutant concentrations in the storm sewers considering the spatial and temporal variability in its decay coefficients, which is not available in any current stormwater model. The VDCS model utilizes the findings of published literature about chloramine dissipation behaviour in the sewer environments to define the decay characteristics. The following chapter includes a full description of the VDCS model development, processes and application along with sample results of carefully-designed simulation scenarios. Further, a complete model description is provided in the form of Python coding is presented in Appendix C. All equations, variables, input data functions and scripts are also provided in Appendix C.

CHAPTER 4

IMPACT OF SPATIAL AND TEMPORAL VARIABILITY IN DECAY COEFFICIENTS ON SIMULTION OF MONOCHLORAMINE DISSIPATION IN STORMWATER SYSTEMS

4.1 Introduction

Chloramine was first used by a treatment plant in Ottawa, Canada, in 1916 to reduce drinking water treatment costs (AWWA, 2006). During chloramination, ammonia is added to convert the residual free chlorine to chloramines. Initially, chlorine and chloramine were both used widely for disinfection purposes; however, after the U.S. Public Health Service observed chlorine's rapid effect on several bacteria in 1943, chloramine use decreased significantly (Crittenden et al., 2012). It was not until the discovery of chlorine disinfection by-products (DBPs) in the 1970s that chloramine started to be used widely as a disinfectant (Connell, 1996) because, (1) although chloramines do form DBPs, they do so to a much lesser degree than chlorine (Zhang et al., 2017); and (2) monochloramine (NH_2Cl), the most dominant chloramine species, has a desirable longer-lasting residual that prolongs its disinfection efficiency (WHO, 2004). By 2008, approximately 30% of U.S. water suppliers used chloramination for disinfection (Maestre et al., 2016), and today it is widely used worldwide as a drinking water secondary disinfectant (Moradi et al., 2017; Wahman and Speitel, 2012), including by the City of Edmonton (CoE) in Alberta, Canada.

Given its long-lasting residual, the DBPs and chloramines in treated drinking water may reach the aquatic environment through their introduction to stormwater drainage systems after outdoor or industrial tap water use (Zhang et al., 2018c). Sources include distribution system leaks and breaks, lawn and garden watering, car and driveway washing, pool emptying, street cleaning, firefighting, construction activities, industrial hydro-testing, and industrial or commercial wash-down (Balling et al., 2008; Manning et al., 1996; Mayer and DeOreo, 1998). In Edmonton, stormwater eventually enters the North Saskatchewan River or tributary creeks from over 200 storm sewer outfalls, from which some of the stormwater system discharges flow directly, without any treatment, into receiving waters (CoE, 2013).

Over the past several decades, a shift has occurred toward the control of the water quality of discharges from urban areas to stream ecosystems (Goulden et al., 2018; Shrestha and He, 2017). In the case of the chloramine discharges in stormwater effluents, a number of studies have demonstrated harmful, and potentially fatal, influences of chlorine on fish habitat and possible changes in species composition (Bellanca et al., 1977; Grothe and Eaton, 1975; Manning et al., 1996; Svecevicius et al., 2005; Zillich, 1972; Zvinavashe et al., 2008). The effects of exposure depend on the concentration, duration, fish species and other environmental factors. Field studies and biological surveys have found a total active chlorine (TAC) concentration exceeding 0.02 mg/L to harm aquatic life, where TAC represents the combination of chloramines and free chlorine species released from chloramines. Consequently, the Canadian Council of Ministers of the Environment (CCME, 2009) issued new Canada-wide guidelines for the protection of aquatic life that lowered the maximum TAC concentration in municipal effluents to 0.02 mg/L. In Edmonton, recent monitoring of the TAC concentrations at selected storm sewer outfalls showed TAC concentrations up to 0.39 mg/L, which are substantially greater (1950% higher) than the reported detrimental level. Combined together, these factors establish requirements to understand and then control chloramine concentrations in stormwater systems.

Comprehensive studies on chloramine dissipation in storm sewer networks are lacking in the literature (Zhang et al., 2018c). Previous studies have addressed TAC dissipation in water distribution networks for human health concerns (Ahn et al., 2012; Alexander and Boccelli, 2010; Fisher et al., 2016; Shang et al., 2008); however, the reactivity between chloramines and a group of substances naturally found in storm sewer environments causes chloramine dissipation to differ significantly in stormwater (Zhang et al., 2018a). Further, the spatial and temporal variability within the stormwater system should be considered (Marsalek, 1991): spatially, with varying characteristics of stormwater effluents per land-use type and human activities (Zhang et al., 2018c), distribution of the decay-inducing parameters within the sewers (Potgieter et al., 2018) such as biofilms, further discussed below, and changes in the properties of the sewer network itself (Savic et al., 2009), which produces varying velocities and consequently travel times; and temporally, as a result of fluctuations in the pollutant mass fluxes over time (Clark, 1998), changes in the levels of the decay-affecting parameters such as temperature (VanBriesen et al., 2011), and the dynamic nature of pipe hydraulics (Westbrook and Digiano, 2009) and decay rates (Jonkergouw et al., 2009). In partcular, decay rates are known to decrease with time (Courtis et

al., 2009), because chloraminated flows traveling in a pipe react with chloramine-consuming substances where present (Sathasivan et al., 2008), both in bulk water and in biofilms at the pipe wall (Hallam et al., 2002). These reactions slow over time as reactants are consumed (Kohpaei et al., 2011; Zhang et al., 2018b). The mathematical representation of these temporal and spatial changes employs varying decay coefficents to model chloramine decay in the stormwater system (Zhang et al., 2018b).

Therefore, there is a real need for a stormwater model that can predict concentrations of pollutants with spatially and temporally variable decay coefficients in stormwater effluents; however, tools capable of simulating such pollutants are lacking. Available software tools such as SWMM, MOUSE and Infoworks WS can simulate first-order decay processes with a constant decay rate for an entire stormwater network over the simulated period of time (Butler and Davies, 2011; Elliott and Trowsdale, 2007; Rubinato et al., 2013). These models contain sophisticated runoff and pipe flow routing modules, and have been applied to study water quality in terms of the transport of suspended solids, heavy metals, phosphorus, COD/BOD in stormwater networks (Becouze-Lareure et al., 2019; Fraga et al., 2016; Lee et al., 2010; May and Sivakumar, 2009; Shon et al., 2012; Zhang et al., 2012). However, they are unsuited to simulation of pollutants with variable decay coefficients.

This paper therefore presents a novel system for simulation and prediction of chloramine concentrations in stormwater effluents throughout a drainage network, including the important spatial and temporal variations in chloramine decay coefficients at different points in that network. This system includes field sampling, laboratory experiments and a stormwater simulation model. First, a number of chemical, physiochemical and biological properties of stormwater were investigated in terms of their effects on chloramine dissipation rates under dry and wet weather conditions (Zhang et al., 2018c, 2018a, 2018b). The temporal and spatial variability of chloramine decay rates was also determined through field samples and laboratory experiments (Zhang et al., 2018c, 2018b). Second, a stormwater model was built, calibrated and validated – as described below – to give satisfactory flow routing and water quality predictions. Third, a new model, called the variable decay coefficient simulator (VDCS), was developed to predict chloramine-related concentrations in a drainage system using temporally- and spatially-variable decay coefficients. Finally, the previously-determined chloramine decay rates were applied to the VDCS model for a

stormwater basin in order to predict pollutant concentrations throughout the stormwater system and particularly at the storm sewer outlet.

This model system allows us to investigate the impact of variable rates of chloramine decay on stormwater model predictions. Specifically, we compare the more commonly-used constant average decay value against, 1) spatially-varying values per land-use, and 2) more comprehensive temporally- and spatially-varying decay rates. We hypothesize that higher spatial and temporal variability in observed decay rates will lead to more accurate model predictions as compared with measured concentrations in the system. Importantly, the system developed in this research is not limited to chloramine. It can be applied to study the dissipation of other degradable pollutants in storm sewers, such as nitrite and organic matter, and to reduce the uncertainties that preclude accurate prediction of their concentrations in different pipe systems. Note that this more-detailed representation of decay variability requires significantly more sampling and modeling effort than an approach that uses a single, average decay coefficient for water quality simulations. However, it should improve the ability of decision makers to anticipate pollutant fluxes in the sewer system and maintain released concentrations below regulated values.

4.2 Literature review

4.3.1 Parameters important for chloramine decay

The dissipation of chlorine and/or chloramine has been studied primarily in water distribution systems (WDS). Chloramine is known to dissipate in these systems through chemical reactivity, bio-degradation and auto-decomposition (Crittenden et al., 2012; Zhang et al., 2018a). Some parameters are known to have a greater effect on the dynamics of chloramine decay, such as natural organic matter (NOM) (Hrudey, 2009; Zhang et al., 2018a), temperature (Adhikari et al., 2012; Regan et al., 2002), pH (Sarker and Sathasivan, 2012), nitrite (Moradi et al., 2017; Sathasivan et al., 2009) and biofilm (Sathasivan et al., 2009, 2008), in addition to other reported parameters, such as bromide (Vikesland et al., 2001), microbiological growth (Herath et al., 2015; Sung et al., 2005), cometabolism (Maestre et al., 2016), alkalinity (Zhang et al., 2017), corrosion (Clark et al., 2006), flow velocity (Westbrook and Digiano, 2009) and pipe materials (Mutoti et al., 2007). The large number of factors involved in chloramine dissipation creates challenges for the modeling of chloramine decay (Mutoti et al., 2007). Further, unlike many stormwater pollutants generated from

deposition on various urban surfaces and accumulated over antecedent dry periods between rainfalls (Wei et al., 2019), chloramine does not exhibit build-up and wash-off characteristics. To date, a single study on chloramine dissipation in stormwater systems (Zhang et al., 2018c) has shown the NOM concentration to be the dominant contributer for monochloramine dissipation in stormwater. It also showed that ammonium can decrease decay rates through promoting the regeneration of NH_2Cl, while reactions with nitrite, organic components, and biofilms accelerate the decay process.

4.3.2 Modeling TAC decay in water networks

The decay of both chlorine and chloramine disinfectant in water networks is generally modeled with first-order kinetics (Ahn et al., 2012; Rossman et al., 1994; Savic et al., 2009), as:

$$\frac{dC}{dt} = -KC \tag{4.1}$$

where C is the concentration and K is the first-order decay constant. Chloramine decay involves two distinct processes: as it travels in pipes, it reacts both with consuming substances that may exist in the bulk fluid, and with the pipe's internal wall material and biofilms. These two processes are known as the bulk decay (K_b) and wall decay (K_w), respectively (Rossman et al., 1994), so that,

$$K = K_b + K_w \tag{4.2}$$

Many attempts have been made to determine K_b and K_w and their associated processes, using laboratory experiments or field measurements with regression analysis – see for instance Ahn et al. (2012), Al-omari et al. (2004), Boccelli et al. (2003), Castro and Neves (2003), Clark et al. (1995), Fisher et al. (2011b), Hallam et al. (2002), Powell et al. (2000) and Vasconcelos et al. (1997). K_b usually varies with temperature, total organic carbon (TOC), transport time and initial Cl concentration and contaminant, while K_w is affected by pipe age, diameter, material, roughness, corrosion and biofilm. In some models, the decay coefficient (K) is simply calibrated to minimize the model error against field measurements (Ahn et al., 2012; Mostafa et al., 2013; VanBriesen et al., 2011).

However, equation (4.1) is not the only first-order decay model available. Other versions of the first-order decay model, such as parallel and limited first-order models were also studied. Some of these models provide a better fit to available data sets, although they are not significantly or consistently better in most cases – see, for instance, Ahn et al. (2012), Helbling and VanBriesen (2009) and Vasconcelos et al. (1997). Other studies focus on second-order decay kinetic models, including those by Clark (1998), Fisher et al. (2011b), and Islam et al. (1997). The second order decay models used to study chlorine decay showed neither considerable nor constant improvements compared to first-order ones. For instance, Boccelli et al. (2003) found second-order models generally equaled or bettered the performance of first-order models, while Kim et al. (2015) compared the performance of 9 different chlorine decay models for a pilot scale water network and found that the first-order model outperformed other models under all studied conditions. Thus, despite the complexity of its decay chemistry, chloramine decay is better represented as a first-order process than chlorine (Fisher et al., 2009); it acts like free chlorine but with slower dissipation (Lee and Heaney, 2003; Maier et al., 2000).

Because temporal and spatial changes in chloramine decay rates do not lend themselves to a simple representation, they can be better modeled in stormwater systems using variable decay coefficients (Kohpaei et al., 2011; Zhang et al., 2018b). Based on actual field sampling results, laboratory experiments (Zhang et al., 2018c, 2018a), and model development in COMSOL (Zhang et al., 2018b), the temporal variation of chloramine decay rates can be described with the following relationship,

$$K_{t,i} = \frac{1}{\alpha\, t + \beta} * (f_i) \tag{4.3}$$

where $K_{t,i}$ is the decay coefficient at time t for land-use i, f is a land-use dependent coefficient described in Zhang et al. (2018b), t is the discharge time in minutes, α =1.73, and β =1.0.

4.3 Methods and material

4.4.1 Location selection

Four study locations were selected to represent major land-uses within two stormwater catchments, Kennedale in north Edmonton and 30th Avenue in south Edmonton; see Fig. 4.1. These locations included, (1) a residential site, as a reference for other land-uses, (2) a park site, for higher application of irrigation and fertilizer compared to residential areas, (3) a commercial site, focusing on automobile dealerships and rental locations, and (4) an industrial site, focusing on pressure vessel fabricator locations.

General characteristics of the stormwater network played an important role in site selection, such as the location of the neighborhood within the pipe system, the presence of stormwater ponds upstream, manhole accessibility for water sampling and existence of monitoring data for water quality and flow. Moreover, long, uninterrupted sections of pipe were preferred to permit attribution of changes in water quality to chemical and biological interactions taking place within the water mass, and to provide sufficient time for such interactions to occur. The sampling location within the network itself was also important, since sampling close to the upstream-end of the stormwater network would ensure that stormwater flows resulted from the catchment under consideration but could lead to limited flow volumes, while sampling farther downstream would make the attribution of contamination to specific sources difficult. Finally, potential neighborhoods with mixed land-uses within or upstream of the neighborhood were avoided, and some neighborhoods were excluded because of high traffic, poor accessibility and sampling difficulty.

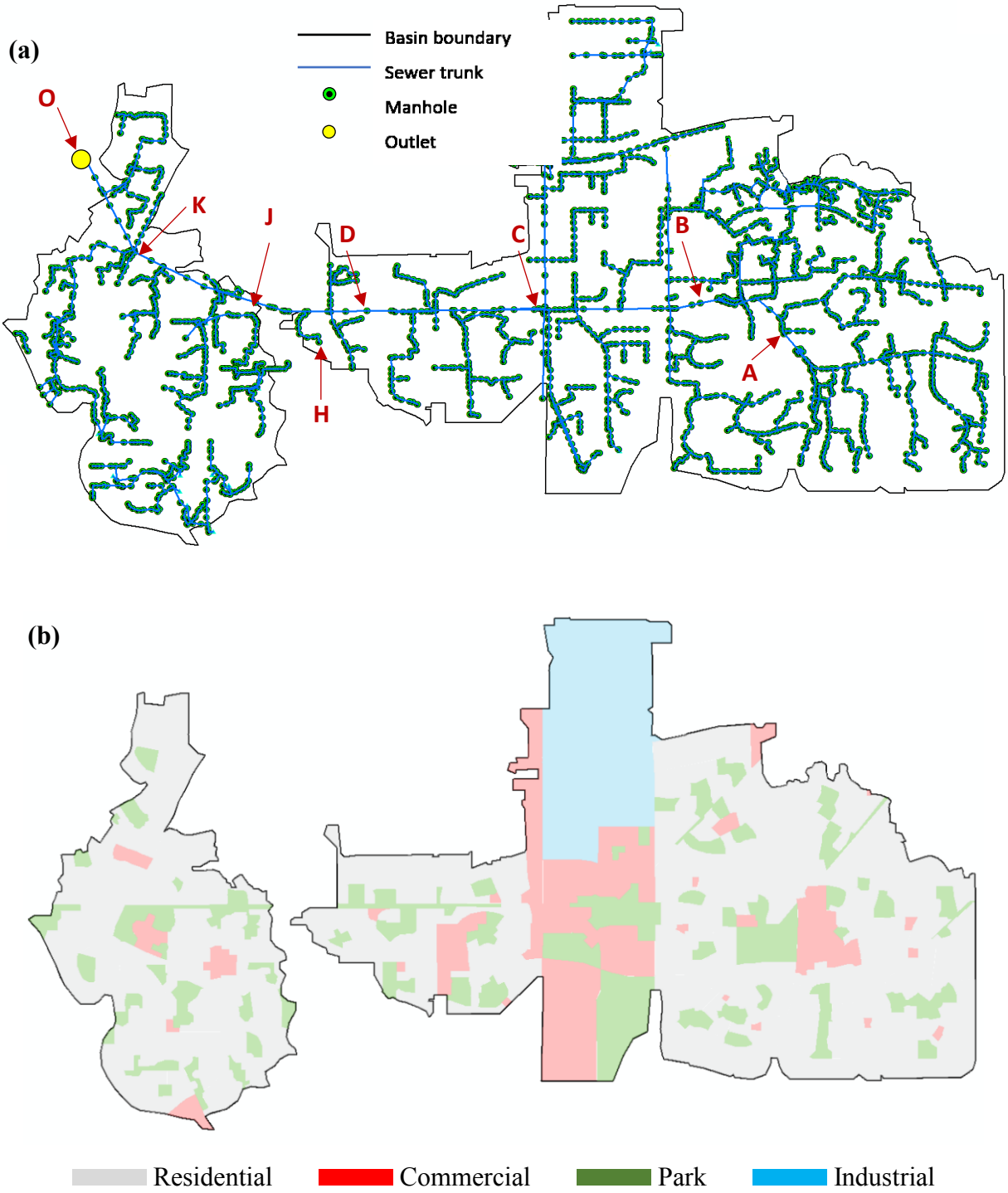

Fig. 4.1 The 30th Avenue stormwater basin in Edmonton, Alberta. (a) Basin boundaries and main sewer system components, labels for significant points on the main trunk. (b) Land-use characterization map

Additional criteria were applied for specific land-use types, similarly to approaches applied by Marsalek (1991) and Zhang et al. (2018b). For the residential location, low-density neighborhoods with relatively higher property values were favored because of their larger lawn areas (Al-Kofahi et al., 2012), and were identified from CoE data and aerial photos, as shown in Fig. 4.2(a). Then, the CoE property assessment values were categorized as shown in Fig. 4.2(b). For the industrial location, pressure-vessel fabricators were selected because of their reliance on large volumes of chloramine-containing potable water for testing vessel integrity. Last, for the commercial site, a cluster of commercial automobile services, including car rental locations, car washes and car dealerships was selected. Fig. 4.3 shows the selected neighborhoods and their associated storm sewer networks and Table 4.1 shows a summary of their storm sewers' characteristics.

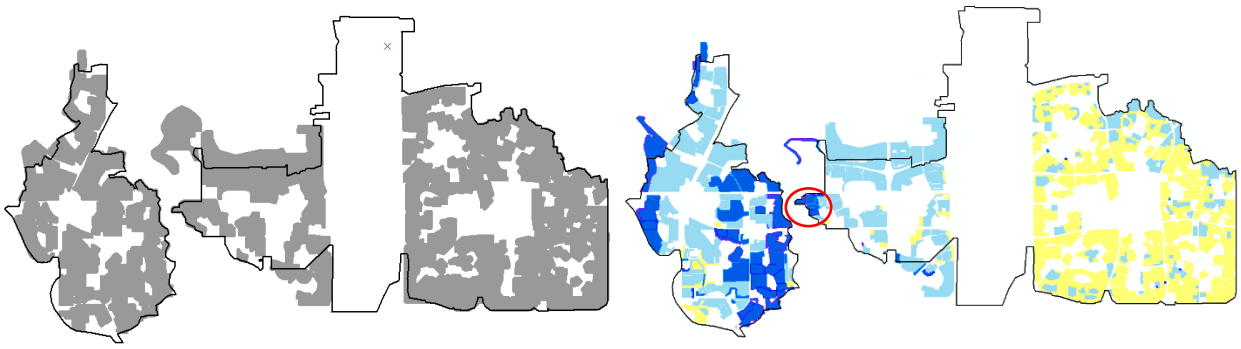

(a) Low-density residency (b) Property assessed value

Fig. 4.2 The selection of the residential study location

4.4.2 Data collection

The City of Edmonton provided a number of data sets that were used first to establish study site selection criteria and then to select the sites themselves. The data comprised (1) GIS data, including aerial images, land-use maps, property assessment maps and digital elevation models (DEM); (2) attributes and layouts of the stormwater network components from the DRAINS database; (3) MIKE URBAN sewer system models built to the trunk level (which represents the main drainage features – pipes with diameters greater than approximately 800 mm); and (4) data about the city's parklands, i.e. area, irrigation status and type of watering source. Online sources including Google

maps and telephone listings were used to find locations of pressure vessel manufacturers and commercial car dealerships in the two basins.

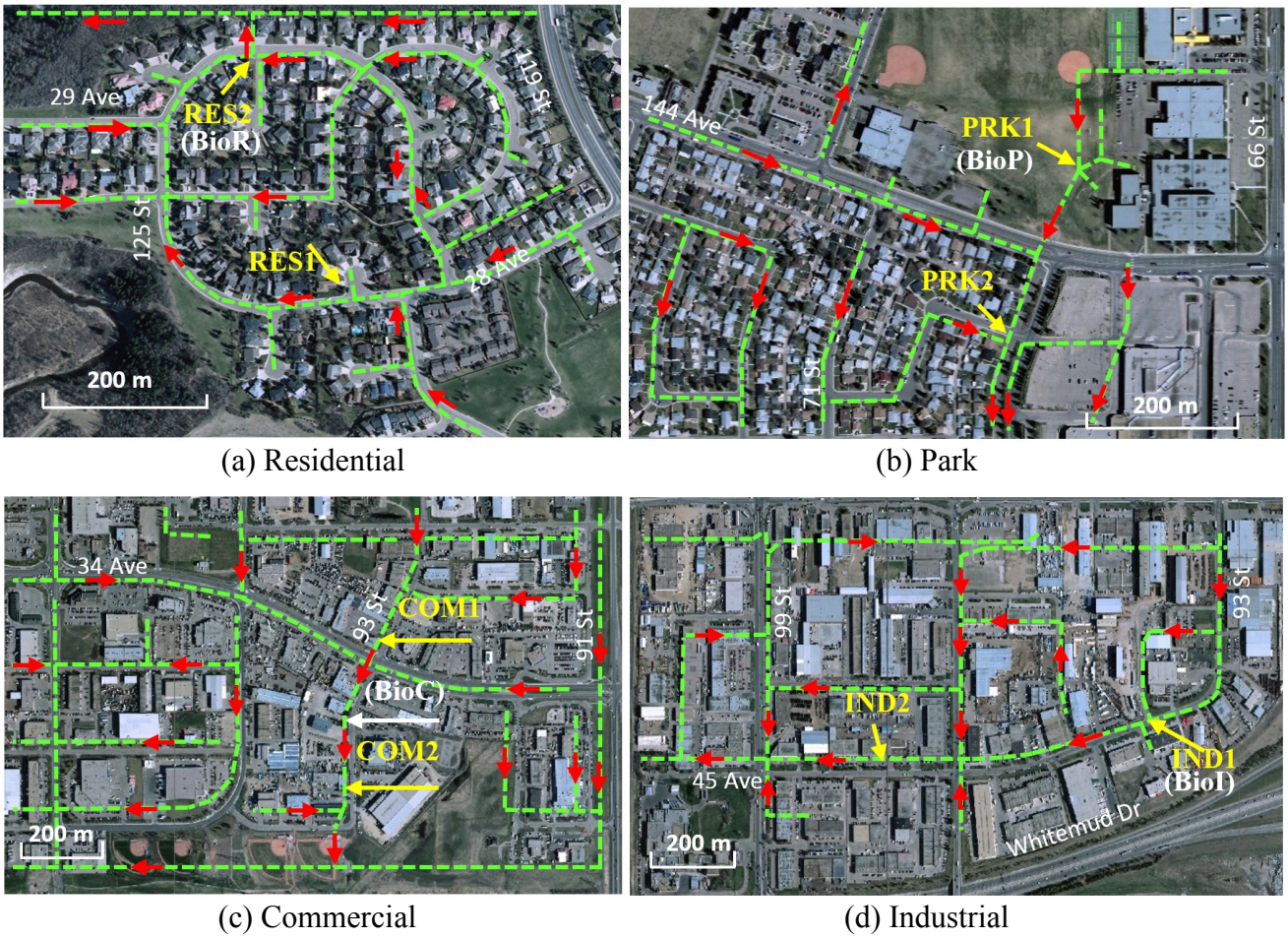

Fig. 4.3 Selected study neighborhoods and their stormwater network (Adapted from Zhang et al., 2018b)

Table 4.1 Average stormwater network properties of the study neighborhoods

Study site	Residential	Commercial	Industrial	Park
Material	Concrete	Concrete	Concrete	Concrete
Diameter (mm)	610	1050	750	375
Slope (%)	0.99	2.03	0.48	0.84
Pipe length (m)	45	95	110	70
Drainage area, ha	34	104	148	27
Imperviousness (%)	62	90	65	51

For calibration and validation of the stormwater model, the following data sets were collected for case study locations: (1) flow metering records from temporary flow meters installed in the summer seasons of 2015, 2016 and 2017 at three locations, one for each of the commercial, industrial and parks land-uses; (2) long-term pipe flow records from other permanent metering stations; and finally (3) long-term rain gauge data for the two stormwater basins.

4.4.3 Stormwater modeling

In many stormwater modeling tools, drainage system simulations and computations are conducted in two distinct stages (Zoppou, 1999), as shown in Fig. 4.4 . The first stage is runoff computations, which simulate the hydrological surface processes and routing of surface flow in modeled catchment areas, based on precipitation input and selected hydrological model parameters and processes (Elliott and Trowsdale, 2007). The second stage is network computations, which uses the computed runoff from the previous stage as a hydraulic load to the collection system (Thorndahl and Schaarup-Jensen, 2007). These steps are described in Zoppou (2001).

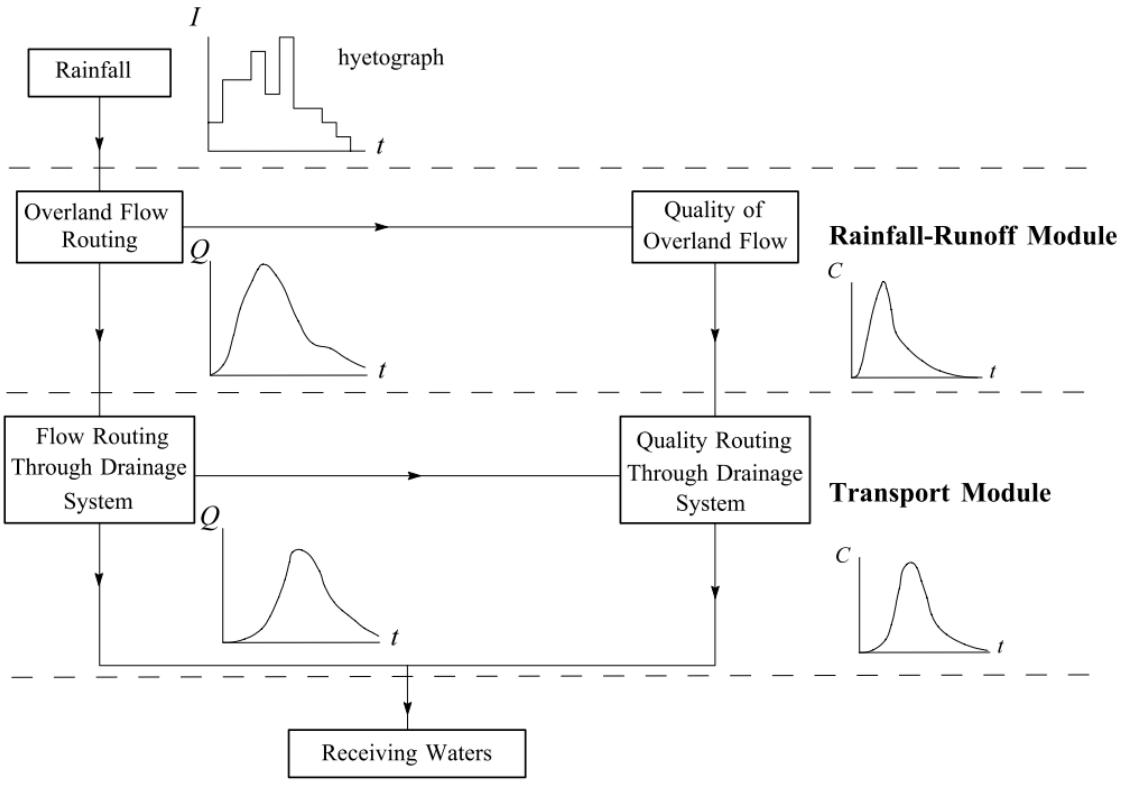

Fig. 4.4 Processes incorporated in a stormwater model (Zoppou, 2001)

The present study uses MIKE URBAN as the stormwater simulation tool. MIKE URBAN can simulate distributed rainfall-runoff and unsteady flow in pipe and channel networks, contains one of the most comprehensive water quality modules (Borah et al., 2009; Carr et al., 2010; Haris et al., 2016), and is used by the CoE for decision support. In terms of water quality, it can simulate pollution transport, dissipation and interaction between different water quality processes such as advection, dispersion, sediment transport and biological processes (DHI, 2017a). However, the water quality module can only simulate first-order decay with a constant decay coefficient. Finally, the selected routing techniques in MIKE URBAN included the kinematic wave method for surface flows and the dynamic wave method for pipe flow, which together balance the need for accurate results with relatively shorter simulation times.

The City of Edmonton provided a MIKE-URBAN stormwater model for the 30th Avenue catchment built to the trunk level. This level of detail allowed the simulation of urban floods, but did not meet requirements for simulating water quality in sewers (Butler and Davies, 2011). Hence, the model was modified to include network components down to the smallest pipe section at the system's upstream ends at all study locations. Next, to calibrate the model, a sensitivity analysis was conducted for 34 parameters to identify critical model inputs; we perturbed parameter values sequentially to examine the related variation in the fit between observations and model predictions, using a procedure adapted from James (2005) and Loucks and van Beek (2017). These parameters included imperviousness, catchment surface properties, infiltration indices, depression and initial losses, and surface roughness. The results showed that model performance was very sensitive to surface roughness, imperviousness and depression storage, while changes in catchment length and infiltration parameters were relatively ineffective. Therefore, GIS applications were used to improve estimates for some model parameters, as described by Liu et al. (2010). Aerial images and land-use maps were used to adjust the imperviousness ratios of each catchment, and digital elevation maps from the CoE improved catchment slope calculations.

The following model efficiency assessment measures were used for model calibration: bR^2 (Moriasi et al., 2007; Zambrano-Bigiarini, 2017), Nash-Sutcliffe efficiency (NSE) (Nash and Sutcliffe, 1970; Ritter and Munoz-Carpena, 2013), RMSE (Legates and McCabe, 1999; Willmott, 1981), and Logarithmic NSE, which is a useful measure for low flow rate performance (Pushpalatha et al., 2012; Ye et al., 1998). From the flow monitoring records of 2015 and 2016,

rainfall events were identified to represent different storm durations, patterns and magnitudes, and their respective sewer flow hydrographs were measured at three different locations within the stormwater basin. These events were then divided into two groups to be used in the calibration and validation processes. A sample of twelve validation results is shown in the Supplementary Materials in Fig. B2 and B3, which compares storm hydrographs from the calibrated MIKE URBAN stormwater model against observed sewer flows. Values of the model efficiency measures used to assess the performance of the stormwater model pre- and post- calibration model and validation are shown in Fig. 4.5, where model accuracy was significantly improved in terms of model prediction errors, and the correlation of both peak and low flows to observed stormwater discharges.

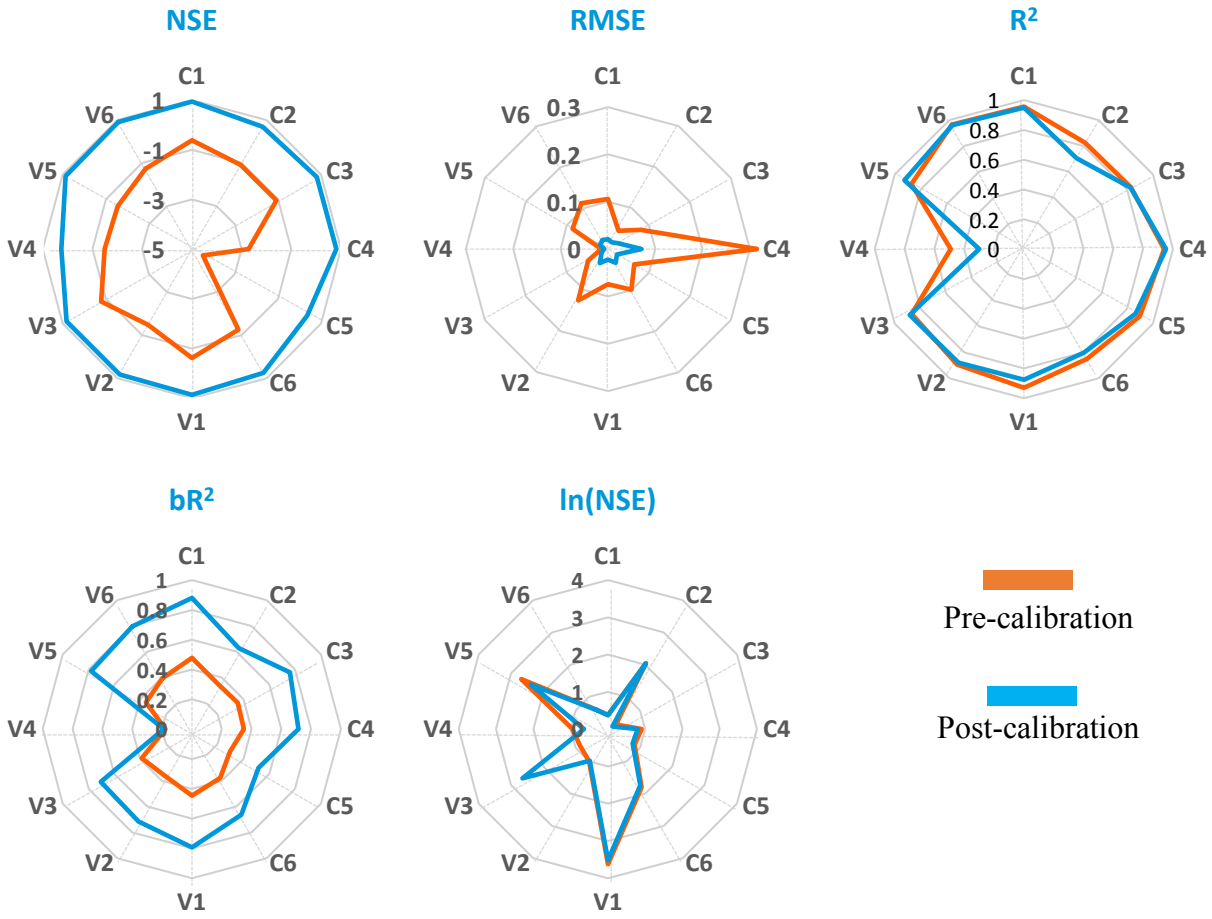

Fig. 4.5 Comparison of pre- and post-calibration model performance
(the C and V indexes denote calibration and validation storm events, respectively)

4.4.4 Python model (VDCS)

Because the available stormwater modeling software packages do not allow the definition of spatially or temporally variable chemical decay coefficients, it was necessary to develop a new simulation tool. The Variable Decay Coefficients Simulator (VDCS), developed in Python, can simulate concentrations of a degradable chemical substance in a water network based on input from existing hydrodynamic simulations. It applies the n^{th} order decay model (Butler and Davies, 2011) to represent the degradation reactions of individual pollutants, as,

$$\frac{dC}{dt} = K[C]^n \tag{4.4}$$

where C is the substance concentration, K is the decay constant, and n is the order of the reaction with respect to that substance. Focusing on chloramine dissipation in this study, the VDCS model applies a first-order decay model following the recommendations and work of Fisher et al. (2009), Lee and Heaney (2003) and Maier et al. (2000); however, VDCS can simulate lower or higher decay orders, if required.

Application of Eq. 4.3 generated the decay rates represented in Fig. 4.6 for the four different land-uses in the current study, where the decay rates start high at the beginning of release events and then decrease over time. Different water characteristics, especially biofilm presence, result in spatial variability in decay rates as well. These differences among land-uses were higher in absolute terms at the beginning of the event and then decreased toward the end of the simulations.

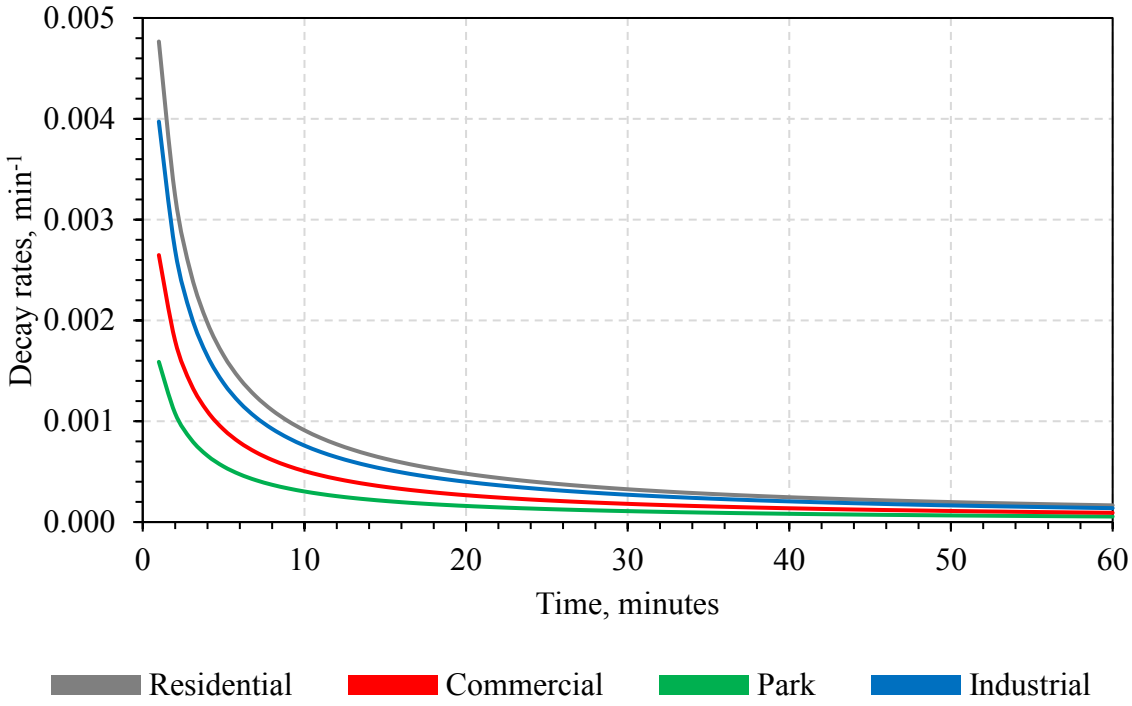

Fig. 4.6 Spatial and temporal variability of chloramine decay rates

The water quality computation process in the VDCS is shown in Fig. 4.7. The first tier represents the required inputs to the VDCS in the form of spreadsheets, either in .csv or .xls file formats. Inputs are categorized into three groups. First, sewer system attribute data are required, which describe different system properties for sewer pipes, manholes, and outlets, in terms of diameters, lengths, material and invert levels, and manhole IDs at both upstream and downstream ends of each pipe in the system. The VDCS uses these data to reconstruct the physical geometry of the water network from upstream branches, diversion and collection nodes, and through to the system outlet. This reproduction of the network layout is required later to determine the paths of pollutants through the sewer system. Second, hydrodynamic results from independent stormwater simulations are imported to provide time series of flow rates and velocities throughout the sewer system. Organization of the hydrodynamic results in spreadsheet form allows the VDCS to import them from any stormwater simulation model. Third, pollutant introduction points such as fire hydrants and industrial releases are defined for specific locations in the drainage system along with variations of their loads over the simulation period. Finally, the decay order is selected, and the

decay rate variation is set to one of three levels, 1) constant average value, 2) spatially-varying per land-use, or 3) varying both spatially and temporally.

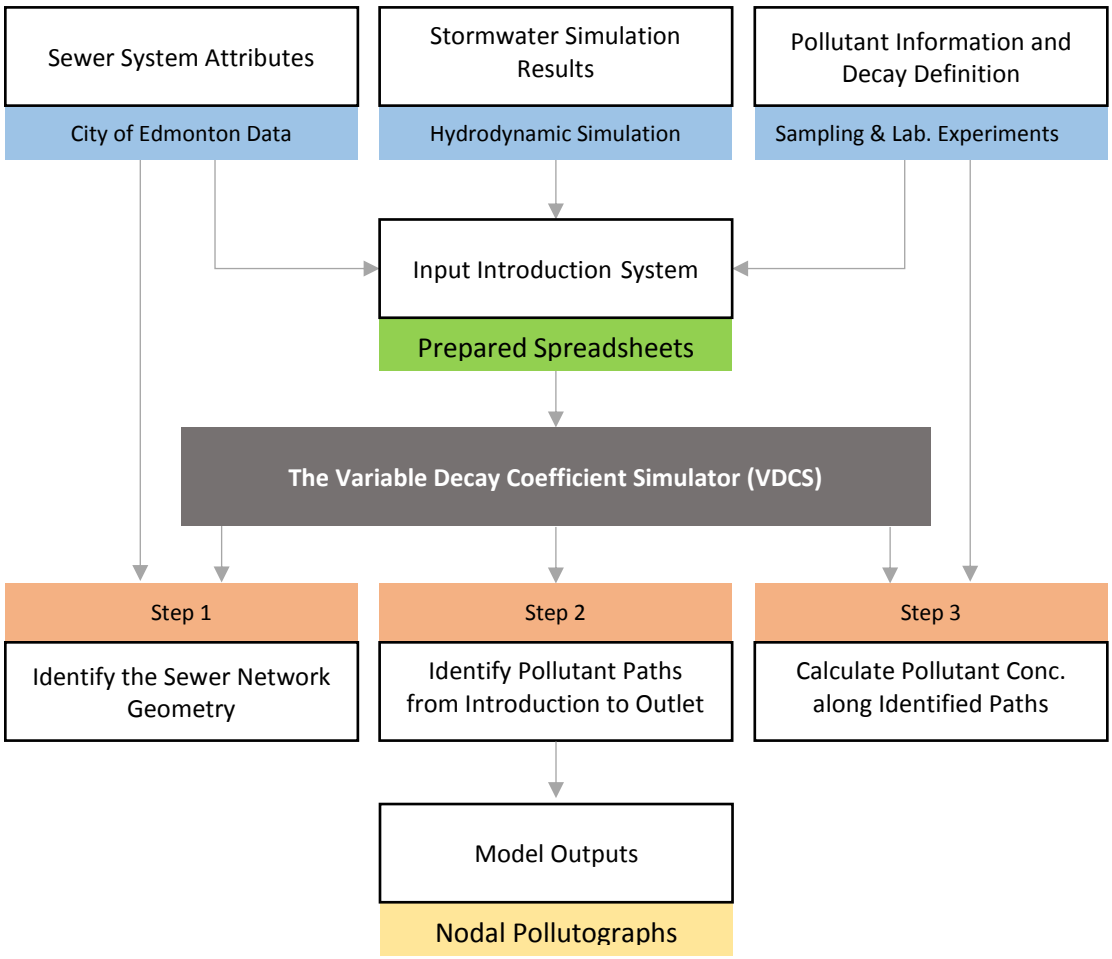

Fig. 4.7 Inputs, process flow and outputs of in the VDCS model

Employing the provided data sets, the VDCS calculates concentrations of the degradable substance along its transit path through the sewer system to the system outlet. The VDCS model computations start by identifying contamination paths, which use the constructed network flow map to trace pollutants from previously-defined introduction points from manhole-to-manhole to the system outlet. The model then identifies common pollution paths stemming from pollutant introductions at different locations in the network and combines their loads in the subsequent water quality computations. Based on the concentration at introduction points and volumetric flow rates, the pollutant load can be calculated and then tracked over the calculated contaminant path

according to the selected decay order. For chloramine dissipation with a first-order decay model, the VDCS calculates the concentration at the downstream node through,

$$C_{DS} = C_{US}\, e^{-Kt} \tag{4.5}$$

where C_{US} and C_{DS} are the chloramine concentrations at upstream and downstream ends of the current sewer link respectively, K is the first-order decay coefficient, and t is the travel time between the upstream and downstream nodes calculated from the pipe length and flow velocity.

Depending on the selected decay coefficient behavior, the VDCS sets the decay coefficient to a constant value or computes it at every timestep from Eq. 4.3. Similarly, beginning at the introduction points and then moving manhole-to-manhole to the system outlet, the VDCS model applies Eq. 4.5 to calculate the concentration downstream based on a known upstream concentration. At diversion or collection points, downstream concentrations are calculated by converting all upstream concentrations to mass fluxes, and then distributing the total mass to the downstream links according to their relative volumetric proportions, assuming uniform and full mixing at all junctions.

The VDCS produces pollutographs for different system nodes, such as manholes and outlets. Results can be exported to spreadsheets or plotted within the Python environment. As presented below in Section 4.5, the VDCS results were verified against the MIKE URBAN stormwater model, using the same inputs and chloramine loads.

4.4 Simulation scenarios

A set of three simulation scenarios was designed to demonstrate the effects of spatial and temporal variation in decay coefficients on chloramine concentrations in a storm sewer system – see Table 4.2. These scenarios investigate the effects of, (1) a constant decay rate, which uses a fixed decay coefficient value throughout the sewer network over the simulation period; (2) a spatially-varying decay rate, which specifies a fixed value for each land-use type; and (3) spatially- and temporally-varying decay rates, that incorporate differences in land-use types and times from initial pollutant

releases. The chloramine decay coefficient values for each scenario are shown in Fig. 4.8, and were determined from field sampling described by Zhang et al. (2018b).

For fixed decay coefficient values, the performance of the VDCS model was tested under both wet and dry weather conditions, defined as zero precipitation preceding and during the simulation period, and consistently matched the chloramine concentrations generated by the MIKE URBAN water quality module ($R^2 = 0.96$). We focus below on dry weather simulations because simulated chloramine concentrations were not significant throughout the sewer network during wet weather periods, as found also in previous studies (Lee et al., 2009; Zhang et al., 2018c).

Table 4.2 Properties of different simulation scenarios

Scenarios		Release type	Chloramine load	Weather condition		Decay rate variation		
				Wet	Dry	Con-stant	Spatial	Temporal
Scenario 1	**A**	Point source	Maximum	X	✓	✓	X	X
	B	Nonpoint source	Average	X	✓	✓	X	X
Scenario 2	**A**	Nonpoint source	Average	X	✓	X	First-flush	X
	B	Nonpoint source	Average	X	✓	X	Average	X
Scenario 3		Nonpoint source	Average	X	✓	X	✓	✓

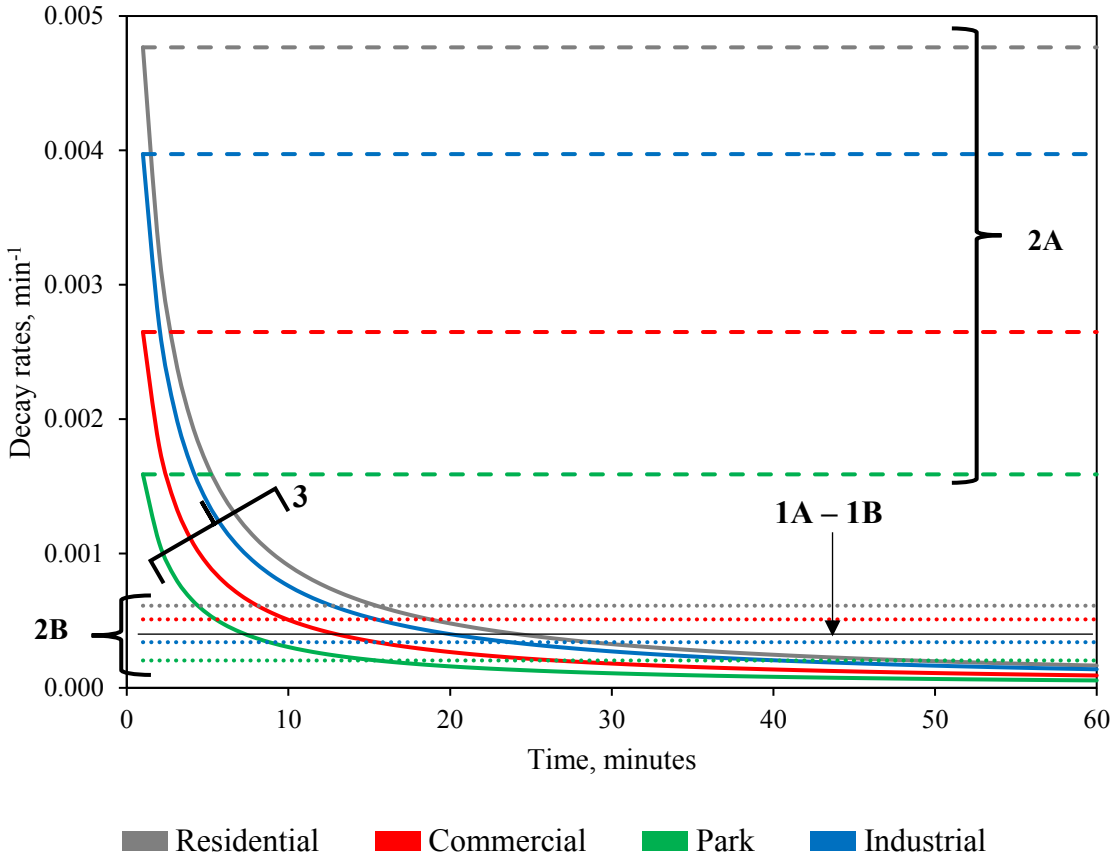

Fig. 4.8 Variability of decay coefficients for different simulation scenarios

4.5.1 Scenario 1: Validation of the Variable Decay Coefficient Simulator

The first set of simulations assesses the performance of the VDCS against the MIKE URBAN model for the 30th Avenue catchment, using a constant decay coefficient as in MIKE URBAN. Therefore, in scenario (1A), an arithmetically-averaged decay coefficient value was applied as an input for both models, as shown in Fig. 4.8. This scenario represents a practical case of a point-source contaminant release from a single fire hydrant to demonstrate the chloramine dissipation process with network flow to the system outlet. A similar approach could be taken to represent the effects of watermain breaks or prohibited industrial releases, potentially important chloramine contamination sources with high flows over a relatively long period of time. The simulated point

source release from a hydrant – next to manhole RES1, Fig. 4.3(a), in the residential neighborhood – was simulated as a constant discharge of 150 L/sec for two. The initial concentration of chloramine was assumed as high as the regulated chloramine limit in drinking water of 2.0 mg/L, which is more conservative as these concentrations might be lower in reality.

Next, to validate VDCS performance under a different set of conditions, scenario (1B) was designed to represent nonpoint source chloramine releases from different land-uses, to replicate more general conditions where chloramine releases occur at the same time from a number of outdoor activities. Scenario (1B) also applies a constant decay rate for both MIKE URBAN and the VDCS, as shown in Fig. 4.8. In addition to model validation, scenario (1B) results are also compared with other scenario results to study the effects of decay coefficient variations on chloramine decay rates.

4.5.2 Scenario 2: Effect of spatially variable decay coefficients

The second set of scenarios investigated the effects of spatially-variable decay coefficients, with coefficient values dependent on the mix of land-uses in each catchment. Temporal variations in decay rates were omitted such that each coefficient was constant over the simulation period, as shown in Fig. 4.8. To provide a plausible lower-bound estimate for the chloramine concentrations at the sewer outfall, the highest plausible decay rate, associated with a first-flush event, was used for scenario (2A). Scenario (2B) was then used to assess a lower, time-averaged decay rate value for each land-use type. Together, this set of simulations illustrates the importance of selecting appropriate decay coefficient values for the different land-use types.

For these scenarios, although the land-uses were limited to four main types (residential, commercial, industrial and parks) with the four individual decay rate values shown in Fig. 4.8, each catchment had unique chloramine load and decay coefficient values based on its drainage area and the proportional mix of the four land-use types. From the field sampling results, to select appropriate time-averaged decay coefficients for these simulations, two decay rates were used as in scenario (1), the first flush decay rate and the average decay rate, which were calculated as:

$$k_i = \sum_{i=1}^{n} k_n \times \varepsilon_n \tag{4.6}$$

where k_i is the land-use averaged decay coefficient of catchment i, k_n is the decay coefficient of land-use n, and ε_n is the percentage of land-use n in catchment i as per the municipal land-use maps.

4.5.3 Scenario 3: Effect of spatially- and temporally-varying decay coefficients

In the last scenario, both spatial and temporal variabilities of the decay coefficients were simulated in the VDCS, as shown in Fig. 4.8. This scenario was intended to represent a more realistic situation in which chloramine decay rates decreased with time, with results applicable for water managers and decision-makers for the regulation and treatment of degradable pollutants. Consequently, scenario (3) represents a conservative case, since the chloramine concentrations it simulates would be expected to be significantly higher throughout the sewer system and at the system outlet than in the other scenarios. The average nonpoint chloramine load used in scenario (1B) and (2) was applied to this scenario.

4.5 Results and discussion

4.6.1 VDCS Model performance assessment

The first set of scenarios was intended to validate the VDCS against results from the MIKE URBAN water quality module. Scenario (1A) simulates chloramine dissipation from a single, potable water point-source, using the pipe flow hydrographs for hydrodynamic simulations from MIKE URBAN shown in Fig. 4.9. Lag and attenuation effects are apparent in the flow hydrograph for discharge introduced at point (H) that traveled downstream through points (J), (K) and (O) – see Fig. 4.1(a) for the locations of these points. Fig. 4.9 also shows that the corresponding chloramine concentrations decreased from an initial concentration of 2.0 mg/L to reach 0.47 mg/L at the system outfall, point (O) – a value that is still considerably higher than the allowable chloramine discharge concentration.

The chloramine concentrations, peaks, and patterns simulated by the VDCS closely matched those produced by the water quality module of MIKE URBAN, as shown in the pollutographs of Fig. 4.9(b). In terms of a statistical assessment of model performance, the VDCS produced very high agreement at all points with MIKE URBAN results: R^2 = 0.98, RMSE= 0.02 mg/L and NSE = 0.96. Further, the small discrepancies between the two results can be attributed to differences in

the hydrodynamic input to the two water quality models. MIKE URBAN used data directly generated from flow routing, while the VDCS used flow parameters at set timestep intervals of 5 minutes.

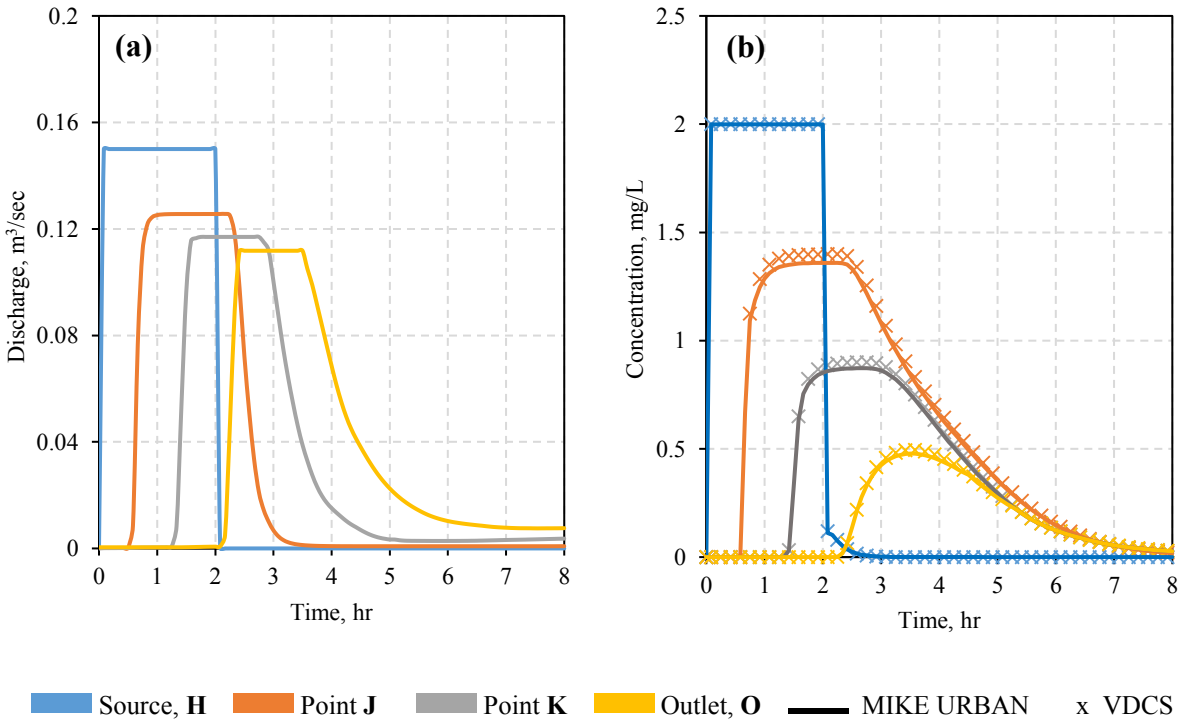

Fig. 4.9 Hydrographs and Pollutographs generated by the VDCS and MIKE URBAN models for three manholes D/S a fire hydrant release; (a) pipe flows, (b) concentrations

An alternative view of scenario (1A) focuses on longitudinal profiles of the chloramine concentration from the source at (H) to the system outfall at (O), a total length of about 5.0 km, for specific initial release times, as shown in Fig. 4.10. For example, after 2 hours (t = 2.0), the chloramine concentration was 2.0 mg/L at point (H) (km = 0.0), dropped to 1.00 mg/L after 2.0 km in the sewer line, and reached 0.0 mg/L after 3.0 km. Likewise, after 8.0 hours (t = 8.0) when the release event ended, chloramine pollution no longer existed at the release point (H), while the maximum chloramine concentration along the release path was 0.53 mg/L at km = 1.75. Longitudinal pollutant concentration profiles, as presented in this work, offer many clear advantages in understanding the transport of any contaminant in a stormwater system. They simplify investigation of the propagation of the pollutant plume through the sewers, identify the

location and value of peak concentrations at different time intervals, and mark time periods after which pollutant concentrations are below regulation limits throughout the water network.

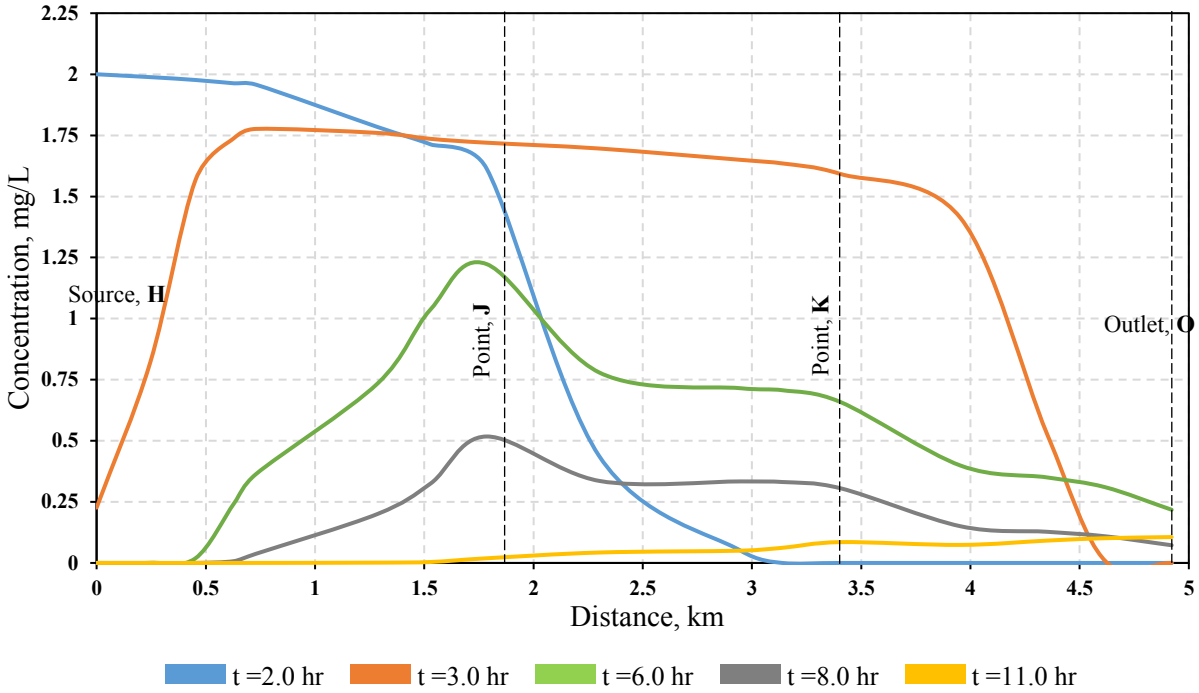

Fig. 4.10 Longitudinal chloramine concentration profiles along the path of scenario (1A)

In scenario (1B), the VDCS was evaluated for nonpoint sources, where chloramine effluents were defined as variable by land-use. The pipe flow hydrographs computed by MIKE URBAN at respective points (A),(B), (C), (D), (J), (K), and (O) on the main trunk – see Fig. 4.1(a) – are shown in Fig. 4.11(a). The passage of the stormwater wave through the drainage system is clearly visible, beginning at point A and then increasing along the main trunk, as the collected stormwater volume increased to reach its peak value at the system outfall (O). Because this scenario represented nonpoint contaminant sources, the shapes of simulated hydrographs and their corresponding pollutographs were affected by many different characteristics of the sub-catchments connected to the key manholes on the main trunk, such as the drainage area, geometry, and land-use types and their distributions within the various sub-basins.

Chloramine concentrations computed for point O with MIKE URBAN and the VDCS – see Fig. 4.11(b) – using the decay rate value for scenario (1B) from Fig. 4.8, were significantly higher than the allowable discharge concentration to surface waters over the entire simulation period. Comparison of the two sets of results also reveals high agreement of the VDCS to MIKE URBAN

values, as shown in Fig. 4.11(b). The average values for the statistical measures were $R^2 = 0.97$, RMSE= 0.026 mg/L, NRMSE = 7.74%, and NSE = 0.94. Note that the slightly higher differences in these measures resulted from the considerably higher flows encountered in scenario (1B).

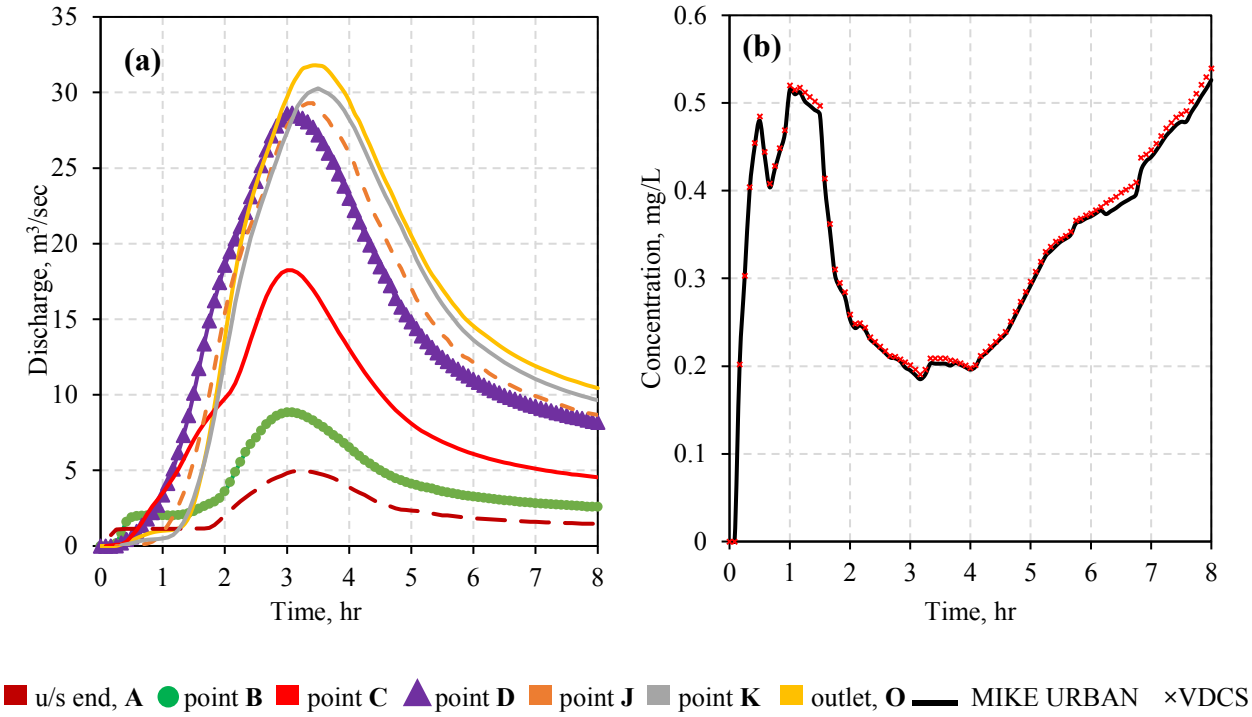

Fig. 4.11 Results of Scenario 1B; (a) pipe flows at 7 different location in the sewer system, (b) pollutograph at the system outlet, O

4.6.2 Spatially-variable decay coefficients

Scenarios (2A) and (2B) focused on model results for spatially-variable but temporally-constant decay coefficient values. Nonpoint source chloramine contaminants introduced to the stormwater model were set at the same level as Scenario (1B), as shown in Fig. 4.8, and pipe flow hydrographs computed by MIKE URBAN are shown in Fig. 4.11(a).

Further, pollutographs at the system outlet, point (O), show chloramine concentrations at the system outlet above the allowable discharge concentration to surface waters. As shown in Fig. 4.12, the average concentrations in scenario (2B) were consistently higher than those of scenario (2A), which used the first-flush decay coefficients, because of the significant difference between

the two decay coefficient values. However, the first-flush values were used to generate a lower-bound scenario for chloramine concentrations, which is not intended to be realistic over the entire simulation period – such high decay rates tend to last only briefly after chloramine introduction, because of the reduction in chloramine dissipation by biofilm over time (Kohpaei et al., 2011; Zhang et al., 2018b).

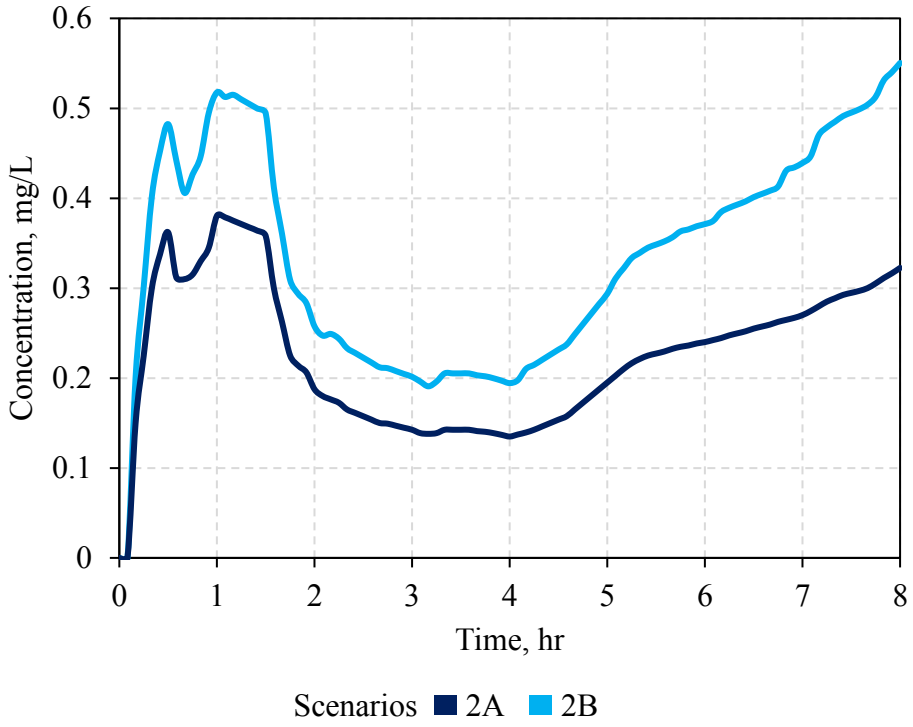

Fig. 4.12 Pollutographs of the system outlet considering fist-flush and avrage decay coefficints, results of second scenario (2A) and (2B)

Interestingly, the differences between the scenario results were not constant throughout the simulation period. For instance, during the first quarter of the simulation period, the difference between the computed concentrations in the two scenarios reached a maximum relative value of 38% for the chloramine levels of Scenario (2A), while the results of Scenario (2B) were 67% higher than Scenario (2A) by the end of the simulation period. Over the full simulation period, the average difference in the two pollutographs was 43%, a significant difference in chloramine concentrations in the sewer system. This comparison illustrates the importance of selecting an appropriate coefficient value, even where the temporal change in decay coefficients is ignored.

4.6.3 Impact of spatial and temporal variability of in the decay coefficient

The scenarios of group (3) incorporated both temporal and spatial variations in the decay coefficient (see Fig. 4.8), and applied the pipe flow hydrographs shown in Fig. 4.11(a). Results from the three varying levels of the decay rates – constant, spatially-variable, and temporally- and spatially-variable – are shown in Fig. 4.13. The following analysis focuses on the stormwater outlet, because of its proximity to the receiving waters.

Overall, the results of spatial disaggregation considered in scenario (2B) showed very high agreement with scenario (1B), because of the small differences in the decay coefficient values between the two scenarios. Interestingly, despite the incorporation of different decay coefficients for specific land-uses in scenario (2B), the spatially-averaged decay coefficient value was quite similar to the single decay coefficient used in scenario (1B) – see Fig. 4.13. However, because this result may have stemmed from the combination of decay coefficient values for the included land-use types, it should not be taken as a general conclusion of the current work.

In contrast to the similarity between scenarios (1B) and (2B), incorporation of both spatial and temporal variations in the decay coefficients in scenario (3) produced a significantly different pollutograph, shown in Fig. 4.13. The maximum simulated concentration in scenario (3) was 0.65 mg/L, which comes closest to 0.7 mg/L, the measured concentration at the system outlet of the 30th Avenue basin during field samples in summer 2015 (Zhang et al., 2018c). Interestingly, the rank of scenario (3) changed over time relative to the other scenarios, from relatively low for the first-quarter of the simulation period, where it lay between the values for scenarios (2B) and (2A), to the highest value in the last three-quarters. Further, as the stormwater volumes collected from farther neighborhoods began to reach the system outlet by the second-third of the simulation period, the differences between the scenarios became more visible with higher chloramine concentrations in scenario (3) than in scenarios (1B) and (2B). This result can be attributed to higher decay rates for case (1B) and (2B) in this part of the simulation period. Finally, in the last-third of the simulation period, the concentrations of scenario (3) were at a maximum of about 100% higher than those predicted in scenario (2A). In absolute terms, the highest predicted chloramine concentrations at the outlet, point (O), were 0.54, 0.32, 0.55 and 0.65 mg/L for

scenarios (1B), (2A), (2B) and (3), respectively, due to the much lower chloramine decay rates in scenario (3) than in the other scenarios.

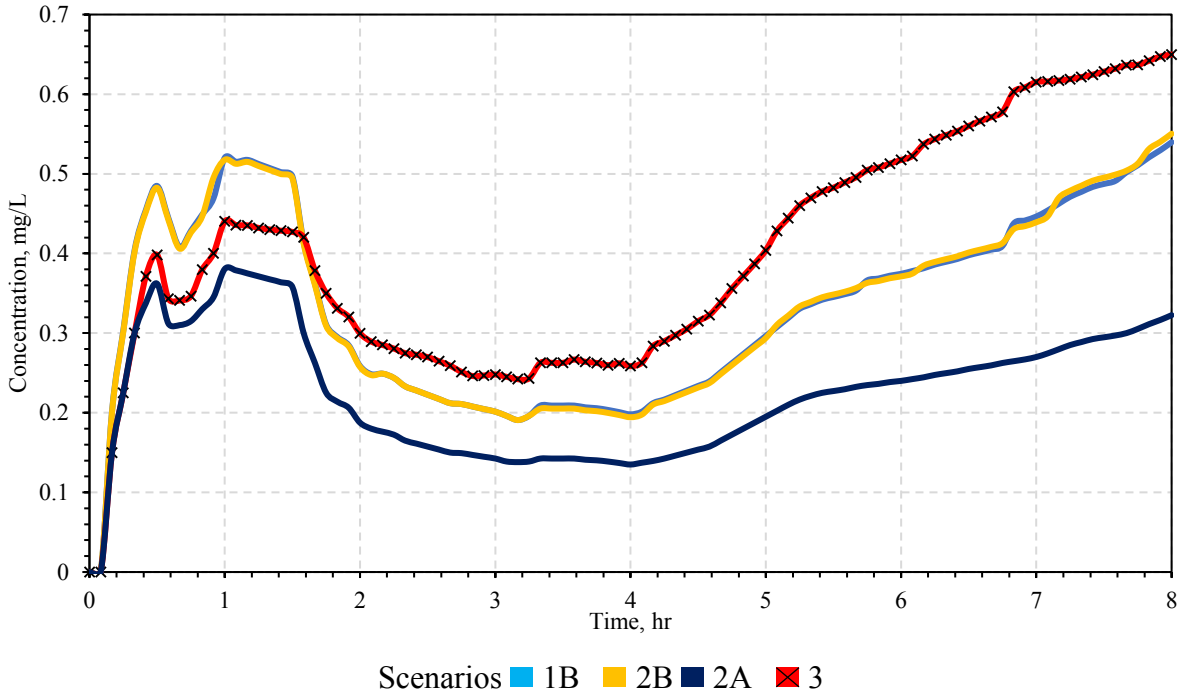

Fig. 4.13 Pollutographs at the system outlet for scenarios (1B), (2A), (2B) and (3)

It is important to consider mass fluxes in addition to concentrations. System operators and managers prioritize pollutant concentrations over mass fluxes, both because concentrations can be measured more easily in the field and because guidelines like those of the CCME focus on maximum allowable concentrations. However, maximum mass fluxes may not occur concurrently with maximum concentrations. For example, in the first-third of the simulation period, the concentrations shown on the pollutograph were relatively high; however, the corresponding mass flux of 0.5 g/sec (at t = 1 hr) was low because of a relatively low discharge at that time. In the middle third, which had the lowest concentrations at the outfall, the maximum discharge occurred and a high mass flux of 5.7 g/sec (at t = 4 hr) resulted. Finally, by the end of the simulation period, with the highest concentrations at the system outfall, the corresponding discharge was relatively low and a similar mass flux of 5.1 g/sec (at t = 7 hr) resulted. The difference between mass fluxes and concentrations shows that care must be taken in the analysis and interpretation of model results, and that a focus only on pollutant concentrations may omit potential environmental

consequences of high mass/low concentration releases of pollutants. Regulators and water managers should incorporate mass fluxes as parameters in guidelines and regulations.

4.6 Conclusions

This study investigated the importance of spatial and temporal variability of monochloramine dissipation rates in stormwater networks. The new Variable Decay Coefficient Simulator model (VDCS) was developed to simulate spatial and temporal variations in coefficient values, and field measurements and results from DHI's MIKE URBAN simulations with constant coefficient values were used to validate model performance. Three scenarios were designed to compare the application of 1) constant decay coefficient values throughout the sewer network over the simulation period, with 2) spatially-varying decay rates per land-use type, and 3) spatially- and temporally-varying decay rates that incorporate changes in coefficient values with time from the initial pollutant releases.

Comparison of the scenario results demonstrated the importance of including both temporal and spatial variations of decay coefficients when simulating degradable chemical pollutants in sewer systems. The combination of spatial and temporal variability in chloramine decay rates affected the predicted chloramine concentrations significantly, with implications for environmental and regulatory measures. To accommodate variable decay rates for degradable chemicals, the available water quality models require modification. In their current state, they omit important dynamics of pollutant concentrations in stormwater systems and may underpredict discharge concentrations, with adverse consequences for the quality of receiving water bodies.

For future studies, an extensive stormwater quality monitoring program is recommended to improve water quality simulations that involve degradable chemicals in stormwater networks. Although resource-intensive and potentially costly, such monitoring programs would improve the estimation of pollutant decay rates, improve understanding of the role of different land-uses and pollutant loads on pollutant concentrations and aid validation of stormwater quality simulations.

Finally, especially for dry weather conditions, close attention should be paid to chloraminated effluents toward the middle and end of the discharge period, rather than at the early stages of release events. After a dry period, which would allow biofilms to accumulate, both chloramine

mass fluxes and concentrations would initially be relatively low, but they rise significantly as decay rates decrease and more distant sections of the drainage system contribute to produce higher flow rates. Results will differ by basin geometry, the mixture of land-uses and system attributes, and water use and quality characteristics, and so pollutants must be assessed for each stormwater basin individually.

CONNECTING TEXT TO CHAPTER 5

The next chapter introduces the procedure of building a practical stormwater quality framework to help decision-makers to assess and control contamination incidents in drainage systems. The framework incorporates; (1) the stormwater simulation model of MIKE URBAN presented in Chapter 3, (2) the water quality simulator of VDCS presented in Chapter 4, and (3) a hazard assessment procedure to develop standalone hazard maps for stormwater basins. That framework is then applied to study chloramine dissipation in the 30th stormwater basin.

CHAPTER 5

A PRACTICAL GIS-BASED HAZARD ASSESSMENT FRAMEWORK FOR WATER QUALITY IN STORMWATER SYSTEMS

5.1 Introduction

Urban stormwater significantly affects the quality of surface waters (He et al., 2011; Konrad, 2005; Paul and Meyer, 2001; Roy et al., 2008). Land-use change, human activity and population growth all aggravate the impact of urban sprawl on the quality of stormwater effluents that eventually reach surface waters (Walsh, 2000; Zhang et al., 2018c). In many cities, stormwater is a significant contributor to local freshwater bodies, and provides a route for pollutant introduction to receiving streams and rivers, impairing local water supplies (Davis et al., 2001; Eriksson et al., 2007; Gnecco et al., 2005; Howell et al., 2012; Roy et al., 2008). In addition to higher runoff volumes and more intensive floods resulting from increased impervious surfaces, urbanization contributes to more severe pollutant loadings (Lee and Heaney, 2003). Several studies have reported the unnecessary risks of polluted stormwater on aquatic ecosystems and human health as it conveys harmful chemicals, sediments, nutrients, heavy metals, microbial pathogens, and waterborne diseases into receiving waters (Bernhardt and Palmer, 2007; Jiang et al., 2015; Makepeace et al., 1995; NRC, 2008).

For instance, Coleman et al. (1974) investigated the effect of urbanization on the microbial content of the North Saskatchewan River and found that urban centers altered the microbial composition of the river to such a degree that its effect was still discernible 480 km downstream from the city. Similarly, Walsh et al. (2016) found that stormwater systems significantly contribute to the degradation of stream ecosystems, alter stream hydrology, and increase the frequency of disturbance to biota in urban environments. Luo et al. (2018) analyzed the potential effects of rapid urbanization on water quality and macroinvertebrate communities of Chinese streams; they found that rapid urbanization has dramatically deteriorated the water quality of streams and threatens aquatic ecosystem health. Further, 91% of the UK river basins considered as at risk are located downstream of heavily altered urban waters (Ellis et al., 2012), and in the US, urban stormwater is considered the primary source of water quality impairments of 13%, 18% and 32% of all rivers,

lakes and estuaries respectively (NRC, 2008). Many studies have found similar patterns, see Meyer et al. (2005).

To control and mitigate these serious environmental risks, water quality monitoring studies have been based for decades on costly, time- and labor-intensive field sampling programs and real-time control (Niu et al., 2014). However, geographic information systems (GIS) can also play a crucial role in managing and modeling many water resources problems related to urban drainage, point- and nonpoint-source pollutants, and water and stormwater systems (Tsihrintzis et al., 1996). Advanced statistical methods have been successfully integrated into GIS applications, which have enhanced the capabilities of water quality assessment over different spatial scales (Machiwal et al., 2018). Over the last decade, many researchers have used GIS-based application in assessing and managing stormwater quality-related risks. Mitchell (2005) developed a GIS model to map 18 key diffuse urban stormwater pollutants in the Aire basin, Yorkshire, UK. Their GIS model successfully identified the locations of scattered pollution hot spots in the stormwater system. In another study, Ellis et al. (2012) developed a GIS-based pollution index to assess risk levels for different urban land-use types using surface impermeability, runoff loads and drainage system best management practices. Wijesiri et al. (2018) employed GIS-Bayesian Networks to model urban water quality and develop health risk maps depending on water pollution. These studies demonstrate an essential need for methods to monitor and predict stormwater quality to ensure that levels of harmful chemicals in surface water systems are maintained below assimilation capacities, and to help decision makers to take appropriate measures.

From an operational perspective, stormwater system managers need reliable and fast tools to assess the severity of unregulated/prohibited point-source contamination spills. Environmental engineers consider pollutant concentrations at the most important point in the system, the system outlet, as the primary concern in managing stormwater effluents to surface waters. Consequently, an effective tool should predict stormwater quality hazards at system outlets as a result of releases from any point in the stormwater basin. However, running simulation models for surface runoff, pipe flow and water quality can be very time-consuming, and by the time results are available, mitigation actions may no longer be necessary. Regulators and decision makers can also benefit from an analysis of points in a system where intervention is necessary after a pollutant release, and where it may dissipate sufficiently that no action is necessary.

Hence, this work introduces a practical, fast and useful tool to assess pollutant concentrations and potential hazards of point-source spills, particularly at system outlets, without the need to conduct resource-intensive simulations. This hazard assessment tool can identify areas in the system that contaminant releases from which generates high pollutant concentrations and consequently can delineate high- and low-risk areas. The solution comes in the form of pollutant concentration and hazard maps. A pollutant concentration map represents the predicted concentration at a system outlet associated with point-source contamination occurring at any location in the stormwater system. Thus, for example, if the pollutant concentration at a specific location on the map is 1.0 mg/L, this means that a pollutant release at this location, although initially higher than 1.0 mg/L at its point of release, would produce a maximum concentration of 1.0 mg/L at the system outlet. Similarly, a hazard map represents the same concept but with a hazard score as a percentage rather than as a concentration. This simple, but effective and accurate, tool will assist and expedite stormwater quality regulation. Such hazard maps can also be generalized to various water systems and extended to different chemical substances and contamination source types as well.

The novel GIS-based hazard assessment framework for stormwater quality introduced here includes stormwater hydrodynamic modeling, pollutant fate and transport modeling, concentration mapping, and hazard estimation and mapping. It therefore comprises four different stages and three individual modeling tools, producing a "4-stage-3-model" framework described below. The goal of implementing this framework is to develop a stand-alone assessment tool for pollution concentrations and water quality hazards so that it can help municipal engineers and planners to better predict water-quality-related risks. Section 5.2 of the paper describes the different stages of the "4-stage-3-model" framework methodology, including the inputs and outputs of each stage and the necessary computations. Section 5.3 presents information on the study area, a stormwater basin in Edmonton, Alberta, Canada, the selected pollutant, monochloramine, and the study scenarios. Section 5.4 provides the results and analysis from application of the framework to the case study, and Section 5.5 concludes the paper.

5.2 Generic framework methodology

This framework adopts a "4-Stage-3-model" methodology (see Fig. 5.1) that incorporates stormwater hydrological, hydraulic and quality simulations, geostatistical mapping analyses, and

pollution hazard assessments. The first three stages were implemented using a stormwater modeling tool, pollution transport and fate model, and GIS-based mapping analyst, respectively. The accuracy of such models determines the reliability of their outcomes, and thus the effectiveness of the decisions taken by system managers, so much care is required in developing and validating their results (Butler and Davies, 2011). The sections below describe each of these steps briefly.

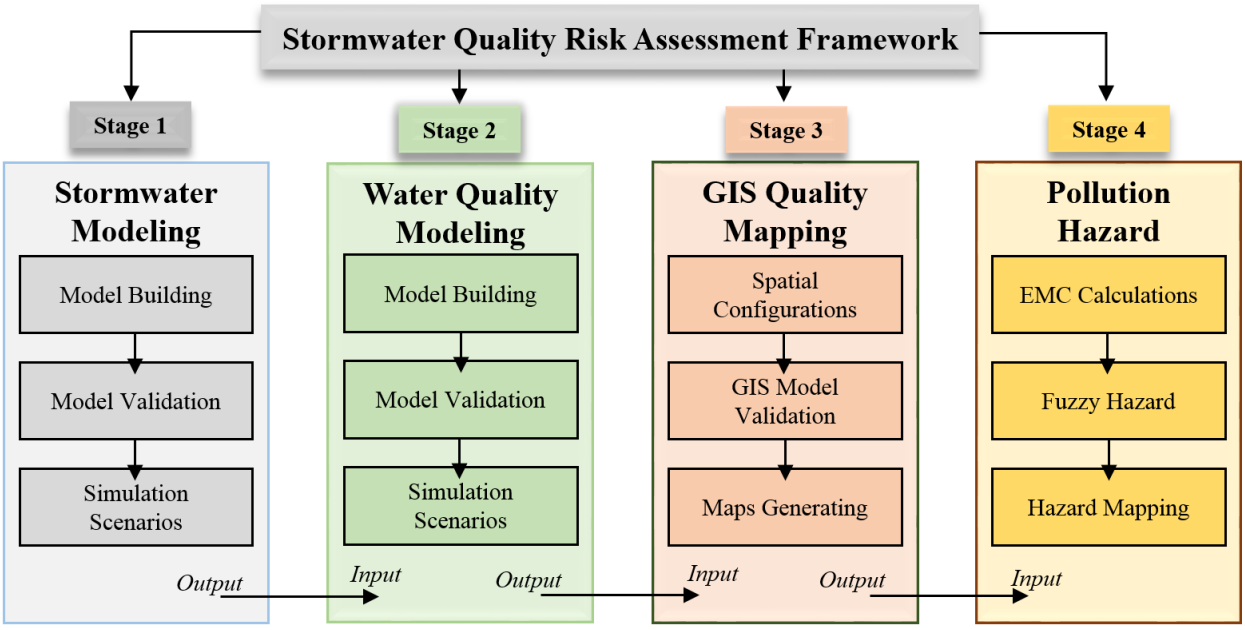

Fig. 5.1 Diagram of the "4-stage-3-model" stormwater quality framework

5.2.1 Stage 1: Stormwater system modeling

Stormwater modeling is the first stage of the framework, as shown in Fig. 5.2, and uses available modeling software packages such as the MOdel for Urban SEwers (MOUSE), StormWater Management Model (SWMM) and infoWorks. Typical stormwater models conduct drainage system computations in two distinct steps (Butler and Davies, 2011). The first step is the runoff computations, which simulate the hydrological surface processes and routing of surface flow in modeled catchment areas based on precipitation input and selected hydrological model parameters and processes (Borah et al., 2009). The second step is the network computations, which use the computed runoff from step one as a hydraulic load to the collection system. Then, the model applies the selected routing model to simulate the hydrodynamics of the pipe flow (Zoppou, 2001).

Once the model is built, a procedure presented in Overton and Meadows (1976) and James (2005) is followed to calibrate and validate the model predictions.

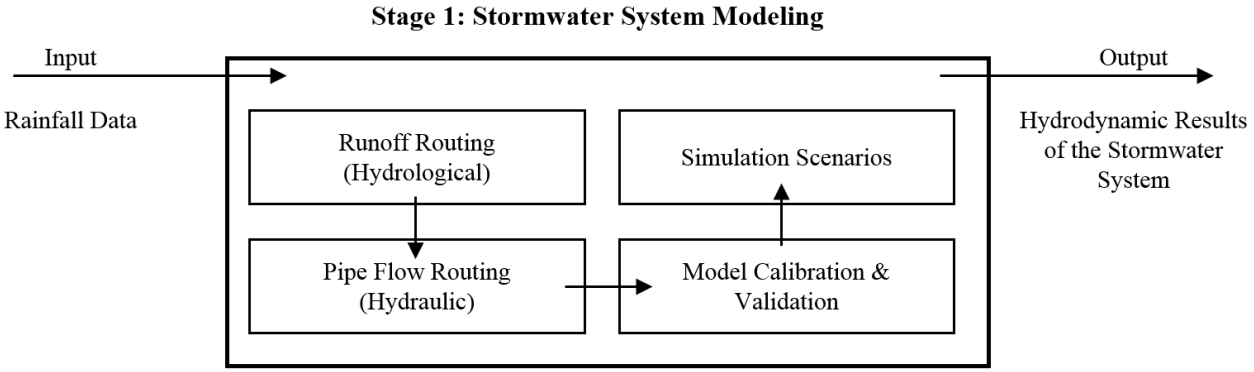

Fig. 5.2 Diagram of Stage (1) Stormwater modeling inputs, outputs and processes

In the present work, DHI's MIKE-URBAN v.2017 stormwater model was selected as the stormwater modeling tool as it can simulate both distributed rainfall-runoff and unsteady flow in pipe and channel networks (Borah et al., 2009; Carr et al., 2010). Delineation of the stormwater basin and its sub-catchments was conducted with standard geospatial analytical tools and GRASS GIS (GRASS, 2016), using data obtained from local administrators including a digital elevation model, land-use data records and stormwater network characteristics. The stormwater model was built, calibrated and validated to give acceptable predictions in terms of runoff and pipe flow routing (Supplementary Fig S.1 and S.2). The calibration involved a sensitivity analysis for 34 parameters to identify critical model inputs, and the model performance was found to be sensitive to surface roughness, imperviousness and depression storage, while changes in catchment length and infiltration parameters were relatively ineffective, see Table 5.1. The model applied kinematic wave and dynamic wave techniques for surface runoff and pipe flow routing, respectively, to achieve the best available accuracy. Storm hydrographs from the stormwater model were validated against historical data from monitoring stations. The model results were in good agreement with both recorded sewer flows in terms of model prediction errors, and correlation of both peak and low flows to observed stormwater discharges, with average $R^2 = 0.95$, NSE = 0.91, RMSE = 0.024 m^3/sec, maximum volume difference+11.3%, total volume error+8.8%, and peak volume error+9.8%. Two sample rainfall events and their associated observed and simulated pipe flows are shown in Fig. 5.3. These results compared favorably with previous studies in the literature (Carr et al., 2010; Shrestha and He, 2017).

Table 5.1 Sensitivity analysis of the stormwater model

	Percentage change in average RMSE				
Perturbation %	**-50**	**-25**	**0**	**25**	**50**
Catchment slope	-2.62	-1.02	0	0.78	1.44
Catchment length	4.46	2.01	0	-1.62	-2.80
Wetting losses	0.05	0.00	0	0.00	0.00
Depression storage (Impervious)	0.97	0.44	0	-0.17	-0.34
Depression storage (Pervious)	2.06	1.07	0	-1.10	-2.25
Manning number (Impervious all)*	-3.56	-1.32	0	0.99	1.69
Manning number (Pervious)	-2.55	-1.04	0	0.76	1.33
Horton's max capacity	0.16	0.07	0	-0.04	-0.16
Horton's min capacity*	23.72	10.58	0	-7.40	-11.27
Imperviousness ratio (Impervious flat)*	-20.49	-10.23	0	10.25	20.48
Imperviousness ratio (Impervious steep)*	-13.01	-6.27	0	6.46	12.98

(*) Indicating relatively sensitive model variables

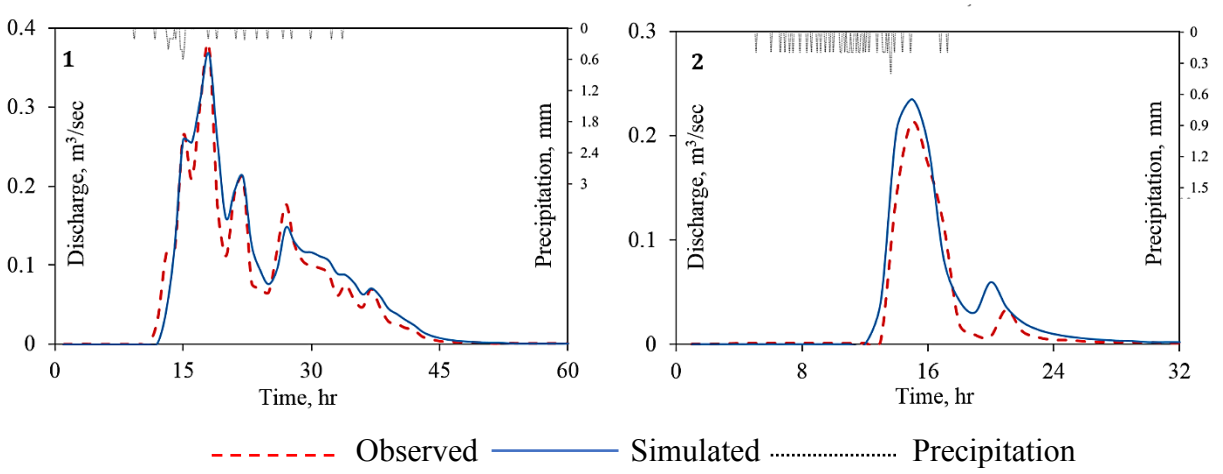

Fig. 5.3 Stormwater model inputs and outputs for two sample storm events

5.2.2 Stage 2: Stormwater quality modeling

Stormwater pollutants can be modeled with a Pipe Advection-Dispersion (AD) model that simulates the transport and dissipation of dissolved materials in the stormwater pipe-flow system (Butler and Davies, 2011). This model can simulate conservative substances as well as non-

conservative substances subject to a linear decay (Islam et al., 1997). An AD simulation must be preceded by a hydrodynamic simulation in order to provide the pipe flow velocities that are used in the one-dimensional AD equation (Islam et al., 1997; Zoppou, 2001), which is given as,

$$\frac{\partial C}{\partial t} = \frac{\partial}{\partial x}\left(D\frac{\partial C}{\partial x}\right) - \frac{\partial C}{\partial x}v - K\,C \tag{5.1}$$

where C is the concentration, K is the linear decay coefficient, x is distance, t is time, and D is the dispersion coefficient, which is considered in MOUSE as a function of the mean flow velocity (v) after Taylor (1954) (Artina et al., 2007). Not all stormwater quality models include dispersion because almost all practical examples of flow in drainage systems are dominated by advection (Butler and Davies, 2011). Hence, a simplified approach can be used to model an individual non-conservative pollutant, using a summary first-order model of the reactions (Savic et al., 2009) where,

$$\frac{dC}{dt} = -KC \tag{5.2}$$

where C is the concentration and K is the first-order decay constant.

However, the water quality modules of available commercial stormwater quality models have limited capacity to simulate degradable chemical substances (Gaafar et al., under review), since their advective-dispersion (AD) calculations only represent first-order decay with a constant decay rate, K, for the entire basin/model (Butler and Davies, 2011; Elliott and Trowsdale, 2007; Rubinato et al., 2013). This approach does not represent other available models for non-conservative pollutants such as second order, parallel first and second orders, and nth order models (Helbling and VanBriesen, 2009; Kohpaei et al., 2011); further, these models typically omit temporal and spatial variations of the decay coefficients (Gaafar et al., under review; Kohpaei et al., 2011; Zhang et al., 2018b). Therefore, the suitability of the available built-in modules depends both on the pollutant under consideration and the acceptable level of accuracy.

In this study, the Variable Decay Coefficient Simulator (VDCS) was used to model stormwater quality (Gaafar et al., under review). The VDCS was developed in Python and validated using results from water quality simulations of MIKE URBAN and a field sampling program. It

simulates the dissipation of point- and nonpoint pollution sources in water distribution and drainage systems, and can simulate different decay orders as well as account for the temporal and spatial variability of decay coefficients. These capabilities specifically suit the simulation of monochloramine decay, as discussed later in Section 5.3.2, since chloramine exhibits spatio-temporal changes in its decay rates (Zhang et al., 2018b). The main structure of the stormwater quality model is shown in Fig. 5.4.

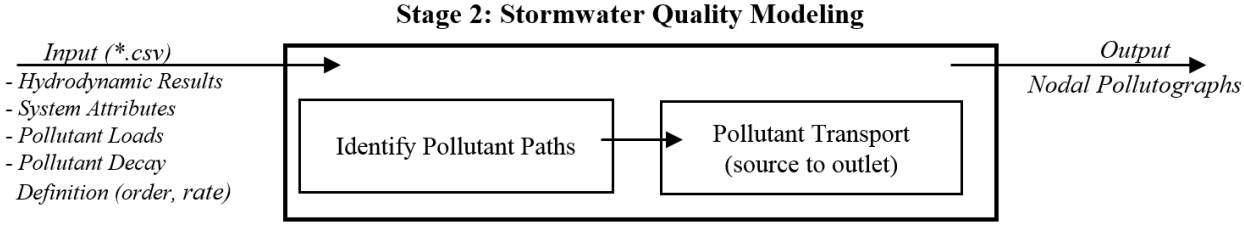

Fig. 5.4 Diagram of Stage (2) Stormwater quality modeling inputs, outputs and processes

The four basic inputs to the VDCS module are: (i) the drainage system characteristics, (ii) pollution data such as introduction points and concentration time series, (iii) data for defining the modeled substance, such as initial concentrations, decay order, and decay coefficient variability, and (iv) results of the hydrodynamic simulations from stage 1. The VDCS model accept inputs in spreadsheet format which makes the model sufficiently flexible to support simulation results from any stormwater model. Next, VDCS utilizes the system characteristics dataset to identify the pollutant path from introduction points to the system outlet and then computes the mass flux at each node using the previously-defined decay order and coefficients. Model outputs are a set of longitudinal concentration profiles and pollutographs at points of interest, most likely control structures or storm sewer outfalls. Further details on the VDCS model structure and computations are available from (Gaafar et al., under review).

5.2.3 Stage 3: Stormwater quality mapping

The third stage of the framework is the development of water quality maps for stormwater pollutants, based on pollution loads from stage 2. To develop standalone concentration maps, simulated pollutant loads are first exported to a GIS-application tool as data records at specific spatial locations defined by longitudes and latitudes in the stormwater network (Ellis et al., 2012). Many GIS-applications provide built-in groups of widely-used mapping models, such as empirical

Bayesian Kriging, radial basis functions, kernel interpolation with barriers and inverse distance weighted models (Nas and Berktay, 2010; Sahu, 2012; Xie et al., 2011). From the imported data values, these models have different approaches to increase the number of records required for accurate mapping in various water resources management applications such as flood risk, natural hazard, groundwater vulnerability and environmental assessment maps (Aydi, 2018; Jiang et al., 2012; Mahmoud, 2014; V. G. Mitchell et al., 2007; Nath et al., 2018; Salman et al., 2019). Fig. 5.5 presents the inputs, outputs and processes of the stormwater quality mapping stage.

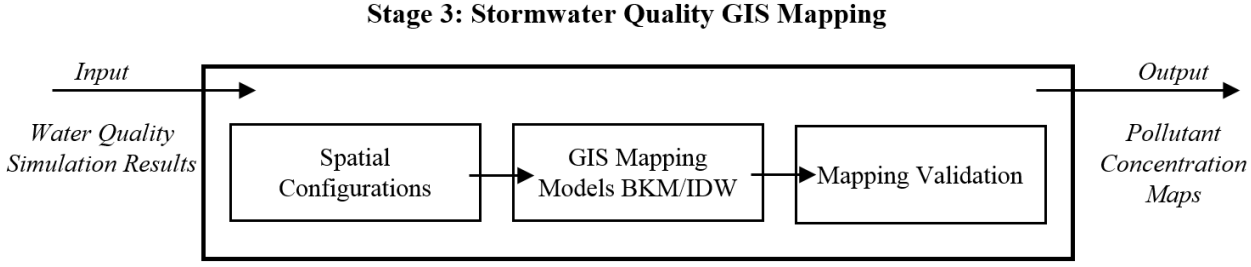

Fig. 5.5 Diagram of Stage (3) GIS-based stormwater quality mapping

In this work, the focus here is on the Inverse Distance Weighted (IDW) and the Bayesian Kriging Model (BKM) modules. The two methods are widely applied for geostatistical analysis (Roy et al., 2018; Sahu, 2012), for soil, air and water quality mapping with high prediction accuracy (Leggett and Bockstael, 2000; Matějíček et al., 2006; Nas and Berktay, 2010; Xie et al., 2011). IDW is a deterministic method, which calculates the concentration at a specific location (L_0) based on the surrounding concentration values as follows,

$$\hat{C}(L_0) = \sum_{i=1}^{m} W_i C(L_1) \tag{5.3}$$

where m is the number of chloramine concentration points, $C(L_1)$, surrounding chloramine concentration locations; W_i is the assigned weight to each measured chloramine concentration. This weight can be determined using the following formula,

$$W_i = \frac{S_{i0}^{-p}}{\sum_{i=1}^{m} S_{i0}^{-p}} \, , \sum_{i=1}^{m} W_i = 1 \tag{5.4}$$

where S_{i0} is the distance between the predicted concentration location, s_0, and the measured concentration, S_i, and p is a parameter that influences the weighting of the measured concentration location.

An alternative is the Bayesian Kriging Model (BKM), which is based on statistical models that include autocorrelation between the measured concentrations. This method can successfully generate prediction maps, provide the accuracy of the predictions, and is more accurate than other kriging methods because it accounts for the uncertainty of semivariogram estimation (Rossi et al., 2018; Roy et al., 2018; Sahu, 2012; Shakeel et al., 2014). In the present study, the unknown chloramine concentration value $f(x)$ at an arbitrary location x is assumed to be a probability of a stochastic function $F(x)$ (i.e. VDCS concentration values). Subjective probabilities are $s(x)$, and their random function is $S(x)$. The first two moments of $S(x)$ are a priori, where $E[S(x)] = \mu_S(x)$ and $Cov[S(x+h), S(x)] = C_S(x+h, x)$, where h is the variogram lag distance between each two points. The covariance can depend on both points $(x + h)$ and (x); therefore, the variogram function for the subjective probabilities can be defined as follows,

$$\gamma_S(x+h, x) = \frac{1}{2}[C_S(x,x) + C_S(x+h, x+h)] - C_S(x+h, x) \tag{5.5}$$

The conditional variogram of $F(x)$ can be expressed as,

$$Var\big[\big(F(x+h) - F(x)\big)|S(x)\big] = 2\gamma_{F|S}(h) \tag{5.6}$$

If $F(x_i)$, $i = 1: n$ is the set of chloramine concentration, BKM predicts the concentration at point x_0 from the following linear estimator,

$$F^*(x_0) = \sum_{i=1}^{n} \tau_i F^T(x_i) + \mu_S(x_i) \tag{5.7}$$

where τ_i is a set of constant weights; and $F^T(x_i)$ is as follow,

$$F^T(x_i) = F(x_i) - \mu_S(x_i) \tag{5.8}$$

By applying the Lagrange multiplier, the following Bayesian kriging model was obtained (Omre, 1987),

$$\sum_{i=1}^{n} \tau_i \left[\gamma_{F|S|}(x_i, x_j) + \gamma_S(x_i, x_j)\right] + L = \gamma_{F|S|}(x_0, x_j) + \gamma_S(x_0, x_j) \tag{5.9}$$

as,

$$\sum_{i=1}^{n} = 1 \text{ with } j = 1, 2, \ldots, n \tag{5.10}$$

where L is a Lagrange multiplier. The estimation error at point x_0 is given by,

$$\sigma^2(x_0) = \sum_{i=1}^{n} \tau_i \left[\gamma_{F|S|}(x_0 - x_j) + \gamma_S(x_0, x_j)\right] - L \tag{5.11}$$

Omre (1987) suggests that an unbiased estimator for $\gamma_{F|S|}(h)$ for all lag distances can be calculated as follows:

$$\gamma_{F|S}(h) = 1/2n_h \sum_{i=1}^{n_h} \Big[(F(x_i + h) - F(x_i))^2 - \left(\mu_S(x_i + h) - \mu_S(x_i)\right)^2 - 2\gamma_S(x_i + h\,, x_i)\Big] \tag{5.12}$$

In this study, ESRI's ArcGIS v.10.3.1 Geostatistical Analyst was employed to develop stormwater quality maps. The IDW and BKM models were applied to produce comprehensive chloramine concentration maps for the study stormwater basin, which are compared and validated in Section 5.4.2.

5.2.4 Stage 4: Stormwater quality hazard mapping

Stage 3 reveals the maximum pollution concentrations from specific sources, which aids identification of worst-case scenarios and helps to keep pollutant concentrations under permissible limits. This outcome provides guidance for stormwater system operators, since regulatory agencies often set guidelines on maximum allowable concentrations, which are relatively straightforward to measure in the sewer system. However, the magnitudes of pollutant loads can vary significantly even for a single release event (He et al., 2010). Therefore, stage 4 aims to provide more insight into contamination pollutographs through an important additional parameter, the total pollutant

mass load (Bertrand-Krajewski et al., 1998). The mapping of stormwater quality hazard requires the three steps shown in Fig 5.6.

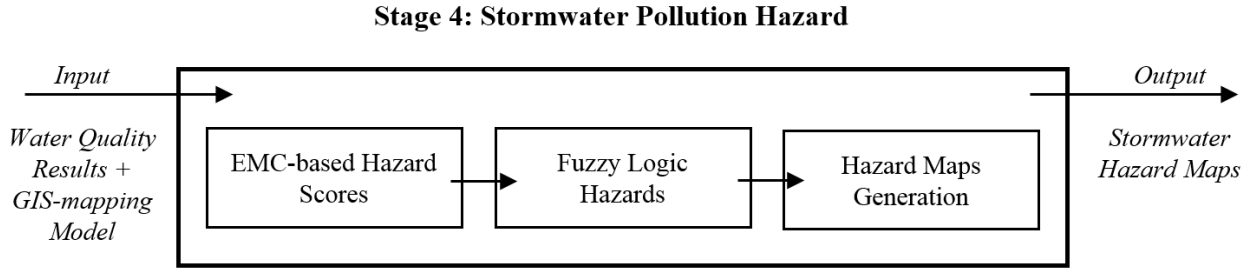

Fig. 5.6 Diagram of Stage (4) GIS-based stormwater quality mapping

First, the Event Mean Concentration (EMC) calculation provides the total mass of a chemical substance at the system outlet divided by the total stormwater volume (Mitchell, 2005) from the results of stormwater hydrodynamic and quality simulations, particularly hydrographs and pollutographs at the system outlets. EMC has been widely applied to assess a variety of pollutants in water resources systems such as total suspended solids (TSS), chemical and bio-chemical oxygen demand (COD and BOD), nitrate, nitrite and nitrogen (NO_2^-, NO_3^-, N), total Kjeldahl nitrogen (TKN), total phosphorus and heavy metals (Becouze-Lareure et al., 2019; Bian et al., 2011; Brezonik and Stadelmann, 2002; Dembélé et al., 2011; Metadier and Bertrand-Krajewski, 2012; Shrestha and He, 2017). It computes a flow-weighted concentration over the storm event duration as,

$$EMC = \frac{\sum C_i \, Q_i \, t_i}{\sum Q_i \, t_i} \tag{5.13}$$

where C_i is the pollutant concentration at time i, Q_i is the flow rate in the i^{th} interval, and t_i is the time interval (Bian et al., 2011). Applying Eq. 5.13, EMC can be then calculated for all pollutant release incidents throughout the study area. EMC values can be calculated either for all, or for only the most critical, weather conditions from the Stage 3 results.

Next, calculated EMCs can be used to generate a stormwater quality hazard score. A hazard score is a percentage value that represents the cumulative environmental risks associated with a stormwater pollutant. Scores range between 0.0 and 100, where 0.0 indicates no hazard. Simple unitless hazard scores can be developed by normalizing concentrations to their maximum,

minimum, mean or standard deviation values in the study area – see for example Mitchell (2005) and Nas and Berktay (2010). More sophisticated hazard scores can be devised by incorporating additional hazard-driving factors. Depending on the system and the pollutant under consideration, the key driving factors can be identified; common factors include proximity to specific land-uses, such as industrial or roadway, soil type, permeability, topography, curve number (CN), traffic volumes, residential density, annual rainfall and ground slope (Aydi, 2018; Nath et al., 2018; Vojtek and Vojteková, 2019). Next, a number of procedures can be applied to rank and weigh identified hazard-driving factors for pollutants, such as fuzzy logic (Pradhan et al., 2009; Yao et al., 2015), analytic hierarchy processes (Aydi, 2018) and artificial neural networks (Liu et al., 2018), in which the affecting factors can be ranked according to their relative effect of the stormwater pollutant (Salman et al., 2019).

To generate hazard risk maps in this study, two hazard assessment tools were used and compared, including the EMC-based hazard score and the fuzzy logic module in ArcGIS. In the first, calculated EMCs were used to calculate chloramine hazard-score percentages. In the second approach with fuzzy logic, the following procedure was followed in ArcGIS. First, based on available literature on chloramine dissipation and pollution susceptibility, a group of factors known to drive chloramine contamination in the sewer system was identified, relevant spatial data were collected, and then the factors were introduced into the ArcGIS environment (Aydi, 2018). Second, each hazard-driving factor is ranked with respect to their relevance to pollution hazard and level of susceptibility into classes ranging from very low to very high pollution hazard (Mahmoud and Gan, 2018), based on an extensive literature review and ranking technique described by Emrouznejad and Ho (2018). For example, different types of land-use (classes) are ranked based on their relative weight on pollutant decay**.** Third, fuzzy membership functions were used to define the individual classes in each map according to their degree of membership. The process of transforming the original input values to the 0–1 membership scale is called the fuzzification process. The classes in each map are assigned fuzzy membership values in an attribute table based on the fuzzy algebraic product operator (Pradhan et al., 2009), which is defined as:

$$\mu_c = \prod_{i=1}^{n} \mu_i \tag{5.14}$$

where μ_c is the fuzzy combination, n number of maps to be combined, μ_i the fuzzy membership function for the i^{th} map. Thus, the possibility of a particular location belonging to one set or multiple sets has only two possibilities, i.e. the location is either a member of a set or it is not. For more details, see Emrouznejad and Ho (2018), Nobre et al. (2007), and Pradhan et al. (2009).

After estimating EMC-based and fuzzy-based hazard scores values across the study area, hazard maps can be developed. A hazard map shows the spatial variation of hazard scores throughout the study area, similar to a concentration map but representing hazard scores instead of pollutant concentrations. As in Stage 3, mapping models can then be utilized to develop the final hazard map(s) for the stormwater system. Information on adopted hazard scores calculations is presented in Section 5.4.3.

5.3 Case study

5.3.1 Study area and data collection

The study area is the 30th Avenue stormwater drainage basin in the City of Edmonton, Alberta, Canada (Fig. 5.7), located between latitudes 53°25'52.4" and 53°30'2" N and longitudes 113°23'38.7" and 113°36'22.2" W, with an approximate area of 5223 ha. The area has a humid continental climate with average annual precipitation of 485 mm, as shown in Fig. 5.8(a); rainfall data are collected through a gauging network shown in Fig. 5.8 (b). The 30th Avenue basin's topographic characteristics are presented in a digital elevation model (DEM, spatial resolution of 1.5 m, resolution of topography 0.1 m) in Fig. 5.8(c). The highest point of the basin is 720 m above sea level. Groundwater resources are very limited. Land-use types, ground slopes and identification numbers of different stormwater catchments are shown in Fig. 5.8(d-e-f),

respectively, based on data obtained from the City of Edmonton online portal (www.data.edmonton.ca).

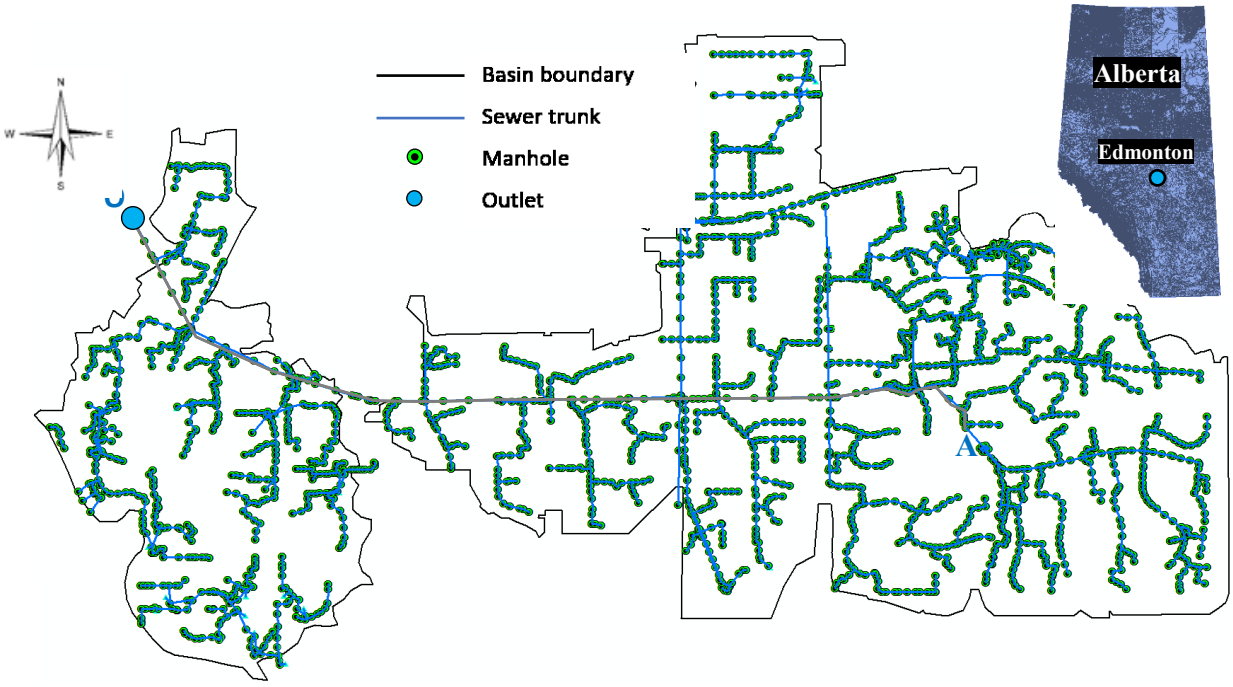

Fig. 5.7 30th Avenue stormwater basin and main components of the sewer system, with the main trunk highlighted between the start point (A) and the outlet point (O)

475mm 500mm

(a) Annual rainfall (mm/yr)

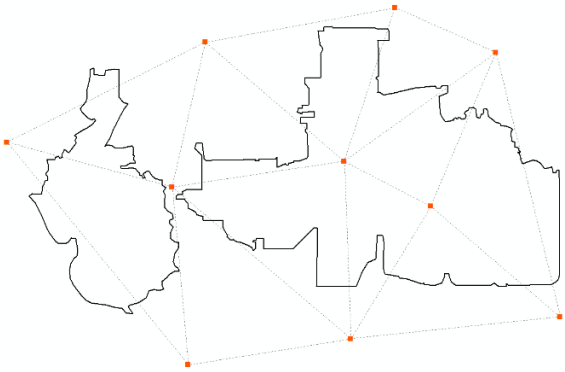

Rain gauge

(b) Rain gauge distribution

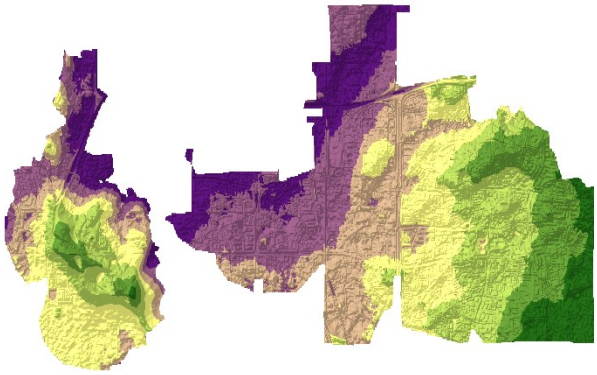

645m 720m

(c) Digital elevation model

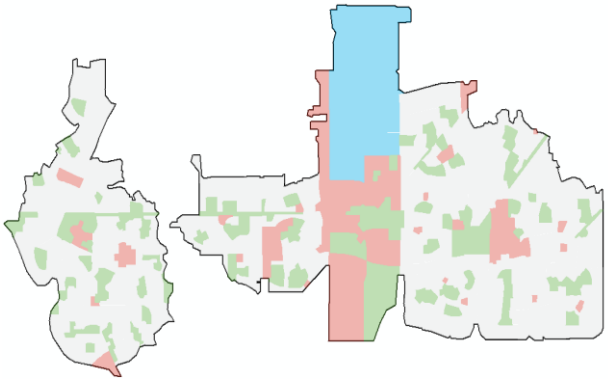

Residential Commercial
Park Industrial

(d) Main Land-use type

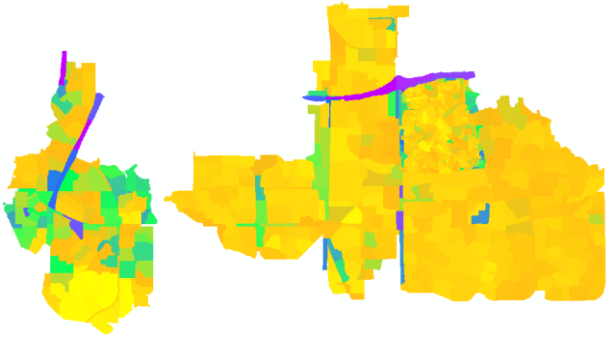

1% 18%

(e) Ground slope

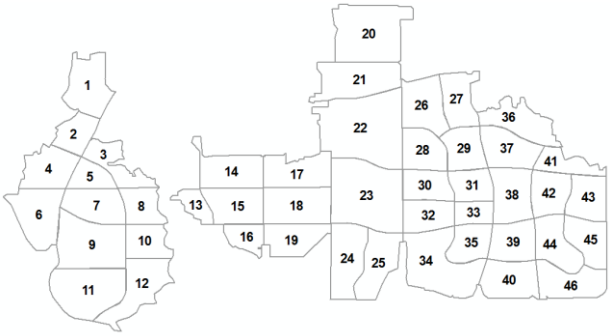

(f) 30th Avenue neighborhoods ID (see also Table E1 in the appendices)

Fig. 5.8 Characterization of the study area (30th Avenue basin)

To validate the stormwater model, additional data sets were collected: (i) temporary pipe flow monitoring for the summer seasons of 2014-2017 at each land-use type (ii) long-term pipe flow

records from permanent metering stations; and (iii) long-term rain gauge data for the stormwater basin. Additional data such as aerial images were obtained from the City of Edmonton, and stormwater network layouts and their attributes were acquired from the DRAINS database.

5.3.2 The Pollutant: Monochloramine

To demonstrate the risk assessment framework, monochloramine (NH_2Cl) was selected as the case study pollutant. NH_2Cl is the dominant disinfectant in chloramination (Zhang et al., 2018a), a drinking water treatment approach used by approximately 30% of U.S. water suppliers as of 2008 (Maestre et al., 2016). As compared with chlorination, NH_2Cl has a desirable longer-lasting residual that prolongs its disinfection efficiency (WHO, 2004). However, chloramines pose environmental concerns as treated drinking water may find its way to the aquatic water system through storm sewers (Zhang et al., 2018c), which can collect chloraminated water from different outdoor tap water uses such as lawn watering, car and driveway washing, pool emptying, street cleaning, firefighting, construction activities, and industrial activities (Balling et al., 2008; Mayer and DeOreo, 1998; Zhang et al., 2018a). In Edmonton, about 200 storm sewer outfalls discharge collected stormwater effluents to the North Saskatchewan River, many of which have no end-of-pipe treatment (CoE, 2013). The Canada-wide Strategy Standard recommended a lower permissible concentration of 0.02 mg/L (CCME, 2009) in surface waters, a level that is a source of concern since recent field sampling programs in Edmonton's storm sewers have shown discharge concentrations as high as 0.77 mg/L (Zhang et al., 2018c).

Few studies have focused on chloramine dissipation in storm sewer networks (Zhang et al., 2018c), and effective simulation tools are lacking because of the complexity and uncertainty associated with the reactivity between chloramines and a large group of other stormwater constituents (Gaafar et al., under review). The decay of both chlorine and chloramine disinfectant in water networks is generally modeled with first-order kinetics (Ahn et al., 2012; Fisher et al., 2009; Savic et al., 2009) as,

$$C_{DS} = C_{US}\, e^{-Kt} \tag{5.15}$$

where C_{US} and C_{DS} are the concentrations at upstream and downstream ends of a sewer pipe respectively, K is the decay coefficient, and t is the travel time through the pipe. However,

chloramine decays according to several pathways including auto-decomposition, and chemical and biological reactions (Ahn et al., 2012). Important parameters include temperature, pH, natural organic matter, nitrite, flow velocity, biofilm, corrosion and microbial growth (Moradi et al., 2017; Sathasivan et al., 2008; Zhang et al., 2018c), the combined effects of which result in varying chloramine decay coefficients both spatially and temporally (Gaafar et al., under review). A combination of field sampling results, laboratory experiments (Zhang et al., 2018c, 2018a), and models (Zhang et al., 2018b) reveals that the spatial- and temporal variability of chloramine decay coefficients can be described with the following relationship,

$$K_{t,i} = \frac{1}{\alpha\, t + \beta} * (f_i) \tag{5.16}$$

where $K_{t,i}$ is the decay coefficient at time t for land-use i, f is a land-use dependent coefficient described in Zhang et al. (2018b), t is the discharge time in minutes, $\alpha = 1.73$, and $\beta = 1.0$.

A number of land-use categories were selected for the case study, (1) residential areas, for outdoor carwash and lawn watering, (2) parks, for denser and higher application of irrigation compared to residential areas, (3) commercial areas, for car washing, and (4) industrial sites, for pressure vessel fabrication. Details of the selection process are provided by Gaafar et al. (under review) and Zhang et al. (2018c). Applying the relationship in Eq. 5.16 for each land-use produces chloramine decay curves for each type, as shown in Fig. 5.9. At the beginning of release events, decay rates were high and then decreased over time, with the highest decay rate observed in residential and industrial areas and somewhat lower rates found in commercial and park areas. More than one hour after release, similar decay rates were observed for the four land-use types.

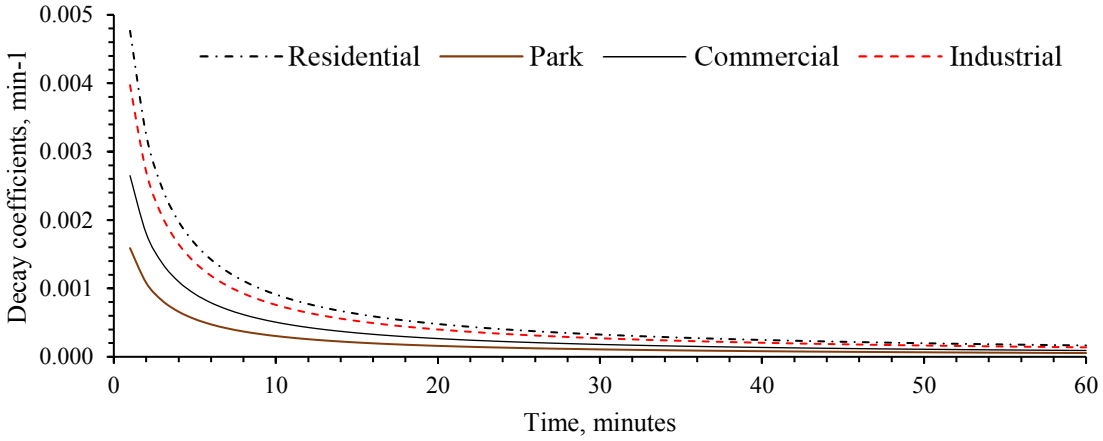

Fig. 5.9 Spatial and temporal variability of chloramine decay rates

To simulate chloramine dissipation and resulting concentrations in the stormwater system – accounting for variability in chloramine decay coefficients over the simulated period – the VDCS model was used to conduct the stormwater quality simulations. Sample VDCS chloramine dissipation outputs are shown in Section 5.4.1.

5.3.3 Simulation scenarios

To provide the stormwater quality hazard maps in a practical, useful format that covers both wet and dry weather conditions (here defined as zero precipitation preceding and during the simulation period), standard wet weather conditions were selected in consultation with Drainage Services personnel at the City of Edmonton. Specifically, three typical design storm hyetographs with return periods of 2, 5 and 10 years were developed, using published IDF curves for Edmonton (Government of Canada, 2015) and the alternating block method (Chow et al., 1988). Fig. 5.10 shows the three hyetographs. All four weather scenarios were defined in the MIKE URBAN stormwater model. Further, based on chloramine-release characteristics described by Zhang et al. (2018b), one incident of a chloramine-containing release was also simulated to represent a hypothetical fire hydrant flow of 150 m^3/sec over 1 hour. Such flows were then simulated individually for multiple different locations in the 30th Avenue stormwater basin to represent realistic scenarios of chloramine release. Maximum initial concentrations of chloramine were set to 2.0 mg/L as per the guidelines of the local water utility and field measurements (Zhang et al., 2018b). In addition to the three design storms, higher return periods were also examined; however,

these storms generated chloramine concentrations below the permissible limit (<0.02 mg/L) throughout the entire stormwater entire basin, and so were omitted.

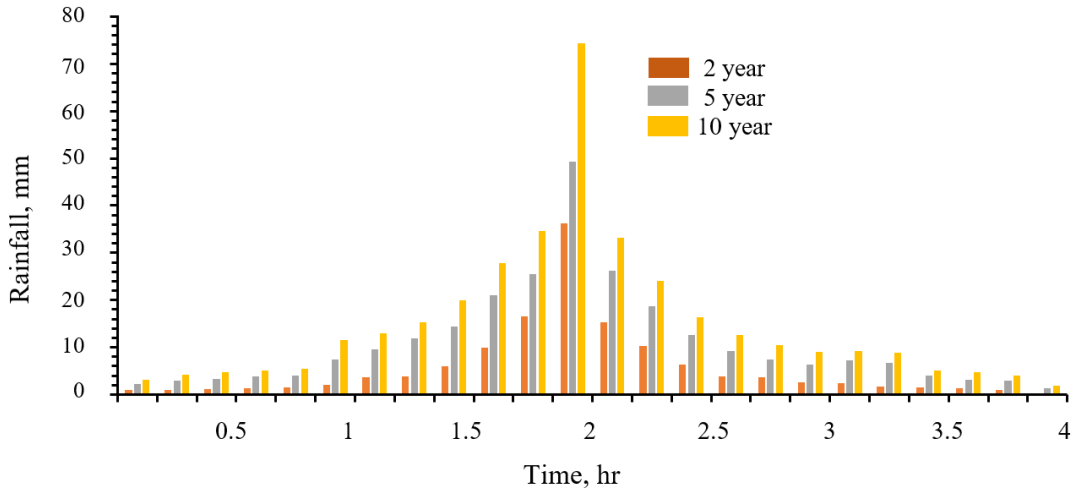

Fig. 5.10 Design storm hyetographs

5.4 Results and analysis

5.4.1 VDCS stormwater quality results

As Stage 2 of the 4-stage-3-model framework, this section describes the results of the stormwater quality simulations conducted with the VDCS models and applies the procedures described in Section 5.2.2. The example results focus on a dry weather flow (DWF) simulation of point-source chloramine pollution, which is introduced at point (A) and then travels downstream through points (B), (D), (J) and (O), along the main trunk (Fig. 5.7). The inflow has a constant chloramine concentration of 2.0 mg/L over a period of 1 hour. As the flow travels through the sewer system, Fig. 5.11(a) shows decreasing chloramine concentrations, with each curve showing the concentration at a different manhole, from the standard 2.0 mg/L at point (A) to 0.25 mg/L at the system outfall, point (O), twelve hours after the release. The concentration at the outlet is significantly higher than a safe chloramine discharge concentration.

As can be seen from Fig. 5.11(a), concentrations decrease slightly with increasing travel time in the main trunk. The longitudinal chloramine concentration profiles in Fig. 5.11(b) show similar trends with distance. The x-axis of this figure represents the length of the main trunk of the sewer system, while each time series shows the concentration for a specific time segment measured from

the beginning of the chloramine release at point (A) to its discharge at point (O). These two figures show the variation of chloramine concentrations spatially and temporally within the sewer system.

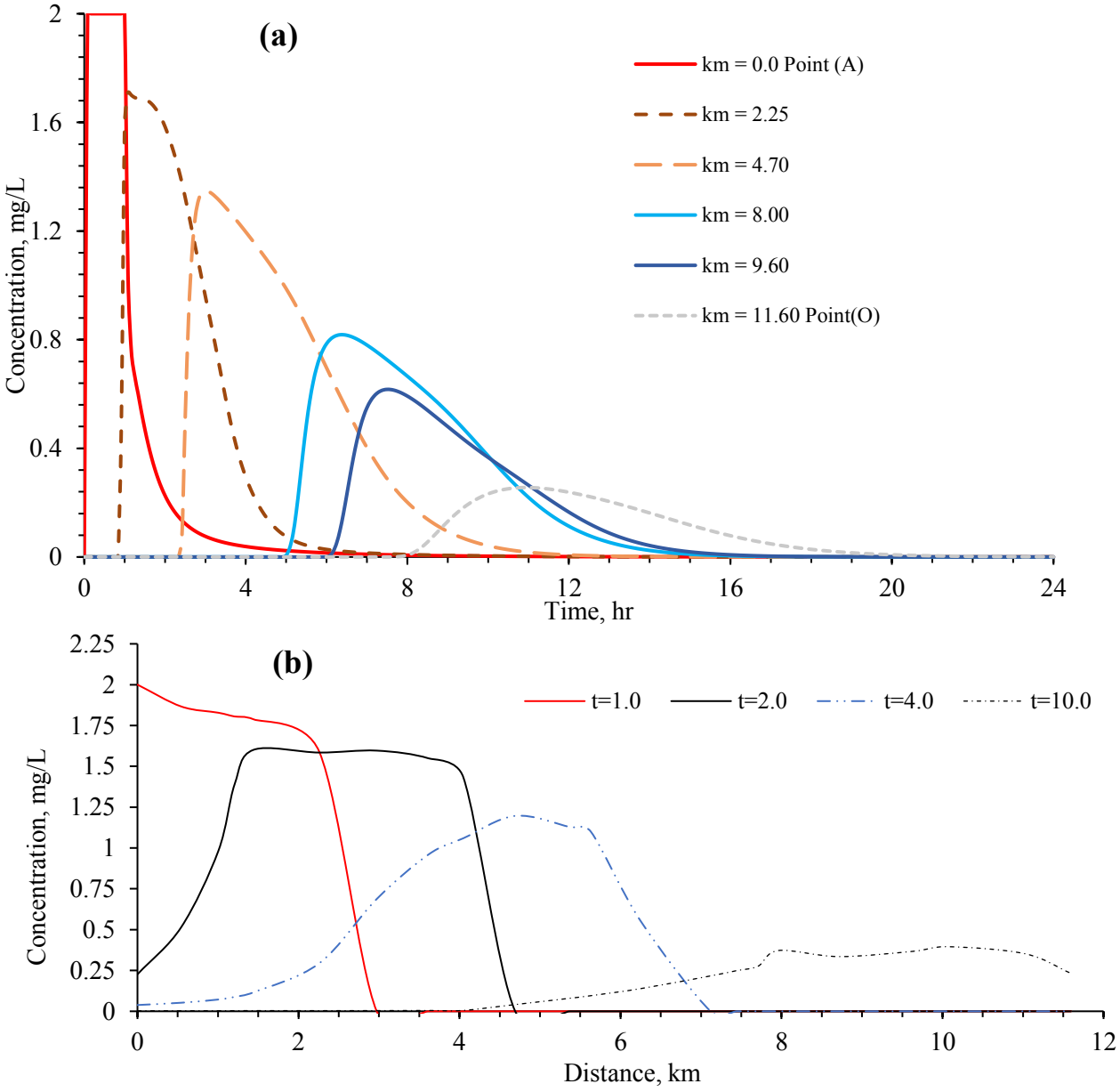

Fig. 5.11 VDCS outputs for a sample chloramine release at the first point on the system's main trunk, (a) pollutographs at different distances downstream from the introduction point (c, t), and (b) longitudinal chloramine concentration profiles along the main trunk line (c,x)

5.4.2 Chloramine concentration maps

Based on the chloramine simulations for the 30th Avenue basin, a geostatistical analysis was conducted as Stage 3 of the framework, as described above in Section 5.2.3. IDW and BKM mapping models were used to map the spatial distribution of chloramine concentration data linked to the stormwater system database built in ArcGIS. The simulated pollutographs from VDCS for all system nodes (manholes and outlets) were exported in spreadsheet (csv) format from Python and then converted into a GIS-compatible format (see Fig. 5.4). These data sets consisted of four different sub-datasets: one for the dry weather conditions, and three for wet weather conditions (2-year, 5-year, and 10-year events).

The concentration maps produced with the BKM and IDW methods are shown in Fig. 5.12 and 5.13, respectively. Although the mapping results generally agree, concentration values for the IDW method were lower than those predicted by the BKM method in some locations. Therefore, we performed cross-validation analyses in ArcGIS to check the accuracy of the concentration maps against point values obtained from VDCS. Fig. 5.14(a) indicates that the BKM methods successfully predicted the concentrations at all the manholes, while the IDW failed at some of them particularly around peak values. For instance, as shown in Fig. 5.14(b), the concentrations predicted by the IDW for manhole numbers 400 to 600 were considerably lower than both the actual values and the BKM predicted values.

The chloramine concentration map for DWF, Fig. 5.12(a), shows the spatial distribution of predicted concentrations from the BKM method. In general, the chloramine concentration over the entire basin is higher than the safe range, with values from 0.076 mg/L at the farthest point downstream to 1.79 mg/L at the upstream end. Fig. 5.12(a) also shows very high concentration zones in the western part of the basin, mainly in neighborhoods 1 to 16 (refer to Fig. 5.8(f) and Supplementary Table 1). In contrast, the concentration map for the 2-year event shows that chloramine concentrations fall within the safe range for 60% of the basin, while the remaining 40% has concentrations from 0.02-0.1 mg/L. This decrease in concentration results from the introduction of wet weather flows in the model, which cause the concentration to decrease with the increase in rainfall. The 5-year event-based concentration map shows a further decline in the concentration in the majority of the 30th Avenue stormwater basin, with about 80% of the basin

falling within the safe range. Areas with higher concentrations (0.02-0.05 mg/L) are mainly in the western end of the basin in neighborhoods 1 to 7, close to the system outfall, see Fig. 5.12(c). Finally, in the 10-year event, the entire basin falls within the safe range, as shown in Fig. 5.12(d).

Overall, these findings reveal that even in the wet weather conditions of 2- and 5-year events, the concentration is higher than the safe range in the northwestern part of the basin. Further, neighborhoods 1 to 7 fall within the very high-risk zones under all weather conditions except for the 10-year event. All these high-risk neighborhoods are in close proximity to the single system outfall to North Saskatchewan River. Note that the distribution of chloramine concentrations within the study area is affected by the fact that the system has a single outfall at the northwest corner, which causes concentrations to decrease as they move upstream from the outfall. In a stormwater system with multiple outlets, pollutant concentrations could vary in a number of different directions, resulting in more complicated dissipation patterns.

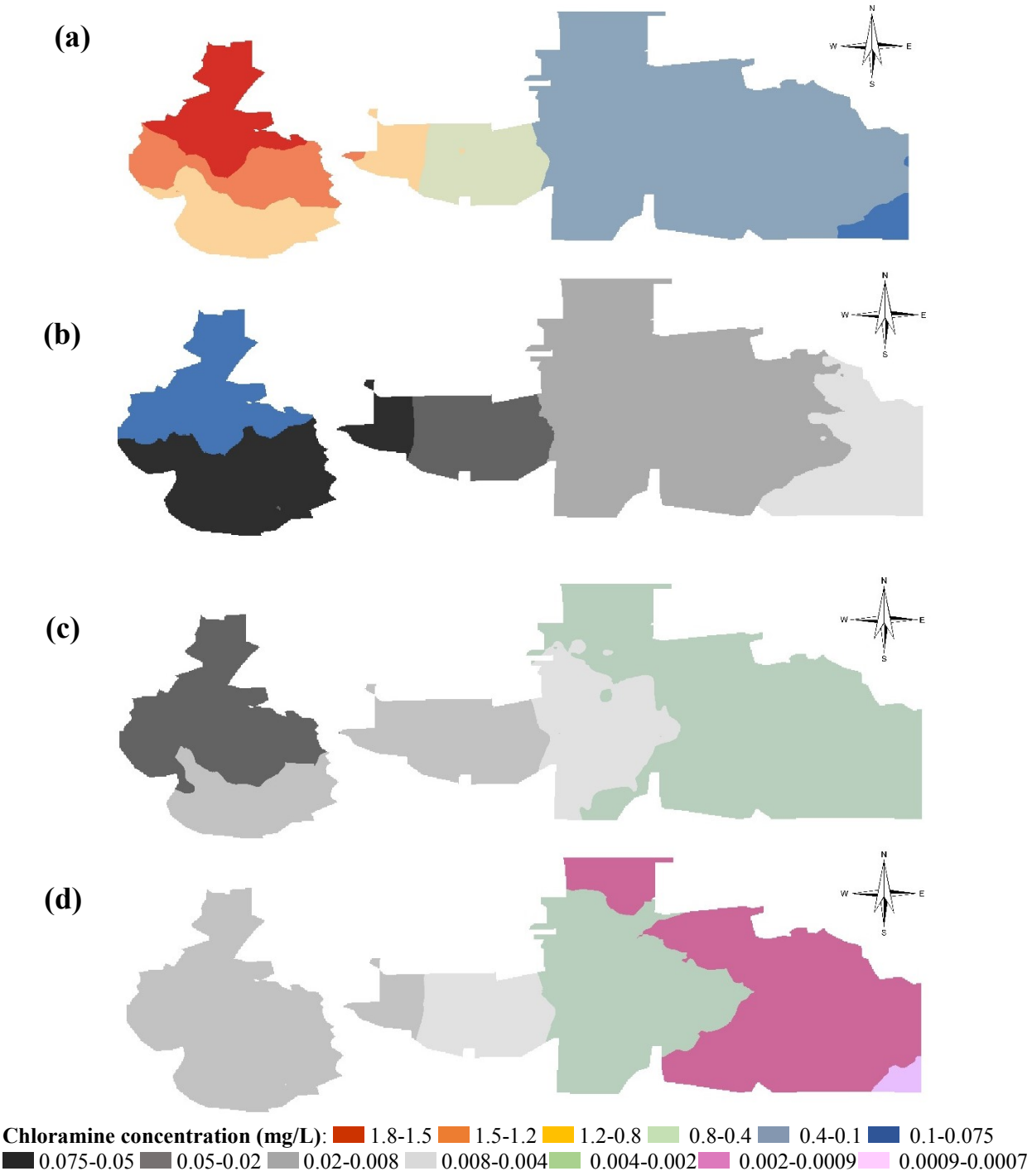

Fig. 5.12 Concentration maps based on BKM method
(a) dry conditions, (b) 2-year event, (c) 5-year event, and (d) 10-year events

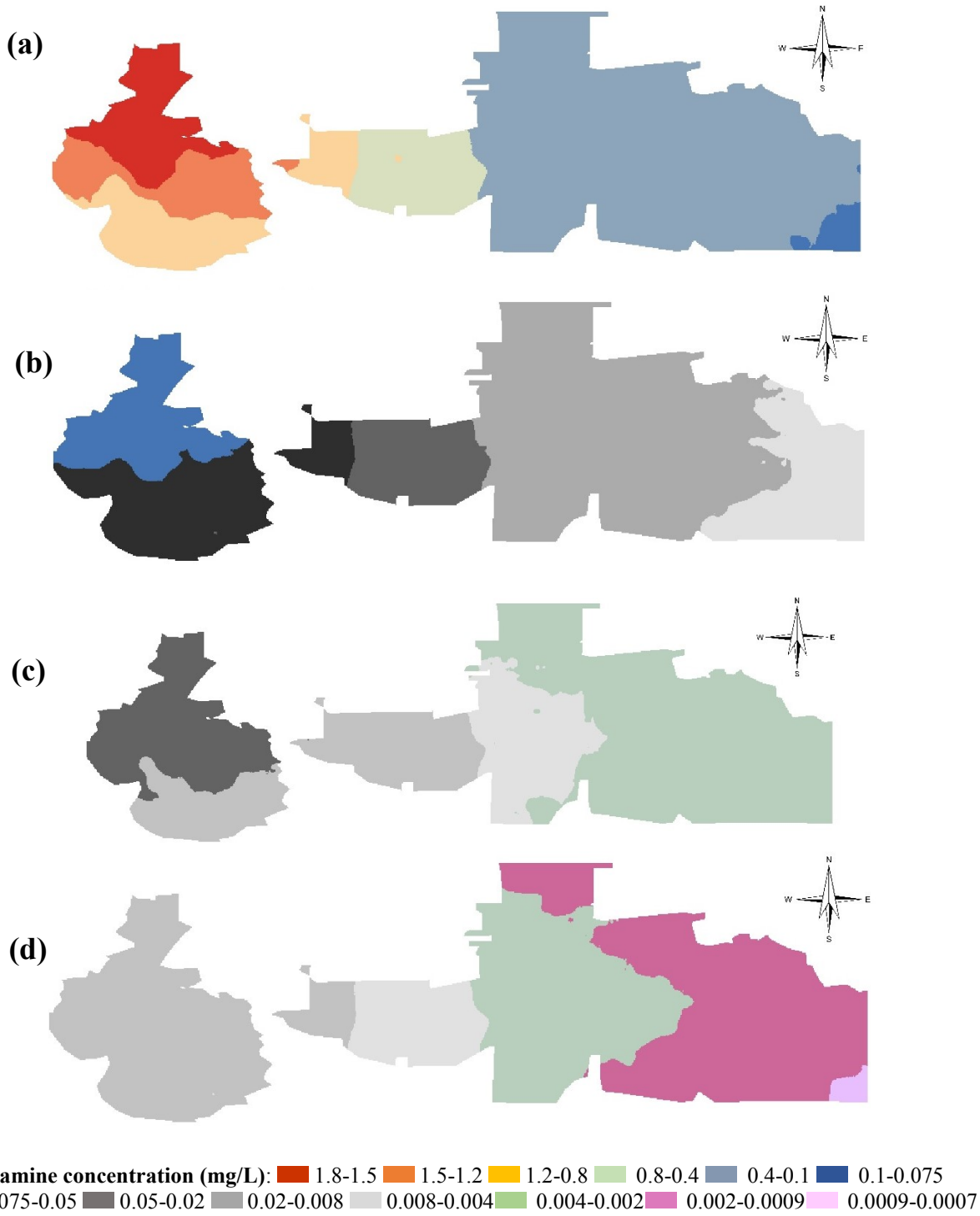

Fig. 5.13 Concentration maps based on IDW model
(a) dry conditions, (b) 2-year event, (c) 5-year event, and (d) 10-year event

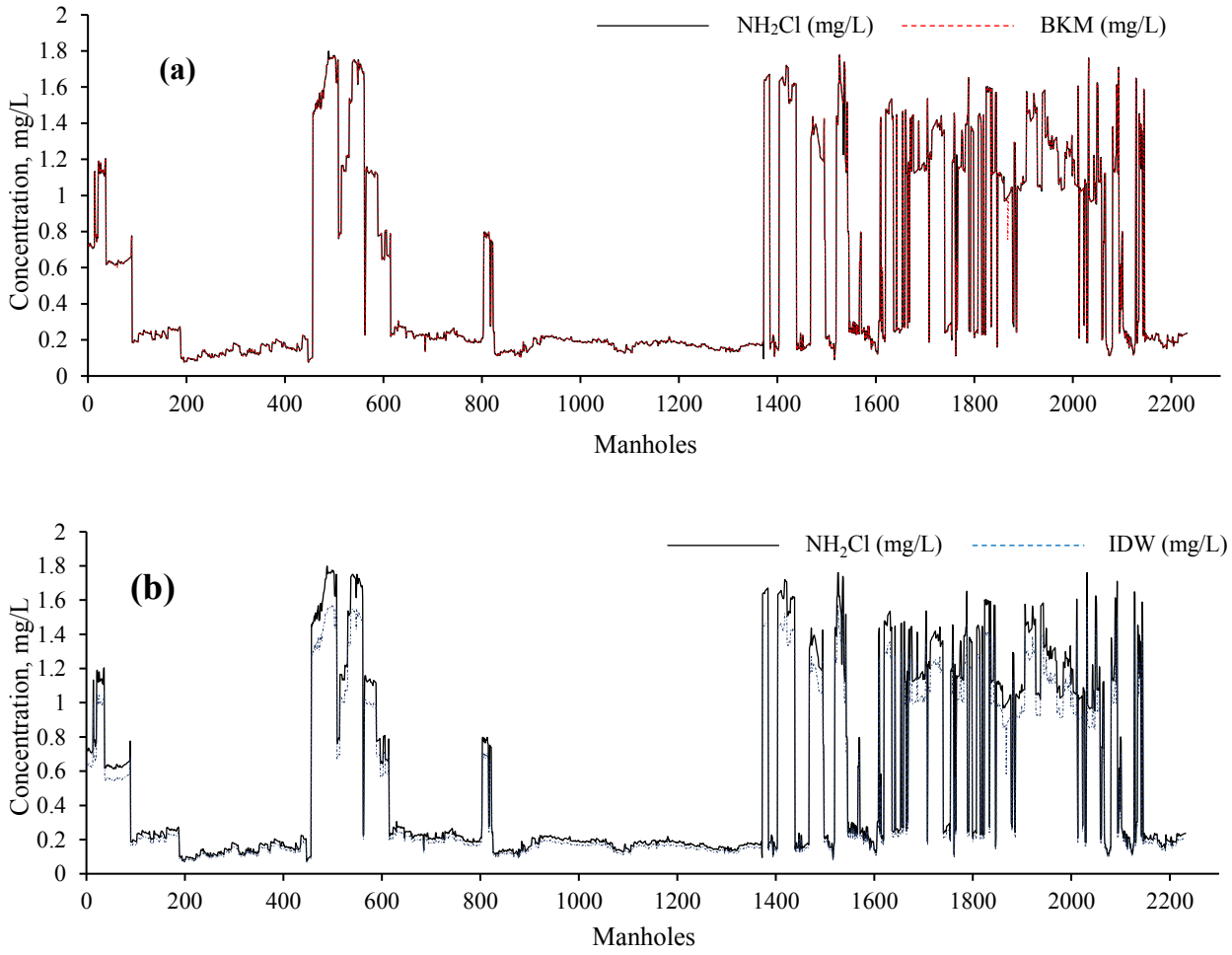

Fig. 5.14 Validations of predicted concentrations for the (a) BKM and (b) IDW models, as compared with VDCS results

5.4.3 Hazard maps

Following the methods presented in Section 5.2.4 for Stage 4, event mean concentrations (EMC) were calculated for all chloramine point-sources considering only the DWF, since it was responsible for the highest chloramine concentrations and associated contamination risk. A simple approach to calculate hazard scores for all chloramine point-sources was adopted, in which the EMCs calculated were normalized by dividing their values by the maximum EMC value encountered in the 30th Avenue basin. Note that these EMC values incorporate a number of factors, including pollution concentration and total mass, stormwater volume, effect of land-use type on chloramine decay rates, and characteristics and layout of the sewer system. Next, the hazard score

percentages over the basin area calculated from the EMC results were imported into the ArcGIS geostatistical analyst to develop a chloramine hazard map with the more accurate BKM model. To aid hazard map interpretation and application, an average hazard score for each sub-catchment was calculated using the arithmetic mean of all hazard values in its smaller constituent catchments. The resulting chloramine pollution hazard map for the 30th Avenue stormwater basin is presented in **Error! Reference source not found.**(a), in which chloramine hazard scores were categorized into t he following hazard ranges based on available information in the literature (Hammouri and El-Naqa, 2008; Mitchell, 2005; Salman et al., 2019; Zhang et al., 2018c): very low (<15), low risk (15 to 30), moderate risk (30 to 50), high risk (50 to 85), and very high risk (>85).

The EMC-based hazard map presents a similar pattern to that of the concentration maps, since the system has only one outlet to the northwest of the system, as shown in **Error! Reference source n ot found.**(a). Approximately 4%, 6%, 14%, 45%, and 51% of the basin were found to be in the very high, high, moderate, low, and very low areas, respectively. Neighborhoods 1 to 7 were all in very high to high risk pollution hazard areas, while industrial land-use areas in neighborhoods 20 to 22 were mainly in very low risk areas, refer to Fig. 5.8(f). Northeastern and southeastern parts of the basin were in no chloramine pollution risk areas: neighborhoods 27, 36, 40, 41, 45 and 46.

Clearly, the distance between the point-source location and the outlet played the main role in determining the total chloramine mass at the system outfall. However, hazard maps based on EMCs produce slightly different spatial distribution patterns from chloramine concentration maps, because the former accounts for the total pollutant mass while the latter shows the maximum concentration reached at each manhole, irrespective of flow volume. The difference between the measures is most obvious in northwestern sub-catchments close to the system outfall, which have higher concentration loads than areas closer to the upstream ends. This is because the variance between EMC and the maximum concentration values is significantly larger close to the system outfall than farther upstream in the system, where EMC and the maximum concentration are typically closer in magnitude.

For fuzzy-based hazards, using available literature on chloramine decay and previous findings of this study, a group of pollution susceptibility factors were identified including EMC values, land-use types, annual average rainfall, ground surface slopes, property assessment values, spatial variations of chloramine decay rates, density of impervious areas and proximity to the sewer network. Each hazard-driving factor had five possible levels: (1) very low, (2) low, (3) moderate, (4) high, and (5) very high pollution susceptibility, ranked according to their relative importance to pollution hazard. The assigned susceptibility factors and explanations are shown in **Error! R eference source not found.**. Next, as discussed in Section 5.2.4, fuzzy memberships were used to define the individual classes in ArcGIS to generate the fuzzy-based hazards. **Error! Reference source not found.**(b) shows the fuzzy-based hazard map for the 30th Avenue stormwater basin. Approximately 13%, 19%, 22%, 34%, and 12% of the basin were found to be in the very high, high, moderate, low, and very low areas, respectively.

Table 5.2 Fuzzy membership classes for chloramine pollution thematic layers

Factor	Categories	Index	Comment
Event mean concentration, mg/L	Very low	1	Hazard severity increases as EMC increases. Classes were defined similarly to EMC-based hazard scores.
	Low	2	
	Moderate	3	
	High	4	
	Very high	5	
Annual rainfall, mm	Moderate	3	Simulation results in section 5.4.2 revealed that more rainfall causes more dilution to chloramine pollution and consequently less risk.
	High	2	
	Very High	1	
Land-use type	Residential	4	Based on field sampling program over two summer seasons at 8 sampling locations covering the four land-use types in the study area (Zhang et al., 2018c).
	Park	3	
	Commercial	3	
	Industrial	2	
Surface slopes, %	< 3	1	Travel times over steeper grounds are much shorter, generating less decay and hence higher pollution risk (cf. the Maceio, Brazil, study conducted by Nobre et al., 2007).
	3 - 6	2	
	6 - 9	3	
	9 - 12	4	
	> 12	5	
Chloramine decay rates	Low	2	Based on chloramine decay curves presented in Section 5.3.2, and values from the literature (Gaafar et al., under review; Zhang et al., 2018b), the decay rates per land-use from high to low were residential, park, commercial and industrial, respectively. The highest decay rate was associated with the lowest hazard and vice versa.
	Moderate	3	
	High	4	
	Very high	5	
Property assessment value, $	<$200k	1	Higher property assessment values are known to be associated with relatively larger lawn and garden areas, and potentially higher chloramine pollution (Al-Kofahi et al., 2012; Gaafar et al., under review; Zhang et al., 2018c).
	$200-$400k	2	
	$400-$600k	2	
	$600-$800k	4	
	>800k	5	
Proximity to the drainage network, m	<100	5	Areas closer to the sewer system can release pollutants faster into the system with higher pollutant concentrations and therefore pose higher risk. See more information at Aydi (2018).
	100-200	3	
	>200	1	
Density of impervious areas	Low	2	Areas with higher imperviousness pose higher pollution risk, see Zoppou (2001) and Lee et al. (2010).
	High	4	

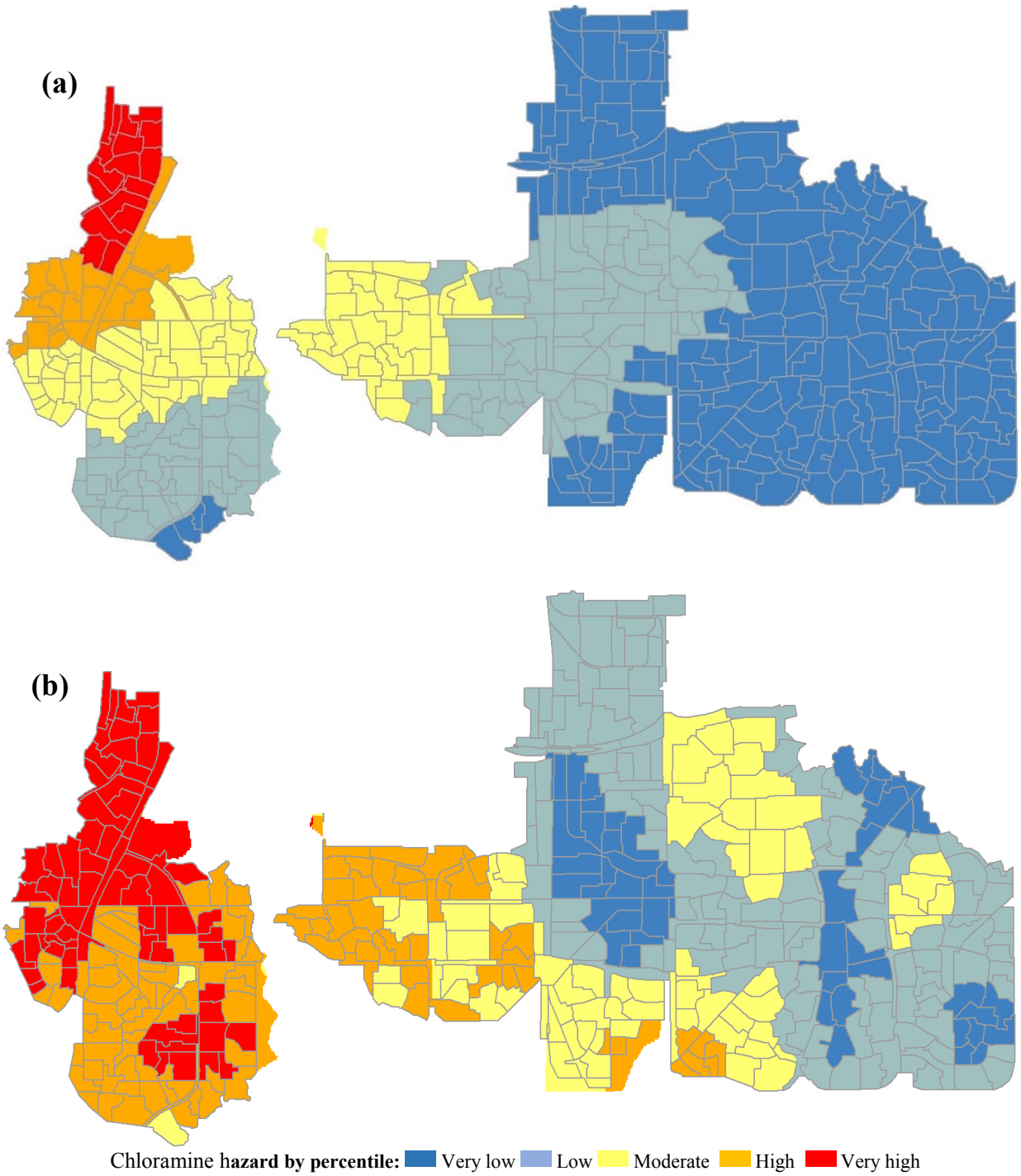

Fig. 5.15 Chloramine pollution hazard map for study area (numbers indicate neighbourhoods) (a) EMC-based and (b) Fuzzy-based

The inclusion of more factors in the fuzzy-based hazard map resulted in greater variation in the spatial pattern of hazard categories, as shown in **Error! Reference source not found.**(b). Mainly affected by land-use types, EMC values and rainfall density, neighborhoods 1 to 5 retained the very high hazard category. Similarly, a cluster of central neighbourhoods, 13 to 17, and eastern neighbourhoods, 42 to 46, retained their general results as subject to high and low hazards, respectively. However, in comparing the EMC-based and fuzzy-based maps, some clusters exhibit more significant changes. For neighbourhoods 9 to 10 in the western part of the basin, the hazard assessment changed from low to high, mainly because of high property assessment values with larger lawn areas and higher potential chloramine inputs. Neighborhoods 24 to 29, 34 and 35 had higher hazard assessments because of higher park areas and a denser stormwater network.

Uncertainties are inherent in all hazard assessment techniques (Nobre et al., 2007); therefore, further investigation would help to provide qualified or comparative analyses between hazard map results. Researchers have attempted to reduce these uncertainties in pollution hazard assessment by accounting for larger numbers of pollution driving factors in fuzzy-based approaches as compared with EMC-based hazards, which mainly focus on pollutant decay mechanisms. Fuzzy-based maps can help to identify potential "hot spots" or assess remediation measures at local locations in the network. To validate the results of the developed hazard methodologies, local authorities should test the accuracy of those two models through collecting extensive pollutant data under varying conditions.

Decision makers should use both concentration maps and hazard maps, since each provides a different perspective on pollutant introduction to surface waters. On one hand, concentration maps can help to evaluate acute changes in the pollution load, and in turn, the need for pollutant control measures in compliance with the local regulations. Because of the nature of the regulations, system operators need to anticipate high concentration incidents regardless of their mass loads. On the other hand, hazard maps can be more important to environmental pollution control and management, since the highest pollutant concentrations can be associated with small stormwater discharges, which makes them a lesser concern for surface water quality (Gaafar et al., under review). The quality of receiving water bodies is not determined by the maximum pollution concentrations of stormwater effluents, as in concentration maps, but rather by the total pollutant mass discharged into the system. To keep pollution levels below the assimilation capacity of

receiving waters, decision makers should take the total pollutant mass into account as well (Brezonik and Stadelmann, 2002; Dembélé et al., 2011).

Some of the considerations taken here were adopted specifically to represent the worst-case scenario for chloramine releases, but other measures should be designed based on the pollutant. For example, DWF represents the lowest rainfall input, which should increase chloramine concentrations. However, other pollutants that accumulate on the ground surface over antecedent dry periods would not share the same characteristics, such as TSS and heavy metals. The hazard score used here is suitable for chloramine, as it builds on calculations that incorporate the factors important for chloramine chemistry in the EMC calculations. Applying the framework to other pollutants may require additional work to determine the factors important in hazard score definitions (Nath et al., 2018; Vojtek and Vojteková, 2019). Once these environmental factors are identified, they should be evaluated and their relative weights on hazard score should be estimated (Liu et al., 2018). Future studies can improve the hazard score calculations by incorporating additional factors that affect the hazard level associated with different pollutants. Ranges of different factors should be assessed to evaluate their potential effect on the pollution hazard. Conducted properly, this hazard assessment methodology can promote taking more effective and faster environmental precautionary measures. Finally, the framework presented here can improve stormwater quality by helping to target monitoring and enforcement resources, leading to higher surface water quality and healthier aquatic ecosystems.

5.4.4 Assessing chloramine pollution hazard

Analyses of chloramine concentration and hazard maps show that significant parts of the 30th Avenue basin can produce significant risks to surface waters from stormwater discharges. Concentrations were generally higher than the allowable chloramine discharge concentration of 0.02 mg/L, especially during dry weather periods. A large number of studies has demonstrated the severity of chloramine on aquatic habitat. According to the US EPA, chloramine concentrations as low as 0.0053 mg/L can cause 50% mortality to some invertebrate species (US EPA, 1984). In addition, high total active chlorine (TAC) can be lethal to crayfish, snails and some fish-food organisms over exposures of 6 min to 48 h (Zhang et al., 2018c). Long-lasting elevated chloramine concentrations can be toxic for fish growth at much lower concentrations, leading to detrimental

environmental risks (Brungs, 1973). In the James River, chloramine toxicity was found to be responsible for major fish kills because of its oxidization of hemoglobin and the resulting death by anoxia (Grothe and Eaton, 1975; Bellanca et al., 1977). Some species are more sensitive to chloramine than others, including invertebrate species such as amphipods, hermit crabs and shrimps, which are sensitive to chlorine exposure at concentrations ranging from 0.090 to 0.687 mg/L (Manning et al., 1996).

5.5 Conclusions

This study presented a new hazard assessment framework and decision support system for better managing point-source pollutants in stormwater effluents and their effects on surface water quality. The primary goal of the 4-stage-3-model framework introduced in this work is to generate reliable standalone concentration and hazard maps that can help municipalities to control pollutant discharges from urban stormwater systems. This framework consists of 1) stormwater hydrological and hydrodynamic simulations that model surface runoff and pipe flows, 2) a stormwater quality model that traces pollutants from introduction points through the sewer system to predict their mass loads and concentrations at the system outlet, 3) a GIS-based model to produce concentration maps, and 4) the generation of stormwater hazard maps from EMC-based and fuzzy-based hazard values.

The 4-stage-3-model framework was applied to chloramine pollution in stormwater discharged to the North Saskatchewan River in Edmonton, Alberta, Canada. Three models were built and used to; 1) simulate surface runoff and pipe flow rates, 2) predict chloramine pollution loads at the system outfall, and 3) develop chloramine concentration and hazard maps for the study area. Two mapping models were applied and validated, Inverse Distance Weighted (IDW) and the Bayesian Kriging Model (BKM), and the BKM model was found to be more accurate in predicting chloramine loads. The framework successfully generated chloramine concentration and hazard maps that showed the spatial variation of hazards of chloramine releases in the study basin. Concentration maps showed that chloramine concentrations over the permissible limits under dry weather flows throughout the basin, and only a design storm of a 10-year return period produced chloramine concentrations below regulation discharge limits. Chloramine hazard maps showed

approximately that 25% and 54% of the basin at moderate to high risk of chloramine-related water pollution as per EMC- and fuzzy-based calculations, respectively.

The new framework for developing concentration and hazard maps can improve water quality management by helping municipalities and water utilities to comply with regulations that usually permit a maximum pollutant concentration in stormwater (concentration maps), and to distinguish areas that pose high risk to receiving waters and that therefore require additional water quality monitoring and enforcement to control prohibited/unregulated releases (hazard risk maps). Further, highlighting areas with low to no-risk of chloramine pollution can optimize local resources by focusing efforts on vulnerable areas with hazardous releases. The framework can be generalized to other chemical substances that impair stormwater quality through either point or non-point source pollution. Its value lies in the production of a tool for stormwater system operators that provides a rapid and accurate pollution hazard assessment without the need to perform time- and labor-intensive calculations on a case-by-case basis and focus mitigation measures on releases from specific locations in the system. Hazard and concentration maps should be used in parallel to anticipate maximum concentrations and to assess potential risks of chloramine pollution.

CHAPTER 6

CONCLUSIONS AND RECOMMENDATIONS

6.1 Summary and conclusions

The aim of the present study was to develop a hazard assessment framework for water quality in storm sewer systems that can simulate chloramine decay and anticipate chloramine-related hazards in stormwater networks. The "4-stage-3-model" framework introduced in this work introduces reliable standalone concentration and hazard maps that can help municipalities to control pollutant discharges from urban stormwater systems in a timely and effective way. Thus, the hazard assessment framework and decision support system can promote better management of point-source pollution sources and in turn their effects on surface water quality. Next, the key conclusions of this work are categorized according to the research objectives presented in Chapter 1.

6.1.1 Building a reliable stormwater simulation model

A stormwater model was built in MIKE URBAN using kinematic wave method for surface runoff routing and dynamic wave method for pipe flow routing, in which both were selected to ensure accuracy of model predictions. Collected rainfall data over two summer seasons of 2015 and 2016 were used as inputs for the hydrological model, while pipe flow monitoring stations inputs and data were used for model calibration and validation. Preliminarily, the model computed pipe flows that were significantly higher than the observed values with peak values about 2.5 times higher than the monitored values.

To assess model sensitivity to perturbations in model inputs, a sensitivity analysis of the model inputs was conducted, and it revealed that;

1. parameters including wetting losses, infiltration exponents and pervious surface roughnesses did not significantly affect model results, while,
2. the most critical parameters were imperviousness ratios, catchment slope and length, and Manning coefficients, and

3. ArcGIS was useful in estimating GIS-based model variables such as catchment slopes and the ratio of impervious surfaces.

To validate model results, twenty-one independent storm events in the summers of 2015 and 2016 were identified along with their related observed pipe flows, with peak flows ranging from 0.12 to 0.63 m^3/sec, and flow duration of between 24 and 60 hours. Half of the data were used for model calibration, and the other half were used for model validation. Then, a group of model efficiency statistical measures were selected including NSE, RMSE and ln(NSE). As a result of model validation, correlation between model predictions and observed pipe flows.The pre-calibration model statistics ($R^2 = 0.84$, NSE = -1.7, RMSE = 0.105 m^3/sec, and ln(NSE) = 2.86) improved considerably compared with the post-calibration values ($R^2 = 0.95$, NSE = 0.91, RMSE = 0.024 m^3/sec, ln(NSE) = 0.59, maximum volume difference +11.3%, total volume error +8.8%, and peak volume error +9.8%). Correlation between model predictions and observed pipe flows was good, in which:

1. The NSE was a better representation of overall improvements in model performance rather than R^2, as it accounts better for the predicted error over the observed variance.
2. Focusing on low flow conditions, model performance was found limited in very low flow conditions (flows<0.05 m^3/s) affected by slight changes in minor losses such as wetting losses and depression storage, not affecting the overall model accuracy because of limited occurrence of such events.
3. The ln(NSE) was not able to reflect model improvements for low flow conditions in all the studied cases. Many assessment measures for low flow were tested; however, none of which performed perfectly.

6.1.2 Building a reliable water quality simulator for chloramine decay

The available stormwater simulation modeling tools do not permit the definition of the spatial and temporal variability of chloramine decay coefficients, so it was necessary to develop a new simulation modeling tool. The new Variable Decay Coefficient Simulator model (VDCS) was developed in Python programming language to trace chloramine inflows from introduction points through the sewer system to predict their mass loads and concentrations at the system outlet. The

advantage of the VDCS model lies in its capability of simulating the spatial and temporal variations in chloramine decay coefficients. The VDCS model collects four input data sets;

1. The sewer system attribute data which describe different stormwater system characteristics for sewer pipes, manholes, and outlets, in terms of diameters, lengths, material and invert levels, and manhole IDs at both upstream and downstream ends of each pipe in the system.
2. The hydrodynamic results of stormwater simulations in the form of time series of flow rates and velocities throughout the sewer system.
3. The chloramine pollutant introduction points such as fire hydrants and industrial releases are defined at respective locations in the drainage system along with variations of their loads over the simulation period.
4. The decay rate variation is set to one of three levels, a) constant average value, b) spatially-varying per land-use, or c) varying both spatially and temporally.

Organization of all inputs in spreadsheet form allows the VDCS to import hydrodynamic results from any stormwater simulation model. The VDCS model utilizes these data to construct the physical geometry of the water network so that it can identify pollutant path and then trace pollutants through the stormwater system.

Results of DHI's MIKE URBAN simulations with constant coefficient values were used to validate model performance. The VDCS produced very high agreements at all points with R^2 = 0.98, RMSE= 0.02 mg/L and NSE = 0.96. Small discrepancies in results can be attributed to differences in the hydrodynamic input to the two water quality models. MIKE URBAN used data directly generated from flow routing, while the VDCS used flow parameters at set timestep intervals of 5 minutes. Therefore, statistically-speaking, the VDCS performance was considered very reliable.

6.1.3 Studying the effect of chloramine decay variability on simulation results

The importance of incorporating the spatial and temporal variability of chloramine decay coefficients in storm sewers was investigated. Three scenarios were designed to compare the application of a) constant decay coefficient values throughout the sewer network over the simulation period, with b) spatially-varying decay coefficients per land-use type, and c) spatially-

and temporally-varying decay rates that incorporate changes in coefficient values with time from the initial pollutant releases. Results revealed the following:

1. Comparison of the scenario results demonstrated the importance of including both the temporal and spatial variations of decay coefficients when simulating degradable chemical pollutants in sewer systems. The combination of spatial and temporal variability in chloramine decay rates affected the predicted chloramine concentrations significantly, reaching concentration values about 100% higher than those predicted neglecting decay variability.
2. Simulation of variable decay coefficients for degradable chemicals should be included in available water quality models. In their current state, these models neglect important pollutant dynamics in stormwater systems that are important for prediction accuracy. Neglecting variable decay coefficients may cause models to underpredict discharge concentrations with adverse consequences for the quality of receiving waters.
3. Maximum mass fluxes may not occur concurrently with maximum concentrations. Currently, system operators and managers prioritize pollutant concentrations over mass fluxes, both because concentrations can be measured more easily in the field and because guidelines like those of the CCME (2014) focus on maximum allowable concentrations. Therefore, it is important to consider mass fluxes in addition to concentrations. Focusing only on pollutant concentrations may ignore potential environmental consequences of high mass/low concentration releases of pollutants. Regulatory agencies should incorporate mass fluxes as parameters in guidelines and regulations.
4. Particularly for dry weather conditions, close attention should be paid to chloraminated flows toward the middle and end of the discharge period, rather than at the early stages of release events. As biofilms accumulate over dry periods, chloramine loads are initially relatively low. As biofilms are consumed, chloramine concentrations rise significantly with decreasing decay rates. However, results will differ by basin geometry, the mixture of land-uses and system attributes, and water use and quality characteristics, and so pollutants must be assessed for each stormwater basin individually.

6.1.4 Developing and validating a GIS model for mapping chloramine concentration

A new approach to the development of chloramine pollutant maps was designed to predict concentrations at the system outlet resulting from point-source pollutant releases. This approach was used to generate two types of maps – concentration and hazard maps – for use as standalone tools to quickly assess the severity of release incidents. Under different weather conditions, two types of maps were devised; 1) a chloramine concentration map represents the pollutant concentration at the system outlet associated with point-source release occurring at any location in the stormwater basin, 2) a hazard map works similarly but rather shows the spatial variation of chloramine hazards instead of concentrations.

Two mapping models, Inverse Distance Weighted (IDW) and the Bayesian Kriging Model (BKM), were applied in ArcGIS. The performance of these models was compared and validated against chloramine concentrations records and the BKM model was found to be more accurate. The error in IDW model predictions was considerably higher for chloramine peak concentrations.

6.1.5 Structuring a hazard assessment framework to stormwater quality

The "4-stage-3-model" hazard assessment framework was constructed to evaluate stormwater pollution risks in stormwater networks. It incorporates a stormwater surface runoff and pipe hydrodynamic model, a stormwater quality model, GIS-based mapping model and GIS-based hazard assessment maps. This framework was applied to study chloramine pollution in stormwater discharged to the North Saskatchewan River in Edmonton, Alberta, Canada. This application required;

1. a stormwater simulation model in MIKE URBAN to simulate surface runoff and pipe flow rates,
2. a newly-developed stormwater quality model (VDCS) to predict chloramine loads at the system outfall considering variability of chloramine decay coefficients, and
3. a mapping model in ArcGIS using Bayesian kriging interpolation to develop chloramine concentration and water quality hazard maps for the study area.

The framework successfully generated chloramine concentration and hazard maps that showed the spatial variation of hazards from chloramine releases over the study basin. Results showed approximately 25% and 54% of the basin at moderate to high risk of chloramine-related water pollution based on EMC and Fuzzy hazards, respectively.

6.1.6 Applying the framework to study chloramine pollution in stormwater systems

A new hazard score system was developed based on EMC values. EMCs calculated were normalized by dividing their values by the maximum EMC value found in the study area. This hazard score is suitable for chloramine, as it builds on calculations that incorporate the factors important for chloramine chemistry in the EMC calculations including pollution concentration and total mass, stormwater volume, effect of land-use type on chloramine decay rates, and characteristics and layout of the sewer system. This EMC-based hazard scores successfully generated a chloramine hazard map that showed the spatial variation of hazards of chloramine releases in the study basin as a result of individual point-source releases.

In the second approach, fuzzy logic, using available literature on chloramine decay and previous findings of this study, factors affecting chloramine pollution in the storm sewer system were identified including EMC values, land-use types, annual average rainfall, ground surface slopes, property assessment values, spatial variations of chloramine decay rates, density of impervious areas and proximity to the sewer network. All relevant spatial data were collected and introduced into the ArcGIS environment. Each hazard-driving factor had five possible levels: (1) very low, (2) low, (3) moderate, (4) high, and (5) very high pollution susceptibility, ranked with respect to their relative weight affecting pollution hazard. Then, fuzzy membership functions were used to define the individual classes in each map according to their degree of membership. These two techniques were applied and their results were compared

6.1.7 Producing hazard assessment maps for chloramine pollution

Concentration maps showed that under dry weather conditions chloramine concentration over the entire basin was higher than the safe range (0.02 mg/L), with a minimum value of 0.076 mg/L. for design storms of 2 and 5-year it was found that 60% and 80% of the 30th Avenue basin developed

concentrations within the safe range. Return periods higher than 5-year posed no significant environmental concerns producing chloramine concentrations below regulation discharge limits over the entire basin. EMC- and fuzzy-based hazard techniques successfully generated chloramine hazard maps for the study area. This application showed that;

1. system operators should not be concerned with chloramine releases approximating hydrant discharge levels outside dry weather and small rainfall periods,
2. hazard and concentration maps should be used in parallel to anticipate maximum concentrations and to assess potential risks of chloramine pollution, since each provides a different purpose. Concentration maps can help to evaluate sudden changes in the pollution load, and in turn, anticipate high concentration incidents regardless of their mass loads. Hazard maps can be more important to environmental pollution control and management, since the highest pollutant concentrations can be associated with small storm discharges, which makes them a lesser concern for surface water quality,
3. the new framework for developing concentration and hazard maps can improve water quality management by helping municipalities and water utilities to comply with regulations that usually permit a maximum pollutant concentration in stormwater (concentration maps), and to distinguish areas that pose high risk to receiving waters and that therefore require additional water quality monitoring and enforcement to control prohibited/unregulated releases (hazard risk maps),
4. this hazard assessment methodology can promote the effectiveness and speed of provided environmental solutions. In addition, this framework can improve stormwater quality by helping to target monitoring and enforcement resources, leading to higher surface water quality and healthier aquatic ecosystems.
5. further, highlighting areas with low to no-risk of chloramine pollution can optimize local resources by focusing efforts on vulnerable areas, and
6. its value lies in the production of a tool for stormwater system operators that provides a rapid and accurate pollution hazard assessment without the need to perform time- and labor-intensive calculations on a case-by-case basis.

6.2 Recommendations

The work presented here related to stormwater quantity and quality modeling and hazard assessment methods could benefit from further study. The following are suggestions for future work on stormwater modeling that may help modelers and system operators to overcome limitations, optimize resources, extend capabilities and widen applications of stormwater models.

6.2.1 For stormwater model developers

Some available stormwater models like MIKE URBAN lack auto-calibration features, which save modelers a lot of time and effort in conducting a large number of simulations during manual calibrations. Some software packages, like PC-SWMM, have features that show approximate changes in the model results that correspond to defined perturbations in model input; such features really aid model validation.

Newly-developed stormwater models have built-in tools to import attributes for different system components from GIS systems like ArcGIS. However, those models do not utilize available GIS data to automatically determine/estimate the key characteristics of model variables. For example, using digital elevation maps, models can easily calculate catchment slope and area, and GIS spatial analysis tools can be devised to delineate catchment areas. Also, image processing tools can identify specific land-use types such as parks and residential areas. Incorporating these tools in the stormwater model environment would make it much easier for modelers to achieve reliable model predictions.

Simulation summary reports of stormwater models can be improved by automatically calculating commonly used statistical measures such as R^2, NSE, RMSE, MAE, and IA. Such additions could help to assess model performance within the model environment.

Available water quality models require improvements to enhance simulation capabilities of different water pollutants with different characteristics. As revealed in this research, the addition of a variable decay coefficient tool would increase the advective dispersion module capability in stormwater models, and in turn, improve model results. Such an improvement can be achieved by allowing the definition of local decay coefficients for user-selected groups of pipe segments.

Uncertainty assessments should be conducted so as to determine various uncertainty sources and allow uncertainty predictions for future stormwater modelling work.

6.2.2 For future studies

The framework developed in this work can be generalized to other chemical substances that impair stormwater quality through either point or non-point source pollution. Considering that some of the steps taken here were adopted specifically to represent the worst-case scenario for chloramine releases, other measures should be designed based on the pollutant. For example, DWF represents the lowest rainfall input, which should result in increased chloramine concentrations at the system outfall. However, other pollutants that accumulate on the ground surface over antecedent dry periods would not share the same characteristics, such as total suspended solids and heavy metals. For each pollutant, the key determinants should be established, and then proper hazard assessment techniques should be applied. Implementing this hazard assessment framework for a complex stormwater pollutant with many decay mechanisms and pathways like chloramine means that the framework is applicable to many other stormwater pollutants.

Such stormwater pollution hazard assessment tool can be generalizable to other Canadian cities and internationally, and can be made flexible enough to apply in the future to study the dissipation of other constituents in sewer systems.

Future studies on risk assessment of chloramine pollution can test the adequacy of different GIS-based hazard assessments tools, such as analytical hierarchy procedure, fuzzy logic and artificial neural networks. Comparison of different assessment tools against actual water quality measurements can help to assess their results and identify the most reliable technique for each stormwater system. Also, different classes of each factor can be assigned and relative weights of affecting-factors can be adjusted.

Future work can improve water quality monitoring by using data loggers and autosamplers to determine pollutant input from specific outdoor uses such as irrigation water application in park areas, commercial outdoor car washers and unregulated industrial releases. Such data would help to identify actual pollutant loads for different land-uses.

Many statistical measures have been designed particularly to assess model performance for low flow conditions, but none of these has been sufficiently tested for different water resources applications. Further, researchers disagree on the most suitable low flow measures. In this research, ln(NSE) was tested and found not to reflect the improvement in model performance through the validation process. Future studies should either evaluate current low flow measures or introduce new measures to better serve different water resources applications.

6.2.3 For municipalities and regulatory agencies

For future studies, an extensive stormwater quality monitoring program is recommended to improve water quality simulations that involve degradable chemicals in stormwater networks. Although resource-intensive and potentially costly, such monitoring programs would improve the estimation of pollutant decay rates, enhance understanding of the role of different land-uses and pollutant loads on pollutant concentrations and aid validation of stormwater quality simulations.

The quality of receiving water bodies is not determined by the maximum pollution concentrations of stormwater effluents, but rather by the total pollutant mass discharged into the system. To keep pollution levels below the assimilation capacity of receiving waters, system managers should take the total pollutant mass into consideration as well. Therefore, new regulations should set limits on mass fluxes along with concentrations to mitigate environmental risks related to stormwater contamination. Scientists should work on tools or procedures to readily estimate pollutant mass at system outlets.

BIBLIOGRAPHY

Adhikari, R.A., Sathasivan, A., Bal Krishna, K.C., 2012. Effect of biofilms grown at various chloramine residuals on chloramine decay. Water Sci. Technol. Water Supply 12, 463. doi:10.2166/ws.2012.015

Ahn, J., Lee, S., Choi, K., Koo, J., 2012. Application of EPANET for the determination of chlorine dose and prediction of THMs in a water distribution system. Sustain. Environ. Res. 22, 31–38.

Al-Kofahi, S.D., VanLeeuwen, D.M., Samani, Z. a., St. Hilaire, R., 2012. Water Budget Calculator Created for Residential Urban Landscapes in Albuquerque, New Mexico. J. Irrig. Drain. Eng. 138, 525–533. doi:10.1061/(ASCE)IR.1943-4774.0000439

Al-omari, A., Chaudhry, H., 2001. Unsteady-State Inverse Chlorine Modelling in Pipe Networks. J. Hydraul. Eng. 127, 669–677.

Al-omari, A., Fayyad, M., Al-nimer, A., 2004. Modelling chlorine residuals at Jabal Amman water supply: Operational paper. J. water supply 53, 351–358.

Alexander, M.T., Boccelli, D.L., 2010. Field Verification of an Integrated Hydraulic and Multi-Species Water Quality Model, in: Water Distribution Systems Analysis. Tuscon, AZ, pp. 687–696. doi:10.1061/41203(425)65

Artina, S., Bolognesi, A., Liserra, T., Maglionico, M., 2007. Simulation of a storm sewer network in industrial area: Comparison between models calibrated through experimental data. Environ. Model. Softw. 22, 1221–1228. doi:10.1016/j.envsoft.2006.11.002

ASCE Task Committee on Definition of Criteria for Evaluation of Watershed Models of the Watershed Managment Committee, I. and D.D., 1993. Evaluation of Watershed Models. J. Irrig. Drain. Eng. 119, 429–442.

AWWA, 2006. Water Chlorination/ Chloramination Practices and Principles, Second. ed. American Water Works Association, Denver, Colorado.

Aydi, A., 2018. Evaluation of groundwater vulnerability to pollution using a GIS-based multi-criteria decision analysis. Groundw. Sustain. Dev. 7, 204–211. doi:10.1016/j.gsd.2018.06.003

Balling, R.C., Gober, P., Jones, N., 2008. Sensitivity of residential water consumption to variations in climate: An intraurban analysis of Phoenix, Arizona. Water Resour. Res. 44, 1–11. doi:10.1029/2007WR006722

Becouze-Lareure, C., Dembélé, A., Coquery, M., Cren-Olivé, C., A, J.-L.B.-K., 2019. Assessment of 34 dissolved and particulate organic and metallic micropollutants discharged at the outlet of two contrasted urban catchments. Sci. Total Environ. 651, 1810–1818. doi:10.1016/j.scitotenv.2018.10.042

Bedient, P.B., Huber, W.C., 2013. Hydrology and floodplain analysis, Fifth. ed. Prentice Hall, Upper Saddle River, NJ.

Bellanca, M.A., Bailey, D.S., Bellanca, A., 1977. Effects of chlorinated effluents on aquatic ecosystem in the lower James River. J. Water Pollut. Control Fed. 49, 639–645.

Bernhardt, E.S., Palmer, M.A., 2007. Restoring streams in an urbanizing world. Freshw. Biol. 52, 738–751. doi:10.1111/j.1365-2427.2006.01718.x

Bertrand-Krajewski, J.L., Chebbo, G., Saget, A., 1998. Distribution of pollutant mass vs volume in stormwater discharges and the first flush phenomenon. Water Res. 32, 2341–2356. doi:10.1016/S0043-1354(97)00420-X

Bian, B., Cheng, X., Li, L., 2011. Investigation of urban water quality using simulated rainfall in a medium size city of China. Environ. Monit. Assess. 183, 217–29. doi:10.1007/s10661-011-1916-y

Blokker, M., Vreeburg, J., Speight, V., 2014. Residual chlorine in the extremities of the drinking water distribution system: The influence of stochastic water demands. Procedia Eng. 70, 172–180. doi:10.1016/j.proeng.2014.02.020

Boccelli, D.L., Tryby, M.E., Uber, J.G., Summers, R.S., 2003. A reactive species model for

chlorine decay and THM formation under rechlorination conditions. Water Res. 37, 2654–2666. doi:10.1016/S0043-1354(03)00067-8

Borah, D.K., Ahmadisharaf, E., Padmanabhan, G., Imen, S., Mohamoud, Y.M., 2019. Watershed Models for Development and Implementation of Total Maximum Daily Loads. J. Hydrol. Eng. 24, 03118001. doi:10.1061/(ASCE)HE.1943-5584.0001724

Borah, D.K., Bera, M., 2004a. Watershed-Scale Hydrologic and Nonpoint- Source Pollution Models : Review of Applications. Am. Soc. Agric. Biol. Eng. 47, 789–803.

Borah, D.K., Bera, M., 2004b. Watershed-scale hydrologic and nonpoint-source pollution models: Review of Applications. Trans. ASAE 47, 789–804.

Borah, D.K., Bera, M., 2003. Watershed-Scale Hydrologic and Nonpoint- Source Pollution Models : Review of Mathematical Bases. Am. Soc. Agric. Biol. Eng. 46, 1553–1566.

Borah, D.K., Weist, J.H., Wall, J.D., Powell, D.N., 2009. Watershed Models for Storm Water Management : Comparing Hydrologic and Hydraulic Procedures. World Environ. Water Resour. Congr. 2009 6517–6526. doi:10.1061/41036(342)660

Borah, D.K., Yagow, G., Saleh, A., Barnes, P.L., Rosenthal, W., Krug, E.C., Hauck, L.M., 2006. Sediment and Nutrient Modeling for TMDL Development and Implementation. Soil Water Div. ASABE 49, 967–986.

Brabec, E., Schulte, S., Richards, P.L., 2002. Impervious Surfaces and Water Quality : A Review of Current Literature and Its Implications for Watershed Planning. J. Plan. Lit. 16, 499–514. doi:10.1177/088541202400903563

Brezonik, P.L., Stadelmann, T.H., 2002. Analysis and predictive models of stormwater runoff volumes, loads, and pollutant concentrations from watersheds in the Twin Cities metropolitan area, Minnesota, USA. Water Res. 36, 1743–1757. doi:10.1016/S0043-1354(01)00375-X

Brungs, W., 1973. Effects of Residual Chlorine on Aquatic Life, Journal - Water Pollution Control Federation.

Butler, D., Davies, J.W., 2011. Urban drainage, Third. ed. Spon Press, New York, NY.

Carr, R., Fontenot, E., Schroeck, J., 2010. City of Los Angeles primary sewer system wet weather flow calibration – MIKE URBAN. DHI, Copenhagen, pp. 1–20.

Castro, P., Neves, M., 2003. Chlorine Decay in Water Distribution Systems Case Study - Lousada Network, in: Environmental 2010: Situation and Perspectives for the European Union. Porto, Portugal, pp. 1–6.

CCME, 2009. Canada-wide Strategy for the Management of Municipal Wastewater Effluent. Whitehorse, Yukon.

Chow, V. Te, Maidment, D.R., Mays, L.W., 1988. Applied Hydrology, Gene. McGraw-Hill Inc., New York, NY. doi:10.1016/0378-1119(91)90258-D

City of Edmonton, 2018. City of Edmonton - EPCOR Drainage Services - Bylaw 18100.

City of Edmonton, 2016. The City of Edmonton Drainage Bylaw - Bylaw 16200. Edmonton Alberta.

City of Edmonton, 2013. EMP Water Quality Summary Report (2001-2011): SSO/Rat Creek CSO Results. Edmonton, Alberta.

Clark, R.M., 1998. Chlorine Demand and TTHM Formation Kinetics: A Second-Order Model. J. Environ. Eng. 124, 16–24. doi:10.1061/(ASCE)0733-9372(1998)124:1(16)

Clark, R.M., Haught, R.C., Panguluri, S., Roman, W., 2006. Predicting the Loss of Chlorine and Chloramine Residuals in Metallic Pipes, in: 8th Annual Water Distribution Systems Analysis Symposium. Cincinnati, Ohio, pp. 1–20. doi:10.1061/40941(247)146

Clark, R.M., Rossman, L.A., Wymer, larry J., 1995. Modelling Distribution System Water Quality: Regulatory Implications. J. Water Resour. Plan. Manag. 121, 423–427.

Coleman, R.N., Campbell, J.N., Cook, F.D., Westlake, D.W., 1974. Urbanization and the microbial content of the north Saskatchewan River. Appl. Microbiol. 27, 93–101.

Connell, G.F., 1996. The Chlorination/chloramination Handbook, First. ed, Water disinfection series. American Water Works Association, Denver, Colorado.

Constans, S., Brémond, B., Morel, P., 2003. Simulation and Control of Chlorine Levels in Water Distribution Networks. J. Water Resour. Plan. Manag. 129, 135–145. doi:10.1061/(ASCE)0733-9496(2003)129:2(135)

Courtis, B.. J.., West, J.R.., Bridgeman, J.., 2009. Temporal and Spatial Variations in Bulk Chlorine Decay within a Water Supply System. J. Environ. Eng. 135, 147–152. doi:10.1061/(ASCE)0733-9372(2009)135:3(147)

Crittenden, J.C., Trussell, R.R., Hand, D.W., Howe, K. j., Tchobanoglous, G., Borchardt, J.H., 2012. MWH's Water Treatment Principles and Design, Third. ed. John Wiley & Sons, Inc, Hoboken, New Jersey.

Davis, A.P., Shokouhian, M., Ni, S., 2001. Loading estimates of lead, copper, cadmium, and zinc in urban runoff specific sources. Chemosphere 44, 997–1009. doi:10.1016/S0045-6535(00)00561-0

Dembélé, A., Bertrand-Krajewski, J.L., Becouze, C., Barillon, B., 2011. A new empirical model for stormwater TSS event mean concentrations (EMCs). Water Sci. Technol. 64, 1926–1934. doi:10.2166/wst.2011.187

Devi, G.K., Ganasri, B.P., Dwarakish, G.S., 2015. A Review on Hydrological Models, in: International Conference on Water Resources, Coastal and Ocean Engineering. pp. 1001–1007.

DHI, 2017a. MIKE URBAN - Collection System User Guide. Copenhagen, Denmark.

DHI, 2017b. MOUSE - Runoff Reference Manual. Copenhagen, Denmark. doi:10.1016/j.matchar.2009.10.005

DHI, 2017c. MOUSE - Pollution Transport Reference Manual. Copenhagen, Denmark.

DHI, 2017d. MOUSE - Pipe Flow Reference Manual. Copenhagen, Denmark.

Dotto, C.B.S., Vezzaro, L., McCarthy, D.T., Deletic, A., Freni, G., Kleidorfer, M., Henrichs, M., Rauch, W., Mannina, G., 2012. Comparison of different uncertainty techniques in urban stormwater quantity and quality modelling. Water Res. 46, 2545–2558. doi:10.1016/j.watres.2012.02.009

Duirk, S.E., Gombert, B., Crou??, J.P., Valentine, R.L., 2005. Modeling monochloramine loss in the presence of natural organic matter. Water Res. 39, 3418–3431. doi:10.1016/j.watres.2005.06.003

Dukan, S., Levi, Y., Piriou, P., Guyon, F., Villon, P., 1996. Dynamic modelling of bacterial growth in drinking water networks. Water Res. 30, 1991–2002. doi:10.1016/0043-1354(96)00021-8

Duncan, H.P., 1995. A Review of Urban Stormwater Quality Processes. Melbourne, Victoria.

Elliott, A.H., Trowsdale, S.A., 2007. A review of models for low impact urban stormwater drainage. Environ. Model. Softw. 22, 394–405. doi:10.1016/j.envsoft.2005.12.005

Ellis, J.B., Revitt, D.M., Lundy, L., 2012. An impact assessment methodology for urban surface runoff quality following best practice treatment. Sci. Total Environ. 416, 172–179. doi:10.1016/j.scitotenv.2011.12.003

Emrouznejad, A., Ho, W., 2018. Fuzzy Analytic Hierarchy Process. Chapman and Hall/CRC, Boca Raton, FL.

Eriksson, E., Baun, A., Scholes, L., Ledin, A., Ahlman, S., Revitt, M., Noutsopoulos, C., Mikkelsen, P.S., 2007. Selected stormwater priority pollutants - a European perspective. Sci. Total Environ. 383, 41–51. doi:10.1016/j.scitotenv.2007.05.028

Fisher, I., Kastl, G., Fayle, B., Sathasivan, A., 2009. Chlorine or Chloramine for Drinking Water Disinfection ? A case study of a new decision framework, in: Ozwater 09. AWA, Sydney, Australia, Melbourne, Australia, p. 8.

Fisher, I., Kastl, G., Sathasivan, A., 2016. Including rechlorination in a suitable chlorine decay model for water distribution networks. Urban Water J. 9006, 1–9.

doi:10.1080/1573062X.2016.1148180

Fisher, I., Kastl, G., Sathasivan, A., 2012. A suitable model of combined effects of temperature and initial condition on chlorine bulk decay in water distribution systems. Water Res. 46, 3293–3303. doi:10.1016/j.watres.2012.03.017

Fisher, I., Kastl, G., Sathasivan, A., 2011a. Evaluation of suitable chlorine bulk-decay models for water distribution systems. Water Res. 45, 4896–4908. doi:10.1016/j.watres.2011.06.032

Fisher, I., Kastl, G., Sathasivan, A., Jegatheesan, V., 2011b. Suitability of Chlorine Bulk Decay Models for Planning and Management of Water Distribution Systems. Crit. Rev. Environ. Sci. Technol. 41, 1843–1882. doi:10.1080/10643389.2010.495639

Fletcher, T.D., Andrieu, H., Hamel, P., 2013. Understanding, management and modelling of urban hydrology and its consequences for receiving waters: A state of the art. Adv. Water Resour. 51, 261–279. doi:10.1016/j.advwatres.2012.09.001

Fraga, I., Charters, F.J., O'Sullivan, A.D., Cochrane, T.A., 2016. A novel modelling framework to prioritize estimation of non-point source pollution parameters for quantifying pollutant origin and discharge in urban catchments. J. Environ. Manage. 167, 75–84. doi:10.1016/j.jenvman.2015.11.003

Gaafar, M., Zhang, Q., Davies, E., 2019. Impact of variability in decay coefficients on simulating monochloramine dissipation in storm sewers. J. Water Resour. Plan. Manag. Under revi, WRENG-4190.

Gamerith, V., Muschalla, D., Könemann, P., Gruber, G., 2009. Pollution load modelling in sewer systems: An approach of combining long term online sensor data with multi-objective auto-calibration schemes. Water Sci. Technol. 59, 73–79. doi:10.2166/wst.2009.772

Garrick, M., Cunnane, C., Nash, J.E., 1978. A criterion of efficiency for rainfall-runoff models. J. Hydrol. 36, 375–381. doi:10.1016/0022-1694(78)90155-5

Gironas, J., Roesner, L. a, Davis, J., 2009. SWMM Applications Manual, Storm Water Management Model Applications Manual. doi:10.1111/j.1752-1688.1990.tb01394.x

Gnecco, I., Berretta, C., Lanza, L.G., La Barbera, P., 2005. Storm water pollution in the urban environment of Genoa, Italy. Atmos. Res. 77, 60–73. doi:10.1016/j.atmosres.2004.10.017

Gobel, P., Dierkes, C., Coldewey, W.G., 2007. Storm water runoff concentration matrix for urban areas. J. Contam. Hydrol. 91, 26–42. doi:10.1016/j.jconhyd.2006.08.008

Goonetilleke, A., Thomas, E., Ginn, S., Gilbert, D., 2005. Understanding the role of land use in urban stormwater quality management. J. Environ. Manage. 74, 31–42. doi:10.1016/j.jenvman.2004.08.006

Goulden, S., Portman, M.E., Carmon, N., Alon-Mozes, T., 2018. From conventional drainage to sustainable stormwater management: Beyond the technical challenges. J. Environ. Manage. 219, 37–45. doi:10.1016/j.jenvman.2018.04.066

GRASS, 2016. GIS Development Team, Geographic Resources Analysis Support System, Open Source Geospatial Foundation, Version 6.4.5. URL http://grass.osgeo.org (accessed 2.24.19).

Grothe, D.R., Eaton, J.W., 1975. Chlorine-Induced Mortality in Fish. Trans. Am. Fish. Soc. 104, 800–802.

Guan, M., Sillanpää, N., Koivusalo, H., 2015. Modelling and assessment of hydrological changes in a developing urban catchment. Hydrol. Process. 29, 2880–2894. doi:10.1002/hyp.10410

Gupta, H. V., Kling, H., Yilmaz, K.K., Martinez, G.F., 2009. Decomposition of the mean squared error and NSE performance criteria: Implications for improving hydrological modelling. J. Hydrol. 377, 80–91. doi:10.1016/j.jhydrol.2009.08.003

Hallam, N.B., West, J.R., Forster, C.F., Powell, J.C., Spencer, I., 2002. The decay of chlorine associated with the pipe wall in water distribution systems. Water Res. 36, 3479–3488. doi:10.1016/S0043-1354(02)00056-8

Hamdy, D., Moustafa, M.A.E., Elbakri, W., 2014. Free residual chlorine calibration by waterCAD at El-NOZHA water network in Alexandria governorate, Egypt. J. Environ. Prot. (Irvine,. Calif). 5, 845–861.

Hammouri, N., El-Naqa, A., 2008. GIS based hydrogeological vulnerability mapping of groundwater resources in Jerash area - Jordan. Geofis. Int. 47, 85–87.

Haris, H., Chow, M.F., Usman, F., Sidek, L.M., Roseli, Z.A., Norlida, M.D., 2016. Urban Stormwater Management Model and Tools for Designing Stormwater Management of Green Infrastructure Practices, in: Proceddings of the 2nd International Conference on Advances in Renewable Energy and Technologies : IOP Conference Series: Earth and Environmental Science (32). IOP Publishing, Putrajaya, Malaysia. doi:10.1088/1755-1315/32/1/012022

He, J., Valeo, C., Chu, A., Neumann, N.F., 2011. Prediction of event-based stormwater runoff quantity and quality by ANNs developed using PMI-based input selection. J. Hydrol. 400, 10–23.

He, J.X., Valeo, C., Chu, A., Neumann, N.F., 2010. Characterizing Physicochemical Quality of Storm-Water Runoff from an Urban Area in Calgary, Alberta. J. Environ. Eng. 136, 1206–1217. doi:10.1061/(ASCE)EE.1943-7870.0000267

Heineman, M., Eichenwald, Z., Gamache, M., Miner, R., Keohan, P., 2013. A Comprehensive Water Quality Model of Boston's Drainage Systems, in: World Environmental and Water Resources Congress 2013. pp. 63–76. doi:doi:10.1061/9780784412947.007

Helbling, D.E., VanBriesen, J.M., 2009. Modeling Residual Chlorine Response to a Microbial Contamination Event in Drinking Water Distribution Systems. J. Environ. Eng. 135, 918–927. doi:10.1061/(ASCE)EE.1943-7870.0000080

Henderson, F.M., 1966. Open Channel Flow. MacMillan Publishing Co., Inc., New York.

Henderson, F.M., Wooding, R.A., 1964. Overland Flow and Groundwater Flow from a Steady Rainfall Finite Duration. J. Geophys. Res. 69, 1531–1540.

Herath, B.S., Sathasivan, A., Lam, H.I., 2015. Can microbes significantly accelerate chloramine decay without severe nitrification? Int. Biodeterior. Biodegrad. 102, 231–236. doi:10.1016/j.ibiod.2015.03.018

House, M., Ellis, J., Herricks, E.E., Hvidtvej-Jacobsen, T., Seager, J., Lijklema, L., Aalderink, H., Clifforde, I.T., 1993. Urban drainage-impacts on receiving water quality. Water Sci. Technol. 27, 117–158.

Howell, E.T., Chomicki, K.M., Kaltenecker, G., 2012. Patterns in water quality on Canadian shores of Lake Ontario: Correspondence with proximity to land and level of urbanization. J. Great Lakes Res. 38, 32–46. doi:10.1016/j.jglr.2011.12.005

Hrudey, S.E., 2009. Chlorination disinfection by-products, public health risk tradeoffs and me. Water Res. 43, 2057–2092. doi:10.1016/j.watres.2009.02.011

Huang, J.J., Mcbean, E.A., 2008. Using Bayesian Statistics to Estimate Chlorine Wall Decay Coefficients for Water Supply System. J. Water Resour. Plan. Manag. 134, 129–137. doi:10.1061/(ASCE)0733-9496(2008)134:2(129)

Hussein, A.O., Shahid, S., Basim, K.N., Chelliapan, S., 2015. Modelling Stormwater Quality of an Arid Urban Catchment. Appl. Mech. Mater. 735, 215–219. doi:10.4028/www.scientific.net/AMM.735.215

Islam, M.R., Chaudhry, M.H., Clark, R.M., 1997. Inverse modeling of chlorine concentration in pipe networks under dynamic condition. J. Environ. Eng. 123, 1033–1039.

Jain, S.K., Sudheer, K.P., 2008. Fitting of Hydrologic Models: A Close Look at the Nash–Sutcliffe Index. J. Hydrol. Eng. 13, 981–986. doi:10.1061/(ASCE)1084-0699(2008)13:10(981)

James, W., 2005. Rules for Responsible Modeling, Forth. ed. CHI, Guelph, Ontario.

Janssen, P.H.M., Heuberger, P.S.C., 1995. Calibration of process-oriented models. Ecol. Modell. 83, 55–66. doi:10.1016/0304-3800(95)00084-9

Jayasooriya, V.M., Ng, A.W.M., 2014. Tools for modeling of stormwater management and economics of green infrastructure practices: A review. Water. Air. Soil Pollut. 225. doi:10.1007/s11270-014-2055-1

Jiang, J., Wang, P., Lung, W. seng, Guo, L., Li, M., 2012. A GIS-based generic real-time risk assessment framework and decision tools for chemical spills in the river basin. J. Hazard. Mater. 227–228, 280–291. doi:10.1016/j.jhazmat.2012.05.051

Jiang, S.C., Lim, K.-Y., Huang, X., McCarthy, D., Hamilton, A.J., 2015. Human and environmental health risks and benefits associated with use of urban stormwater. Wiley Interdiscip. Rev. Water 2, 683–699. doi:10.1002/wat2.1107

Jonkergouw, P.M.R., Khu, S.T., Savic, D.A., Zhong, D., Hou, X.Q., Zhao, H. Bin, 2009. A variable rate coefficient chlorine decay model. Environ. Sci. Technol. 43, 408–414. doi:10.1021/es8012497

Karamouz, M., Moridi, A., Nazif, S., 2010. Urban Water Engineering and Management. Taylor & Francis Group, Boca Raton, FL. doi:10.1080/02508068008685882

Kastl, G.J., Fisher, I.H., Jegatheesan, V., 1999. Evaluation of chlorine decay kinetics expressions for drinking water distribution systems modelling. J. water supply Res. Technol. - AQUA 48, 219–226.

Kessler, E., Neas, B., 1994. On correlation, with applications to the radar and raingage measurement of rainfall. Atmos. Res. 34, 217–229. doi:10.1016/0169-8095(94)90093-0

Kim, H., Kim, S., Koo, J., 2015. Modelling chlorine decay in a pilot scale water distribution system subjected to transient. Procedia Eng. 119, 370–378. doi:10.1016/j.proeng.2015.08.897

Kohpaei, A.J., Sathasivan, A., Aboutalebi, H., 2011. Effectiveness of parallel second order model over second and first order models. Desalin. Water Treat. 32, 107–114. doi:10.5004/dwt.2011.2685

Konrad, C.P., 2005. Hydrologic Changes in Urban Streams and Their Ecological Significance, in: American Fisheries Society Symposium. pp. 157–177. doi:10.1109/IEMBS.2005.1616849

Kowalska, B., Kowalski, D., Widomski, M.K., 2013. Modelling of Hydraulics and Pollutants

Transport in Sewer Systems. Lublin University of Technology, Lublin, Poland.

Krause, P., Boyle, D.P., 2005. Advances in Geosciences Comparison of different efficiency criteria for hydrological model assessment. Adv. Geosci. 5, 89–97. doi:10.5194/adgeo-5-89-2005

Lee, D.-J., Choi, J.-H., Chung, J., Lee, Y.-W., Kim, Y.-I., 2009. Effect of Infiltration and Inflow in Dry Weather on Reducing the Pollution Loading of Combined Sewer Overflows. Environ. Eng. Sci. 26, 897–906. doi:10.1089/ees.2008.0038

Lee, J.G., Heaney, J.P., 2003. Estimation of Urban Imperviousness and its Impacts on Storm Water Systems. J. Water Resour. Plan. Manag. 129, 419–426.

Lee, L.-Y., Lu, C.-S., Chang, R., 2003. Exploration of the mutuality and variation correlating combined chlorine concentrations with other factors in the water distribution system. J. Chinese Inst. Eng. 26, 343–352. doi:10.1080/02533839.2003.9670786

Lee, S.-B., Yoon, C.-G., Jung, K.W., Hwang, H.S., 2010. Comparative evaluation of runoff and water quality using HSPF and SWMM. Water Sci. Technol. 62, 1401–1409. doi:10.2166/wst.2010.302

Legates, D.R., McCabe, G.J., 1999. Evaluating the use of "goodness-of-fit" measures in hydrologic and hydroclimatic model validation. Water Resour. Res. 35, 233–241.

Leggett, C.G., Bockstael, N.E., 2000. Evidence of the effects of water quality on residential land prices. J. Environ. Econ. Manage. 39, 121–144. doi:10.1006/jeem.1999.1096

Liggett, J.A., 1994. Govering Equations for Free Surface Flows, in: CHAUDHRY, M.H., MAYS, L.W. (Eds.), Computer Modeling of Free-Surface and Pressurized Flows. Pullman, WA, p. 736.

Liu, A., Egodawatta, P., KjØlby, M.J., Goonetilleke, A., 2010. Development of pollutant build-up parameters for MIKE URBAN for Southeast Queensland, Australia, in: Proceedings of the International MIKE by DHI Conference, 6–8 September, 2010, Copenhagen, Denmark. DHI, Copenhagen, Denmark, pp. 15–22.

Liu, Y., Zhang, J., Zhao, Y., 2018. The risk assessment of riverwater pollution based on a modified non-linear model. Water (Switzerland) 10, 1–12. doi:10.3390/w10040362

Loucks, D.P., van Beek, E., 2017. Water resource systems planning and management. doi:10.1007/978-3-319-44234-1

Luo, K., Hu, X., He, Q., Wu, Z., Cheng, H., Hu, Z., Mazumder, A., 2018. Impacts of rapid urbanization on the water quality and macroinvertebrate communities of streams: A case study in Liangjiang New Area, China. Sci. Total Environ. 621, 1601–1614. doi:10.1016/j.scitotenv.2017.10.068

Machiwal, D., Cloutier, V., Güler, C., Kazakis, N., 2018. A review of GIS-integrated statistical techniques for groundwater quality evaluation and protection. Environ. Earth Sci. 77, 1–30. doi:10.1007/s12665-018-7872-x

Maestre, J.P., Wahman, D.G., Speitel, G.E., 2016. Monochloramine cometabolism by Nitrosomonas europaea under drinking water conditions. Environ. Sci. Technol. Downloaded, 1–29. doi:DOI: 10.1021/acs.est.5b05641

Mahmoud, S.H., 2014. Investigation of rainfall-runoff modeling for Egypt by using remote sensing and GIS integration. Catena 120, 111–121. doi:10.1016/j.catena.2014.04.011

Mahmoud, S.H., Gan, T.Y., 2018. Urbanization and climate change implications in flood risk management: Developing an efficient decision support system for flood susceptibility mapping. Sci. Total Environ. 636, 152–167. doi:10.1016/j.scitotenv.2018.04.282

Maier, S.H., Powell, R.S., Woodward, C.A., 2000. Calibration and comparison of chlorine decay models for a test water distribution system. Water Res. 34, 2301–2309. doi:10.1016/S0043-1354(99)00413-3

Makepeace, D.K., Smith, D.W., Stanley, S.J., 1995. Urban Stormwater Quality: Summary of Contaminant Data. Crit. Rev. Environ. Sci. Technol. 25, 93–139. doi:10.1080/10643389509388476

Mannina, G., Viviani, G., 2010. An urban drainage stormwater quality model: Model

development and uncertainty quantification. J. Hydrol. 381, 248–265. doi:10.1016/j.jhydrol.2009.11.047

Manning, T.M., Wilson, S.P., Chapman, J.C., 1996. Toxicity of chlorine and other chlorinated compounds to some Australian aquatic organisms. Bull. Environ. Contam. Toxicol. 56, 971–976. doi:10.1007/s001289900140

Mansell, M., Rollet, F., 2008. The effect of surface texture on evaporation, infiltration and storage properties of paved surfaces, in: 11th International Conference on Urban Drainage. Scotland, UK, pp. 71–76. doi:10.2166/wst.2009.323

Marsalek, J., 1991. Pollutant Loads in Urban Stormwater: Review of Methods for Planning-Level Estimates. Am. Water Resour. Assoc. 27, 283–291. doi:10.1111/j.1752-1688.1991.tb03133.x

Maruéjouls, T., Lessard, P., Vanrolleghem, P.A., 2014. Calibration and validation of a dynamic model for water quality in combined sewer retention tanks. Urban Water J. 11, 668–677. doi:10.1080/1573062X.2013.847462

Matějíček, L., Engst, P., Jaňour, Z., 2006. A GIS-based approach to spatio-temporal analysis of environmental pollution in urban areas: A case study of Prague's environment extended by LIDAR data. Ecol. Modell. 199, 261–277. doi:10.1016/j.ecolmodel.2006.05.018

May, D.B., Sivakumar, M., 2009. Prediction of urban stormwater quality using artificial neural networks. Environ. Model. Softw. 24, 296–302. doi:10.1016/j.envsoft.2008.07.004

Mayer, P.W., DeOreo, W.B., 1998. Residential End Uses of Water, American Water Works Association.

McCuen, R.H., Knight, Z., Cutter, A.G., 2006. Evaluation of the Nash–Sutcliffe Efficiency Index. J. Hydrol. Eng. 11, 597–602. doi:10.1061/(ASCE)1084-0699(2006)11:6(597)

Metadier, M., Bertrand-Krajewski, J.L., 2012. The use of long-term on-line turbidity measurements for the calculation of urban stormwater pollutant concentrations, loads, pollutographs and intra-event fluxes. Water Res. 46, 6836–6856.

doi:10.1016/j.watres.2011.12.030

Meyer, J.L., Paul, M.J., Taulbee, W.K., 2005. Stream ecosystem function in urbanizing landscapes. J. North Am. Benthol. Soc. 24, 602–612. doi:10.1899/04-021.1

Miguntanna, N.S., Egodawatta, P., Kokot, S., Goonetilleke, A., 2010. Determination of a set of surrogate parameters to assess urban stormwater quality. Sci. Total Environ. 408, 6251–6259. doi:10.1016/j.scitotenv.2010.09.015

Miller, J.E., 1984. Basic Concepts of Kinematic-Wave Models, U.S. Geological Survey Professional Paper 1302.

Milne, G.D., Stanley, S.J., Smith, D.W., 1993. Residual chlorine decay in a broad, shallow river. Water Res. 27, 993–1001. doi:10.1016/0043-1354(93)90063-N

Mitchell, G., 2005. Mapping hazard from urban non-point pollution: a screening model to support sustinable urban drainage planning. J. Environ. Manage. 74, 1–9. doi:10.1016/j.jenvman.2004.08.002

Mitchell, V., Duncan, H., Inma, R., Rahilly, M., Stewart, J., Vieritz, A., Holt, P., Grant, A., Fletcher, T.D., Coleman, J., Maheepala, S., Sharma, A., Deletic, A., Breen, P., 2007. State of the art review of integrated urban water models, in: Brelot, E. (Ed.), NOVATECH 2007 - 6th International Conference on Sustainable Techniques and Strategies in Urban Water Management. Lyon, France, pp. 507–514.

Mitchell, V.G., Duncan, H., Inman, M., Rahilly, M., Stewart, J., Vieritz, a, Holt, P., Grant, a, Fletcher, T., Coleman, J., Et Al., 2007. Integrated Urban Water Modelling–Past, Present, and Future. Rainwater Urban Des. 2007 Jt. 13th Int. Rainwater Catchment Syst. Conf. 5th Int. Water Sensitive Urban Des. Conf. 21–23.

Monteiro, L., Figueiredo, D., Dias, S., Freitas, R., Covas, D., Menaia, J., Coelho, S.T., 2014. Modeling of chlorine decay in drinking water supply systems using EPANET MSX. Procedia Eng. 70, 1192–1200. doi:10.1016/j.proeng.2014.02.132

Moradi, S., Liu, S., Chow, C.W.K., van Leeuwen, J., Cook, D., Drikas, M., Amal, R., 2017.

Developing a chloramine decay index to understand nitrification: A case study of two chloraminated drinking water distribution systems. J. Environ. Sci. (China) 57, 170–179. doi:10.1016/j.jes.2016.11.007

Moriasi, D.N., Arnold, J.G., Van Liew, M.W., Binger, R.L., Harmel, R.D., Veith, T.L., 2007. Model evaluation guidelines for systematic quantification of accuracy in watershed simulations. Trans. ASABE 50, 885–900. doi:10.13031/2013.23153

Mostafa, N.G., Matta, M.E., Halim, H.A., 2013. Simulation of Chlorine Decay in Water Distribution Networks Using EPANET – Case Study. J. Civ. Environ. Res. 3, 100–113.

Mutoti, G., John D. Dietz, Arevalo, J., Taylor, J.S., 2007. Combined Chlorine dissipation: Pipe material, water quality, and hydraulic effects. Am. Water Work. Assoc. 99, 96–106.

Nagatani, T., Yasuhara, K., Murata, K., Takeda, M., Nakamura, T., Fuchigami, T., Terashima, K., 2006. Residual Chlorine Decay Simulation in Water Distribution System, in: The 7th International Symposium on Water Supply Technology. Yokohama, Japan, pp. 1–11.

Nas, B., Berktay, A., 2010. Groundwater quality mapping in urban groundwater using GIS. Environ. Monit. Assess. 160, 215–227. doi:10.1007/s10661-008-0689-4

Nash, J.E., Sutcliffe, J. V, 1970. River Flow Forecasting Through Conceptual Models Part I-a Discussion of Principles*. J. Hydrol. 10, 282–290. doi:10.1016/0022-1694(70)90255-6

Nath, B.K., Chaliha, C., Bhuyan, B., Kalita, E., Baruah, D.C., Bhagabati, A.K., 2018. GIS mapping-based impact assessment of groundwater contamination by arsenic and other heavy metal contaminants in the Brahmaputra River valley: A water quality assessment study. J. Clean. Prod. 201, 1001–1011. doi:10.1016/j.jclepro.2018.08.084

National Research Counsil NRC, 2008. Urban Stormwater Management in the United States. Washington, DC.

Nejjari, F., Puig, V., Perez, R., Quevedo, J., Cuguero, M.A., Sanz, G., Mirats, J.M., 2014. Chlorine decay model calibration and comparison: Application to a real water network. Procedia Eng. 70, 1221–1230. doi:10.1016/j.proeng.2014.02.135

Niu, C., Zhang, Y., Zhou, Y., Shi, K., Liu, X., Qin, B., 2014. The potential applications of real-time monitoring of water quality in a large shallow lake (Lake Taihu, China) using a chromophoric dissolved organic matter fluorescence sensor. Sensors (Switzerland) 14, 11580–11594. doi:10.3390/s140711580

Nobre, R.C.M., Rotunno Filho, O.C., Mansur, W.J., Nobre, M.M.M., Cosenza, C.A.N., 2007. Groundwater vulnerability and risk mapping using GIS, modeling and a fuzzy logic tool. J. Contam. Hydrol. 94, 277–292. doi:10.1016/j.jconhyd.2007.07.008

Novak, P., Guinot, V., Jeffrey, A., Reeve, D.E., 2010. Hydraulic Modelling - an introduction Principles, methods and applications. Spon Press, New York, NY.

Obropta, C.C., Kardos, J.S., 2007. Review of urban stormwater quality models: Deterministic, stochastic, and hybrid approaches. J. Am. Water Resour. Assoc. 43, 1508–1523. doi:10.1111/j.1752-1688.2007.00124.x

Omre, H., 1987. Bayesian kriging-Merging observations and qualified guesses in kriging. Math. Geol. 19, 25–39. doi:10.1007/BF01275432

Oudin, L., Andréassian, V., Mathevet, T., Perrin, C., Michel, C., 2006. Dynamic averaging of rainfall-runoff model simulations from complementary model parameterizations. Water Resour. Res. 42, 1–10. doi:10.1029/2005WR004636

Overton, D.E., Meadows, M.E., 1976. Stormwater Modeling Projects. ACADEMIC PRESS, INC., New York.

Ozdemir, O.N., Ucak, A., 2002. Simulation of Chlorine Decay in Drinking Water Distribution Systems. J. Environ. Eng. 128, 31–39. doi:10.1061/(ASCE)0733-9372(2002)128:1(31)

Paul, M.J., Meyer, J.L., 2001. Streams in the Urban Landscape. Annu. Rev. Ecol. Syst. 32, 333–365. doi:10.1146/annurev.ecolsys.32.081501.114040

Porretta-Brandyk, L., Chormanski, J., Brandyk, A., Okruszko, T., 2011. Automatic Calibration of the WetSpa Distributed Hydrological Model for Small Lowland Catchments, in: Mirosław-Swiatek, D., Okruszko, T. (Eds.), Modelling of Hydrological Processes in the

Narew Catchmentt: Earth and Planetary Sciences. Springer-Verlag Berlin Heidelberg, Berlin, pp. 43–62. doi:10.1007/978-3-642-19059-9

Potgieter, S., Pinto, A., Sigudu, M., du Preez, H., Ncube, E., Venter, S., 2018. Long-term spatial and temporal microbial community dynamics in a large-scale drinking water distribution system with multiple disinfectant regimes. Water Res. 139, 406–419. doi:10.1016/j.watres.2018.03.077

Powell, J.C., Hallam, N.B., West, J.R., Forster, C.F., Simms, J., 2000. Factors which dontrol bulk chlorine decay rates. Water Res. 34, 117–126.

Pradhan, B., Lee, S., Buchroithner, M.F., 2009. Use of geospatial data and fuzzy algebraic operators to landslide-hazard mapping. Appl. Geomatics 1, 3–15. doi:10.1007/s12518-009-0001-5

Pushpalatha, R., Perrin, C., Moine, N. Le, Andreassian, V., 2012. A review of efficiency criteria suitable for evaluating low-flow simulations. J. Hydrol. 420–421, 171–182. doi:10.1016/j.jhydrol.2011.11.055

Regan, J.M., Harrington, G.W., Daniel, R., Noguera, D.R., 2002. Ammonia- and Nitrite-Oxidizing Bacterial Communities in a Pilot-Scale Chloraminated Drinking Water Distribution System. Appl. Environ. Microbiol. - Am. Soc. Microbiol. 68, 73–81. doi:10.1128/AEM.68.1.73–81.2002

Reusser, D.E., Blume, T., Schaefli, B., Zehe, E., 2009. Analysing the temporal dynamics of model performance for hydrological models. Hydrol. Earth Syst. Sci. 13, 999–1018. doi:10.5194/hessd-5-3169-2008

Ritter, A., Munoz-Carpena, R., 2013. Performance evaluation of hydrological models: Statistical significance for reducing subjectivity in goodness-of-fit assessments. J. Hydrol. 480, 33–45. doi:10.1016/j.jhydrol.2012.12.004

Rossi, L., Calizza, E., Careddu, G., Rossi, D., Orlandi, L., Jona-Lasinio, G., Aguzzi, L., Costantini, M.L., 2018. Space-time monitoring of coastal pollution in the Gulf of Gaeta,

Italy, using Δ15N values of Ulva lactuca, landscape hydromorphology, and Bayesian Kriging modelling. Mar. Pollut. Bull. 126, 479–487. doi:10.1016/j.marpolbul.2017.11.063

Rossi, L., Chevre, N., Fankhauser, R., Margot, J., Curdy, R., Babut, M., Barry, D.A., 2013. Sediment contamination assessment in urban areas based on total suspended solids. Water Res. 47, 339–350. doi:10.1016/j.watres.2012.10.011

Rossman, L.A., Clark, R.M., Grayman, W.M., 1994. Modeling Chlorine Residuals in Drinking-Water Distribution Systems. J. Environ. Eng. 120, 803–820. doi:10.1061/(ASCE)0733-9372(1994)120%3A4(803)

Roy, A.H., Wenger, S.J., Fletcher, T.D., Walsh, C.J., Ladson, A.R., Shuster, W.D., Thurston, H.W., Brown, R.R., 2008. Impediments and solutions to sustainable, watershed-scale urban stormwater management: Lessons from Australia and the United States. Environ. Manage. 42, 344–359. doi:10.1007/s00267-008-9119-1

Roy, V., Simonetto, A., Leus, G., 2018. Spatio-temporal field estimation using kriged kalman filter (KKF) with sparsity-enforcing sensor placement. Sensors (Switzerland) 18. doi:10.3390/s18061778

Rubinato, M., Shucksmith, J., Saul, A.J., Shepherd, W., 2013. Comparison between InfoWorks hydraulic results and a physical model of an Urban drainage system. Water Sci. Technol. 68, 372–379. doi:10.2166/wst.2013.254

Sahu, S.K., 2012. A Bayesian Kriged-Kalman model for short-term fore- casting of air pollution levels. J. R. Stat. Soc. Ser. C 54, 223–244.

Salman, S.A., Arauzo, M., Elnazer, A.A., 2019. Groundwater quality and vulnerability assessment in west Luxor Governorate, Egypt. Groundw. Sustain. Dev. 8, 271–280. doi:10.1016/j.gsd.2018.11.009

Sarker, D.C., Sathasivan, A., 2012. Nitrification control by adjusting pH in severely nitrified bulkwaters. Water Sci. Technol. Water Supply 12, 683–690. doi:10.2166/ws.2012.042

Sathasivan, A., Chiang, J., Nolan, P., 2009. Temperature dependence of chemical and

microbiological chloramine decay in bulk waters of distribution system. Water Sci. Technol. Water Supply 9, 493–499. doi:10.2166/ws.2009.387

Sathasivan, A., Fisher, I., Tam, T., 2008. Onset of severe nitrification in mildly nitrifying chloraminated bulk waters and its relation to biostability. Water Res. 42, 3623–3632. doi:10.1016/j.watres.2008.05.010

Savic, D. a., Kapelan, Z.S., Jonkergouw, P.M.R., 2009. Quo vadis water distribution model calibration? Urban Water J. 6, 3–22. doi:10.1080/15730620802613380

Shakeel, M., Hussain, T., Hussain, M., Faisal, M., Soomro, Z.A., Hussain, I., 2014. Distribution of Total Dissolved Solids in Drinking Water by Means of Bayesian Kriging and Gaussian Spatial Predictive Process. Water Qual. Expo. Heal. 6, 177–185. doi:10.1007/s12403-014-0123-9

Shamseldin, A.Y., 1997. Application of a neural network technique to rainfall-runoff modelling. J. Hydrol. 199, 272–294. doi:10.1016/S0022-1694(96)03330-6

Shang, F., Uber, J.G., Rossman, L. a, 2008. Modeling reaction and transport of multiple species in water distribution systems. Environ. Sci. Technol. 42, 808–814. doi:10.1021/es072011z

Shang, F., Uber, J.G., Rossman, L.A., 2007. EPANET Multi-Species Extension User's Manual. Cincinnati, OH.

Shon, T.S., Kim, S.D., Cho, E.Y., Im, J.Y., Min, K.S., Shin, H.S., 2012. Estimation of NPS pollutant properties based on SWMM modeling according to land use change in urban area. Desalin. Water Treat. 38, 267–275. doi:10.1080/19443994.2012.664382

Shorshani, M.F., Bonhomme, C., Petrucci, G., André, M., Seigneur, C., 2014. Road traffic impact on urban water quality: A step towards integrated traffic, air and stormwater modelling. Environ. Sci. Pollut. Res. 21, 5297–5310. doi:10.1007/s11356-013-2370-x

Shrestha, D., He, J., 2017. Characterization and Modeling of Urban Water Quality in the City of Calgary, Canada. Nat. Resour. 08, 513–530. doi:10.4236/nr.2017.88032

Stephenson, D., Meadows, M.E., 1986. Kinematic Hydrology and Modelling. Elsevier Science Publishers B.V., Amsterdam.

Sung, W., Huang, X., Wei, I.W., 2005. Treatment and distribution system effects on chloramine decay, pH, nitrification, and disinfection by-products: case study. J. Water Resour. Plan. Manag. 131, 201–207. doi:10.1061/(ASCE)0733-9496(2005)131:3(201)

Svecevicius, G., Syvokiene, J., Stasiunaite, P., Mickeniene, L., 2005. Acute and chronic toxicity of chlorine dioxide (ClO2) and chlorite (ClO2 -) to rainbow trout (Oncorhynchus mykiss). Environ. Sci. Pollut. Res. 12, 302–305. doi:10.1065/espr2005.04.248

Tamminen, S., Ramos, H., Covas, D., 2008. Water supply system performance for different pipe materials part I: Water quality analysis. Water Resour. Manag. 22, 1579–1607. doi:10.1007/s11269-008-9244-x

Temprano, J., Arango, O., Cagiao, J., Suarez, J., Tejero, I., 2006. Stormwater quality calibration by SWMM: A case study in Northern Spain. Water SA 32, 55–63. doi:10.1080/09593332308618381

Thorndahl, S., Schaarup-Jensen, K., 2007. Comparative analysis of uncertainties in urban surface runoff modelling, in: 6th International Conference on Sustainable Techniques and Strategies in Urban Water Management, , June 25-28 2007. Novatech2007, Lyon, France, pp. 1631–1638.

Tsihrintzis, V.A., Hamid, R., 1998. Runoff quality prediction from small urban catchments using SWMM. Hydrol. Process. 12, 311–329. doi:10.1002/(SICI)1099-1085(199802)

Tsihrintzis, V.A., Hamid, R., 1997a. Modeling and management of urban stormwater runoff quality: a review. Water Resour. Manag. 11, 137–164. doi:10.1023/A:1007903817943

Tsihrintzis, V.A., Hamid, R., 1997b. Urban Stormwater Quantity/Quality Modelling Using the SCS Method and Imperical Equations. J. Am. Water Resour. Assoc. 33, 163–176.

Tsihrintzis, V.A., Hamid, R., Fuentes, H.R., 1996. Use of Geographic Information Systems (GIS) in water resources: A review. Water Resour. Manag. 10, 251–277.

doi:10.1007/BF00508896

US EPA, 2002. Guidance for Quality Assurance Project Plans for Modeling. Washington, DC.

US EPA, 1988. Ambient Water Quality Criteria for Chloride. Washington, DC. doi:EPA 440/5-88-001

US EPA, 1984. EPA Ambient Water Quality Criteria for Chlorine. Washington DC.

VanBriesen, J.M., Parks, S.L.I., Helbling, D.E., T.McCoy, S., 2011. Chlorine ResidualManagement forWater Distribution System Security, in: Clark, R.M. (Ed.), Handbook of Water and Wastewater Systems Protectio. Springer, New York, NY, pp. 27–46. doi:10.1007/978-1-4614-0189-6

Vasconcelos, J.J., Rossman, L.A., Grayman, W.M., Boulos, P.F., Clark, R.M., 1997. Kinetics of Chlorine Decay. J. Am. Water Work. Assoc. 89, 54–65.

Vaze, J., Chiew, F.H.S., 2003. Comparative evaluation of urban storm water quality models. Water Resour. Res. 39, 1280. doi:10.1029/2002WR001788

Vikesland, P.J., Ozekin, K., Valentine, R.L., 2001. Monochloramine decay in model and distribution system waters. Water Res. 35, 1766–1776. doi:10.1016/S0043-1354(00)00406-1

Vojtek, M., Vojteková, J., 2019. Flood Susceptibility Mapping on a National Scale in Slovakia Using the Analytical Hierarchy Process. Water 11, 364. doi:10.3390/w11020364

Vuţă, L., Pîrăianu, V., 2008. Infoworks WS and epanet v2 - Modeling the water distribution networks. UPB Sci. Bull. Ser. D Mech. Eng. 70, 91–102.

Wahman, D.G., Speitel, G.E., 2012. Relative importance of nitrite oxidation by hypochlorous acid under chloramination conditions. Environ. Sci. Technol. 46, 6056–6064. doi:10.1021/es300934x

Walsh, C.J., 2000. Urban impacts on the ecology of receiving waters: a framework for

assessment, conservation and restoration. Hydrobiologia 431, 107–114.

Walsh, C.J., Booth, D.B., Burns, M.J., Fletcher, T.D., Hale, R.L., Hoang, L.N., Livingston, G., Rippy, M.A., Roy, A.H., Scoggins, M., Wallace, A., 2016. Principles for urban stormwater management to protect stream ecosystems. Freshw. Sci. 35, 398–411. doi:10.1086/685284

Wang, Y., Luan, Q., Wang, H., Liu, J., Ma, J., 2019. Risk Assessment of Rainstorm Waterlogging in New District Based on MIKE Urban, in: Dong, W., Lian, Y., Zhang, Y. (Eds.), Sustainable Development of Water Resources and Hydraulic Engineering in China. Springer, Cham, Switzerland, pp. 29–40.

Węglarczyk, S., 1998. The interdependence and applicability of some statistical quality measures for hydrological models. J. Hydrol. 206, 98–103. doi:10.1016/S0022-1694(98)00094-8

Wei, T., Wijesiri, B., Jia, Z., Li, Y., Goonetilleke, A., 2019. Re-thinking classical mechanistic model for pollutant build-up on urban impervious surfaces. Sci. Total Environ. 651, 114–121. doi:10.1016/j.scitotenv.2018.09.013

Westbrook, A., Digiano, F.A., 2009. Rate of chloramine decay at pipe surfaces. J. / Am. Water Work. Assoc. 101, 59–70. doi:10.1002/j.1551-8833.2009.tb09924.x

WHO, 2004. Monochloramine in Drinking-water, Background document for development of WHO Guidelines for Drinking-water Quality.

Wijesiri, B., Deilami, K., McGree, J., Goonetilleke, A., 2018. Use of surrogate indicators for the evaluation of potential health risks due to poor urban water quality: A Bayesian Network approach. Environ. Pollut. 233, 655–661. doi:10.1016/j.envpol.2017.10.076

Wilcox, B.P., Rawls, W.J., Brakensiek, D.L., Wight, J.R., 1990. Predicting runoff from Rangeland Catchments: A comparison of two models. Water Resour. Res. 26, 2401–2410. doi:10.1029/WR026i010p02401

Willmott, C.J., 1981. On the validation of models. Phys. Geogr. doi:10.1080/02723646.1981.10642213

Wong, T., Koh, X., 2008. Which model type is best for deterministic rainfall-runoff modelling?, in: Robinson, L.N. (Ed.), Water Resources Research Progress. Nova Science Publishers, New York, pp. 241–260.

Wong, T.S.W., 2009. Kinematic-Wave Rainfall-Runoff Formulas. Nova Science Publishers, Inc., New York.

Wooding, R.A., 1965. A Hydraulic Model for the Catchment-Stream Problem. J. Hydrol. 3, 254–267.

Xie, Y., Chen, T. Bin, Lei, M., Yang, J., Guo, Q.J., Song, B., Zhou, X.Y., 2011. Spatial distribution of soil heavy metal pollution estimated by different interpolation methods: Accuracy and uncertainty analysis. Chemosphere 82, 468–476. doi:10.1016/j.chemosphere.2010.09.053

Yao, H., Li, W., Qian, X., 2015. Identification of major risk sources for surface water pollution by risk indexes (RI) in the multi-provincial boundary region of the taihu basin, China. Int. J. Environ. Res. Public Health 12, 10150–10170. doi:10.3390/ijerph120810150

Yapo, P.O., Gupta, H.V., Sorooshian, S., 1998. Multi-objective global optimization for hydrologic models. J. Hydrol. 204, 83–97. doi:10.1016/S0022-1694(97)00107-8

Ye, W., Jakeman, A.J., Young, P.C., 1998. Identification of improved rainfall-runoff models for an ephemeral low-yielding Australian catchment. Environ. Model. Softw. 13, 59–74. doi:10.1016/S1364-8152(98)00004-8

Zambrano-Bigiarini, M., 2017. Goodness of fit functions for numerical and graphical comparison of simulated and observed time series for hydrological modelling.

Zhang, Q., Davies, E.G.R., Bolton, J., Liu, Y., 2017. Monochloramine Loss Mechanisms in Tap Water. Water Environ. Res. 89, 1999–2005. doi:10.2175/106143017X14902968254421

Zhang, Q., Davies, E.G.R., Bolton, J.R., Liu, Y., 2018a. Monochloramine loss mechanisms and dissolved organic matter characterization in stormwater. Sci. Total Environ. 631–632, 745–754. doi:10.1016/j.scitotenv.2018.02.335

Zhang, Q., Gaafar, M., Davies, E.G.R., Bolton, J.R., Liu, Y., 2018b. Monochloramine Dissipation in Storm Sewer Systems : Field Testing and Model Development. Water Sci. Technol. 78, 2279–2287.

Zhang, Q., Gaafar, M., Yang, R.C., Ding, C., Davies, E.G.R., Bolton, J.R., Liu, Y., 2018c. Field data analysis of active chlorine-containing stormwater samples. J. Environ. Manage. 206, 51–59. doi:10.1016/j.jenvman.2017.10.009

Zhang, W., Che, W., Liu, D.K., Gan, Y.P., Lv, F.F., 2012. Characterization of runoff from various urban catchments at different spatial scales in Beijing, China. Water Sci. Technol. 66, 21–27. doi:10.2166/wst.2012.156

Zhang, W., Li, T., Dai, M., 2015. Uncertainty assessment of water quality modeling for a small-scale urban catchment using the GLUE methodology: a case study in Shanghai, China. Environ. Sci. Pollut. Res. 22, 9241–9249. doi:10.1007/s11356-015-4085-7

Zillich, J. a, 1972. Toxicity of combined chlorine residuals to freshwater fish. J. Water Pollut. Control Fed. 44, 212–220.

Zoppou, C., 2001. Review of urban storm water models. Environ. Model. Softw. 16, 195–231. doi:10.1016/S1364-8152(00)00084-0

Zoppou, C., 1999. Review of Storm Water Models. CSIRO L. Water. Technical No 52/99. doi:ISBN 0 643 06075 8

Zvinavashe, E., Van Den Berg, H., Soffers, A.E.M.F., Vervoort, J., Freidig, A., Murk, A.J., Rietjens, I.M.C.M., 2008. QSAR models for predicting in vivo aquatic toxicity of chlorinated alkanes to fish. Chem. Res. Toxicol. 21, 739–745. doi:10.1021/tx700367c

APPENDIX A

DESCRIPTION OF COLLECTED DATA

Table A1 Collected data description, source and application

Item	Source	Format	Description	Data application			
				Stormwater modeling	Water quality simulations	Concentration maps	Hazard assessment
A) GIS Data							
Aerial images	City of Edmonton, update version 2014	Raster images	Satellite raster images that cover the area of the 30th Avenue and Kennedale stormwater basins	■	■	■	■
DEM	City of Edmonton, update version 2013	Shapefile Feature Class	digital elevation models with spatial resolution of 1.5 m, and resolution of topography of 0.1 m	■			■
Land-use data	City of Edmonton, update version 2015	Shapefile Feature Class	Simplified land-use types were used to represent spatial variability of land-use across the study area.	■	■		■
Property assessment maps	City of Edmonton, update version 2015	KML files	Data was downloaded directly from the City's open portal (ww.edmonton.ca)	■			■
Low development residential uses	Developed based on Google maps, update version 2016	KML files	Based on aerial images and the provided property assessment data by the City of Edmonton, the low development residential land-use was estimated.	■			■
Parklands locations	Developed based on Google maps, update version 2016	KML files	Location of different parks within the study area and accessibility.	■			
Stormwater ponds locations	Developed based on Google maps, update version 2016	KML files	Location of different wet stormwater ponds within the study area.	■			
Locations of pressure vessel manufacturers	Developed based on Google, Alberta Pressure Vessel Manufacturing Sector website and telephone listings, update version 2016	KML files	Spatial distribution of pressure vessel manufacturers in Edmonton different wet stormwater ponds within the study area.	■			
Locations of car services vendors	Developed based on Google maps and telephone listings	KML files	Automobile-related service providers such as car rental agencies, car washers and dealerships	■			
Catchment Slopes	Developed from DEM	File System Raster	Using DEM data, catchment slopes were estimated using geospatial analyst in ArcGIS.	■			■

Impervious surfaces density	Developed from aerial images and land-use maps.	Shapefile Feature Class	Based on roofline data provided by the CoE and special GIS layers prepared for roadways, parking areas and driveways.	■			■
Neighborhoods	City of Edmonton	Shapefile Feature Class	Sub catchments / neighborhoods in the study area.			■	■
Average annual rainfall for Edmonton	Environment Canada	Excel sheets	Historical rainfall data collected over the last decade was used to develop average annual rainfall for Edmonton (Environment Canada, 2018).				■
B) Sewer system attributes							
Sewer system attributes	City of Edmonton, update version 2015	DGN files and spreadsheets	attributes and layouts of the stormwater network components from the DRAINS database.	■	■	■	■
MIKE URBAN models	City of Edmonton, update version 2015	DHI MOUSE files	Models of the two study basins were provided uncalibrated to the trunk level.	■			
Parklands attributes	City of Edmonton, update version 2016	Excel sheets	Data about the city's parklands, including area, irrigation status, metering and type of watering source.	■			
C) Other							
Rainfall data	City of Edmonton, update version 2017	Spreadsheets	Long-term rainfall data was provided for a network of rain gauges in and around the study basins.	■			
Pipe flow monitoring data	City of Edmonton	Spreadsheets	Temporary pipe flow monitoring values for the summer seasons of 2015 and 2016 at one permeant and three temporary locations.	■			
Field sampling results	Collected	Spreadsheets	Field data collection over the two summers of 2015 and 2016, data available at Zhang et al. (2018a, 2018b, 2018c).		■	■	■
Design storm data	Government of Canada	Charts	IDF curves for Edmonton were obtained and used to calculate design storms of return periods of 2, 5 and 10 years (Government of Canada, 2018).				■
Chloramine decay	Zhang et al (2018a, 2018b, 2018c)	Collected	Land-use dependent coefficients for commercial, residential, industrial and park areas were 0.00888, 0.00089, 0.00846 and 0.0019 respectively.		■	■	■

APPENDIX B
ADDITIONAL INFORMATION ON THE STORMWATER MODEL IN MIKE URBAN

This section presents the main settings used to build the stormwater model of the 30th Avenue stormwater basin in MIKE URBAN. As discussed earlier, the kinematic wave and dynamic wave modules were used to conduct the surface runoff and pipe flow routings, respectively.

B1 System definitions

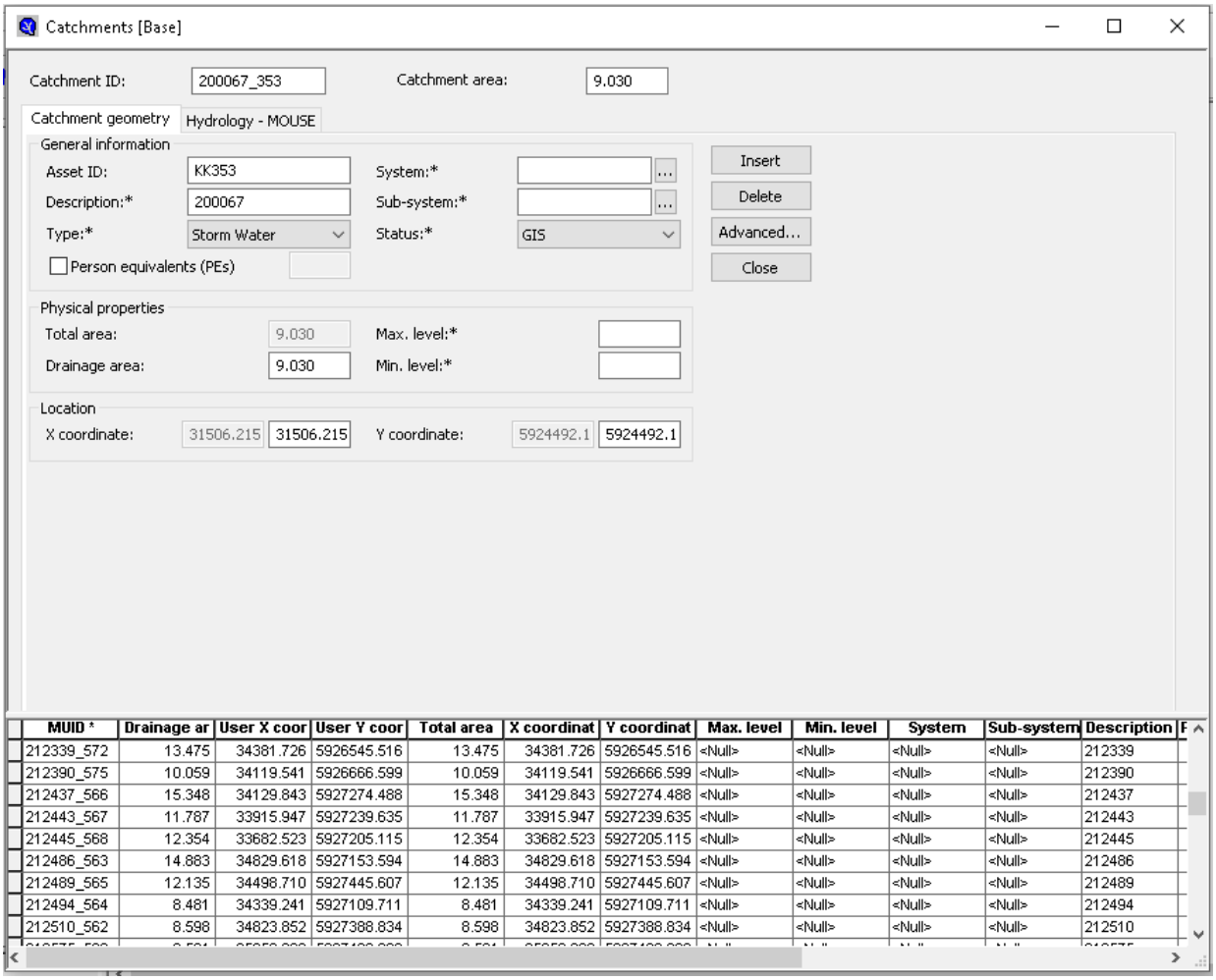

MUID *	Drainage ar	User X coor	User Y coor	Total area	X coordinat	Y coordinat	Max. level	Min. level	System	Sub-system	Description
212339_572	13.475	34381.726	5926545.516	13.475	34381.726	5926545.516	<Null>	<Null>	<Null>	<Null>	212339
212390_575	10.059	34119.541	5926666.599	10.059	34119.541	5926666.599	<Null>	<Null>	<Null>	<Null>	212390
212437_566	15.348	34129.843	5927274.488	15.348	34129.843	5927274.488	<Null>	<Null>	<Null>	<Null>	212437
212443_567	11.787	33915.947	5927239.635	11.787	33915.947	5927239.635	<Null>	<Null>	<Null>	<Null>	212443
212445_568	12.354	33682.523	5927205.115	12.354	33682.523	5927205.115	<Null>	<Null>	<Null>	<Null>	212445
212486_563	14.883	34829.618	5927153.594	14.883	34829.618	5927153.594	<Null>	<Null>	<Null>	<Null>	212486
212489_565	12.135	34498.710	5927445.607	12.135	34498.710	5927445.607	<Null>	<Null>	<Null>	<Null>	212489
212494_564	8.481	34339.241	5927109.711	8.481	34339.241	5927109.711	<Null>	<Null>	<Null>	<Null>	212494
212510_562	8.598	34823.852	5927388.834	8.598	34823.852	5927388.834	<Null>	<Null>	<Null>	<Null>	212510

Fig. B1 Definition of the catchment geometry

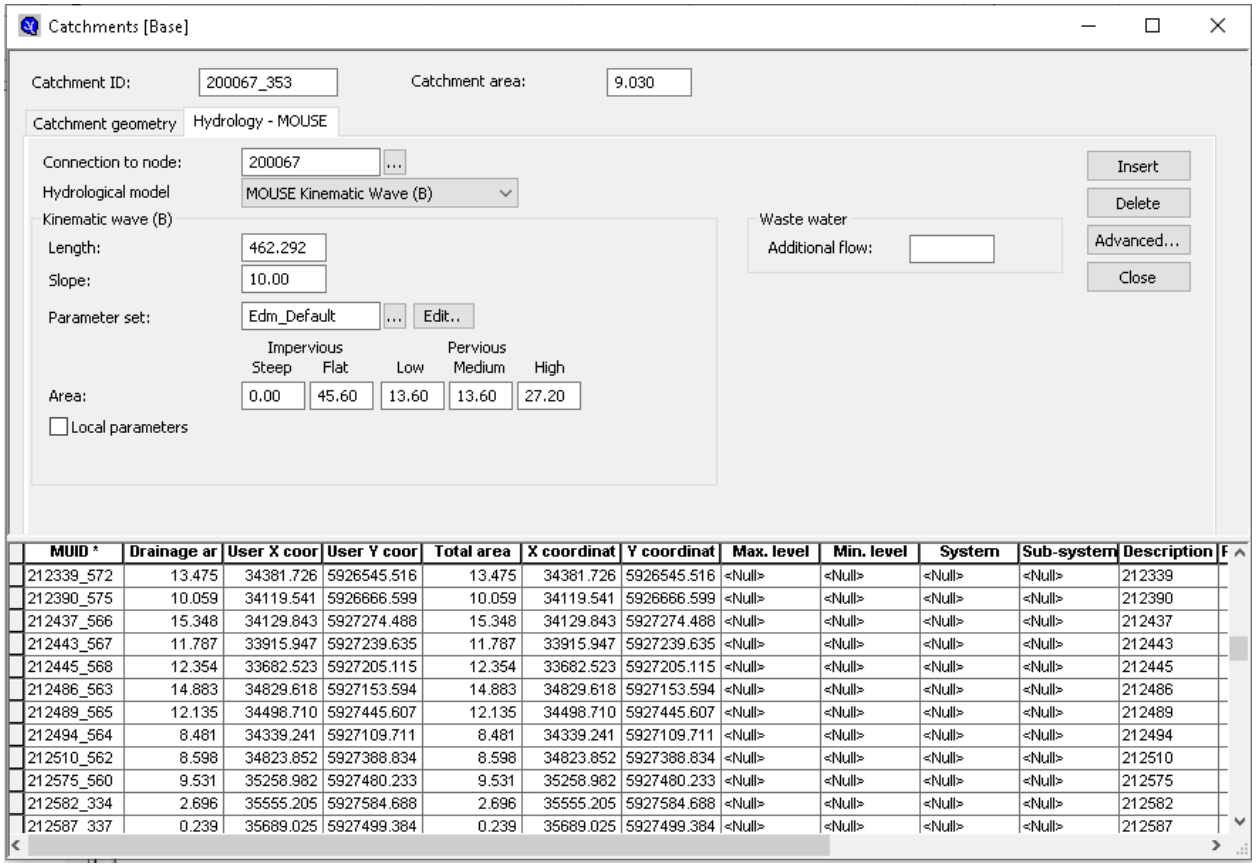

MUID *	Drainage ar	User X coor	User Y coor	Total area	X coordinat	Y coordinat	Max. level	Min. level	System	Sub-system	Description
212339_572	13.475	34381.726	5926545.516	13.475	34381.726	5926545.516	<Null>	<Null>	<Null>	<Null>	212339
212390_575	10.059	34119.541	5926666.599	10.059	34119.541	5926666.599	<Null>	<Null>	<Null>	<Null>	212390
212437_566	15.348	34129.843	5927274.488	15.348	34129.843	5927274.488	<Null>	<Null>	<Null>	<Null>	212437
212443_567	11.787	33915.947	5927239.635	11.787	33915.947	5927239.635	<Null>	<Null>	<Null>	<Null>	212443
212445_568	12.354	33682.523	5927205.115	12.354	33682.523	5927205.115	<Null>	<Null>	<Null>	<Null>	212445
212486_563	14.883	34829.618	5927153.594	14.883	34829.618	5927153.594	<Null>	<Null>	<Null>	<Null>	212486
212489_565	12.135	34498.710	5927445.607	12.135	34498.710	5927445.607	<Null>	<Null>	<Null>	<Null>	212489
212494_564	8.481	34339.241	5927109.711	8.481	34339.241	5927109.711	<Null>	<Null>	<Null>	<Null>	212494
212510_562	8.598	34823.852	5927388.834	8.598	34823.852	5927388.834	<Null>	<Null>	<Null>	<Null>	212510
212575_560	9.531	35258.982	5927480.233	9.531	35258.982	5927480.233	<Null>	<Null>	<Null>	<Null>	212575
212582_334	2.696	35555.205	5927584.688	2.696	35555.205	5927584.688	<Null>	<Null>	<Null>	<Null>	212582
212587_337	0.239	35689.025	5927499.384	0.239	35689.025	5927499.384	<Null>	<Null>	<Null>	<Null>	212587

Fig. B2 Definition of the catchment surface hydrology

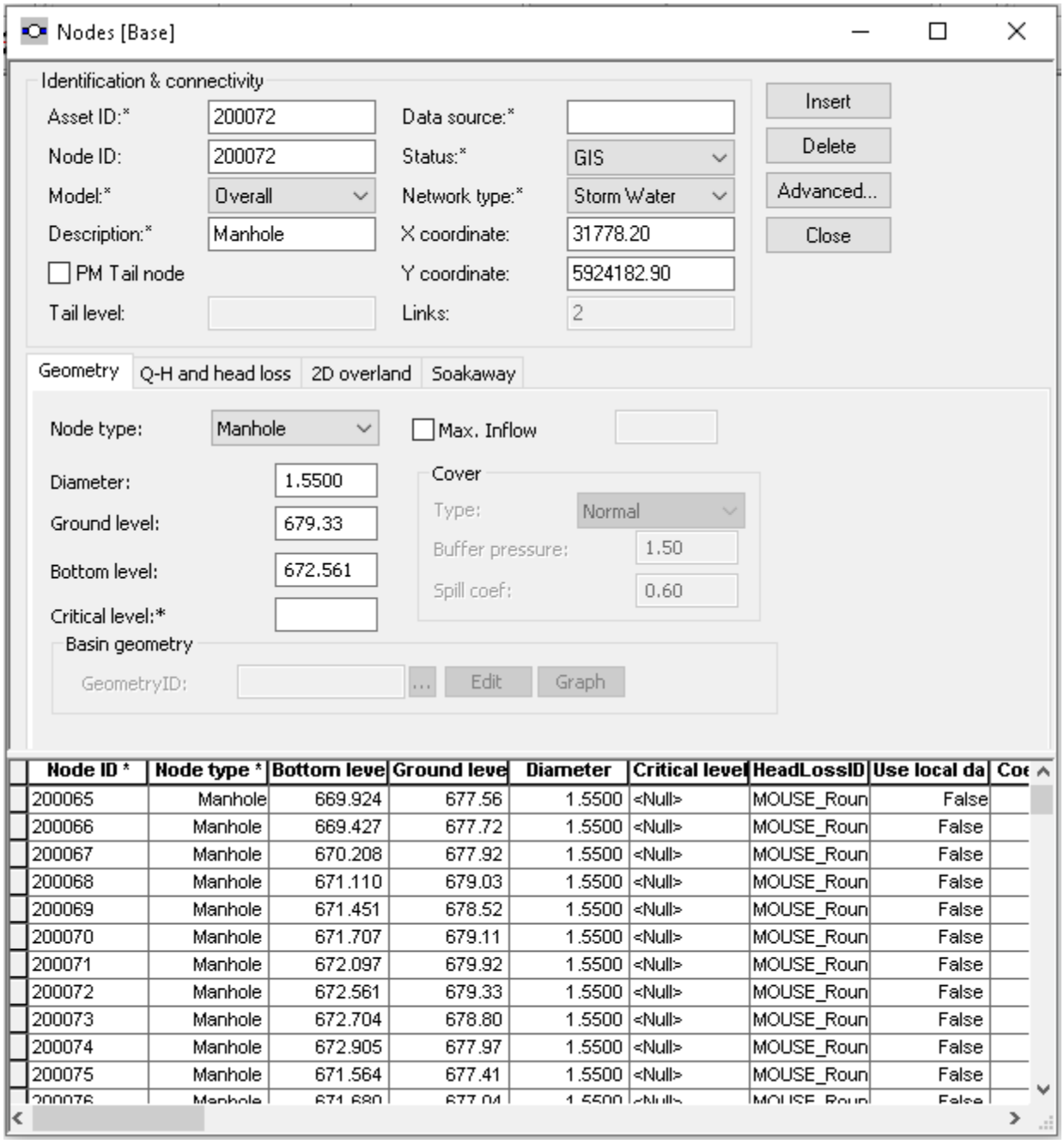

Fig. B3 Definition of the system nodes in MIKE URBAN

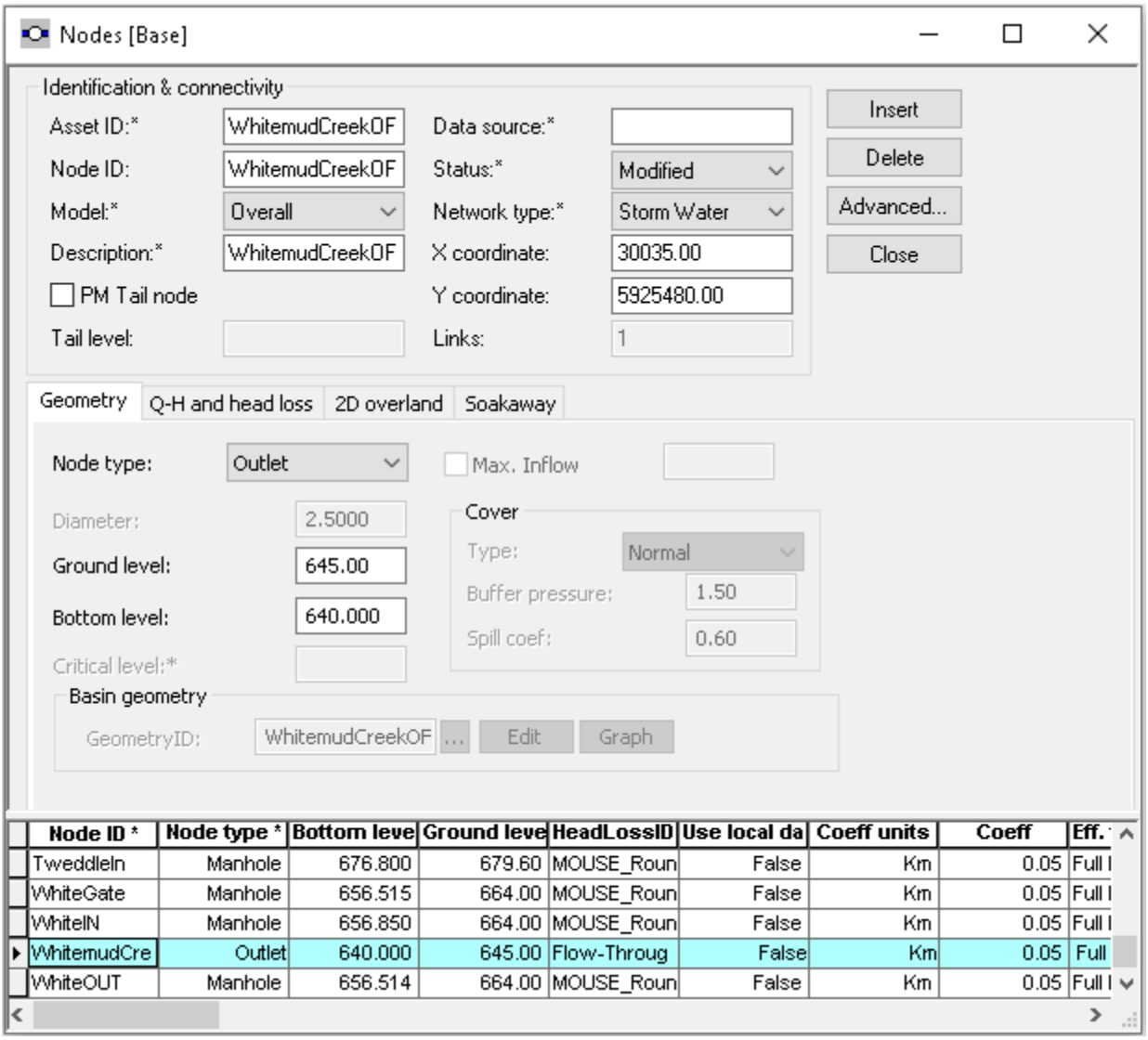

Fig. B4 Definition of the system outlet nodes in MIKE URBAN

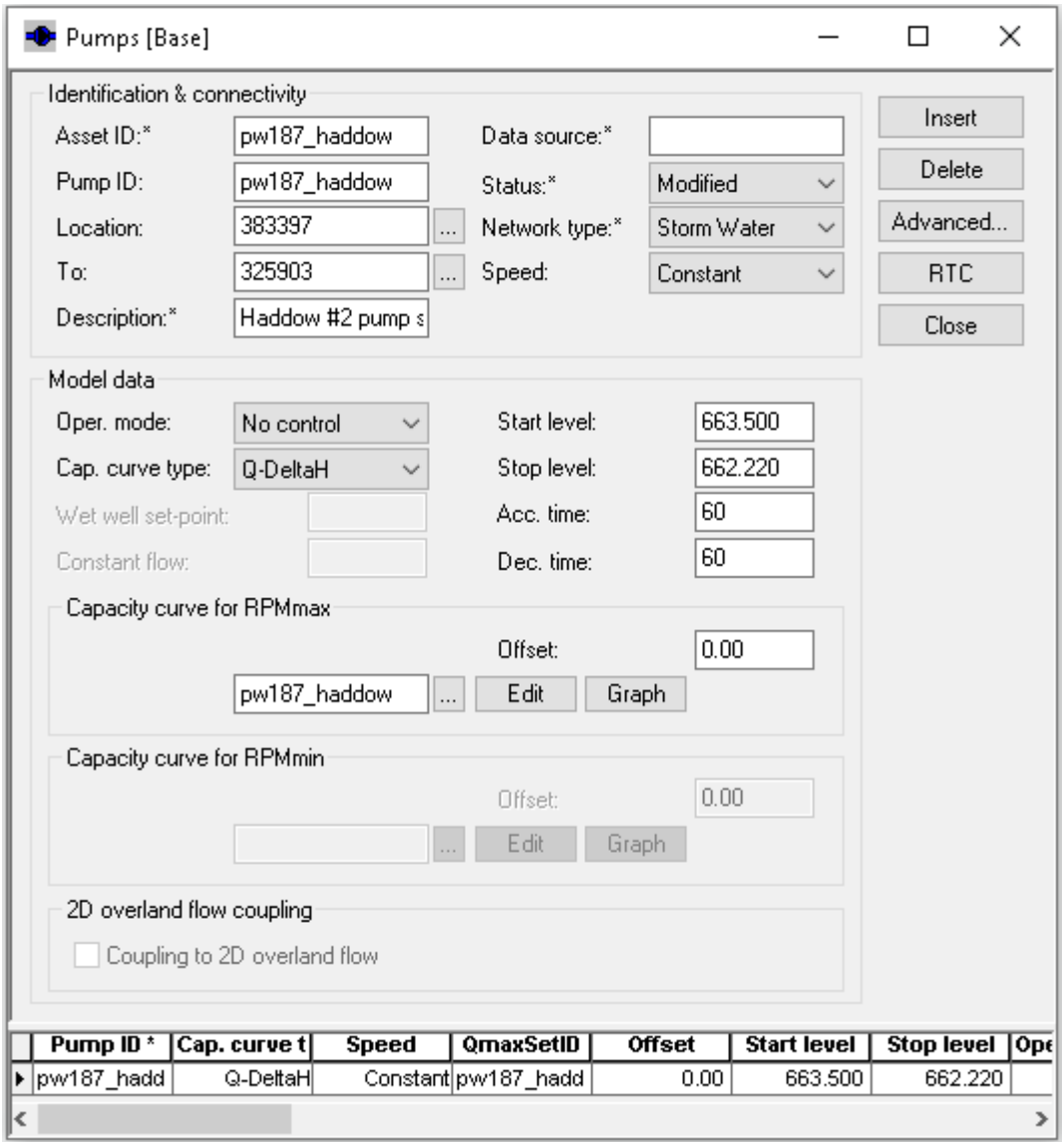

Fig. B5 Definition of a stormwater pump in MIKE URBAN

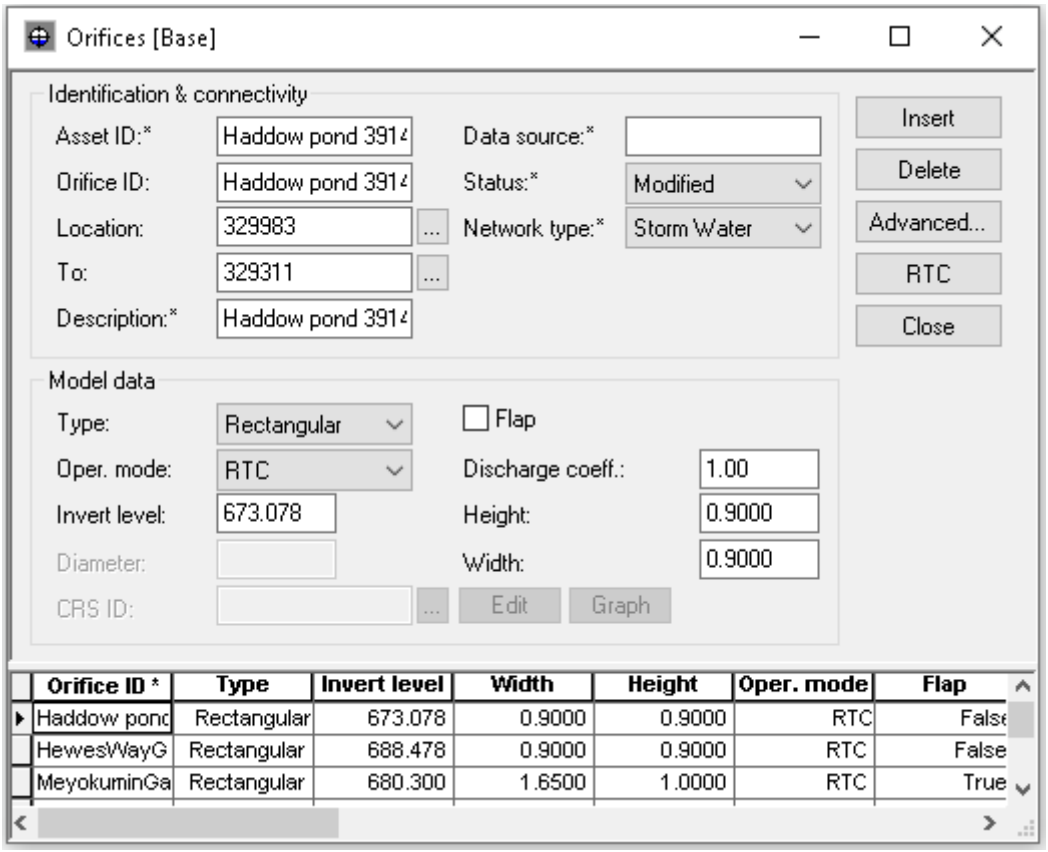

Fig. B6 Definition of a stormwater orifice in MIKE URBAN

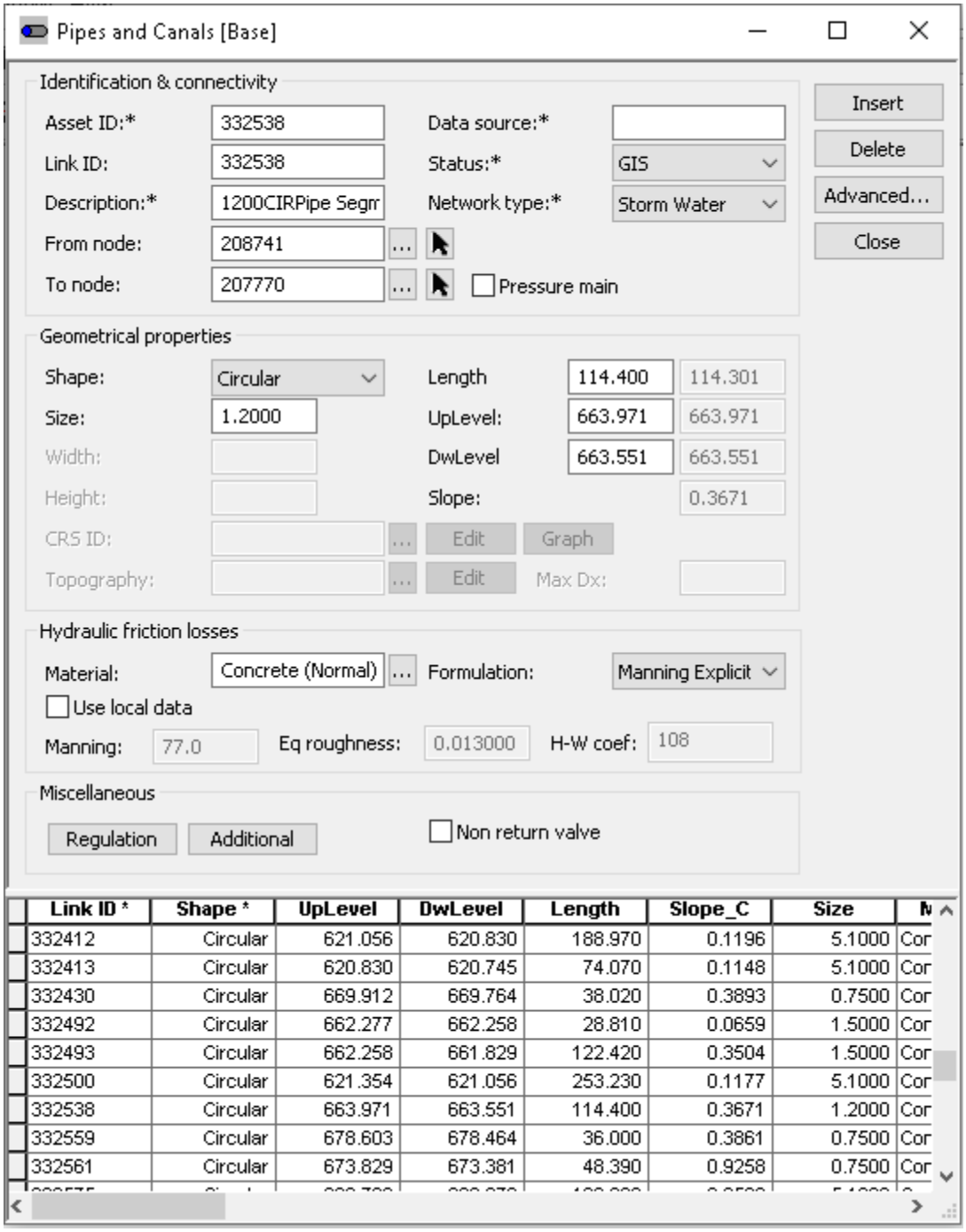

Link ID *	Shape *	UpLevel	DwLevel	Length	Slope_C	Size	M
332412	Circular	621.056	620.830	188.970	0.1196	5.1000	Cor
332413	Circular	620.830	620.745	74.070	0.1148	5.1000	Cor
332430	Circular	669.912	669.764	38.020	0.3893	0.7500	Cor
332492	Circular	662.277	662.258	28.810	0.0659	1.5000	Cor
332493	Circular	662.258	661.829	122.420	0.3504	1.5000	Cor
332500	Circular	621.354	621.056	253.230	0.1177	5.1000	Cor
332538	Circular	663.971	663.551	114.400	0.3671	1.2000	Cor
332559	Circular	678.603	678.464	36.000	0.3861	0.7500	Cor
332561	Circular	673.829	673.381	48.390	0.9258	0.7500	Cor

Fig. B7 Definition of the stormwater pipes in MIKE URBAN

B2 Module parameters

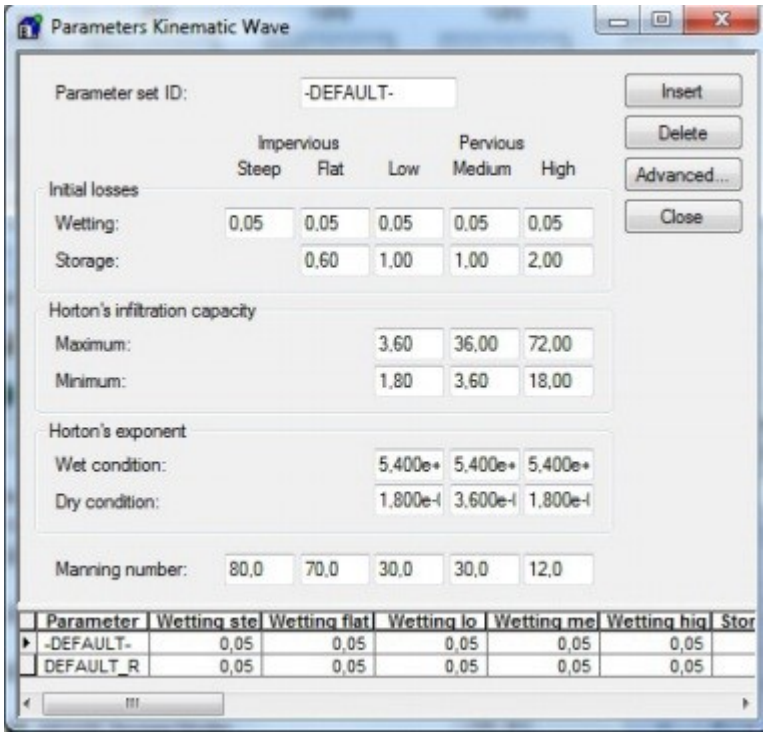

Fig. B8 The global Kinematic Wave Model editor in MIKE URBAN

Table B1 The Kinematic Wave Model calibrated parameters for the 30th Avenue basin

Model Parameter	Unit	Minimum	Average	Maximum
Wetting losses (impervious steep)	m	$5.0x10^{-4}$	$7.0x10^{-4}$	$9.0x10^{-4}$
Wetting losses (impervious flat)	m	$5.0x10^{-4}$	$7.0x10^{-4}$	$9.0x10^{-4}$
Wetting losses (pervious low)	m	$5.0x10^{-4}$	$7.0x10^{-4}$	$9.0x10^{-4}$
Wetting losses (pervious medium)	m	$5.0x10^{-4}$	$7.0x10^{-4}$	$9.0x10^{-4}$
Wetting losses (pervious high)	m	$5.0x10^{-4}$	$7.0x10^{-4}$	$9.0x10^{-4}$
Storage losses (impervious flat)	m	$1.0x10^{-3}$	$2.0x10^{-3}$	$4.0x10^{-3}$
Storage losses (pervious low)	m	$9.0x10^{-3}$	$1.1x10^{-2}$	$2.5x10^{-2}$
Storage losses (pervious medium)	m	$9.0x10^{-3}$	$1.1x10^{-2}$	$2.5x10^{-2}$
Storage losses (pervious high)	m	$9.0x10^{-3}$	$1.1x10^{-2}$	$2.5x10^{-2}$
Horton's infiltration maximum capacity (pervious low)	m/s	$8.0x10^{-7}$	$4.0x10^{-6}$	$8.0x10^{-6}$
Horton's infiltration maximum capacity (pervious medium)	m/s	$2.5x10^{-6}$	$6.0x10^{-6}$	$1.25x10^{-5}$
Horton's infiltration maximum capacity (pervious high)	m/s	$4.2x10^{-6}$	$8.1x10^{-6}$	$2.1x10^{-5}$
Horton's infiltration minimum capacity (pervious low)	m/s	$8.0x10^{-7}$	$1.0x10^{-6}$	$1.2x10^{-6}$
Horton's infiltration minimum capacity (pervious medium)	m/s	$9.5x10^{-7}$	$1.12x10^{-6}$	$1.425x10^{-6}$
Horton's infiltration minimum capacity (pervious high)	m/s	$1.1x10^{-6}$	$1.35x10^{-6}$	$1.65x10^{-6}$
Horton's exponent wet conditions (pervious low)	N/A	$9.0x10^{-4}$	$1.2x10^{-3}$	$1.2x10^{-3}$
Horton's exponent wet conditions (pervious medium)	N/A	$9.0x10^{-4}$	$1.2x10^{-3}$	$1.2x10^{-3}$
Horton's exponent wet conditions (pervious high)	N/A	$9.0x10^{-4}$	$1.2x10^{-3}$	$1.2x10^{-3}$

Horton's exponent dry conditions (pervious low)	N/A	$3.0x10^{-5}$	$3.0x10^{-5}$	$3.0x10^{-5}$
Horton's exponent dry conditions (pervious medium)	N/A	$3.0x10^{-5}$	$3.0x10^{-5}$	$3.0x10^{-5}$
Horton's exponent dry conditions (pervious high)	N/A	$3.0x10^{-5}$	$3.0x10^{-5}$	$3.0x10^{-5}$
Manning number (impervious steep)	N/A	48.0	52.0	56.0
Manning number (impervious flat)	N/A	48.0	52.0	56.0
Manning number (pervious low)	N/A	26.0	28.0	30.0
Manning number (pervious medium)	N/A	26.0	28.0	30.0
Manning number (pervious high)	N/A	3.3	3.3	3.3
Manning number (concrete pipe)	N/A	68	77	85

APPENDIX C

VARIABLE DECAY COEFFICIENT SIMULATOR: MODEL DISCRIPTION, USE GUIDE, AND MODEL CODE

This appendix describes the different component of the Variable Decay coefficient Simulator (VDCS), its modeling interface, inputs and input files, and how to run. The appendix also provides the model code in Python. This appendix is supplemented with the information provided for the model development as discussed in both Chapter 4 and Chapter 5. Therefore, this document is not a standalone but rather complements the model description provided earlier.

C1 About Python

The VDCS model is implemented using a programming language called Python. Python is an interpreted, high-level, general-purpose programming coding language, created by Guido van Rossum and first released in 1991, which is available for free from the Python Software Foundation, at (https://www.python.org/).

The installment guide of Python and the user's guide can be accessed through the website of Python at (https://www.python.org/doc/). Fig. C1 shows the user interface of Python.

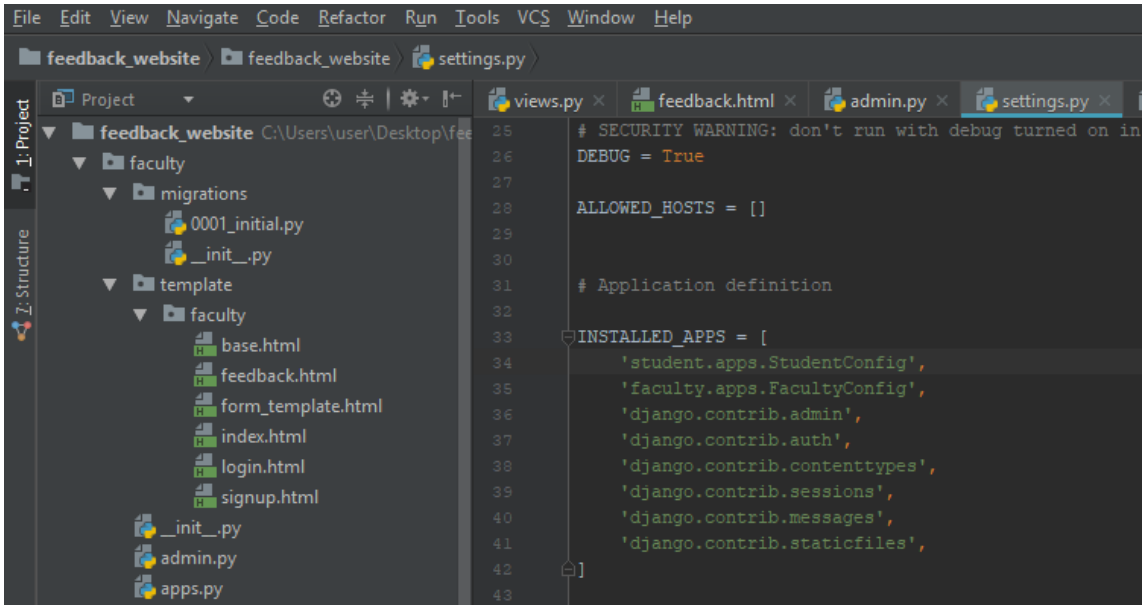

Fig. C1 User interface of Python

C2 Model structure

The water quality computation process in the VDCS is shown in Fig. C2. The first tier represents the required inputs to the VDCS. The second tier represents the model computations. The last tier is for the model outputs.

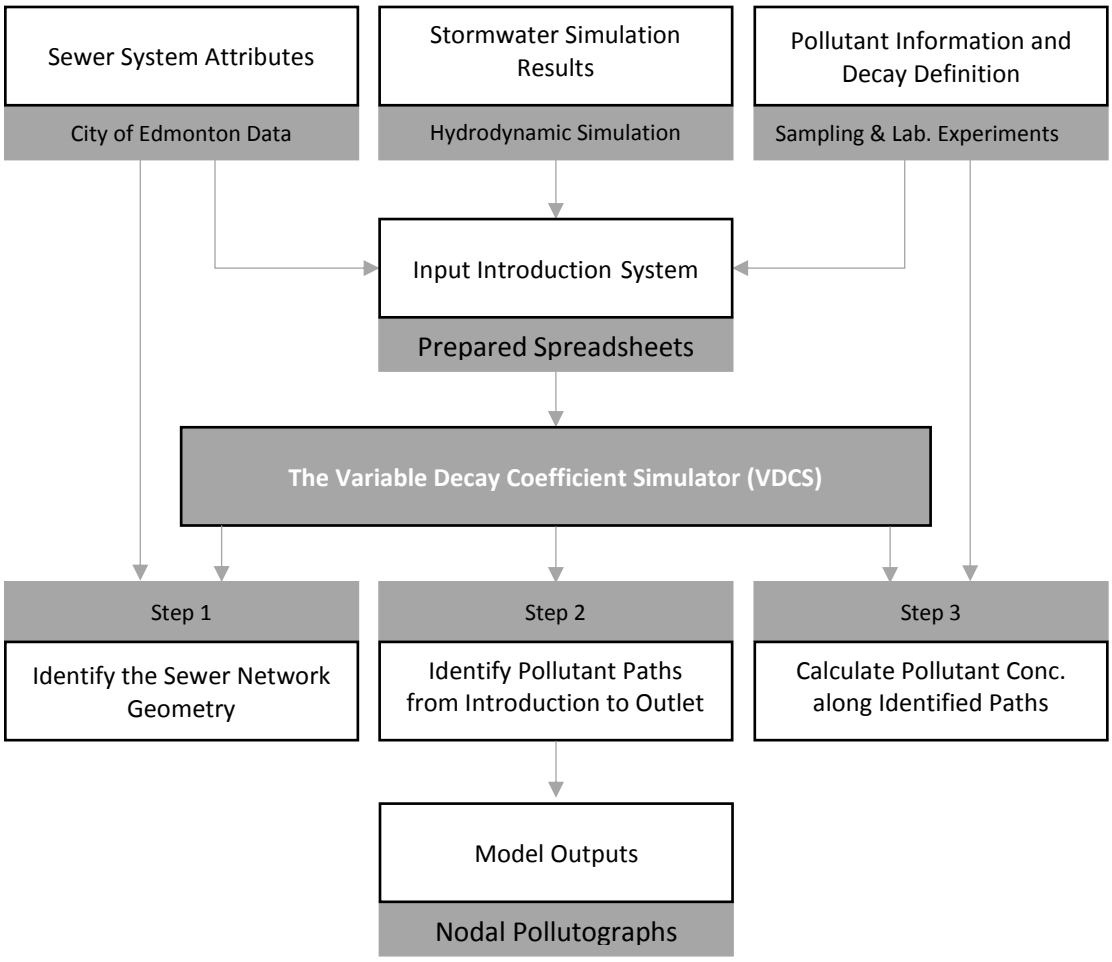

Fig. C2 Simplified schematic diagram of inputs, process flow and outputs of in the VDCS model

C3 Model inputs

For simplicity, the VCDS reads the required inputs from files in the form of spreadsheets, either in .csv or .xls file formats. Inputs are categorized into three groups. First, sewer system attribute data are required, which describe different system properties for sewer pipes, manholes, and outlets, in terms of diameters, lengths, material and invert levels, and manhole IDs at both upstream and downstream ends of each pipe in the system. The VDCS uses these data to reconstruct the physical geometry of the water network from upstream branches, diversion and collection nodes, and through to the system outlet. This reproduction of the network layout is required later to determine the paths of pollutants through the sewer system. A sample of this input is shown in Fig. C3.

	A	B	C	D	E	F	H	I	K	P	Q
1	Input 1										
2	Pipe ID	Diameter	Material	Slope %	Length	U/S ID	U/S Invert	/S Elevatio	D/S ID	1/n	LandUse
3	77623	0.9	Concrete (Normal)	1.8257584	89.99	200349	665.444	663.801	200350	77	Residential
4	328800	1.2	Concrete (Normal)	0.4636234	56.08	200350	663.472	663.212	200328	77	Residential
5	77603	1.2	Concrete (Normal)	0.5162331	99.18	200328	663.182	662.67	200329	77	Residential
6	77670	1.2	Concrete (Normal)	0.4793077	90.13	200394	661.941	661.509	200395	77	Residential
7	77671	1.2	Concrete (Normal)	0.5470801	121.92	200329	662.639	661.972	200394	77	Residential
8	79354	1.2	Concrete (Normal)	0.2401808	35.39	208402	660.844	660.759	510464	77	Residential
9	79355	1.2	Concrete (Normal)	0.7593239	37.27	208403	660.255	659.972	208404	77	Residential
10	79360	1.2	Concrete (Normal)	0.4669847	39.83	208407	661.03	660.844	208402	77	Residential
11	79364	1.2	Concrete (Normal)	0.5544475	75.21	200395	661.478	661.061	208407	77	Residential
12	500464	1.2	Concrete (Normal)	0.2024708	29.14	510464	660.759	660.7	208403	77	Residential
13	79356	1.2	Concrete (Normal)	0.7703358	55.69	208404	659.972	659.543	208393	77	Residential
14	79357	1.35	Concrete (Normal)	0.6913254	45.42	208393	659.39	659.076	329414	77	Residential
15	328798	1.35	Concrete (Normal)	0.154424	23.96	329414	659.076	659.039	510472	77	Residential
16	500472	1.35	Concrete (Normal)	0.951348	32.27	510472	659.039	658.732	391011	77	Residential
17	391012	1.35	Concrete (Normal)	1.0706045	21.67	391011	658.732	658.5	208405	77	Residential
18	103778	3.0734	Concrete (Normal)	0.0044267	22.59	208405	637.612	637.611	329399	77	Residential

Fig. C3 System attributes input

Second, hydrodynamic results from independent stormwater simulations are imported to provide time series of flow rates and velocities throughout the sewer system. Organization of the hydrodynamic results in spreadsheet form allows the VDCS to import them from any stormwater simulation model. A sample input of the hydrodynamic simulation results is shown in Fig. C4.

	A	B	C	D	E	F	G	H	I	J	K	L	M	N	O	P	Q
1	**Input 2**																
2	**pipe ID**	**77623**		**328800**		**77603**		**77671**		**77670**		**79364**		**79360**		**79354**	
3	**Time**	**Q**	**V**	**Q**	**V**	**Q**	**V**	**Q**	**V**	**Q**	**V**	**Q**	**V**	**Q**	**V**	**Q**	**V**
4	2015-07-25 16:00	0	0	0	0	0	0	0	0	0	0	0	0	0	0	0	0
5	2015-07-25 16:05	0	0	0.1	0.912	0.099	0.914	0.088	1.109	0.045	1.13	0.011	0.911	0.001	0.26	0	0
6	2015-07-25 16:10	0	0	0.1	0.907	0.1	0.875	0.1	0.883	0.097	0.957	0.088	1.006	0.078	0.796	0.067	0.716
7	2015-07-25 16:15	0	0	0.1	0.907	0.1	0.875	0.1	0.873	0.1	0.922	0.099	0.967	0.098	0.773	0.097	0.718
8	2015-07-25 16:20	0	0	0.1	0.907	0.1	0.875	0.1	0.873	0.1	0.919	0.1	0.963	0.1	0.77	0.1	0.718
9	2015-07-25 16:25	0	0	0.1	0.907	0.1	0.875	0.1	0.873	0.1	0.919	0.1	0.963	0.1	0.77	0.1	0.718
10	2015-07-25 16:30	0	0	0.1	0.907	0.1	0.875	0.1	0.873	0.1	0.919	0.1	0.963	0.1	0.77	0.1	0.718
11	2015-07-25 16:35	0	0	0.1	0.907	0.1	0.875	0.1	0.873	0.1	0.919	0.1	0.963	0.1	0.77	0.1	0.718
12	2015-07-25 16:40	0.001	0.332	0.101	0.911	0.101	0.876	0.1	0.874	0.1	0.916	0.101	0.965	0.101	0.771	0.1	0.719
13	2015-07-25 16:45	0.006	0.789	0.108	0.93	0.107	0.89	0.104	0.886	0.102	0.908	0.106	0.98	0.104	0.781	0.104	0.727
14	2015-07-25 16:50	0.011	0.966	0.118	0.944	0.116	0.906	0.114	0.906	0.11	0.909	0.117	1.006	0.114	0.803	0.113	0.747
15	2015-07-25 16:55	0.017	1.103	0.128	0.961	0.126	0.92	0.124	0.922	0.12	0.909	0.131	1.031	0.128	0.827	0.126	0.771
16	2015-07-25 17:00	0.026	1.255	0.142	0.985	0.14	0.94	0.136	0.945	0.131	0.908	0.149	1.061	0.145	0.855	0.143	0.798
17	2015-07-25 17:05	0.03	1.313	0.15	0.99	0.149	0.948	0.148	0.959	0.144	0.919	0.166	1.084	0.164	0.878	0.162	0.824
18	2015-07-25 17:10	0.039	1.426	0.165	1.015	0.162	0.967	0.158	0.976	0.154	0.915	0.183	1.107	0.18	0.898	0.178	0.845
19	2015-07-25 17:15	0.046	1.495	0.176	1.026	0.175	0.979	0.172	0.994	0.168	0.925	0.202	1.132	0.199	0.921	0.197	0.869
20	2015-07-25 17:20	0.056	1.582	0.191	1.046	0.189	0.996	0.185	1.012	0.18	0.928	0.222	1.155	0.219	0.942	0.217	0.892
21	2015-07-25 17:25	0.065	1.659	0.206	1.063	0.204	1.012	0.201	1.031	0.196	0.937	0.245	1.181	0.242	0.964	0.239	0.917
22	2015-07-25 17:30	0.074	1.724	0.22	1.078	0.218	1.026	0.215	1.048	0.211	0.946	0.268	1.203	0.264	0.984	0.262	0.94

Fig. C4 Input of the hydrodynamic simulation results

Third, pollutant introduction points such as fire hydrants and industrial releases are defined for specific locations in the drainage system along with variations of their loads over the simulation period. A sample of this input is shown in Fig. C5.

	A	B	C	D	E	F	G	H	I	J	K	L	M
1	Input 3												
2	No of Chloramine itroduction points	1											
3	chloramine inflows at:	MH ID	46259	MH ID	77670	MH ID	36789	MH ID	79364	MH ID	89562	MH ID	73852
4	Time	Q	conc	Q	conc	Q	conc	Q	conc	Q	conc	Q	conc
5	2015-07-25 16:00	0.1	2	0.1	2	0.1	2	0.1	2	0.1	2	0.1	2
6	2015-07-25 16:05	0.1	2	0.1	2	0.1	2	0.1	2	0.1	2	0.1	2
7	2015-07-25 16:10	0.1	2	0.1	2	0.1	2	0.1	2	0.1	2	0.1	2
8	2015-07-25 16:15	0.1	2	0.1	2	0.1	2	0.1	2	0.1	2	0.1	2
9	2015-07-25 16:20	0.1	2	0.1	2	0.1	2	0.1	2	0.1	2	0.1	2
10	2015-07-25 16:25	0.1	2	0.1	2	0.1	2	0.1	2	0.1	2	0.1	2
11	2015-07-25 16:30	0.1	2	0.1	2	0.1	2	0.1	2	0.1	2	0.1	2
12	2015-07-25 16:35	0.1	2	0.1	2	0.1	2	0.1	2	0.1	2	0.1	2
13	2015-07-25 16:40	0.1	2	0.1	2	0.1	2	0.1	2	0.1	2	0.1	2
14	2015-07-25 16:45	0.1	2	0.1	2	0.1	2	0.1	2	0.1	2	0.1	2
15	2015-07-25 16:50	0.1	2	0.1	2	0.1	2	0.1	2	0.1	2	0.1	2
16	2015-07-25 16:55	0.1	2	0.1	2	0.1	2	0.1	2	0.1	2	0.1	2
17	2015-07-25 17:00	0.1	2	0.1	2	0.1	2	0.1	2	0.1	2	0.1	2
18	2015-07-25 17:05	0.1	2	0.1	2	0.1	2	0.1	2	0.1	2	0.1	2
19	2015-07-25 17:10	0.1	2	0.1	2	0.1	2	0.1	2	0.1	2	0.1	2
20	2015-07-25 17:15	0.1	2	0.1	2	0.1	2	0.1	2	0.1	2	0.1	2
21	2015-07-25 17:20	0.1	2	0.1	2	0.1	2	0.1	2	0.1	2	0.1	2
22	2015-07-25 17:25	0.1	2	0.1	2	0.1	2	0.1	2	0.1	2	0.1	2
23	2015-07-25 17:30	0.1	2	0.1	2	0.1	2	0.1	2	0.1	2	0.1	2

Fig. C5 Input of the hydrodynamic simulation results

Finally, the decay order is selected, and the decay rate variation is set to one of three levels, 1) constant average value, 2) spatially-varying per land-use, or 3) varying both spatially and temporally. Varying decay coefficients are introduced in this input, as shown in Fig. C6.

	A	B	C	D	E
1	**Input 4**			Select	
2			1	2	3
3	**Pollutant Variability**	**2**	constant	Spatial only	Temporal & Spatial
4	**Land-use type**	**Residential**	**Commercial**	**Insustrial**	**Park**
5	**Time**	**K_R**	**K_C**	**K_I**	**K_P**
6	2015-07-25 16:00	0	0	0	0
7	2015-07-25 16:05	0.0048	0.00395	0.0028	0.0017
8	2015-07-25 16:10	0.0048	0.00395	0.0028	0.0017
9	2015-07-25 16:15	0.0048	0.00395	0.0028	0.0017
10	2015-07-25 16:20	0.0048	0.00395	0.0028	0.0017
11	2015-07-25 16:25	0.0048	0.00395	0.0028	0.0017
12	2015-07-25 16:30	0.0048	0.00395	0.0028	0.0017
13	2015-07-25 16:35	0.0048	0.00395	0.0028	0.0017
14	2015-07-25 16:40	0.0048	0.00395	0.0028	0.0017
15	2015-07-25 16:45	0.0048	0.00395	0.0028	0.0017
16	2015-07-25 16:50	0.0048	0.00395	0.0028	0.0017
17	2015-07-25 16:55	0.0048	0.00395	0.0028	0.0017
18	2015-07-25 17:00	0.0048	0.00395	0.0028	0.0017
19	2015-07-25 17:05	0.0048	0.00395	0.0028	0.0017

Fig. C6 Input of the pollutant decay variability definition

C4 Model process

Employing the provided data sets, the VDCS calculates concentrations of the degradable substance along its transit path through the sewer system to the system outlet. The VDCS model computations start by identifying contamination paths, which use the constructed network flow map to trace pollutants from previously-defined introduction points from manhole-to-manhole to the system outlet. The model then identifies common pollution paths stemming from pollutant introductions at different locations in the network and combines their loads in the subsequent water quality computations. Based on the concentration at introduction points and volumetric flow rates, the pollutant load can be calculated and then tracked over the calculated contaminant path according to the selected decay order. For chloramine dissipation with a first-order decay model, the VDCS calculates the concentration at the downstream node through,

$$C_{DS} = C_{US}\, e^{-Kt} \tag{C1}$$

where C_{US} and C_{DS} are the chloramine concentrations at upstream and downstream ends of the current sewer link respectively, K is the first-order decay coefficient, and t is the travel time between the upstream and downstream nodes calculated from the pipe length and flow velocity. the temporal variation of chloramine decay rates can be described with the following relationship,

$$K_{t,i} = \frac{1}{\alpha\, t + \beta} * (f_i) \tag{C2}$$

where $K_{t,i}$ is the decay coefficient at time t for land-use i, f is a land-use dependent coefficient, t is the discharge time in minutes, α =1.73, and β =1.0.

Depending on the selected decay coefficient behavior, the VDCS sets the decay coefficient to a constant value or computes it at every timestep from Eq. C2. Similarly, beginning at the introduction points and then moving manhole-to-manhole to the system outlet, the VDCS model applies Eq. C1 to calculate the concentration downstream based on a known upstream concentration. At diversion or collection points, downstream concentrations are calculated by converting all upstream concentrations to mass fluxes, and then distributing the total mass to the downstream links according to their relative volumetric proportions, assuming uniform and full mixing at all junctions.

C5 Model output

The VDCS produces pollutographs for different system nodes, such as manholes and outlets. Results can be exported to spreadsheets (.csv or .xls) or plotted within the Python environment.

C6 Model code

The code of the VDCS model is presented below in the format of the Python coding.

```
#Importing modules
import csv
import scipy
import numpy as np
import pylab as py
import pandas as pd
import math
import datetime
import matplotlib.pyplot as plt
import sys
'''
# Globally divert all print statements to THIS TXT file:
import sys
sys.stdout =
open("c:\\Users\\MGaafar\\PycharmProjects\\no_1\\Results.txt", "w")
print ("test sys.stdout")
'''

### [1] FIRST importing the MU Simulation results csv file : pipe
flows,(T, Q, V)
print ("\n [1] Imported data from MU\'s simulations \n", "-"*45)
    ## Listing IDs of pipes imported from MU's simulation
with open('1.csv') as file_1a:      #describe location (path)
    myReader1a = list(csv.reader(file_1a, delimiter="|"))    #Name the
file = describe delimiter

    MU_pipes = myReader1a[0][1:]  # Reading pipe IDs of MU simulation
starting row [0], column [1]:[end]
    MU_pipes = list(filter(None, MU_pipes))  # this line to remove any
empty strings processed as pipe IDs
print ("Number of pipes imported from MU hydrodynamic simulation file:",
len(MU_pipes))
print ("With Pipe IDs: ", MU_pipes, "\n")

    ##Pipes time series
        # importing data from 1.csv
file_1b = "1.csv"  #opening the 1.csv again different method to get time
series data
myReader1b = [line.strip().split('|') for line in open(file_1b)] # to
transfrom data
del myReader1b[0:2] # Removing the first TWO header rows from the
myReader1b List
```

```
print myReader1b
        # initializing a new time series list to store pipes time-series
data into
No_timesteps = len(myReader1b)          #No of data lines in the time
series for Q and V
print ("No. of time series found:", No_timesteps)
timeStep = 300                          #CHANGE it to readable afterwards:
in seconds = 5min*60=300 sec
No_columns1 = len(MU_pipes) * 2 + 1     # each pipe has Q and v columns
plus one for time/date column
timeSeries_1 = [[] for i in range(No_columns1)]
print timeSeries_1   # one list has each col as a sub-list

# Saving data in the new time series list
for i in range(No_timesteps):      # To switch col to rows and rows to col
between myReader1b and timeseries_1
    for j in range(No_columns1):        # i is the row number from 0 to
length of list myReader1b
        item_ij = myReader1b[i][j]      # j column of data like time, Q or
v
        timeSeries_1[j].append(item_ij)         #every loop the new row
item item_ij get added to list

print('MU\'s pipes time-series data (strings) :',timeSeries_1)
print ("MU\'s pipes time-series data (strings) :")

for i in range(No_columns1): # i column in timeseries_3
    if i!=0:     #For the date/time col only
        for j in range(No_timesteps):        # i is the row number from 0
to length of list myReader3b
            timeSeries_1[i][j] = str(timeSeries_1[i][j])      # j column
of data like time, Q or C
col_width = 18  # col width to enter
for row in timeSeries_1:
    print ("".join(word.ljust(col_width) for word in row))

# transforming data in time-series list to floats and date/time

for i in range(No_columns1): # i column in timeseries_3

    if i==0:     #For the date/time col only
        for j in range(No_timesteps):
            timeSeries_1[i][j] =
datetime.datetime.strptime(timeSeries_1[i][j], "%Y-%m-%d %H:%M") #time
format

    else:       # all other columns 'str' to 'float'
        for j in range(No_timesteps):        # i is the row number from 0
to length of list myReader3b
```

```
            timeSeries_1[i][j] = float(timeSeries_1[i][j])      # j column
of data like time, Q or C
                #every loop the new row item item_ij get added to list

#print 'MU\'s pipes time-series data (adjusted) :', timeSeries_1

#Extracting separate DateTime, V and Q time series:

DT_timeSeries_1=[]    #starting DateTime list
Q_timeSeries_1=[]           #starting Discharge nested list, list for each
pipe
V_timeSeries_1=[]           #starting Velocity nested list, list for each
pipe

for i in range(No_timesteps): # i row in timeseries_1
    DT_timeSeries_1.append(timeSeries_1[0][i]) #time format

for i in range(len(MU_pipes)):
    Q_timeSeries_1.append(timeSeries_1[2*i+1])  #picking only the odd
columns after the time column
    V_timeSeries_1.append(timeSeries_1[2*i+2]) #picking only the even
columns after the time column

print("DateTime :", DT_timeSeries_1)
print("Discharge :", Q_timeSeries_1)
print("velocity :", V_timeSeries_1)


### [2] Second second csv data (pipe data): Using a dictionary within a
list
print ("\n"," [2] Pipe attributes data from the city of Edmonton \n", "-
"*55)
    ## Building the pipes dictionary
pipes = []
with open('2.csv', 'r') as file_2:
    myReader2 = csv.reader(file_2, delimiter="|")
    next(myReader2)
    i = 1    #To initiate the dictionary ID
    for row in myReader2:
        pipes.append({'dictID': i, 'pipeID': row[0], 'Diameter':
float(row[1]), 'Slope': float(row[3])/100, 'Length': float(row[4]),
'typeUS': row[6], 'pipeUS': row[5], 'typeDS': row[11], 'pipeDS' : row[10],
'pipe1/N' : float(row[15]), 'pipeLandUse' : row[16]})
        i = i + 1

    ## Printing pipes{} dictionary values:
      # following 1st method: (Read comment below)

    ## There are TWO ways to print data in the pipes{} dictionary:
```

```
        # 1st method
print ('\nSewer network attributes :\nDrainage pipes attributes :')
for i in range(len(pipes)):
    print (pipes[i])

'''
        # 2nd method
for i in pipes:
     print i

    ## How to access a dictionary key value present inside a list
x = pipes[0]['pipeID']       # Remember 1st = [0], last = [n-1]
print x

for i in range(len(pipes)):
    y = pipes[i]['pipeID']
    print y
'''

#Listing all MHs found in the pipe Data
print ("\n","  List of All Manholes in the sewer network \n", "-"*40)
MHs=[]  #starting the list
for i in range(len(pipes)):
    item_US = pipes[i]['pipeUS']
    item_DS = pipes[i]['pipeDS']
    MHs.append(item_US);MHs.append(item_DS) #adding all US and DS MHs to
the list
MHs = sorted(set(MHs))  #set() to remove duplicates and sorted() to sort
alphabetically

print("No. of network Manholes:",len(MHs),"\t","Found Manhole IDs:",MHs)

### [3] Third importing chloramine-introducing manholes (pollutants data):
Using a dictionary within a list
print ("\n [3] Importing data of chloraine inflows\n", "-"*42)

with open('3.csv', 'r') as file_3a:
    myReader3a = list(csv.reader(file_3a, delimiter="|"))

    ##Number of chloramine MHs
    No_chl_int_MHs = int(myReader3a[0][1])  # Reading the Number of
chloramine-introducing MHs # transferring to integer
    print ('Number of chloramine-introducing MHs : ', No_chl_int_MHs)

    ## Listing IDs of chloramine MHs
    chl_int_MHs = myReader3a[0][3:] # Reading chloramine-introducing MHs
IDs starting row [0], column [3]:[end]
    chl_int_MHs = list(filter(None, chl_int_MHs)) # this line to remove
any empty strings processed as MHs IDs
```

```
    print ('List of chloramine-introducing MHs : ', chl_int_MHs)
    print ("Checking all MHs are processed in the MHs IDs list : ",
bool(len(chl_int_MHs)== No_chl_int_MHs))

    ##MHs time series
        # importing data from 3.csv
file_3b = "3.csv"  #opening the 3.csv
myReader3b = [line.strip().split('|') for line in open(file_3b)] # to
transfrom data in file_3b to each line to a list of stings using '\t' as a
separator
del myReader3b[0:3] # Removing the first three header rows from the
myReader3b List
#print myReader3b
        # initializing a new time series list to store MHs time-series
data into
No_columns3 = No_chl_int_MHs * 2 + 1    # each MH has Q and C columns plus
one for time/date column
timeSeries_3 = [[] for i in range(No_columns3)]
print timeSeries_3   # one list has each col as a sub-list

# Saving data in the new time series list
for i in range(No_timesteps):      # To switch col to rows and rows to col
between myReader3b and timeseries_3
    for j in range(No_columns3):        # i is the row number from 0 to
length of list myReader3b
        item_ij = myReader3b[i][j]      # j column of data like time, Q or
C
        timeSeries_3[j].append(item_ij)         #every loop the new row
item item_ij get added to list

print ('\nChloramine concentrations time-series :\nMHs time-series data
(strings) :',timeSeries_3)

# transforming data in time-series list to floats and date/time
for i in range(No_columns3): # i column in timeseries_3
    if i==0:     #For the date/time col only
        for j in range(No_timesteps):
            timeSeries_3[i][j] =
datetime.datetime.strptime(timeSeries_3[i][j], "%Y-%m-%d %H:%M") #time
format

    else:       # all other columns 'str' to 'float'
        for j in range(No_timesteps):        # i is the row number from 0
to length of list myReader3b
            timeSeries_3[i][j] = float(timeSeries_3[i][j])      # j column
of data like time, Q or C
                #every loop the new row item item_ij get added to list

print ('MHs time-series data (adjusted) :',timeSeries_3)
```

```
#Extracting separate Q_MHs and C time series
Q_MHs_timeSeries_3=[]    #starting Discharge nested list, list for each
pipe
C_timeSeries_3=[]  #starting concentrations nested list, list for each
pipe

for i in range(No_chl_int_MHs):
    Q_MHs_timeSeries_3.append(timeSeries_3[2*i+1])  #picking only the odd
columns after the time column
    C_timeSeries_3.append(timeSeries_3[2*i+2]) #picking only the even
columns after the time column

print ("Manholes discharges :", Q_MHs_timeSeries_3)
print ("inflow concentrations :", C_timeSeries_3)

### [4] Forth importing the un-chlorminated inflows at MHMU Simulation
results csv file : pipe flows,(T, Q, V)
print ("\n [4] Importing Un-chloraminted inflows data from MU\'s
simulations \n", "-"*65)
    ## Listing IDs of pipes imported from MU's simulation
with open('4.csv') as file_4a:      #describe location (path)
    myReader4a = list(csv.reader(file_4a, delimiter="|"))    #Name the
file = describe delimiter

    un_Chl_MH_inflows = myReader4a[0][1:]  # Reading pipe IDs of MU
simulation starting row [0], column [1]:[end]
    un_Chl_MH_inflows = list(filter(None, un_Chl_MH_inflows))  # this line
to remove any empty strings processed as pipe IDs
    No_of_un_Chloraminated_inflows = len (un_Chl_MH_inflows)  # each pipe
has Q and v columns plus one for time/date column
print ("Number of Un-chloraminated inflow found : ",
No_of_un_Chloraminated_inflows)
print ("Linked to the following MHs : ", un_Chl_MH_inflows, "\n")

    ##un-chloraminated inflow timeseries
        # importing data from 4.csv
file_4b = "4.csv"  #opening the 4.csv again different method to get time
series data
myReader4b = [line.strip().split('|') for line in open(file_4b)] # to
transfrom data in file_4b to each line to a list of stings using '|' as a
separator
del myReader4b[0:2] # Removing the first TWO header rows from the
myReader4b List, 2 not included
print ("Data imported as is:",myReader4b)

        # initializing a new time series list to store MHs discharges
found
timeSeries_4 = [[] for i in range(No_of_un_Chloraminated_inflows+1)] #each
```

```
MH has one sub-list
print ("Time series 4 initiated:",timeSeries_4)   # one list has each col
as a sub-list

        # Saving data in the new time series list
for i in range(No_timesteps):      # To switch col to rows and rows to col
between myReader1b and timeseries_1
    for j in range(No_of_un_Chloraminated_inflows+1):        # i is the
row number from 0 to length of list myReader4b
        item_ij = myReader4b[i][j]      # j column of data like time or Q
        timeSeries_4[j].append(item_ij)         #every loop the new row
item item_ij get added to list

del timeSeries_4[0:1] # Removing the first list from the timeSeries_4
List, note 1 not included; time/date column
print ("Time series 4 :", timeSeries_4)

        #Starting a new un-chloraminated MHs inflows time series
un_Chloraminated_inflows_timeSeries_4 = [[] for i in
range(No_of_un_Chloraminated_inflows)] #each MH has one sub-list
print ("Un-chloraminated MHs inflows (empty list) :",
un_Chloraminated_inflows_timeSeries_4)

        # transforming data in timeseries_4 to the new list of
un_chlo_inflows only, all floats and skip the time/date column
for i in range(No_of_un_Chloraminated_inflows): # i list in timeseries_4
    for j in range(No_timesteps):  # j is for each time step, the row
number from 0 to length of list timeSeries_4
        item_ij = float(timeSeries_4[i][j])      # string to float
        un_Chloraminated_inflows_timeSeries_4[i].append(item_ij) # every
loop the new row item item_ij get added to list

print ("Un-chloraminated MHs inflows :",
un_Chloraminated_inflows_timeSeries_4)

### Tracking MHs downstream every chloramine-introducing MH:
    ##Starting new Lists each has No. of sub-lists = No. of chl MHs
MH_tracking_MHs = [[] for i in range(No_chl_int_MHs)]   #to extract all
MHs D/S of each chl MH
MH_tracking_pipes = [[] for i in range(No_chl_int_MHs)] #to extract all
pipes D/S of each chl MH

    ##Filling the MHs list
print ("\nTotal number of sewer pipes :",len(pipes))
for i in range(No_chl_int_MHs):      #For every chl MH
    item_US = chl_int_MHs[i]           # the most US item is the chl-int
MH
    MH_tracking_MHs[i].append(item_US)  # adding 1st item to MHs list
    for k in range(len(pipes)):         #to scroll over the whole list of
```

```
pipes again
        for j in range(len(pipes)):         # for all items j in the list
pipes
            if item_US == pipes[j]['pipeUS']:   # if the US of the item j
is the US/item
                MH_tracking_MHs[i].append(pipes[j]['pipeDS'])   # adding
the D/S of that item to the MHs list
                item_US= pipes[j]['pipeDS']                     # Now the
D/S of that item becomes the U/S of the next one

print ('MHs path D/S chloramine-introducing MHs :', MH_tracking_MHs)

    ##Filling the pipes list13313#$

for i in range(No_chl_int_MHs):      #For every chl MH
    item_US = chl_int_MHs[i]           # the most US item is the chl-int
MH
    #MH_tracking_pipes[i].append(item_US)  # adding 1st item to pipes list
    for k in range(len(pipes)):  # to scroll over the whole list of pipes
again
        for j in range(len(pipes)):         # for all items j in the list
pipes
            if item_US == pipes[j]['pipeUS']:   # if the US of the item j
is the US/item
                MH_tracking_pipes[i].append(pipes[j]['pipeID'])   # adding
the pipeID of that item to the pipes list
                item_US = pipes[j]['pipeDS']                    # Now the
D/S of that pipe becomes the U/S of the next one

print ('Pipes D/S chloramine-introducing MHs :', MH_tracking_pipes)

    ##Identifying common paths (occurrences)
chl_pipes_flat_list = [item for sublist in MH_tracking_pipes for item in
sublist]
chl_MHs_flat_list = [item for sublist in MH_tracking_MHs for item in
sublist]

"""
which means?
for sublist in MH_tracking_pipes:
    for item in sublist:
        flat_list.append(item)
"""

import collections
No_chloramine_sources_pipes = collections.Counter(chl_pipes_flat_list)
print ('No. of chloramine sources U/S each pipe :',
No_chloramine_sources_pipes)
No_chloramine_sources_MHs = collections.Counter(chl_MHs_flat_list)
```

```
print ('No. of chloramine sources U/S each MH :',
No_chloramine_sources_MHs)
# another way to count specific item -->  list.count('item')

### Forth: First-order decay model calculations
print ("\n [4] First-order decay model calculations \n", "-"*42)

###Calculating travel times in every pipe in the network (individually):

    #Building the list of single pipe travel time
print ("\n  Calculating pollutant travel time in each pipe separately:\n",
" -"*28)

single_pipe_travel_time = [[] for i in range(len(pipes))]    #intializing
the list for every pipe
print ("All travel time items saved in one nested list of length = ",
len(single_pipe_travel_time), "pipes")
print ("The single pipe travel times empty list :",
single_pipe_travel_time,"\n")

    #Filling the single pipe travel time List:
for j in range(len(pipes)):
    length_x = pipes[j]['Length']                          #calling each
pipe length
    for k in range(No_timesteps):
        vel_jk= V_timeSeries_1[j][k]             #calling the velocity
value from its list
        tt_x = round(length_x/vel_jk,0) if vel_jk != 0 else 0   # calc
travel time = L/v #to avoid Div/0 error
        tt_seconds = datetime.timedelta(seconds=tt_x)  #convert to time
variables NOT USED LATER
        single_pipe_travel_time[j].append(tt_x)     #updating travel_time
list
    print ("Pipe",pipes[j]['pipeID'], "Travel Times in sec :",
(single_pipe_travel_time [j]))
#print (single_pipe_travel_time, "\n")

###Accumulative travel time for  pipes in each chloramine path:
------------------------------------------------------------------

print ("\n  Calculating accumulative travel time up to each pipe\n", " -
"*28)

    #Building the accumulated travel time list (3rd order list) [pipes]
acc_travel_times_pipe = [[] for i in range(No_chl_int_MHs)] # No. of sub-
lists = No. of MH paths
for i in range(No_chl_int_MHs):
    for j in range(len(MH_tracking_pipes[i])):
        acc_travel_times_pipe[i] = [[] for k in
```

```
range(len(MH_tracking_pipes[i]))] #No. of sub-sub-lists = No. of pipes in
each MH paths
print ("Accumulative travel time items saved in a list of
[",No_chl_int_MHs,"] nested lists  = ",No_chl_int_MHs,"of chl. paths")
print ("The accumulative travel times (pipes) empty list :",
acc_travel_times_pipe)

    #Filling the accumulated time travel list
for i in range(No_chl_int_MHs):             #i every MH path (list)
    print ("\nChloramine source No.", i+1, ", with Manhole ID :",
chl_int_MHs[i],  ". Pipes in this path:")

    for j in range(len(MH_tracking_pipes[i])):      #j every pipe in i
every MH path
        pipeID_x = MH_tracking_pipes[i][j]  # calling ID of pipe no.j

        for k in range(len(pipes)):         #Only to get the DictID for
each pipe in j
            if pipeID_x == pipes[k]['pipeID']:
                dictID_x = pipes[k]['dictID'] # calling dictID of pipe
no.j
        print ("\tAt location :", j + 1, " pipe ID: ", pipeID_x, ",with
DictID:", dictID_x)

        for k in range(No_timesteps):  #for every time step
            if j==0:        #for the first pipe j=0 in each MH path i

acc_travel_times_pipe[i][j].append(single_pipe_travel_time[dictID_x-1][k])
#importing travel time data for 1st pipe

            else:           # for the following pipes accumulating begins
                #before adding travel times must convert time strings TO
datetime
                previous_pipe_value = acc_travel_times_pipe[i][j-1][k]
                current_pipe_value = single_pipe_travel_time[dictID_x -
1][k]
                acc_travel_times_pipe[i][j].append(current_pipe_value +
previous_pipe_value)

        print ("\t\ttravel time to end of pipe", MH_tracking_pipes[i][j],
":", acc_travel_times_pipe[i][j])

##Accumulative travel time for  Manholes in each chloramine path:
print("\n  Calculating accumulative travel time up to each Manhole\n", " -
" * 30)
    # Building the accumulated travel time list (3rd order list)
[Manholes]
acc_travel_times_MH = [[] for i in range(No_chl_int_MHs)]  # No. of sub-
lists = No. of MH paths
```

```
for i in range(No_chl_int_MHs):
    for j in range(len(MH_tracking_MHs[i])):
        acc_travel_times_MH[i] = [[] for k in
range(len(MH_tracking_MHs[i]))]  # No. of sub-sub-lists = No. of MHs in
each MH paths
print("Accumulative travel time items saved in a list of [",
No_chl_int_MHs, "] nested lists  = ", No_chl_int_MHs,"of chl. paths")
print("The accumulative travel times (MHs) empty list :",
acc_travel_times_MH)

    # Filling the accumulated time travel list
for i in range(No_chl_int_MHs):  # i every MH path (list)
    print("\nChloramine source No.", i + 1, ", with Manhole ID :",
chl_int_MHs[i], ". Pipes in this path:")

    for j in range(len(MH_tracking_MHs[i])):  # j every MH in i every MH
path
        # To get pipedID and DictID of the pipe U/S of each MH j
        MH_ID_x = MH_tracking_MHs[i][j]  # calling ID of MH no.j
        pipeID_x = "No chloramine pipes U/S"    #apply only for 1st MH in
each path, , for next MHs value will be over-written
        dictID_x = "N/A"        #apply only for 1st MH in each path, for
next MHs value will be over-written

        for k in range(len(pipes)):  # Only to get the PipeID and DictID
for the pipe U/S of this MH j
            if MH_ID_x == pipes[k]['pipeDS'] and pipes[k]['pipeID'] in
MH_tracking_pipes[i]:
                pipeID_x = pipes[k]['pipeID']
                dictID_x = pipes[k]['dictID']  # calling dictID of pipe
no.j
        print("\tAt location :", j, " MH ID: ", MH_ID_x, "chl. Pipe U/S:",
pipeID_x, ",with DictID:", dictID_x)

            #Now travel times of first MH (j=0) in each path i
        for k in range(No_timesteps):  # for every time step
            # adding delay time at MHs:
            Delay_time_at_MH = 0       #define delay time at a single MH
in Seconds
            if j == 0:  # for the first MH j=0 in each MH path i
                acc_travel_times_MH[i][j].append(0)  # setting first MH
value to Zero

            elif j==1:  # for the second MH (j=1) in each MH path i

acc_travel_times_MH[i][j].append(single_pipe_travel_time[dictID_x -
1][k]+Delay_time_at_MH)  # importing travel time data for 1st pipe to 2nd
MH (j=1)
            else:
```

```
                previous_MH_value = acc_travel_times_MH [i][j-1][k]
                current_MH_value = single_pipe_travel_time [dictID_x-1][k]

acc_travel_times_MH[i][j].append(current_MH_value+previous_MH_value+Delay_
time_at_MH)


        print("\t\ttravel time to manhole No.", MH_tracking_MHs[i][j],
":", acc_travel_times_MH[i][j])


###Ccalculating pollutant Mass from single sources:
print ("\n  Calculation of Pollutant Mass D/S each introduction MH \n", "
-" * 18)

        #Building the pollutant mass matrix for manholes (3rd order list)
pol_assembly_MH = [[] for i in range(No_chl_int_MHs)] # No. of sub-lists =
No. of chloramine paths
for i in range(No_chl_int_MHs):
    for j in range(len(MH_tracking_MHs[i])):
        pol_assembly_MH[i] = [[[],[]] for k in
range(len(MH_tracking_MHs[i]))]
        #No. of sub-sub-lists = No. of MHs in each MH paths each sublist
has two lists [time],[c]
print ("The MHs pollution assembly matrix (Empty List):", pol_assembly_MH)

for i in range(No_chl_int_MHs):             #i every chloramine path
(list)
    print ("\n", "-" *2, "Pollutant Mass D/S chloramine source No.", i+1,
", Manhole No.", chl_int_MHs[i],  ". MHs in this path:")

    # Calling Data of all first MHs (IDs, Dicts, chl_sources U/S)
    for j in range(len(MH_tracking_MHs[i])):      #j every MH in i every
MH path

        ##Getting the current MH data [ID, No. of chl sources US, pipes US
and DS, MHs US]
            # getting the ID of MH no.j
        MH_x_ID = MH_tracking_MHs[i][j]
            # getting the ID of the MH just US of MH no.j
        MH_US_x_ID = MH_tracking_MHs[i][j-1] if j != 0 else "N/A"
            # getting No. of chloramine sources US of MH no.j
        MH_x_No_chl_sources = No_chloramine_sources_MHs[MH_x_ID]
            # getting pipe_ID of the next pipe D/S  on the current chlo
path --> so MH is U/s of it
        pipe_US_x_ID = MH_tracking_pipes[i][j - 1] if j != 0 else "N/A"
        print ("pipe US ID : ",pipe_US_x_ID)

        if j < len(MH_tracking_MHs[i])-1:      #as long as it is not the
```

```
last MH
            pipe_DS_x_ID = MH_tracking_pipes[i][j]
        else:
            pipe_DS_x_ID = "N/A"      # Last MH has no D/S pipe

        #print ("pipe DS ID : ", pipe_DS_x_ID)
        for k in range (len (pipes)):

            if pipe_US_x_ID == pipes[k]['pipeID']:
                pipe_US_x_dictID = pipes[k]['dictID']
                #print ("pipe US dict ID : ",pipe_US_x_dictID)
            if pipe_DS_x_ID == pipes[k]['pipeID']:
                pipe_DS_x_dictID = pipes[k]['dictID']
                #print ("pipe DS dict ID : ", pipe_DS_x_dictID)


        # bring all the U/S and D/S pipes and MHs:
        pipe_dictID_DS_x = [pipes[k]['dictID'] for k in range(len(pipes))
if MH_ID_x == pipes[k]['pipeUS']]  # calling dictID of pipe k
        pipe_dictID_US_x = [pipes[k]['dictID'] for k in range(len(pipes))
if MH_ID_x == pipes[k]['pipeDS']]  # calling dictID of pipe k, that will
bring all pipes u/s
        MH_dictID_US_x =[]      # to get the ID of the closest MHs U/S -->
so MH is D/s of all of them
        for x in pipe_dictID_US_x:
            MH_ID_US_x = [pipes[k]['pipeUS'] for k in range(len(pipes)) if
x == pipes[k]['dictID']]  # calling dictID of pipe k

        # Which account for the conc.
        for k in range(len(pipes)):
            if MH_x_ID == pipes[k]['pipeUS']:
dictID_DS_x.append(pipes[k]['dictID'])
            if MH_x_ID == pipes[k]['pipeDS']:
dictID_US_x.append(pipes[k]['dictID'])

        print ("\n\tDS MH No.", j, " of ID:", MH_x_ID,"\t", "No. sources
US:", MH_x_No_chl_sources,"\t", "ID next pipe DS:", pipe_DS_x_ID,"\t", "ID
first pipe US:", pipe_US_x_ID,"\t", "ID first MH US:", MH_US_x_ID)

    # Calculating initial pollutant Mass (Mo) in every first receiving MHs
(j=0) in every chloramine path (i)

        # Now calculating and filling the first MH list with (time, Co)
        for k in range(No_timesteps):  # k  --> for every time step,
''''''''+1 because first time it goes in the j==0 direction
            if j == 0:  # for the first MH j=0 in each chloramine path i
               # MHs with No un-chloraminated inflows
                # Now calling each first MH data
                Datetime_MH_0 = timeSeries_3[j]                    #print
```

```
("\t\tDateTime:", Datetime_MH_0)  # first list in timeSeries_3 is the
datetime series
                Q_MH_0 = Q_MHs_timeSeries_3[i]                      #print
("\t\tQ_MHs_0:", Q_MH_0)
                C_MH_0 = C_timeSeries_3[i]                        #print
("\t\tC_MH_0:", C_MH_0)

                #calculation of (Co)
                Q_pipe_0 = Q_timeSeries_1[pipe_DS_x_dictID - 1]
#print ("\t\tQ_pipe_0:", Q_pipe_0, "\n")

                # Calculating Co (c_first) for pipe j due to mixing at
introduction MH i
                c_fisrt_MH_0 = round(C_MH_0[k] * Q_MH_0[k] /
Q_pipe_0[k],3) if Q_pipe_0[k] != 0 else 0

                pol_assembly_MH[i][j][0].append(Datetime_MH_0[k])  # [i]MH
path, [j]MH in that path,[0]first list is always for time
                pol_assembly_MH[i][j][1].append(c_fisrt_MH_0)  # [i]MH
path, [j]MH in that path,[1]second list is always for conc.


                # Calculating Mo (M_first) for pipe j due from given Co
and Q at introduction MH i
                mass_fisrt_MH_0 = round(C_MH_0[k] * Q_MH_0[k],4)
#mass in grams

                pol_assembly_MH[i][j][0].append(Datetime_MH_0[k])  # [i]MH
path, [j]MH in that path,[0]first list is always for time
                pol_assembly_MH[i][j][1].append(mass_fisrt_MH_0)  # [i]MH
path, [j]MH in that path,[1]second list is always for Mass.

                print (pol_assembly_MH[i][j][0], pol_assembly_MH[i][j][1])

print(len(pol_assembly_MH[i][j][0]),len(pol_assembly_MH[i][j][1]))

            else: # for every other MH j>=0, in each chloramine path i

                decayCoeff = 0.50  # unit = hr^(-1)
                delaytime = 0  # unit is seconds

                ## Now calling previous MH data All Lists at [j-1]
                print ("j-1:", len (pol_assembly_MH[i][j-1][0]), len
(pol_assembly_MH[i][j-1 ][1]))
                previous_MH_time = pol_assembly_MH[i][j - 1][0]  #
datetime of the Mass list
                print (previous_MH_time)
                print (len(previous_MH_time))
```

```
                previous_MH_mass = pol_assembly_MH[i][j - 1][1]  # Mass
list
                print (previous_MH_mass)
                print (len(previous_MH_mass))

                previous_MH_ID = MH_tracking_MHs[i][j - 1]  # previous MH
ID
                print (previous_MH_ID)

                previous_pipe_tt =
single_pipe_travel_time[(pipe_US_x_dictID - 1)]
                print(previous_pipe_tt)
                print (len(previous_pipe_tt))

                # Calculating time to the current MH = previous_MH_time +
Previous pipe tt
                tt_MH_x = previous_pipe_tt[k] + delaytime  # the travel
time value, still as a float
                print (tt_MH_x)

                Datetime_MH_x = previous_MH_time[k] + datetime.timedelta
(seconds=tt_MH_x)  # adding the travel time to the datetime object
                mass_US_MH_x = previous_MH_mass[k]  # calling the mass of
the first U/S MH, mass_US_MH_x

                # Calculating pipe-end mass at each MH(j)
                mass_end_MH_x = round (mass_US_MH_x * math.exp (-1 *
decayCoeff * tt_MH_x / 60 / 60),6);  # print ("\t\tc_end_MH_x:",
c_end_MH_x)

                pol_assembly_MH[i][j][0].append ((Datetime_MH_x))  # [i]MH
path, [j]MH in that path,[0]always for time list
                pol_assembly_MH[i][j][1].append (mass_end_MH_x)  # [i]MH
path, [j]MH in that path,[1]always for mass list



                    if c_end_MH_x == 0.0: pass # to skip all zero
velocityvalues --> zero travel time values also zero conncentration values
tra
                    else:
                        pol_assembly_MH[i][j][0].append((Datetime_MH_x))
# [i]MH path, [j]MH in that path,[0]always for time list
                        pol_assembly_MH[i][j][1].append(c_end_MH_x)  #
[i]MH path, [j]MH in that path,[1]always for conc. list


            #round first acc travel time up
        from datetime import datetime, timedelta
```

```
        def RoundUp_dt(dt, deltaUP): #round the time up to closest
timestep
            return dt + (datetime.min - dt) % deltaUP
        def RoundDown_dt(dt, deltaDown): #round the time down to closest
timestep
            return dt + (datetime.min - dt) % deltaDown -
timedelta(minutes=(timeStep/60))

        pol_assembly_MH[i][j][0][0]=
RoundUp_dt(pol_assembly_MH[i][j][0][0], timedelta(minutes=(timeStep/60)))
#modify the first value only
        pol_assembly_MH[i][j][0][-1] =
RoundDown_dt(pol_assembly_MH[i][j][0][-1],
timedelta(minutes=(timeStep/60)))#modify the last value only


        print ("\t\tDatetime:", (pol_assembly_MH[i][j][0]), "\n",
"\t\tMass:", pol_assembly_MH[i][j][1])
        print (len(pol_assembly_MH[i][j][0]),
len(pol_assembly_MH[i][j][1]))

#Modification of Manhole mass decay data:   Edit times and interpolate
mass between
print ("\n  Modification of Time and Mass Time Series \n", " -" * 28)
print ("\n  Editing DateTime object to match timesteps and end with last
timestep, interpolate mass values \n")

        #Building the modified pollution matrix for manholes (3rd order
list)
mod_pol_assembly_MH = [[] for i in range(No_chl_int_MHs)] # No. of sub-
lists = No. of chloramine paths
for i in range(No_chl_int_MHs):                #

    for j in range(len(MH_tracking_MHs[i])):

        mod_pol_assembly_MH[i] = [[[],[]] for k in
range(len(MH_tracking_MHs[i]))]
        #No. of sub-sub-lists = No. of MHs in each MH paths each sublist
has two lists [time],[c]
print ("The modified MHs' pollution assembly matrix (Empty List):",
mod_pol_assembly_MH)

        #all other MHs need editing DateTime and interpolation of mass
for i in range(No_chl_int_MHs):                #i for every chloramine
path (list)
    for j in range(len(MH_tracking_MHs[i])):      #j for every MH in i
every MH path
            # First MH in every path needs NO-Edit, copy directly from
pol_assembly_MH
```

```
        if j==0:  # only for the first MH j=0, in every path i
            added_time_lists = pol_assembly_MH[i][j][0]
            added_mass_lists = pol_assembly_MH[i][j][1]

        if j!=0:    #to except the 1st MH (j=0) in every path i
                #adding Original time lists to every MH time list

            added_time_lists = pol_assembly_MH[i][j][0] + DT_timeSeries_1
# add the two time lists

                # adding list of (None or 1000 mass grams) to previously
calculated mass in MH_pol_assm
            mass_imaginary_list = [1000] * No_timesteps    #None list of
the same length of the original time series
            added_mass_lists = pol_assembly_MH[i][j][1] +
mass_imaginary_list  # add the two mass lists

                # Zip(T,C) together and then and sort according to
DateTime value
            added_time_lists, added_mass_lists =
zip(*sorted((zip(added_time_lists, added_mass_lists))))
                # Converting sorted (T,C)back to lists again
            added_time_lists, added_mass_lists = (list (t) for t in zip
(*sorted (zip (added_time_lists, added_mass_lists))))

                # finding 1st calculated mass value in the added mass list
            first_calc_mass_value = next(item for item in added_mass_lists
if item is not 1000)
                # finding the index of 1st calc mass value in the added
mass list
            index_1st_calc_mass_value = added_mass_lists.index
(first_calc_mass_value)

            #Interpolation of mass between None values
            for k in range(len(added_time_lists)):    #for all values in
the combined Datetime series

                # before 1st calculated mass all values set to zero
                if k < index_1st_calc_mass_value:  # all cono. before the
first cono value
                    added_mass_lists[k] = 0.000  # all these None values
are set to Zero
                #before 1st calculated mass all values set to zero

                else:       #for all other mass values after the first
calculated mass value
                    if added_mass_lists[k] is not 1000:  # if there is
already a calculated value
```

```
                        pass  # Do nothing

                    else:  # If there is an imaginary value there of (None
or 100), we will replace it with interpolated one

                        M_before = added_mass_lists[k - 1]   #mass before
that value
                        T_before = added_time_lists[k - 1]   #DateTime
before that value

                        T_current = added_time_lists[k]

                        for nxt_valu in range (k+1, len
(added_time_lists)):  # searching for the next calculated mass
                            if added_mass_lists[nxt_valu] is not 1000:  #
So it got a value
                                if  added_time_lists[nxt_valu] not in
DT_timeSeries_1:  # and with NOT original timestep
                                    M_after = added_mass_lists[nxt_valu]
# calling the next calculated C value
                                    T_after = added_time_lists[nxt_valu]
# calling the corresponding T value
                                    break       #Once found break out loop

                        diff_T_before = T_current - T_before  # DT diff
before
                        diff_T_before = diff_T_before.seconds  # convert
to seconds
                        diff_T_after = T_after - T_current  # DT diff
after
                        diff_T_after = diff_T_after.seconds  # convert to
seconds
                        diff_T_total = T_after - T_before  # DT diff total
                        diff_T_total = diff_T_total.seconds  # convert to
seconds

                        #mass Interpolation function
                        M_current = 1 / diff_T_total * (diff_T_after *
M_before + diff_T_before * M_after) if diff_T_total != 0 else 0  #
interpolation, if for DIV/0

                        '''
                        #print statment to check interpolation calculation
                        if i==15 and j==21:
                            print("\nCurrent Time
Slot",T_current,"\tbefore",T_before , "\tafter",T_after ,
"\n\tdiff_T_before",diff_T_before,"\tdiff_T_after", diff_T_after,
"\tdiff_T_total",diff_T_total, "\n\tM before:", M_before, "\tM after:",
M_after,"\n\t\tinterpolation M", M_current)
```

```
                        '''

                        #replacing with the calculated mass
                        added_mass_lists[k] = round (M_current, 8)  #
coping it to the pol assembly

        print (len(added_mass_lists))
        mod_pol_assembly_MH[i][j][0] = added_time_lists
        mod_pol_assembly_MH[i][j][1] = added_mass_lists  # all other MHs
need editing DateTime and interpolation of mass

        print ("path:", i,"\t","MH No.:",j,"\t","DT:",
mod_pol_assembly_MH[i][j][0])
        print ("path:", i, "\t", "MH No.:", j, "\t", "C:",
mod_pol_assembly_MH[i][j][1])

    #Removing time values not in the original time series
for i in range(No_chl_int_MHs):  # i for every chloramine path (list)
    for j in range(len(MH_tracking_MHs[i])):  # j for every MH in i every
MH path
            # First MH in every path needs NO-Edit, copy directly from
pol_assembly_MH

        added_time_lists = mod_pol_assembly_MH[i][j][0]
        added_mass_lists = mod_pol_assembly_MH[i][j][1]

        print(len(added_time_lists))
        for k in added_time_lists:  # for all values in the combined
Datetime series
            index_k = added_time_lists.index(k)

            if k not in DT_timeSeries_1: #if time value in the original
timeSeries

                added_time_lists[index_k]=1000      #replace time value
with a 1000
                added_mass_lists[index_k]=1000     #and replace its mass
with 1000 too.

                #Now delete all 1000s from both lists
        added_time_lists = list(filter(lambda x: x !=1000,
added_time_lists))
        added_mass_lists = list(filter(lambda x: x !=1000,
added_mass_lists))

        #Removing replicant time values and mass values
        for ki in added_time_lists:  # for all values in the combined
Datetime series
            index_ki = added_time_lists.index(ki) #Index current
```

```
            index_kj = index_ki + 1 if ki != added_time_lists[-1] else
index_ki #index next, for last one=index last one
            kj = added_time_lists[index_kj]       #next Time value

                #Removing time replicants
            if ki== kj and ki != added_time_lists[-1]: #current=next, and
not for last object
                    #calculating avergae mass for replicant DT values
                mav= 1/2*(added_mass_lists[index_ki]+
added_mass_lists[index_kj])
                added_mass_lists[index_kj]= mav     #replacing mass with
average value

                added_time_lists[index_ki] = 1000  # replace time value
with a 1000
                added_mass_lists[index_ki] = 1000  # and replace its mass
with 1000 too.

            # Now delete all 1000s from both lists
        added_time_lists = list (filter (lambda x: x != 1000,
added_time_lists))
        added_mass_lists = list (filter (lambda x: x != 1000,
added_mass_lists))

        mod_pol_assembly_MH[i][j][0] = added_time_lists
        mod_pol_assembly_MH[i][j][1] = added_mass_lists

        print ("T", len (added_time_lists))
        print ("M", len (added_mass_lists))
        print (len(added_mass_lists))
        print ("path:", i,"\t","MH No.:",j,"\t","DT:",
mod_pol_assembly_MH[i][j][0])
        print ("path:", i, "\t", "MH No.:", j, "\t", "Mass:",
mod_pol_assembly_MH[i][j][1])

    #editing odd mass values by averiging them
for i in range(No_chl_int_MHs):  # i for every chloramine path (list)
    for j in range(len(MH_tracking_MHs[i])):  # j for every MH in i every
MH path
        for k in range(1,(len(mod_pol_assembly_MH[i][j][1])-1)):  #except
the first and last items
            variance = 1.20   #allowable diff beetween

            x_before = mod_pol_assembly_MH[i][j][1][k-1]
            x_after = mod_pol_assembly_MH[i][j][1][k+1]
            x_current = mod_pol_assembly_MH[i][j][1][k]

            if x_current > (x_before*variance) and x_current >
(x_after*variance):
```

```
                print ("UP",i, j, k, x_before, x_current, x_after)#to see
values odd values before
                x_current = (x_before+x_after)/2
                mod_pol_assembly_MH[i][j][1][k] = x_current
                print ("UP",i, j, k, x_before, x_current, x_after)

            if x_current < (x_before/variance) and x_current <
(x_after/variance):
                print ("DN",i,j,k,x_before,x_current,x_after)
                x_current = (x_before+x_after)/2
                mod_pol_assembly_MH[i][j][1][k] = x_current
                print ("DN",i,j,k,x_before, x_current, x_after)


#trial data extraction
# Printing mass-time values  #EDIT MH ID below:
for i in range (len(pol_assembly_MH[0][73][0])):
    print (pol_assembly_MH[0][73][0][i])
#Mass values
for i in range (len(pol_assembly_MH[0][73][1])):
    print (pol_assembly_MH[0][73][1][i])

for i in range (len(mod_pol_assembly_MH[0][73][0])):
    print (mod_pol_assembly_MH[0][73][0][i])
#Mass values
for i in range (len(mod_pol_assembly_MH[0][73][1])):
    print (mod_pol_assembly_MH[0][73][1][i])

##### NEXT: Assemble collected mass at each MH:
print ("\n","  Pollutographs of Manholes in the sewer network \n", "-"*40)
#Manholes with zero sources U/S

        # starting a new MH pollutographs time series
MH_pollutographs = [[[],[]] for i in MHs] #each MH has one sub-list
print(MH_pollutographs)
#filling Date-Time lists:
for i in range(len(MH_pollutographs)):
    MH_pollutographs[i][0]= DT_timeSeries_1

for i in MHs:

    MH_ID_i = i                 #ID of curernt MH
    index_MH_i = MHs.index(i)   #index of current MH in the [MHS] list

    MH_pollutographs[index_MH_i][0] = DT_timeSeries_1  # this MH time
series is set to original timeseries

    if i not in No_chloramine_sources_MHs: #MH not D/S of chl sources
```

```
        MH_pollutographs[index_MH_i][1] = [0.00] * No_timesteps
        print("Zero chloramine sources U/S of MH ID :", i)

    if i in No_chloramine_sources_MHs:

        #all other MH
        No_chl_sources_i = No_chloramine_sources_MHs[i]
        print ("Pollutograph of MH ID: ",i,"\tNo. of chloramine sources
U/S :", No_chl_sources_i)

        # pipes U/S of current MH
        pipes_US_MH_i =[]   #New lists One for Pipe IDs
        pipes_US_MH_i_dict = []  # And One for Dict IDs
        for k in range(len(pipes)):
            if i == pipes[k]['pipeDS']:  # if MH i is the DS pipe k (so
pipe k is u/S of MH i)
                pipes_US_MH_i.append(pipes[k]['pipeID'])
                pipes_US_MH_i_dict.append (pipes[k]['dictID'])
                print("\tpipes U/S :", pipes_US_MH_i, "with dictIDs:",
pipes_US_MH_i_dict)


        #Un-chloraminated Q at MH:
        if i in un_Chl_MH_inflows:
            index_MH_i_unchl = un_Chl_MH_inflows.index(i)
            Q_unchl_MH_i =
un_Chloraminated_inflows_timeSeries_4[index_MH_i_unchl]
        else:
            Q_unchl_MH_i = [0.00] * No_timesteps
            print("\tNo Un-chloraminated inflow")
        # [2] preparing the Discharge matrices, first: Chloraminated
inflow at each MH
        # Chloraminated Q at MH:
        if i in chl_int_MHs:
            index_MH_i_chl = chl_int_MHs.index(i)
            Q_chl_MH_i = Q_MHs_timeSeries_3[index_MH_i_chl]
            C_chl_MH_i = C_timeSeries_3[index_MH_i_chl]
            print ("\tChloraminated inflow defined")
        else:
            Q_chl_MH_i = [0.00] * No_timesteps
            print ("\tNo Chloraminated inflow defined")

        total_MH_Q = [0.00] * No_timesteps
        for j in range (len (DT_timeSeries_1)):
            for k in pipes_US_MH_i_dict:
                total_MH_Q[j] = total_MH_Q[j] + Q_timeSeries_1[k-1][j]

            total_MH_Q[j] = total_MH_Q[j] + Q_chl_MH_i[j] +
Q_unchl_MH_i[j]
```

```
        print ("\ttotal MH Q :", total_MH_Q)

        total_MH_mass = [0.00] * No_timesteps
        counter_mass = 0
        for j in range(len(MH_tracking_MHs)):
            for k in range(len(MH_tracking_MHs[j])):

                if MH_ID_i == MH_tracking_MHs[j][k]:
                    for x in range(len(DT_timeSeries_1)):
                        total_MH_mass[x] =
round(mod_pol_assembly_MH[j][k][1][x]+ total_MH_mass[x], 5)
                    counter_mass = counter_mass +1
        print( "\ttotal MH mass added : ", counter_mass, "\tmass:",
total_MH_mass )

        final_MH_conc = [0.00] * No_timesteps
        for j in range (len (DT_timeSeries_1)):

            final_MH_conc[j] = round (total_MH_mass[j] / total_MH_Q[j], 5)
if total_MH_Q[j] != 0 else 0

        print ("\tFinal MH concentration : ", final_MH_conc)

# [1] preparing the Discharge of un-chloramineated Q at MH i


#### Finally, find the resultant concentrations at each D/S MH

        #starting two lists for Q pipes and
        MH_pollutographs = [[[], []] for i in MHs]  # each MH has one sub-
list
        MH_pollutographs = [[[], []] for i in MHs]  # each MH has one sub-
list

print ("\nTotal number of sewer pipes :",len(pipes))
for i in range(No_chl_int_MHs):      #For every chl MH
    item_US = chl_int_MHs[i]           # the most US item is the chl-int
MH
    MH_tracking_MHs[i].append(item_US)  # adding 1st item to MHs list
    for k in range(len(pipes)):         #to scroll over the whole list of
pipes again
        for j in range(len(pipes)):         # for all items j in the list
pipes
            if item_US == pipes[j]['pipeUS']:   # if the US of the item j
is the US/item
                MH_tracking_MHs[i].append(pipes[j]['pipeDS'])   # adding
the D/S of that item to the MHs list
                item_US= pipes[j]['pipeDS']                     # Now the
```

```
D/S of that item becomes the U/S of the next one

print ('MHs path D/S chloramine-introducing MHs :', MH_tracking_MHs)

    ##Filling the pipes list
for i in range(No_chl_int_MHs):      #For every chl MH
    item_US = chl_int_MHs[i]           # the most US item is the chl-int
MH
    #MH_tracking_pipes[i].append(item_US)  # adding 1st item to pipes list
    for k in range(len(pipes)):  # to scroll over the whole list of pipes
again
        for j in range(len(pipes)):         # for all items j in the list
pipes
            if item_US == pipes[j]['pipeUS']:   # if the US of the item j
is the US/item
                MH_tracking_pipes[i].append(pipes[j]['pipeID'])   # adding
the pipeID of that item to the pipes list
                item_US = pipes[j]['pipeDS']                      # Now the
D/S of that pipe becomes the U/S of the next one

No_chloramine_sources_pipes = collections.Counter(chl_pipes_flat_list)
print ('No. of chloramine sources U/S each pipe :',
No_chloramine_sources_pipes)
No_chloramine_sources_MHs = collections.Counter(chl_MHs_flat_list)
print ('No. of chloramine sources U/S each MH :',
No_chloramine_sources_MHs)
# another way to count specific item -->  list.count('item')

MHs=[]  #starting the list
for i in range(len(pipes)):
    item_US = pipes[i]['pipeUS']
    item_DS = pipes[i]['pipeDS']
    MHs.append(item_US);MHs.append(item_DS) #adding all US and DS MHs to
the list
MHs = sorted(set(MHs))  #set() to remove duplicates and sorted() to sort
alphabetically

print("No. of network Manholes:",len(MHs),"\t","Found Manhole IDs:",MHs)
'''
'''
for i in range(No_chl_int_MHs):  # i for every chloramine path (list)
    for j in range(len(MH_tracking_MHs[i])):  # j for every MH in i every
MH path
        for k in range(1,(len(mod_pol_assembly_MH[i][j][1])-1)):  #except
the first and last items
            variance = 1.20   #allowable diff beetween

            x_before = mod_pol_assembly_MH[i][j][1][k-1]
            x_after = mod_pol_assembly_MH[i][j][1][k+1]
```

```
            x_current = mod_pol_assembly_MH[i][j][1][k]

            if x_current > (x_before*variance) and x_current >
(x_after*variance):
                print ("UP",i, j, k, x_before, x_current, x_after)#to see
values odd values before
                x_current = (x_before+x_after)/2
                mod_pol_assembly_MH[i][j][1][k] = x_current
                print ("UP",i, j, k, x_before, x_current, x_after)

            if x_current < (x_before/variance) and x_current <
(x_after/variance):
                print ("DN",i,j,k,x_before,x_current,x_after)
                x_current = (x_before+x_after)/2
                mod_pol_assembly_MH[i][j][1][k] = x_current
                print ("DN",i,j,k,x_before, x_current, x_after)

'''

'''

#trial data extraction
# Printing mass-time values  #EDIT MH ID below:
for i in range (len(pol_assembly_MH[0][73][0])):
    print (pol_assembly_MH[0][73][0][i])
#Mass values
for i in range (len(pol_assembly_MH[0][73][1])):
    print (pol_assembly_MH[0][73][1][i])

for i in range (len(mod_pol_assembly_MH[0][73][0])):
    print (mod_pol_assembly_MH[0][73][0][i])
#Mass values
for i in range (len(mod_pol_assembly_MH[0][73][1])):
    print (mod_pol_assembly_MH[0][73][1][i])

##### NEXT: Assemble collected mass at each MH:
print ("\n","  Pollutographs of Manholes in the sewer network \n", "-"*40)
#Manholes with zero sources U/S

        # starting a new MH pollutographs time series
MH_pollutographs = [[[],[]] for i in MHs] #each MH has one sub-list
print(MH_pollutographs)
#filling Date-Time lists:
for i in range(len(MH_pollutographs)):
    MH_pollutographs[i][0]= DT_timeSeries_1

for i in MHs:

    MH_ID_i = i                 #ID of curernt MH
```

```
    index_MH_i = MHs.index(i)   #index of current MH in the [MHS] list

    MH_pollutographs[index_MH_i][0] = DT_timeSeries_1  # this MH time
series is set to original timeseries

    if i not in No_chloramine_sources_MHs: #MH not D/S of chl sources

        MH_pollutographs[index_MH_i][1] = [0.00] * No_timesteps
        print("Zero chloramine sources U/S of MH ID :", i)

    if i in No_chloramine_sources_MHs:

        #all other MH
        No_chl_sources_i = No_chloramine_sources_MHs[i]
        print ("Pollutograph of MH ID: ",i,"\tNo. of chloramine sources
U/S :", No_chl_sources_i)

        # pipes U/S of current MH
        pipes_US_MH_i =[]   #New lists One for Pipe IDs
        pipes_US_MH_i_dict = []  # And One for Dict IDs
        for k in range(len(pipes)):
            if i == pipes[k]['pipeDS']:  # if MH i is the DS pipe k (so
pipe k is u/S of MH i)
                pipes_US_MH_i.append(pipes[k]['pipeID'])
                pipes_US_MH_i_dict.append (pipes[k]['dictID'])
                print("\tpipes U/S :", pipes_US_MH_i, "with dictIDs:",
pipes_US_MH_i_dict)


        #Un-chloraminated Q at MH:
        if i in un_Chl_MH_inflows:
            index_MH_i_unchl = un_Chl_MH_inflows.index(i)
            Q_unchl_MH_i =
un_Chloraminated_inflows_timeSeries_4[index_MH_i_unchl]
        else:
            Q_unchl_MH_i = [0.00] * No_timesteps
            print("\tNo Un-chloraminated inflow")
        # [2] preparing the Discharge matrices, first: Chloraminated
inflow at each MH
        # Chloraminated Q at MH:
        if i in chl_int_MHs:
            index_MH_i_chl = chl_int_MHs.index(i)
            Q_chl_MH_i = Q_MHs_timeSeries_3[index_MH_i_chl]
            C_chl_MH_i = C_timeSeries_3[index_MH_i_chl]
            print ("\tChloraminated inflow defined")
        else:
            Q_chl_MH_i = [0.00] * No_timesteps
            print ("\tNo Chloraminated inflow defined")
```

```
        total_MH_Q = [0.00] * No_timesteps
        for j in range (len (DT_timeSeries_1)):
            for k in pipes_US_MH_i_dict:
                total_MH_Q[j] = total_MH_Q[j] + Q_timeSeries_1[k-1][j]

            total_MH_Q[j] = total_MH_Q[j] + Q_chl_MH_i[j] +
Q_unchl_MH_i[j]

        print ("\ttotal MH Q :", total_MH_Q)

        total_MH_mass = [0.00] * No_timesteps
        counter_mass = 0
        for j in range(len(MH_tracking_MHs)):
            for k in range(len(MH_tracking_MHs[j])):

                if MH_ID_i == MH_tracking_MHs[j][k]:
                    for x in range(len(DT_timeSeries_1)):
                        total_MH_mass[x] =
round(mod_pol_assembly_MH[j][k][1][x]+ total_MH_mass[x], 5)
                    counter_mass = counter_mass +1
        print( "\ttotal MH mass added : ", counter_mass, "\tmass:",
total_MH_mass )

        final_MH_conc = [0.00] * No_timesteps
        for j in range (len (DT_timeSeries_1)):

            final_MH_conc[j] = round (total_MH_mass[j] / total_MH_Q[j], 5)
if total_MH_Q[j] != 0 else 0

        print ("\tFinal MH concentration : ", final_MH_conc)

plt.plot(mod_pol_assembly_MH[18][10][0], mod_pol_assembly_MH[18][10][1],
'r') # plotting t, a separately
plt.plot(mod_pol_assembly_MH[18][10][0], mod_pol_assembly_MH[18][10][1],
'b') # plotting t, b separately
plt.plot(mod_pol_assembly_MH[18][10][0], mod_pol_assembly_MH[18][10][1],
'g') # plotting t, c separately
plt.show()

plt.plot(mod_pol_assembly_MH[0][4][0], mod_pol_assembly_MH[0][4][1], 'r')
# plotting t, a separately
plt.plot(mod_pol_assembly_MH[1][3][0], mod_pol_assembly_MH[1][3][1], 'b')
# plotting t, b separately
plt.plot(mod_pol_assembly_MH[2][2][0], mod_pol_assembly_MH[2][2][1], 'g')
# plotting t, c separately
plt.show()
```

APPENDIX D
SUPPLEMENTARY MATERIAL FOR CHAPTER 4

The MIKE URBAN stormwater model sensitivity was tested. Fig. D1 shows the model sensitivity, presented as a change in the root mean square error (RMSE) on the vertical axis, to perturbations in model inputs such as catchment properties, storage and wetting losses, Manning coefficients and imperviousness ratios. Fig. D2 shows pre-calibration results and Fig. D3 shows post-calibration results for the stormwater model. Table D1 provides statistical measures of MIKE URBAN model performance for twelve sample storm events, both pre- and post-calibration.

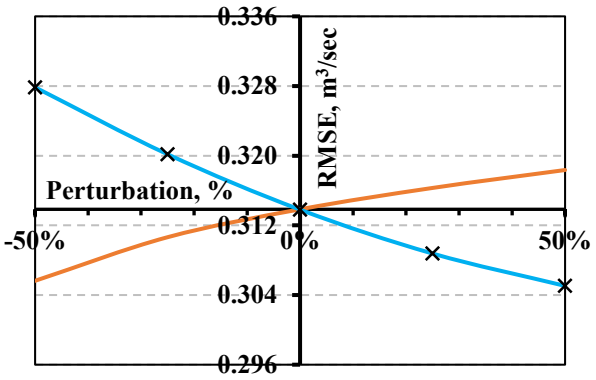

Catchment slope Catchment length

(a) Catchment properties

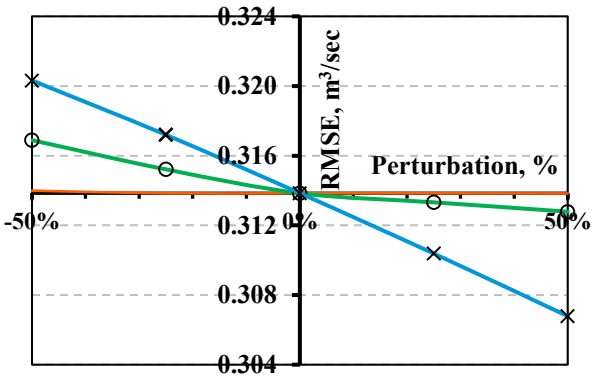

Wetting Impervious surf. Perv. surf.

(b) Storage/Wetting losses

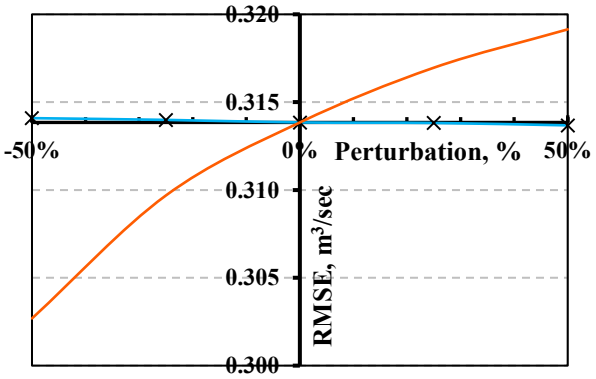

Impervious surfaces Pervious surfaces

(c) Manning coefficient

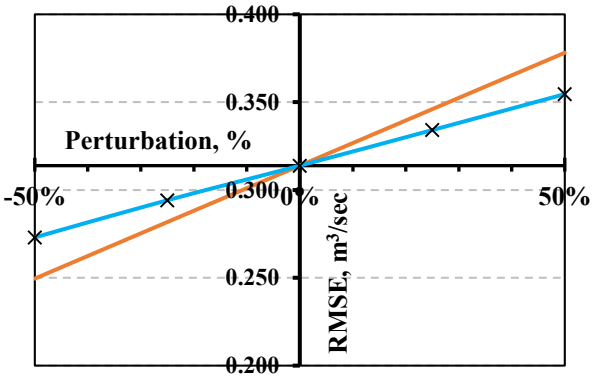

Steep surfaces Flat surfaces

(d) Imperviousness ratio

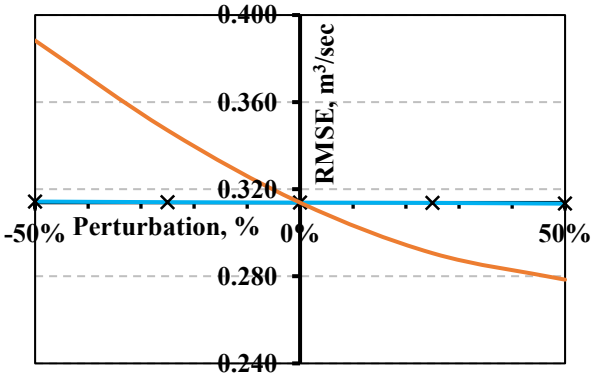

Minimum capacity Maximum capacity

(e) Horton capacity

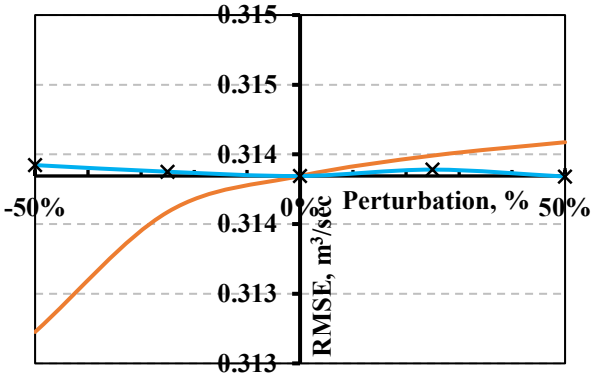

Dry Wet

(f) Horton's exponent

Fig. D1 Results of sensitivity analyses

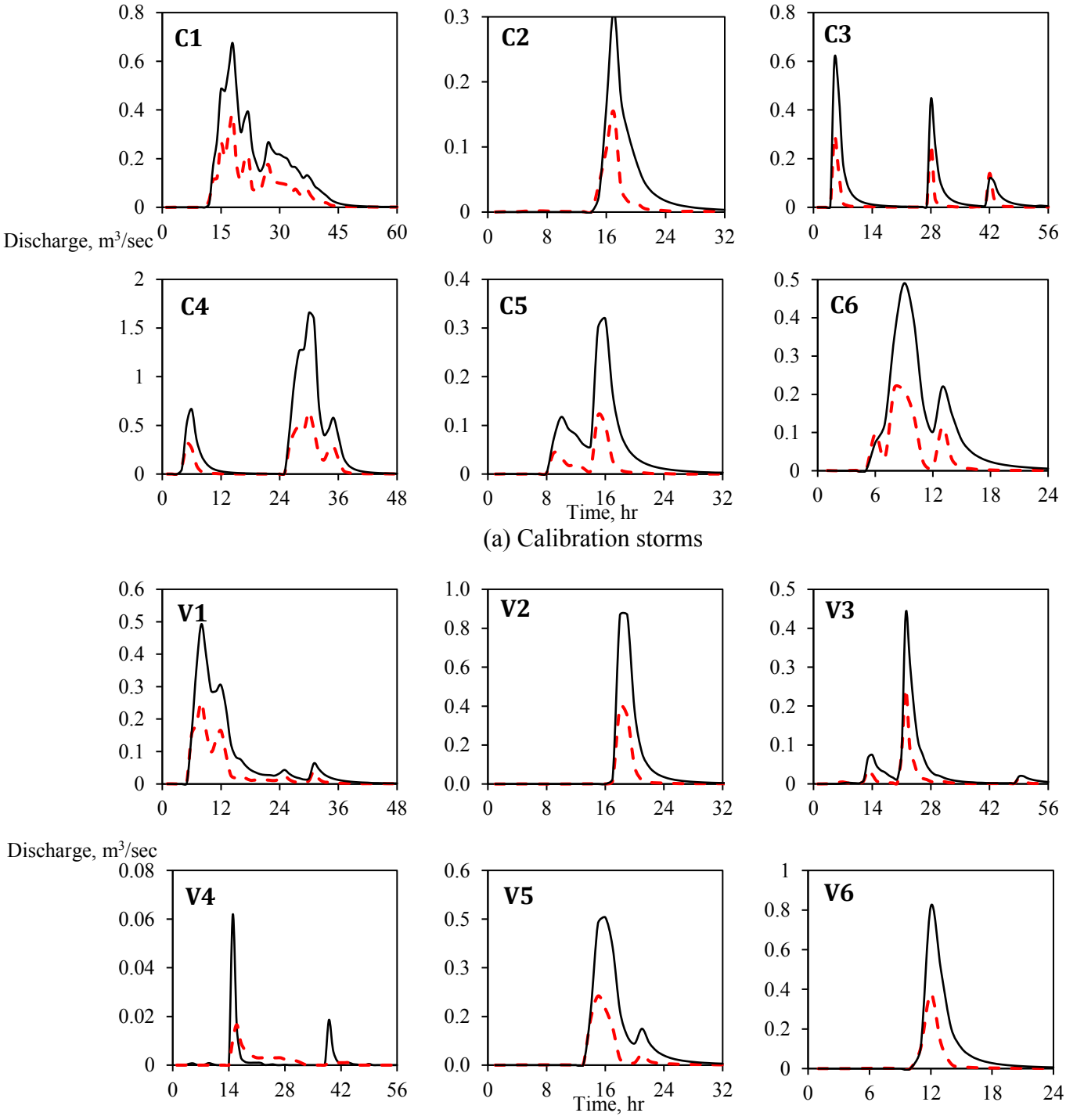

Fig. D2 Pre-calibration model results for some storm events

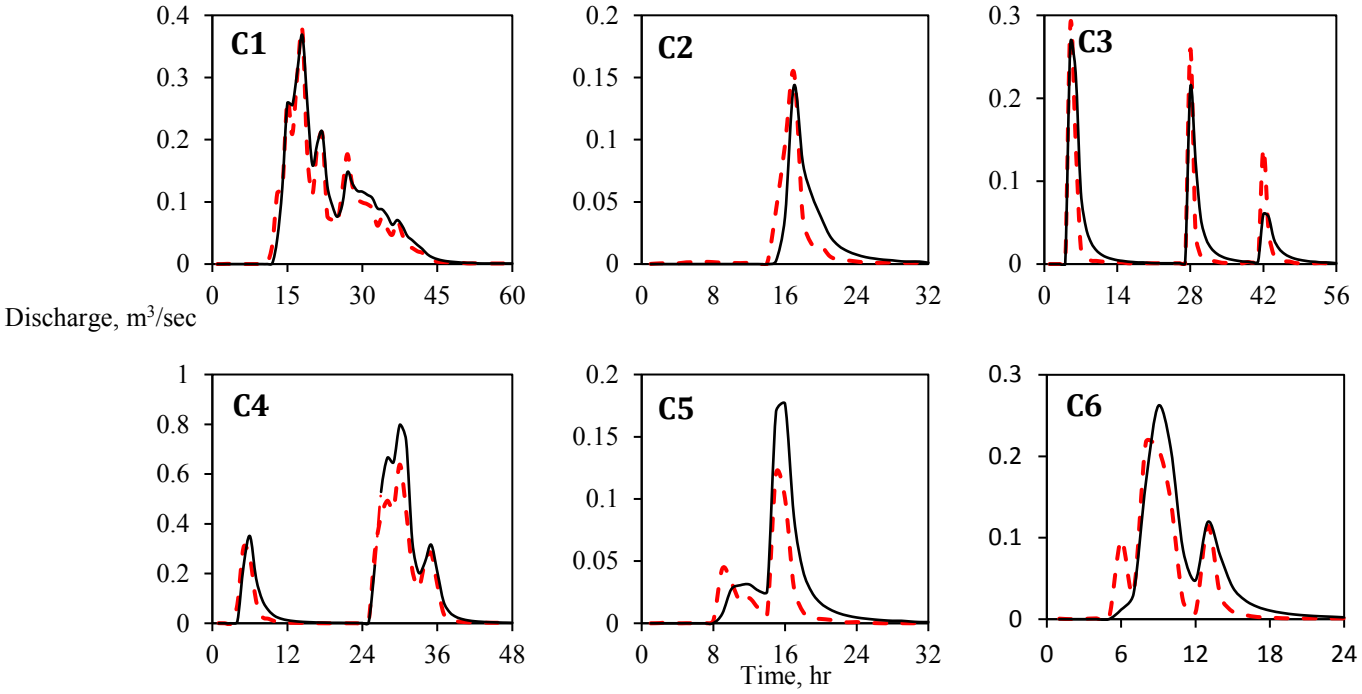

(a) Calibration storms

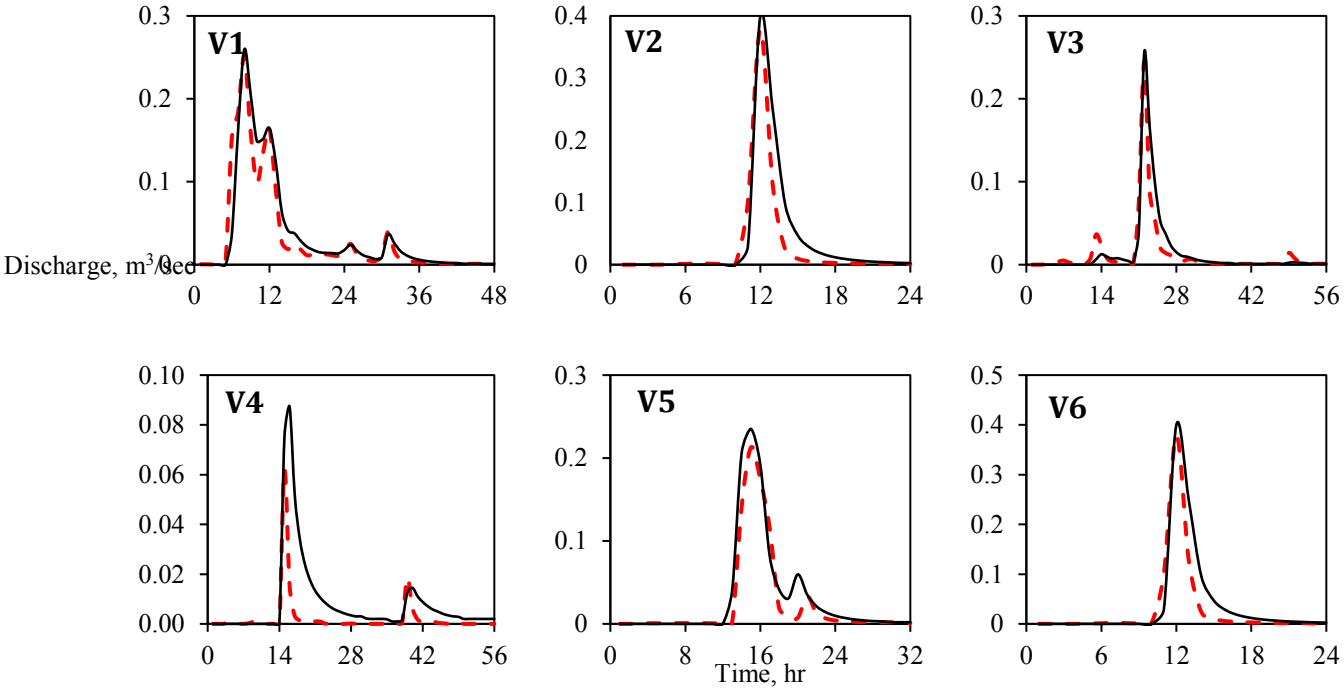

(b) Validation storms

Observed — Simulated

Fig. D3 Post-calibration model results for some storm events

Table D1 Efficiency assessment measures for a sample group of storm events

Pre-calibration model statistics

Storm	C1	C2	C3	C4	C5	C6	V1	V2	V3	V4	V5	V6	Average
Duration	60	32	56	48	32	24	48	24	56	56	32	48	N/A
NSE	-0.621	-1.082	-1.070	-2.719	-4.485	-1.259	-0.620	-1.487	-0.786	-1.484	-1.551	-1.267	-1.536
RMSE (m^3/s)	0.106	0.045	0.081	0.315	0.064	0.099	0.074	0.125	0.048	0.014	0.086	0.112	0.098
R^2	0.956	0.823	0.828	0.941	0.899	0.848	0.930	0.894	0.869	0.490	0.871	0.966	0.860
Slope (b)	0.500	0.426	0.429	0.371	0.331	0.447	0.480	0.404	0.447	0.364	0.408	0.409	0.418
Ln (NSE)	0.384	2.045	0.247	0.901	0.831	1.802	3.622	0.999	0.868	0.953	2.683	0.601	2.862
bR^2	0.478	0.351	0.355	0.349	0.297	0.379	0.446	0.361	0.388	0.178	0.356	0.395	0.361

Post-calibration model statistics

Storm	C1	C2	C3	C4	C5	C6	V1	V2	V3	V4	V5	V6	Average
Duration	60	32	56	48	32	24	48	24	56	56	32	48	N/A
NSE	0.939	0.692	0.805	0.814	0.353	0.748	0.863	0.817	0.823	0.253	0.874	0.939	0.912
RMSE (m^3/s)	0.021	0.017	0.025	0.071	0.022	0.033	0.022	0.034	0.015	0.008	0.019	0.021	0.022
R^2	0.949	0.704	0.826	0.953	0.865	0.803	0.876	0.878	0.883	0.299	0.925	0.949	0.961
Slope (b)	0.927	0.892	0.920	0.751	0.597	0.827	0.905	0.814	0.800	1.598	0.844	0.927	0.829
Ln (NSE)	0.374	2.029	0.140	0.805	0.763	1.738	3.517	0.980	2.645	0.638	2.385	0.374	0.592
bR^2	0.880	0.627	0.760	0.715	0.517	0.664	0.793	0.715	0.706	0.187	0.780	0.880	0.797

APPENDIX E

SUPPLEMENTARY MATERIAL FOR CHAPTER 5

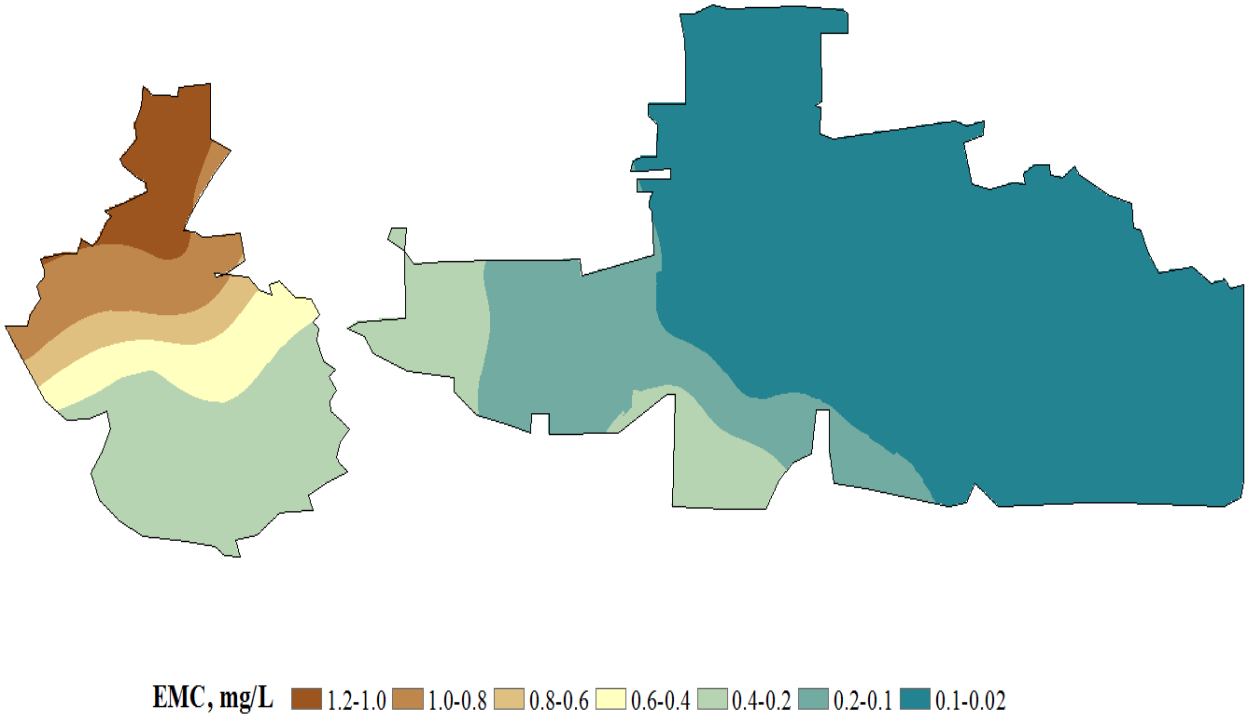

Fig. E1 EMC spatial distribution map

Table E1 Sub catchments / Neighbourhoods in the study area

No.	Neighbourhood	No.	Neighbourhood
1	RAMSAY HEIGHTS	24	SOUTH EDMONTON COMMON
2	RHATIGAN RIDGE	25	RESEARCH AND DEVELOPMENT PARK
3	OGILVIE RIDGE	26	TWEDDLE PLACE
4	HENDERSON FALCONER	27	MICHAELS PARK
5	CARTER CREST	28	RICHFIELD
6	HADDOW	29	LEE RIDGE
7	LEGER	30	TIPASKAN
8	HODGSON	31	KAMEYOSEK
9	TERWILLEGAR TOWNE	32	MEYONOHK
10	MAGRATH HEIGHTS	33	MILL WOODS PARK
11	SOUTH TERWILLEGAR	34	MENISA SATOO
12	MACTAGGART	35	EKOTA
13	BLUE QUILL ESTATES	36	GREENVIEW
14	SWEET GRASS	37	HILLVIEW
15	BLUE QUILL	38	TAWA
16	SKYRATTLER	39	MEYOKUMIN
17	STEINHAUER	40	SAKAW
18	ERMINESKIN	41	MINCHAU
19	KEHEEWIN	42	WEINLOS
20	CORONET ROSEDALE	43	BISSET
21	PAPASCHASE	44	POLLARD MEADOWS
22	STRATHCONA INDUSTRIAL PARK	45	DALY GROVE
23	PARSONS INDUSTRIAL	46	CRAWFORD PLAINS

APPENDIX F

ASSOCIATED PUBLICATIONS

Table F1 Related publications on chloramine decay in water distribution and storm sewers

No.	Publication		
1	Title	:	Monochloramine Loss Mechanisms in Tap Water
	Authors	:	Qianyi Zhang, Evan Davies, James Bolton and Yang Liu
	Journal	:	Water Environment Research, Volume 98(11), p 1999-2005 (2017)
	DOI	:	10.2175/106143017X14902968254421
2	Title	:	Field data analysis of active chlorine-containing stormwater samples
	Authors	:	Qianyi Zhang, Mohamed Gaafar, Rong-Cai Yang, Chen Ding, Evan Davies, James Bolton and Yang Liu
	Journal	:	Journal of Environmental Management, Volume 206, p 51-59 (2018)
	DOI	:	10.1016/j.jenvman.2017.10.009
3	Title	:	Monochloramine loss mechanisms and dissolved organic matter characterization in stormwater
	Authors	:	Qianyi Zhang, Evan Davies, James Bolton and Yang Liu
	Journal	:	Science of the Total Environment, Volume 631, p 745-754 (2018)
	DOI	:	10.1016/j.scitotenv.2018.02.335
4	Title	:	Monochloramine dissipation in storm sewer systems: field testing and model development
	Authors	:	Qianyi Zhang, Mohamed Gaafar, Evan Davies, James Bolton and Yang Liu
	Journal	:	Water Science & Technology, Volume 78 (11), p 2279-2287 (2018)
	DOI	:	https://doi.org/10.2166/wst.2018.512